hAGT inhibitors as chemotherapy enhancers

Maria Tintoré Gazulla

UNIVERSITAT DE BARCELONA

FACULTAT DE FARMÀCIA

“hAGT inhibitors as chemotherapy enhancers”

Maria Tintoré Gazulla

2015

UNIVERSITAT DE BARCELONA

FACULTAT DE FARMÀCIA

Programa de Doctorat en Biotecnologia

hAGT inhibitors as chemotherapy enhancers

Memòria presentada per Maria Tintoré Gazulla per a optar al títol de doctor per la Universitat de Barcelona

Dr. Carme Fàbrega Claveria
Directora

Dr. Ramón Eritja Casadellà
Director

Dr. Glòria Rosell Pellisé
Tutora

Maria Tintoré Gazulla

Barcelona, 2015

The work described in this thesis has been performed in the Institute for Advanced Chemistry of Catalonia (CSIC) and in the Institute for Research in Biomedicine of Barcelona, IRB Barcelona. Chapter 5 is the result of a short stay of 4 months in the University of Milan.

I am grateful for a FIS contract (grant PI06/1250, Fondo de Investigaciones Sanitarias) and a predoctoral fellowship from MINECO (Spanish Ministry of Economy and Competitiveness) FPI (BES-2011-043815) associated to the project CTQ2010-20541-C03-01 and for a short stay grant from MINECO (EEBB-C-13-00369).

Durant aquest temps al laboratori he tingut la sort de conèixer molta gent maca. Voldria agrair especialment als meus companys del laboratori de Química dels Àcids Nucleics tot el que he après, tant científica com personalment. Gràcies al Ramon per donar-me l'oportunitat d'entrar en aquest magnífic grup. A la Carme, que em va ensenyar gairebé a utilitzar una pipeta i de qui he après que el més important en la recerca són la paciència i el rigor. A l'Anna, que m'ha cuidat com una mare. Al Santi, per la seva paciència amb els meus múltiples dubtes sobre síntesi química; a la Sònia, sempre disposada a donar un cop de mà amb els HPLC, els MALDIs o el que faci falta; i a l'Adele, per la seva disponibilitat i ajuda amb els cultius cel·lulars. Al Rubén per la seva ajuda amb els experiments de masses i per tots els bons moments i consells. Al Nacho, que m'aguanta amb alegria les invasions de papers a la seva taula i els robatoris de calculadores i bolis. I a la resta de persones que han passat pel lab durant aquest temps, de qui he pogut aprendre moltes coses.

Vull agrair molt a la Stefi la seva carinyosa acollida durant la meva estada al seu laboratori a Milà. I a la Laura, el Leo, la Gigliola, la Sabrina i l'Angela.

També vull mencionar els meus companys estudiants de doctorat, en especial a l'Albert, per tots els berenars en què hem convertit un moment de desànim per experiments que no sortien en unes bones rialles. Al Michael i l'Andrey pels dinars i ping-pongs compartits. I als meus companys i amics del màster, en especial a la Laura per la seva ajuda durant l'escriptura de la tesi i al Jesús per donar-me un cop de mà amb l'estadística.

Moltes gràcies als meus amics de farmàcia pel seu suport, amb ells vaig començar l'aventura de la ciència. Agraeixo molt al Germán la seva ajuda amb el disseny de la portada de la tesi. I gràcies també al Carlos Roca, la Laia i la resta d'amics per la seva curiositat i interès, em fa molta il·lusió que amics que treballen en camps tan allunyats tinguin tantes ganes de saber el què faig.

Per últim, vull agrair moltíssim als meus pares i als meus germans la seva implicació i il·lusió i sobre tot, al Xavi, que m'ha ajudat, m'ha donat ànims, m'ha preguntat i s'ha escoltat les presentacions, m'ha preparat el tupper moltíssimes vegades i sobre tot, m'ha recolzat en tot moment.

INDEX

ABBREVIATIONS

^{3}H-MNU: Tritiated 1-methyl-1-nitrosourea

3'-Dabsyl CPG: 1-(4,4'-Dimethoxytrityloxy-3-[O-(N-4'-sulfonyl-4-(dimethylamino)-azobenzene)-3-aminopropyl]-propyl-2-O-succinoyl-long chain alkylamino-CPG

3'-Dabcyl CPG: 1-(4,4'-Dimethoxytrityloxy)-3-[O-(N-4'-carboxy-4-(dimethylamino)- azobenzene)-3-aminopropyl)]-propyl-2-O-succinoyl-long chain alkylamino-CPG

6'-FAM: 6-[(3',6'-dipivaloylfluoresceinyl)-carboxamido]-hexyl-1-O-[(2-cyanoethyl)-(*N,N*-diisopropyl)]-phosphoramidite

Ac: acetyl

Ac_2O: acetic anhydride

ACN: acetonitrile

AcOEt: ethyl acetate

AFM: atomic force microscopy

anh: anhydrous

Ape1: human apurinic/apyrimidinic endonuclease

Ar: aromatic

$Au(OOCCH_3)$: gold acetate

AuNPs: gold nanoparticles

AuSPIONs: gold-coated superparamagnetic iron oxide nanoparticles

BCNU: 1,3-Bis(2-chloroethyl)-1-nitrosourea or carmustine

BME: 2-mercaptoethanol

Bz: benzyl

Bzl: benzoyl

Cpd: compound

CPG: controlled pore glass

Dabcyl: 4-(4-(dimethylamino)phenyl-azobenzoic acid

Dabsyl: *N*-4'-sulfonyl-4-(dimethylamino)-azobencene)-3-aminopropyl

DCM: dichloromethane

DEAD: diethyl azodicarboxylate (IUPAC diethyl diazenedicarboxylate)

DIEA: *N,N*-Diisopropylethylamine

DLS: dynamic light scattering

dmf: dimethylformamidino group

DMAP: *N,N*-dimethylaminopyridine

DMF: *N,N*-dimethylformamide

DMSO: dimethylsulfoxide

DMT: 4,4'-dimethoxytrityl

DMT-Cl: 4,4'-dimethoxytrityl chloride

DTT: dithiothreitol

EDTA: ethylenediaminetetraacetic acid

ESI: electrospray ionization

EtTFA: ethyl trifluoroacetate

FAM/F: fluoresceine

^{F}G: O^6-fluorescein-benzylguanosine

FITC: fluorescein isothiocyanate

FL: full length

FRET: fluorescence resonance energy transfer

GST: gluthatione-S-transferase

hAGT: human O^6-alkylguanine-DNA alkyltransferase

HBA: hydrogen bond acceptors

HBD: hydrogen bond donors

HPLC: high performance liquid chromatography

IC_{50}: inhibitory concentration 50%

IPTG: isopropyl-β-D-1-thiogalactopyranoside

LCAA: long chain amino alkyl

LD_{50}: lethal dose 50%

MALDI: matrix-assisted laser diserption/ionization

MeOH: methanol

MB: molecular beacon

MNU: 1-methyl-1-nitrosourea

MTT:(3-(4,5-dimethylthiazol-2-yl)-2,5-diphenyltetrazolium bromide)

NMR: nuclear magnetic resonance.

NPs: nanoparticles

OD: optical density

O^6-MeG: O^6-methylguanine

PAGE: polyacrylamide gel electrophoresis

PBS: phosphate-buffered saline buffer

PPh_3: triphenylphosphine

PrePro: prescission protease

Pyr: pyridine

^{Q}T: (N-4'-carboxy-4-(dimethylamino)-azobenzene)-aminohexyl-3-acrylamido]-2'-deoxyuridine

RP-HPLC: reverse phase high pressure liquid chromatography

rt: room temperature

SPIONs: superparamagnetic iron oxide nanoparticles

TBA: thrombin-binding aptamer

cTBA: complementary TBA

TCA: trichloroacetic acid

TEA: triethylamine

TCEP·HCl: tris(2-carboxyethyl)phosphine hydrochloride

TEAAc: triethylammonium acetate

TEM: transmission electron microscopy

TFA: trifluoroacetic acid

THAP: 2',4',6'-trihydroxyacetophenone monohydrate

THF: tetrahydrofurane

Thr: α-thrombin

TLC: thin-layer chromatography

Tm: melting temperature

TMAOH: tetramethylammonium hydroxide

TOF: time of flight

Tris: tris(hydroxymethyl)aminomethane

UV: ultraviolet

VS: virtual screening

Introduction

Deoxyribonucleic acid (DNA)

The DNA double helix was first described by Watson and Crick in 1953.[1] Since then, the scientific advances based in DNA have been prodigious and far beyond expectations in many fields, reaching areas as diverse as medicine, basic biology, genetics, forensics, archeology among others, and culminating in the sequencing of the human genome.[2]

Deoxyribonucleic acid is a self-assembling biopolymer that encodes the genetic information used in the development and functioning of all known living organisms and many viruses. DNA, together with proteins and carbohydrates, compose the three major macromolecules essential for all forms of life. DNA forms double helices directed by canonical Watson-Crick base pairing and is stabilized by hydrogen bonds, π-π stacking and hydrophobic interactions.[1] The two DNA strands are composed of simpler units called nucleotides. Each nucleotide is composed of a nitrogen-containing nucleobase—either guanine (G), adenine (A), thymine (T), or cytosine (C)—as well as a monosaccharide sugar called deoxyribose and a phosphate group. The four nucleobases are classified in pyrimidines and purines, depending on their structure: pyrimidines (T and C) consist of a single heterocycle of six atoms and purines (A and G) are composed by a pyrimidine ring fused to an imidazole ring (figure 1). Nucleotides are joined to one another by covalent bonds between the sugar of one nucleotide and the phosphate of the next, resulting in a chain formed by an alternating sugar-phosphate backbone. According to base pairing rules (A with T and C with G), hydrogen bonds bind the nitrogenous bases of the two separate polynucleotide strands to make double-stranded DNA. This double helix is further stabilized by π-π stacking and hydrophobic interactions.

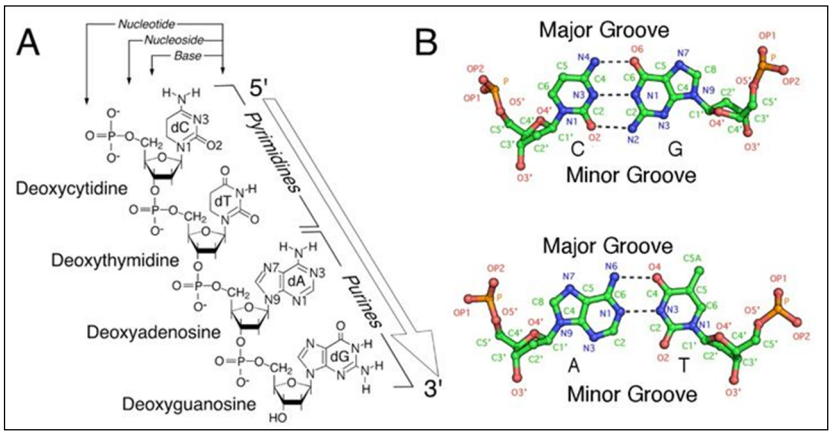

Figure 1. 1A. Representation of the four nucleotides, covalently linked by phosphate bonds. **1B.** Watson-Crick canonical base pairing, C-G and A-T. Non-covalent hydrogen bonds between the pairs are shown as dashed lines. Adapted from ref [3].[3]

DNA structures

DNA exists in many possible conformations that include A-DNA, B-DNA, and Z-DNA forms (figure 2), although only B-DNA and Z-DNA have been directly observed in functional organisms.[4] The conformation adopted by DNA depends on its hydration level, its sequence, the amount and direction of supercoiling, the chemical modifications of its bases, the type and concentration of metal ions, as well as the presence of polyamines in solution.[5] The more compact A form of DNA has 11 base pairs per turn and exhibits a large tilt of the base pairs with respect to the helix axis. In addition, the A form has a central whole (figure 2, left). This helical form is adopted by RNA–DNA and RNA–RNA helices.[6] The B-form of DNA, usually found in cells, consists of well-defined structures that are repeated along the strands: the helical turn measures ~ 3.4 nm, the helical diameter ~ 2.0 nm and the twist angle between base-pairs in solution ~ 34.3º (figure 2, centre).[1] In contrast, the Z-DNA helix is left-handed and has a structure that is repeated every 2 base pairs (figure 2, right). The major and minor grooves, unlike A- and B-DNA, show little difference in width.[7] Formation of this structure is generally unfavourable, as it is a form of higher energy than B-DNA, although certain conditions can promote it, such as alternating purine-pyrimidine sequence, negative DNA supercoiling or high salt and some cations, all requiring physiological conditions. Z-DNA can form a junction with B-DNA (called a "B-to-Z junction box") in a structure which involves the extrusion of a base pair.[8] The Z-DNA conformation has been difficult to study because it does not exist as a stable feature of the double helix. Instead, it is a transient structure that is occasionally induced by biological activity and then quickly disappears.[9]

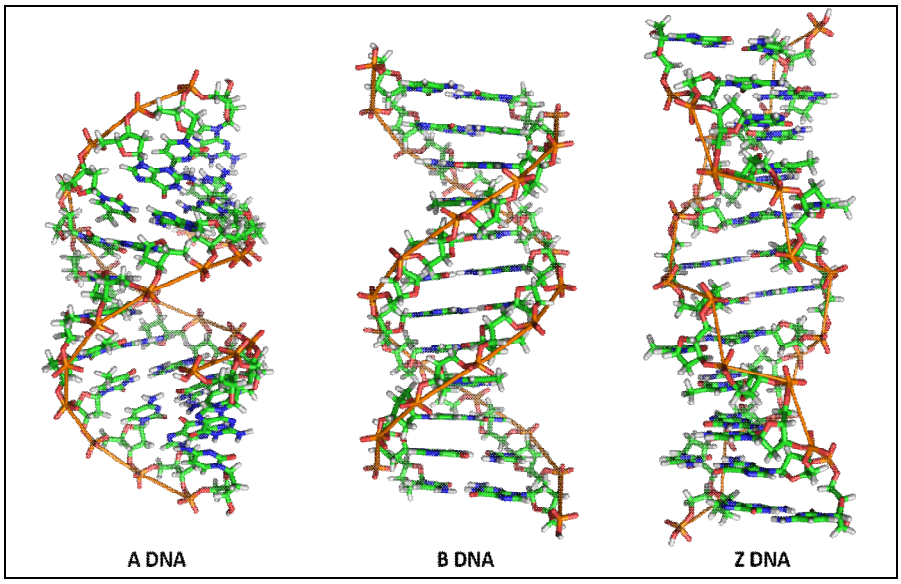

Figure 2. Different types of DNA conformation. A-DNA is the more compact form of DNA, with 11 base-pairs per turn, and it is typical of RNA-DNA and RNA-RNA lattices. B-DNA, the most common conformation of DNA in

nature, is right-handed and possesses a well-defined structure. Z-DNA is conferred as a zig-zag and is a form of higher energy than B-DNA.

The remarkable flexibility of nucleic acids allows them to form a great variety of structures, in addition to the double helix described above, as for example triplexes, *i-motif*s and G-quadruplexes. This flexibility is caused mainly by the high degree of freedom of the deoxyribose ring, and secondly, by the rotation of the glycosidic bond and the phosphate backbone.

Triplex forming oligonucleotides (TFOs)[10] bind in the major groove of duplex DNA with high specificity and affinity. A DNA triplex is formed when pyrimidine or purine bases occupy the major groove of the DNA double helix forming Hoogsteen pairs with purines of the Watson-Crick base-pairs. Intermolecular triplexes are formed between triplex forming oligonucleotides (TFO) and target sequences on duplex DNA[11] (figure 3).[12] TFO should have the identical sequence of the complementary strand of the associating strand in the DNA duplex, while the direction of the TFO relies on the type of DNA triplex. Depending on which bases (pyrimidine or purine) of the TFO interact with the purine base of the duplex, there are two kinds of DNA triplexes: parallel and anti-parallel, respectively.[12] Because of these characteristics, TFOs have been proposed as homing devices for genetic manipulation *in vivo* to alter gene expression and mediate genome modification.[13]

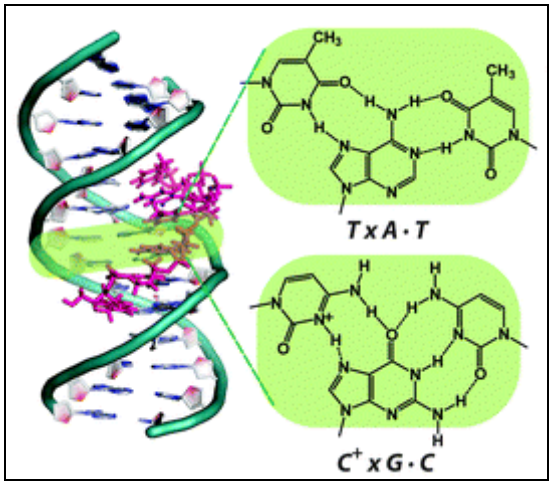

Figure 3. Parallel triplex which consists of T × A·T and C+ × G·C triads (light green). Triplex forming oligonucleotide (TFO), bound at the major groove of the DNA duplex, is coloured in pink. Adapted from ref. [12].

In contrast, the *i*-motif is an intercalated structure formed by association in a head to tail orientation of two parallel duplexes whose strands are held together by hemiprotonated C:C(+) pairs [14] (figure 4). Due to the hemiprotonated nature of the C:C(+) pairs, the formation of *i*-motifs often requires acidic conditions. However, depending on

particular C-rich sequences, *i*-motifs can fold close to neutral pH.[15] The *i*-motif may be formed by a single strand containing four cytidine repeats, by association of two strands containing two cytidine repeats or by four strands containing a single cytidine stretch. *In vivo*, intramolecular *i*-motifs can be found in C-rich sequences of centromeric and telomeric sequences in the chromosome.

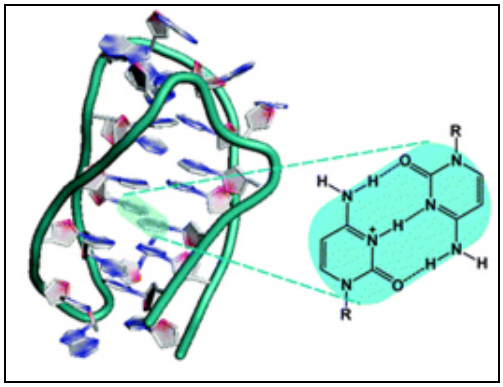

Figure 4. Representation of an *i*-motif quadruplex structure, with its hemiprotonated C:C+ base pair in cyan. Adapted from ref. [12].

G-quadruplexes and TBA

G-quadruplexes are a family of four-stranded DNA structures stabilized by the stacking of guanine tetrads, in which four planar guanines form a cyclic array of Hoogsteen hydrogen bonds stabilized by the presence of monovalent cations[16] (figure 5A). However, most divalent cations have the capacity to induce the dissociation of G-quadruplex structures.[17] These G-rich regions are connected by lateral, central or diagonal loops of diverse sizes and composition that form base-pairing alignments, which in turn stack with the terminal G-tetrads, thus further stabilizing G-quadruplex structures.[18] G-quadruplexes can be folded from a single G-rich sequence intramolecularly or by the intermolecular association of two (dimeric) or four (tetrameric) separate strands (figure 5B). In addition, quadruplexes can adopt different topologies with varying loop configurations, depending on how the guanine bases are arranged.[16d] In the case of intermolecular quadruplexes, if the 5'-3' direction of all the strands is the same, the quadruplex is termed parallel (figure 5C). In contrast, intermolecular G-quadruplexes are antiparallel if the strands are arranged in different directions. For intramolecular quadruplexes, if one or more of the runs of guanine bases has a 5'-3' direction opposite to the other runs of guanine bases, the quadruplex is said to have adopted an antiparallel topology (figure 5C).

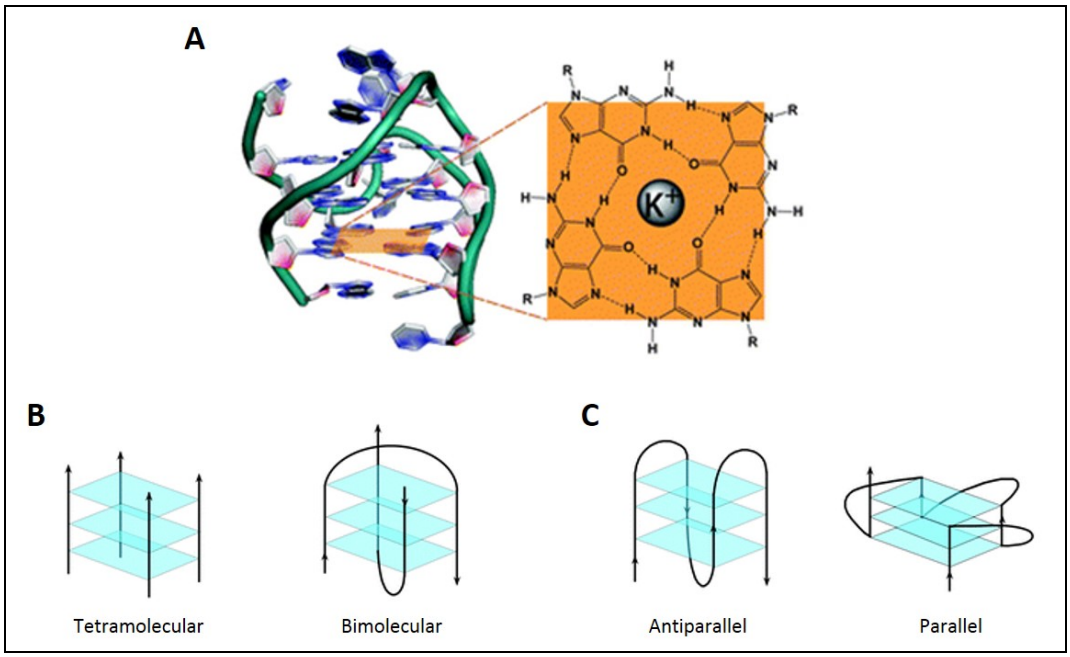

Figure 5. A. Structure of a G-quadruplex structure with the square and planar arrangement of four guanines forming a G-quartet. Adapted from ref. [12] **B.** Schematic representation of intermolecular quadruplexes, tetra and bimolecular. **C.** Schematic representation of intramolecular quadruplexes, antiparallel and parallel respectively. Adapted from ref. [19][19]

Modifications in the base composition of the tetrads are poorly tolerated by these structures. As an example, inosine [20] and O^6-methylguanosine [21], (figure 6) both nucleosides containing non-natural bases, can form a smaller number of hydrogen bonds, provoking the loss of the quadruplex conformation.[22]

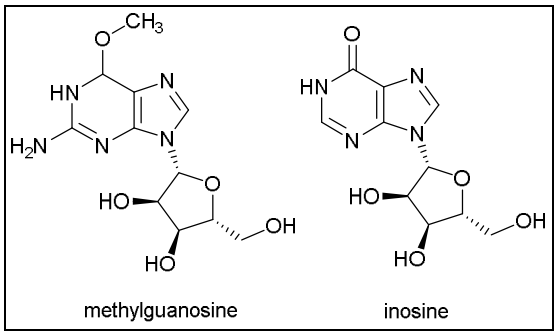

Figure 6. Chemical structure of methylguanosine and inosine.

There is evidence that G-quadruplexes can be formed *in vivo*[23] and present great biological relevance. They can be found in the telomere, the final region of the chromosome composed by repetitions of non-coding G-rich sequences, which protects the end of the chromosome from deterioration or from fusion with neighbouring chromosomes.[24] In addition, these sequences can be found in gene promoters regions, suggesting that their function may be related with gene regulation at the transcription level.[25] Furthermore, a great variety of proteins can recognize and interact with

oligonucleotide aptamers that possess a G-quadruplex structure, as the G-quadruplex aptamers that inhibit the HIV integrase.[26]

In particular, the α-thrombin binding aptamers (TBA) are well characterized chair-like, antiparallel quadruplex structures that bind specifically to α-thrombin at nanomolar concentrations and therefore have interesting anticoagulant properties.[27] α-thrombin is able to interact with two different TBAs in two binding sites of the protein.[28] These two sequences are known to bind specifically and cooperatively to two specific and almost opposite epitopes of α-thrombin when folded into their quadruplex structure.[28b] TBA1 is a 15mer nucleotide composed of two G-tetrads that are connected by three edge-wise loops, forming a well-characterized intramolecular chair-like, antiparallel quadruplex which binds α-thrombin in its primarily fibrinogen exosite.[28a] In contrast, TBA2, a 29mer nucleotide that forms a combined quadruplex/duplex structure, interacts with α-thrombin in its heparin-binding exosite, placed in the opposite side of the protein[28b] (figure 7).

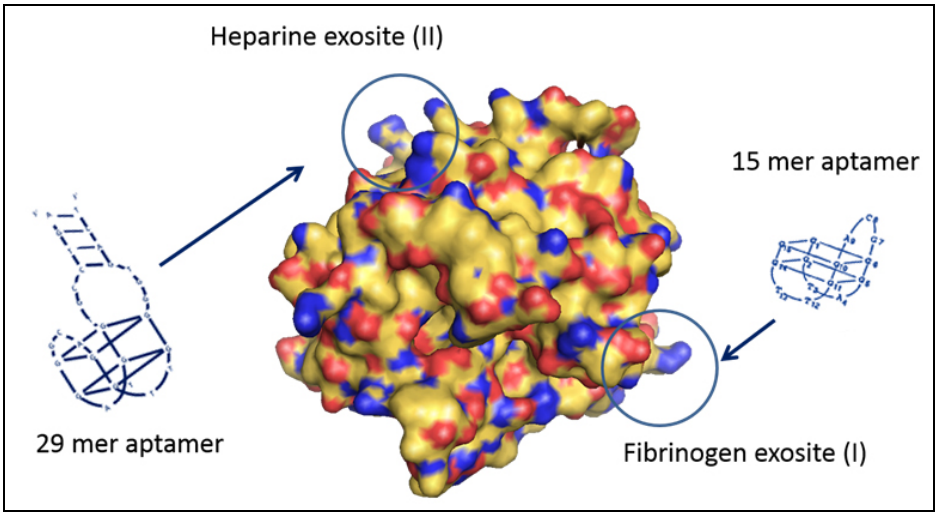

Figure 7. α-thrombin interaction with the α-thrombin binding aptamers. The fibrinogen exosite (I) of α-thrombin interacts with the 15mer aptamer while the heparine exosite (II) is recognized by the longer aptamer (29mer).

DNA stability, damage and repair

DNA may suffer structural damage that can alter or eliminate the cell's ability to transcribe the encoded genes.[29] DNA damage occurs at a rate of 10,000 to 1,000,000 molecular lesions per cell per day, which constitutes only 0.000165% of the human genome,[30] and plays a major role in mutagenesis, carcinogenesis and ageing. These reactions are triggered by exposure to environmental factors and exogenous chemicals, or they can result from metabolic processes inside the cell.[31] Environmental and exogenous DNA damage can be caused by the UV radiation of the sun,[32] other radiation frequencies, as X-

rays and gamma radiation,[33] and human-made mutagenic chemicals,[34] specially aromatic compounds that act as intercalating agents.[35] Some viruses can also cause mutations in DNA during their replication cycle inside the host cell.[36] In contrast, endogenous damage is caused by spontaneous mutations and replication errors,[37] or by reactive oxygen species produced from normal metabolic byproducts.[38]

There are several types of damage to DNA due to exogenous factors and endogenous cellular processes:[39] oxidation of bases, as for example 8-oxo-7,8-dihydroguanine (8-oxoG);[40] alkylation of bases[41] (usually methylation), such as formation of 7-*N*-methylguanine,[42] 3-*N*-methyladenine[43] and 6-O-methylguanine;[44] or hydrolysis of bases, such as deamination,[45] depurination,[46] and depyrimidination.[47] Other damage includes bulky adduct formation, mismatch of bases due to errors in DNA replication and crosslinks of different types.[48]

Cells must repair DNA damage to prevent mutations from propagating and accumulating, and to maintain genome integrity and stability. The persistence of unrepaired DNA damage results in accumulation of mutations, cell cycle arrest and apoptosis.[49] DNA damage alters the spatial configuration of the helix and such alterations can be detected by the cell, inducing several mechanisms for DNA repair.[50] The ATM and ATR genes often initiate the DNA damage response, activating signal transduction pathways that arrest the cell cycle and increase the expression of DNA repair genes.[51] Enzymes involved in different pathways as the base-excision, the nucleotide excision, the mismatch repair, the double-strand break, and other DNA repair processes (figure 8) all respond in a pre- and post-transcriptionally regulated fashion to DNA damage. Nevertheless, cells unable to sense and repair DNA damage may continue to grow and divide, eventually causing cellular dysfunction and death, a hallmark of diseases such as neurological defects and infertility. In addition, deregulation of DNA damage sensing can also yield an increased mutation rate, potentially causing uncontrolled cell growth and cancer.

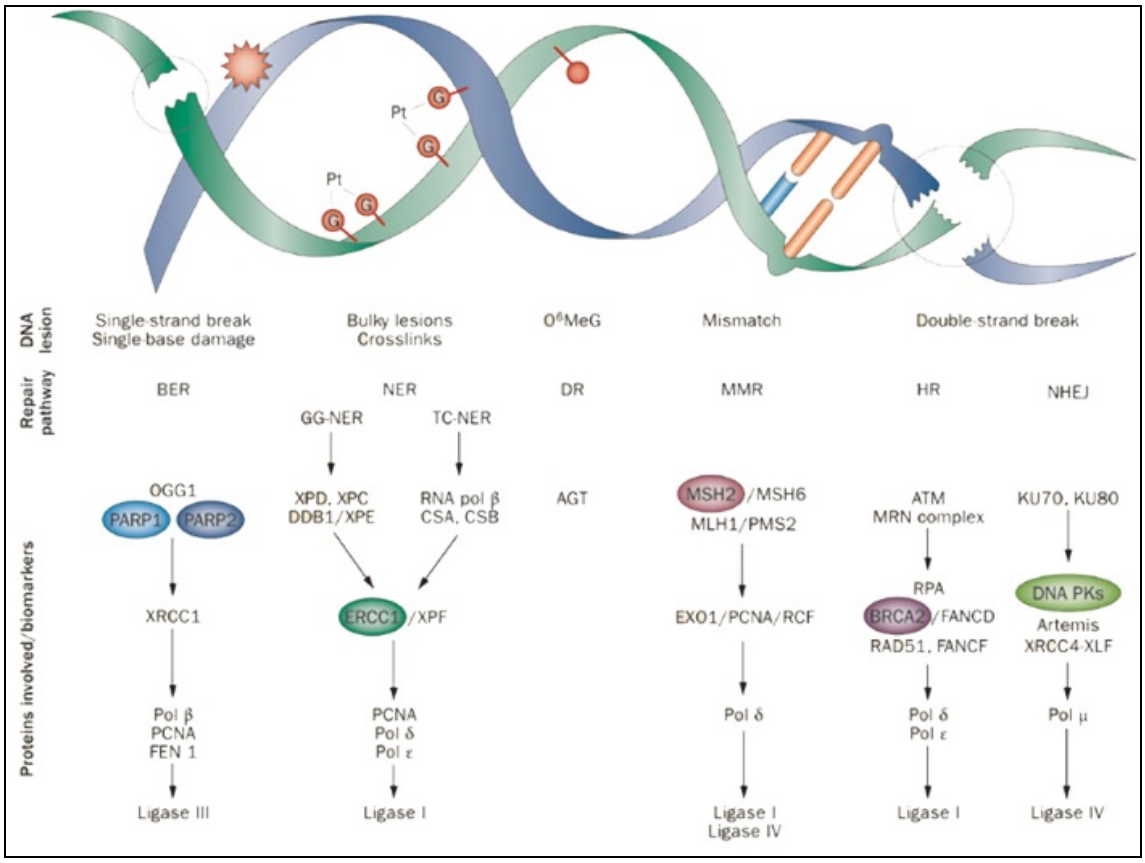

Figure 8. Scheme of the different types of damage that DNA can suffer with their according DNA repair pathways. Adapted from ref. [52]

The base excision repair (BER) pathway is a major mechanism for dealing with a variety of lesions in DNA produced by alkylation.[53] This pathway is initiated by specific DNA glycosylases, which recognize and excise the damaged base to generate an apurinic/apyrimidinic (AP) site. AP endonuclease 1 (Ape1)[54] cleaves the phosphodiester backbone adjacent to the 5' site of the AP site, generating a 3' hydroxyl and 5'-deoxyribose phosphate termini.[54d] Polymerase β removes the 5'-deoxy ribose phosphate, fills in the one-nucleotide gap, and the consequent nick is ligated by DNA ligase I or by DNA ligase III/XRCC1[47, 55] (figure 9). Ape1 is a fundamental protein in this essential repair pathway and it is thought to be responsible for 95% of total AP endonuclease activity in human cell lines.[56]

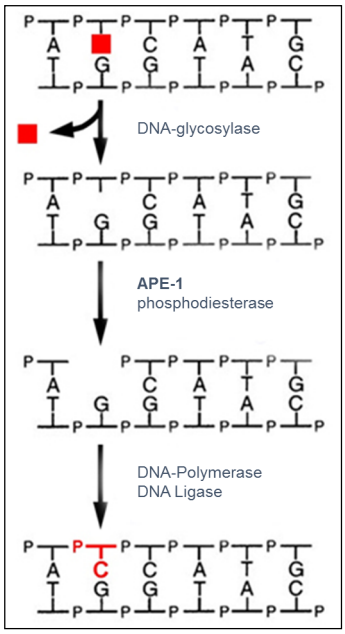

Figure 9. Schematic representation of the enzymes involved in the base excision repair pathway.

Other DNA repair mechanisms are based on a single reaction modulated by a single enzyme. For example, the DNA repair O^6-alkylguanine DNA alkyltransferase (AGT or MGMT) is in charge of repairing alkylating damage, removing alkyl adducts from the O^6 position of guanines. The human AGT (hAGT), the most thoroughly characterized AGT protein, repairs alkylated DNA by flipping the damaged base out of the helix, and the alkyl group is transferred from the point of lesion to the active site Cys145 residue to be repaired.[57] Once alkylated, this protein is degraded by the ubiquitin pathway.[58] hAGT is normally present in all cells, but its overexpression can be triggered in tumoral cells that are being attacked by alkylating chemotherapeutic agents.

DNA alkylating agents as chemotherapy for cancer

Alkylating agents are chemotherapeutic anticancer drugs that produce their cytotoxic effect by generating alkylation and adducts at multiple sites in DNA.[59] DNA repair pathways induced by chemotherapeutic drugs as alkylating agents have a key role in the prognosis and evolution of multiple cancers.[60] The simultaneous treatment with alkylating agents and inhibitors of DNA repair proteins sensitizes tumoral cells to chemotherapy and results in a better outcome and prognosis.[61] An example of it is the identification and characterization of small molecules that inhibit the repair endonuclease activity of APE-1,[62] including methoxyamine (MX), lucanthone and 7-nitroindole-2-carboxilic acid (NCA). All three compounds were able to enhance the effects of

methylmethane sulfonate (MMS) or temozolamide (TMZ) in ovarian,[63] breast,[63b, 64] colon[65] and HT1080 fibrosarcoma cancer cells.[66]

Another subset of alkylating agents, which includes nitrosoureas and temozolamide, have a preference for alkylating guanine at the O^6 position, which is the most important in terms of mutagenesis and carcinogenesis.[42, 44, 67] In particular, 1,3-bis-(2-chloroethyl)-1-nitrosourea (BCNU or carmustine) attacks initially at the O^6 guanine position, causing its rearrangement in a cyclic intermediate due to the attack at the N^1 position of guanine, giving rise to N^1,O^6-ethanoguanine.[68] Finally, a cross-link with the opposite cytosine is formed (figure 10) and, as a consequence, DNA replication is blocked, producing G2/M arrest.[69]

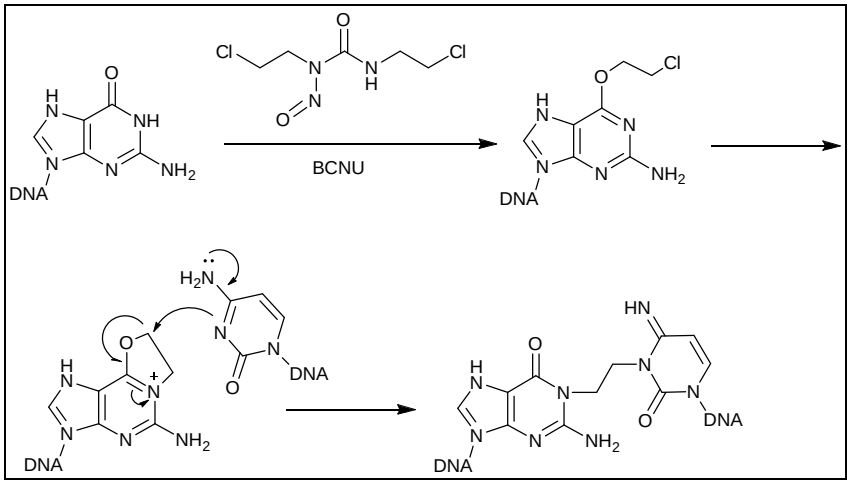

Figure 10. Mechanism of action of 1,3-bis-(2-chloroethyl)-1-nitrosourea, which alkylates the O^6 position of guanines, causing a crosslink with the opposite cytosine.

The DNA-repair O^6-alkylguanine DNA alkyltransferase (hAGT) is in charge of removing alkyl adducts from the O^6 position of guanines, blocking their cytotoxic effects and playing an important role as a chemotherapy resistance mechanism (figure 11).[70]

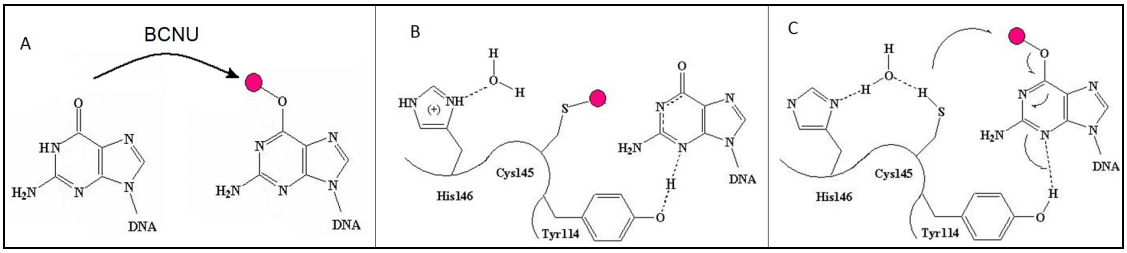

Figure 11. Mechanism of action of the repair reaction of hAGT. **A.** Carmustine or BCNU (bis-chloroethylnitrosourea) introduces alkyl groups in the O^6 position of guanines. **B.** The active site cystine 145 removes the alkylation through a nucleophilic attack S_N2. **C.** The guanine is restored while the active site of hAGT remains covalently linked to the alkyl group and the protein undergoes a process of ubiquitination and degradation.

It is well established that tumor cells frequently express higher levels of this protein, which appears to be predictive of poor response to chemotherapeutic drugs. This effect has been observed in a large number of cancers, ranging from colon cancer, lung tumors, breast cancer, pancreatic tumors, non-Hodgkin's lymphoma, myeloma and glioblastoma multiforme, among others.[71] Additionally, methylation of hAGT promoter and consequently hAGT complete depletion has been associated with longer survival in patients with gliomas under radiation-chemotherapy combining treatment.[72] Therefore, pharmacological inhibition of hAGT has the potential to enhance cytotoxicity of a diverse range of anticancer agents.[73] Adducts formed at the O^6 position of the guanine are of major importance in both the initiation of mutations and in the cytotoxic effects of these agents. For all these reasons, hAGT is considered relevant as a prognosis marker of cancer and represents a potential therapeutic target.[70c] Several research groups have focussed their research on the identification of small molecules capable of inhibiting hAGT activity and enhancing the cytotoxic effect of the alkylating agents in tumour cells.[74]

Over the last years, a number of drugs have been shown to inactivate hAGT in cells, human tumour models and cancer patients, and O^6-benzylguanine and O^6-[4-bromothenyl]guanine have been used in clinical trials. These agents also inactivate MGMT in normal tissues and hence exacerbate the toxic side effects of the alkylating drugs, requiring dose reduction.[75] In addition, they possess poor pharmacokinetic conditions[76] and also produce myelosupression.[77]

DNA Nanotechnology

At the end of the XX century, Ned Seeman set the bases for the use of DNA as a scaffold for nanoscale building material.[78] The remarkable specificity of the molecular recognition between complementary nucleotides in the DNA base pairing has made it an attractive molecule for scientists and engineers interested in micro- and nano-fabrication. Its predictability, rigidity, and precise structural control, as well as the creation of algorithms for *de novo* design of new self-assembled structures,[79] make it a useful building material to develop different kinds of nanotechnological platforms. Compared to other self-assembling molecules, DNA nanostructures offer programmable interactions and surface features for the precise positioning of other nanoparticles and biomolecules.[80]

Seeman's original goal was the creation of regular 3D lattices of DNA which could be used as scaffolding for the rapid, orderly binding of biological macromolecules to speed the formation of suitable crystals for 3D protein structure elucidation in x-ray diffraction studies.[78] This concept gave rise to the tile-based assembly method, used to synthesize two-dimensional periodic lattices[81] and three-dimensional architectures as for example a cube in solution[82] and different polyhedra in solid phase.[83] Some examples of 3D DNA constructs are represented in figure 12.[84]

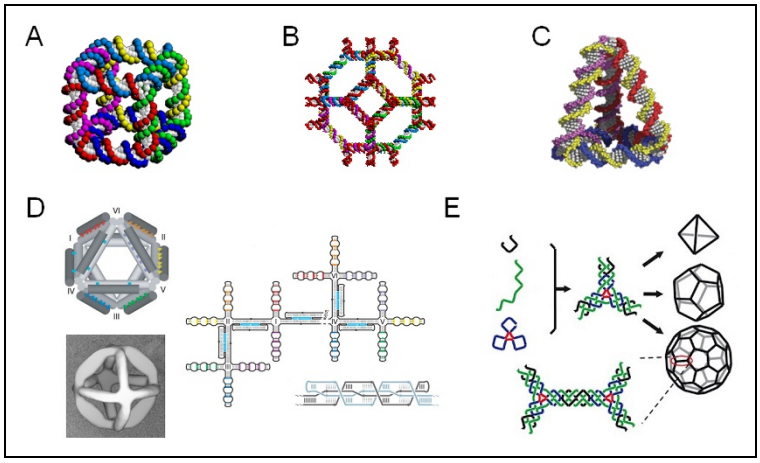

Figure 12. A. Schematic representation of a tridimensional cube, containing twelve equal-length double-helical edges arranged around eight vertices. Adapted from ref. [82] **B.** Double-helical representation of an ideal truncated octahedron. Adapted from ref. [83b] **C**. Schematic representation of a DNA tetrahedron. Adapted from ref. [83c] **D**. Reconstituted 3D image of an octahedron. Secondary structures of the octahedron consisted of different DNA motifs for 3D formation. Adapted from ref. [83a] **E**. Scheme of the polyhedral structures: a tetrahedron, a dodecahedron and a bucky ball were assembled from three-point star building blocks. Adapted from reference [83d].

DNA Origami

Another important breakthrough in the structural DNA nanotechnology field has been the development of DNA origami by Paul Rothemund,[85] where a long scaffold strand of 7

kilobase, the M13 phage genome, is folded with the help of hundreds of short 'staples' to create a rational desired two-dimensional shape (figure 13). Since then, various DNA motifs have been designed in 2D and 3D, and extensive studies are currently ongoing to apply these nanostructures to a large amount of biomedical, computational and molecular motor purposes.

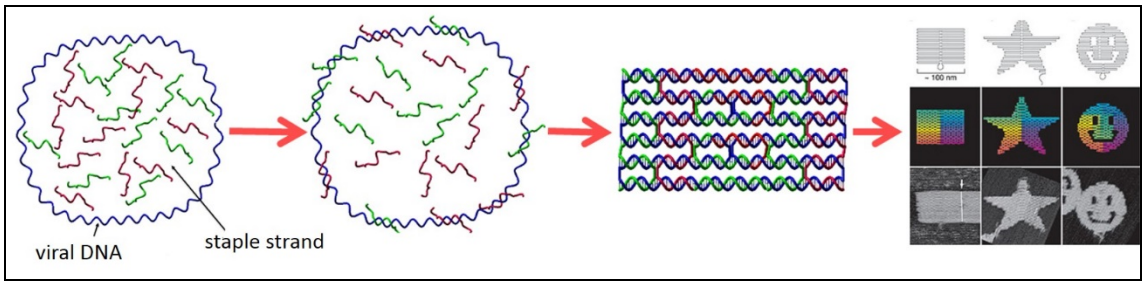

Figure 13. Scheme of the formation of a DNA origami by the annealing of a viral circular scaffold and the complementary staple strands. Adapted from ref [87].

DNA origami is a versatile tool for the self-assembly of other molecular species[86] and constitutes an excellent platform to create a variety of new nanoscale devices[87] with great biological potential and applications.[88] As examples, Yao and co-workers have used the DNA origami as an addressable support for label-free detection of RNA hybridization[89] and later, Seeman and co-workers have developed a nanosensor to detect single nucleotide polymorphism (SNP).[90] Both strategies represent an innovative way to use the DNA origami methodology to create a nanosensor for biomedical applications at the single molecule level using atomic force microscopy (AFM) (figure 14A). In addition, DNA origami has been applied for the study of DNA repair proteins, as represented in figure 14B, where the methyl transfer reaction of *Eco*RI is visualized in a frame-like DNA origami. In this particular case, Sugiyama and collaborators studied by AFM the regulation of DNA methylation using different tensions of double strands. They introduced two different double helical tensions (tense and relaxed) into an origami frame, to control the methyl transfer reaction of *Eco*RI and examine the structural effect of this methylation.[91] Endo *et al.* further evolved this idea to create a versatile nanochip for direct analysis of DNA base-excision repair. In this case, the studied enzymes were 8-oxoguanine glycosylase (hOgg1) and t4 pyrimidine dimer glycosylase (PDG).[92] The exact positioning and displacement of the enzymes in the reaction can be monitored and analyzed.

Another relevant application of the DNA origami is its potential use as drug delivery systems with high biocompatibility: for example, a logic-gated DNA nano-pill was designed for the selective delivery of molecular payloads to the cell and is represented in figure 14C.[93] These nanopills are capable of inducing a great variety of responses in cell behavior. Another cutting-edge design of DNA origami related with cellular biology was

the design of DNA-based channel that can punch pores into the lipidic cell membrane which are able to discriminate single DNA molecules (figure 14D).[94] This could be of great interest for the delivery of oligonucleotide-based drugs for gene therapy, which do not enter the cell easily due to their chemical features.

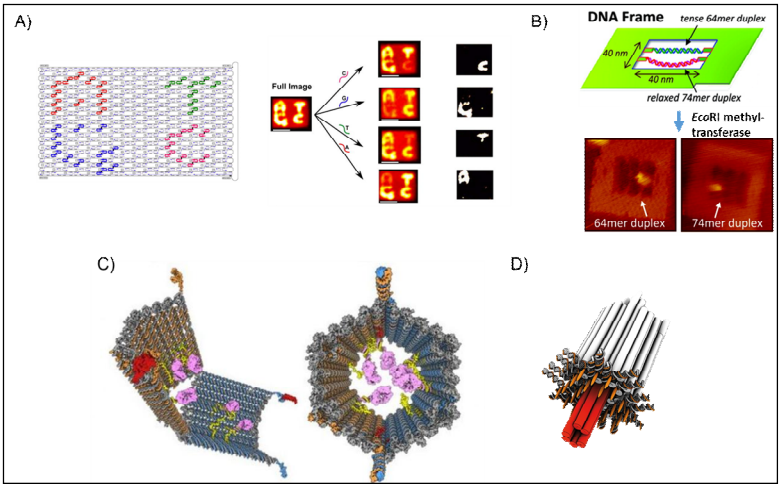

Figure 14. A. Detection of single molecule polymorphisms via atomic force microscopy over an origami surface. Adapted from ref. [90]. **B.** Methyl transfer reaction of *Eco*RI and analysis of the structural effect of this methylation using a same frame-like design of DNA origami. Adapted from ref. [91] **C.** DNA-origami based channel that can punch pores into the lipidic cell membrane, with ability to discriminate single DNA molecules. Adapted from ref. [93]. **D.** Logic-gated DNA nano-pill for the selective delivery of molecular payloads to the cell. Adapted from ref. [94].

Further development of DNA nanotechnology holds great potential for biological applications, hopefully for biomedical approaches with highly programmable and controllable abilities in the very near future.

DNA Nanoparticles

In recent years, a great variety of chemical methods has been developed to synthesize functionalized nanoparticles for biomedical applications such as drug delivery, cancer therapy, diagnostics, tissue engineering and molecular biology, and the structure-function relationship of these functionalized nanoparticles has been extensively examined.[95]

Nanoparticles are particles between 1 and 100 nanometres in size. In nanotechnology, a particle is defined as a small object that behaves as a whole unit with respect to its transport and properties. Particles are classified according to their composition and diameter. Their properties allow the functionalization with diverse biomolecules, including DNA, by different chemical means.

In particular, the controlled assembly and disassembly of gold nanoparticles (AuNPs) has been a subject of great interest over the past decade due to the potential applications of these particles in nanobiotechnology.[96] Their unique physical properties,[97] particularly their localized surface plasmon resonance (LSPR)[98] and their efficient interaction with molecules with a free thiol group, make AuNPs attractive building blocks for nanoscale electronic and photonic devices.[99] Due to the strong interaction between gold and thiols (-SH), a single monolayer of DNA around the gold particle can be obtained. The negative charge repulsion of the phosphate backbone of DNA orients the DNA strands out into solution with a unique footprint that is dependent on gold nanoparticle size and packing density. Since the first DNA sensor was designed by Mirkin and co-workers,[100] the development of AuNP-based colorimetric biosensors has been increasingly applied for the detection of a large variety of targets, including nucleic acids, proteins, saccharides, small molecules, metal ions, and even cells. This technique takes advantage of the colour change that arises from the interparticle plasmon coupling during AuNP aggregation (red-to-purple or blue) or redispersion of an AuNP aggregate (purple-to-red) (figure 15).[96a, 96b, 96g] It is quickly becoming an important alternative to conventional detection techniques, as fluorescence-based assays, and holds great potential in clinical diagnostics, drug discovery, and environmental contaminant analysis, among others.

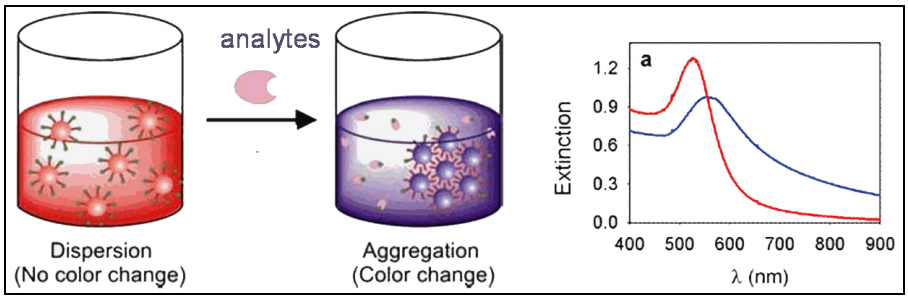

Figure 15. Schematic representation of the colorimetric change suffered by gold colloid upon aggregation and its UV spectra displacement. Adapted from ref [103].[101]

In contrast, super paramagnetic iron oxide nanoparticles possess different interesting features for nanomedicine. SPION are one of the most promising agents in diagnostics, due to their advantages as MRI contrast agents.[102] Under an applied magnetic field, SPION shorten the spin-spin relaxation time (T2) of the proton, which results in darkening of MR images. A schematic representation of this process is shown in figure 16.[103]

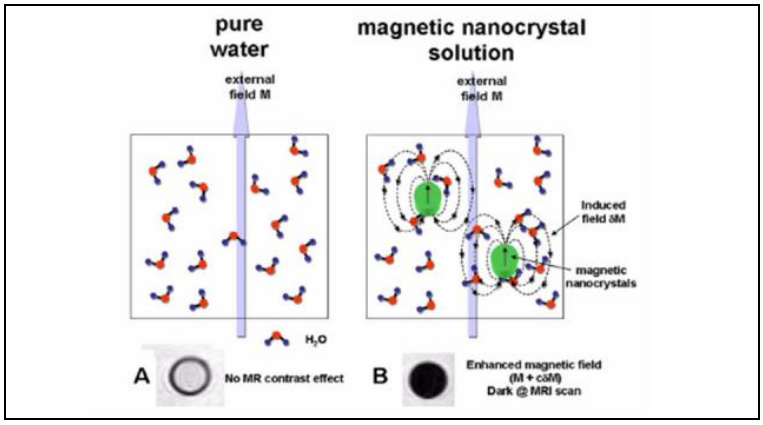

Figure 16. Super paramagnetic iron oxide nanoparticles as negative contrast agents. Under an applied magnetic field, SPION shorten the spin-spin relaxation time (T2) of the proton, which results in darkening of MR images. Adapted from ref. [103]

In comparison with the traditional gadolinium-based contrast agents, SPION produce lower toxicity, stronger enhancement of proton relaxation and have a lower detection limit.[104] Furthermore, SPION have several other applications in biomedicine, especially for delivery purposes and biosensing, due to their reduced size and ability to be transported in biological systems.[105] Their functionalization with DNA is not straightforward, as iron oxide interacts poorly with biomolecules. For this reason, organic compounds are used for their coating, focusing in two major objectives: preserve the magnetic properties of magnetic iron oxides and enhance their biocompatibility.[106]

Gold and iron-based magnetic nanoparticles seem to be one of the most promising nanoparticles for biomedical applications for their unique properties. The combination of them through a gold coating over the magnetic core provides the benefits from both nanoparticles, adding the magnetic properties to the robust chemistry provided by the thiol functionalization of the gold coating (figure 17).[107] As a result, an increasing number of laboratories is working on the synthesis and applications of this type of gold-coated nanoparticles.[105c, 105d, 108]

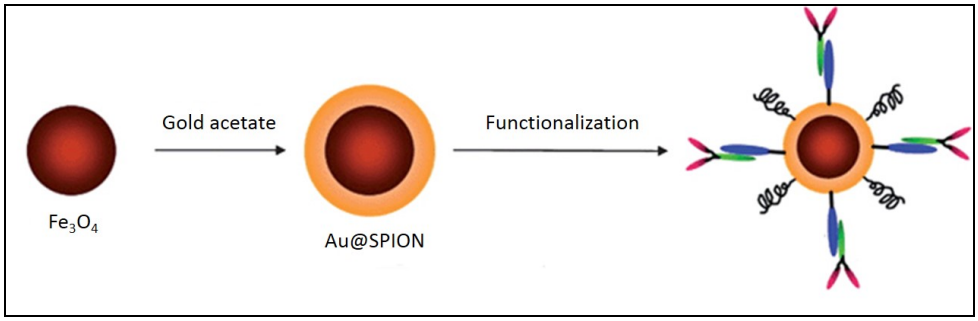

Figure 17. Steps in the synthesis and functionalization of gold-coated magnetic nanoparticles. Adapted from ref [107].

As mentioned before, DNA functionalized nanoparticles are suitable for several applications, as drug delivery or the development of sensors for the detection of biomolecules. Nanoparticles provide the benefits from controlled drug delivery and cell-specific targeting, compared to the traditional forms of drug administration. A drug is transported to the place of action, hence, its influence on vital tissues and undesirable side effects can be minimized. Accumulation of therapeutic compounds in the target site increases and, consequently, the required doses of drugs are lower.[109] However, for nanoformulations used in drug delivery the focus in most researches is mainly on the reduction of toxicity of the incorporated drug, whereas the possible toxicity of the carrier used is not considered. Their toxicity due to bioaccumulation still needs to be studied and minimized, as the kind of hazards they may cause are beyond that produced by the chemicals or biomolecules with which they are functionalized.

The detection potency of nanoparticles is multidisciplinary, as the combination of their features permits the use of different techniques. SPIONs' and AuSPIONs' magnetic properties allow the detection of biomolecules by means of Magnetic Resonance Imagining, because they are contrast agents for image enhancement and the change in contrast (T_2) caused by biological reactions resulting in nanoparticles aggregation can be easily detected.[105e] AuSPIONs and AuNPs have a surface plasmon maximum at 520 nm that shifts to higher wavelengths when precipitation occurs, allowing the use of UV-

spectroscopy as a detection method. And finally, aggregation of the three types of nanoparticles can be detected by Dynamic Light Scattering, measuring the differences in diameter upon several changes caused by biological reactions. Due to all their features, nanoparticles can provide promising and multidisciplinar detection systems for biomedical applications.

References:

[1] J. D. Watson, F. H. Crick, *Nature* **1953**, *171*, 737-738.

[2] a) F. Sanger, G. M. Air, B. G. Barrell, N. L. Brown, A. R. Coulson, C. A. Fiddes, C. A. Hutchison, P. M. Slocombe, M. Smith, *Nature* **1977**, *265*, 687-695; b) K. B. Mullis, F. A. Faloona, *Methods Enzymol.* **1987**, *155*, 335-350; c) F. W. Studier, *Proc Natl Acad Sci U S A* **1989**, *86*, 6917-6921; d) A. Martin-Gallardo, W. R. McCombie, J. D. Gocayne, M. G. FitzGerald, S. Wallace, B. M. Lee, J. Lamerdin, S. Trapp, J. M. Kelley, L. I. Liu, et al., *Nat Genet* **1992**, *1*, 34-39; e) X. C. Huang, M. A. Quesada, R. A. Mathies, *Anal. Chem.* **1992**, *64*, 2149-2154.

[3] P. Shing Ho and Megan Carter (2011). DNA Structure: Alphabet Soup for the Cellular Soul, DNA Replication-Current Advances, Dr Herve Seligmann (Ed.), ISBN: 978-953-307-593-8, InTech, DOI: 10.5772/18536. Available from: http://www.intechopen.com/books/dna-replication-current-advances/dna-structure-alphabet-soup-for-the-cellular-soul

[4] A. Ghosh, M. Bansal, *Acta Crystallogr D Biol Crystallogr* **2003**, *59*, 620-626.

[5] H. S. Basu, B. G. Feuerstein, D. A. Zarling, R. H. Shafer, L. J. Marton, *J Biomol Struct Dyn* **1988**, *6*, 299-309.

[6] Saenger W. Principles of nucleic acids structure, Springer-Verlag, New York, 1984

[7] F. M. Pohl, T. M. Jovin, *J Mol Biol* **1972**, *67*, 375-396.

[8] M. de Rosa, D. de Sanctis, A. L. Rosario, M. Archer, A. Rich, A. Athanasiadis, M. A. Carrondo, *Proc Natl Acad Sci U S A* **2010**, *107*, 9088-9092.

[9] H. Zhang, H. Yu, J. Ren, X. Qu, *Biophys J* **2006**, *90*, 3203-3207.

[10] G. Felsenfeld, A. Rich, *Biochim Biophys Acta* **1957**, *26*, 457-468.

[11] M. D. Frank-Kamenetskii, S. M. Mirkin, *Annu Rev Biochem* **1995**, *64*, 65-95.

[12] J. Choi, T. Majima, *Chem Soc Rev* **2011**, *40*, 5893-5909.

[13] a) H. E. Moser, P. B. Dervan, *Science* **1987**, *238*, 645-650; b) M. Grigoriev, D. Praseuth, A. L. Guieysse, P. Robin, N. T. Thuong, C. Helene, A. Harel-Bellan, *Proc Natl Acad Sci U S A* **1993**, *90*, 3501-3505.

[14] a) K. Gehring, J. L. Leroy, M. Gueron, *Nature* **1993**, *363*, 561-565; b) H. A. Day, P. Pavlou, Z. A. Waller, *Bioorg Med Chem* **2014**, *22*, 4407-4418; c) S. A. Benabou, A.; Eritja, R.; González, C.; Gargallo, R., *RSC Advanced* **2012**.

[15] K. Guo, A. Pourpak, K. Beetz-Rogers, V. Gokhale, D. Sun, L. H. Hurley, *J Am Chem Soc* **2007**, *129*, 10220-10228.

[16] a) I. Smirnov, R. H. Shafer, *Biochemistry* **2000**, *39*, 1462-1468; b) B. I. Kankia, L. A. Marky, *J Am Chem Soc* **2001**, *123*, 10799-10804; c) N. V. Hud, F. W. Smith, F. A.

Anet, J. Feigon, *Biochemistry* **1996**, *35*, 15383-15390; d) S. Burge, G. N. Parkinson, P. Hazel, A. K. Todd, S. Neidle, *Nucleic Acids Res* **2006**, *34*, 5402-5415.

[17] S. W. Blume, V. Guarcello, W. Zacharias, D. M. Miller, *Nucleic Acids Res* **1997**, *25*, 617-625.

[18] S. Neidle, *Curr Opin Struct Biol* **2009**, *19*, 239-250.

[19] G. Song, J. Ren, *Chem Commun (Camb)* **2010**, *46*, 7283-7294.

[20] A. G. Petrovic, P. L. Polavarapu, *J Phys Chem B* **2008**, *112*, 2255-2260.

[21] C. S. Mekmaysy, L. Petraccone, N. C. Garbett, P. A. Ragazzon, R. Gray, J. O. Trent, J. B. Chaires, *J Am Chem Soc* **2008**, *130*, 6710-6711.

[22] M. Trajkovski, P. Sket, J. Plavec, *Org Biomol Chem* **2009**, *7*, 4677-4684.

[23] a) L. Oganesian, T. M. Bryan, *Bioessays* **2007**, *29*, 155-165; b) M. L. Duquette, P. Handa, J. A. Vincent, A. F. Taylor, N. Maizels, *Genes Dev* **2004**, *18*, 1618-1629.

[24] J. R. Williamson, M. K. Raghuraman, T. R. Cech, *Cell* **1989**, *59*, 871-880.

[25] S. Rankin, A. P. Reszka, J. Huppert, M. Zloh, G. N. Parkinson, A. K. Todd, S. Ladame, S. Balasubramanian, S. Neidle, *J Am Chem Soc* **2005**, *127*, 10584-10589.

[26] J. R. Wyatt, T. A. Vickers, J. L. Roberson, R. W. Buckheit, Jr., T. Klimkait, E. DeBaets, P. W. Davis, B. Rayner, J. L. Imbach, D. J. Ecker, *Proc Natl Acad Sci U S A* **1994**, *91*, 1356-1360.

[27] A. Avino, C. Fabrega, M. Tintore, R. Eritja, *Curr Pharm Des* **2012**, *18*, 2036-2047.

[28] a) L. C. Bock, L. C. Griffin, J. A. Latham, E. H. Vermaas, J. J. Toole, *Nature* **1992**, *355*, 564-566; b) D. M. Tasset, M. F. Kubik, W. Steiner, *J Mol Biol* **1997**, *272*, 688-698.

[29] T. Lindahl, *Nature* **1993**, *362*, 709-715.

[30] B. A. Lodish H, Matsudaira P, Kaiser CA, Krieger M, Scott MP, Zipursky SL, Darnell J. *Molecular Biology of the Cell*, New York, NY., **2004**.

[31] a) R. De Bont, N. van Larebeke, *Mutagenesis* **2004**, *19*, 169-185; b) S. Burney, J. L. Caulfield, J. C. Niles, J. S. Wishnok, S. R. Tannenbaum, *Mutat Res* **1999**, *424*, 37-49.

[32] a) S. E. Mancebo, S. Q. Wang, *Rev Environ Health* **2014**, *29*, 265-273; b) A. Kammeyer, R. M. Luiten, *Ageing Res Rev* **2015**, *21*, 16-29.

[33] a) D. J. Shah, R. K. Sachs, D. J. Wilson, *Br J Radiol* **2012**, *85*, e1166-1173; b) A. I. Gaziev, *Radiats Biol Radioecol* **2013**, *53*, 117-136.

[34] D. O. Carpenter, S. Bushkin-Bedient, *J Adolesc Health* **2013**, *52*, S21-29.

[35] a) M. D. Faddeeva, T. N. Beliaeva, *Tsitologiia* **1991**, *33*, 3-31; b) L. B. Hendry, V. B. Mahesh, E. D. Bransome, Jr., D. E. Ewing, *Mutat Res* **2007**, *623*, 53-71.

[36] Y. Chen, V. Williams, M. Filippova, V. Filippov, P. Duerksen-Hughes, *Cancers (Basel)* **2014**, *6*, 2155-2186.

[37] a) G. R. Stuart, Y. Oda, J. G. de Boer, B. W. Glickman, *Genetics* **2000**, *154*, 1291-1300; b) B. A. Kunz, K. Ramachandran, E. J. Vonarx, *Genetics* **1998**, *148*, 1491-1505.

[38] C. Nathan, A. Cunningham-Bussel, *Nat Rev Immunol* **2013**, *13*, 349-361.

[39] K. S. Gates, *Chem Res Toxicol* **2009**, *22*, 1747-1760.

[40] P. Fortini, B. Pascucci, E. Parlanti, M. D'Errico, V. Simonelli, E. Dogliotti, *Mutat Res* **2003**, *531*, 127-139.

[41] F. Drablos, E. Feyzi, P. A. Aas, C. B. Vaagbo, B. Kavli, M. S. Bratlie, J. Pena-Diaz, M. Otterlei, G. Slupphaug, H. E. Krokan, *DNA Repair (Amst)* **2004**, *3*, 1389-1407.

[42] R. Saffhill, G. P. Margison, P. J. O'Connor, *Biochim Biophys Acta* **1985**, *823*, 111-145.

[43] D. E. Shuker, E. Bailey, A. Parry, J. Lamb, P. B. Farmer, *Carcinogenesis* **1987**, *8*, 959-962.

[44] B. Singer, *Cancer Res* **1986**, *46*, 4879-4885.

[45] a) R. Shapiro, M. Danzig, *Biochemistry* **1972**, *11*, 23-29; b) R. Shapiro, R. S. Klein, *Biochemistry* **1966**, *5*, 2358-2362; c) L. A. Frederico, T. A. Kunkel, B. R. Shaw, *Biochemistry* **1990**, *29*, 2532-2537; d) T. Lindahl, B. Nyberg, *Biochemistry* **1974**, *13*, 3405-3410; e) P. Karran, T. Lindahl, *Biochemistry* **1980**, *19*, 6005-6011.

[46] a) P. Auerbach, R. A. Bennett, E. A. Bailey, H. E. Krokan, B. Demple, *Proc Natl Acad Sci U S A* **2005**, *102*, 17711-17716; b) S. Boiteux, M. Guillet, *DNA Repair (Amst)* **2004**, *3*, 1-12.

[47] A. B. Robertson, A. Klungland, T. Rognes, I. Leiros, *Cell Mol Life Sci* **2009**, *66*, 981-993.

[48] a) P. A. Muniandy, J. Liu, A. Majumdar, S. T. Liu, M. M. Seidman, *Crit Rev Biochem Mol Biol* **2010**, *45*, 23-49; b) N. R. Jena, *J Biosci* **2012**, *37*, 503-517; c) D. M. Noll, T. M. Mason, P. S. Miller, *Chem Rev* **2006**, *106*, 277-301; d) Y. Huang, L. Li, *Transl Cancer Res* **2013**, *2*, 144-154; e) B. Said, M. K. Ross, T. Salib, R. C. Shank, *Carcinogenesis* **1995**, *16*, 3057-3062.

[49] a) H. Fung, B. Demple, *Mol Cell* **2005**, *17*, 463-470; b) L. A. Loeb, B. D. Preston, *Annu Rev Genet* **1986**, *20*, 201-230.

[50] B. Demple, *Curr Biol* **1995**, *5*, 719-721.

[51] J. Smith, L. M. Tho, N. Xu, D. A. Gillespie, *Adv Cancer Res* **2010**, *108*, 73-112.

[52] http://jonlieffmd.com/blog/the-many-ways-neurons-repair-their-own-dna.

[53] S. S. Wallace, *DNA Repair (Amst)* **2014**, *19*, 14-26.

[54] a) L. Harrison, A. G. Ascione, D. M. Wilson, 3rd, B. Demple, *J Biol Chem* **1995**, *270*, 5556-5564; b) L. Hughesdavies, T. Galanopoulos, L. Harrison, M. Maxwell, H. Antoniades, B. Demple, *Int J Oncol* **1995**, *6*, 749-752; c) D. M. Wilson, 3rd, R. A. Bennett, J. C. Marquis, P. Ansari, B. Demple, *Nucleic Acids Res* **1995**, *23*, 5027-5033;

d) D. M. Wilson, 3rd, M. Takeshita, A. P. Grollman, B. Demple, *J Biol Chem* **1995**, *270*, 16002-16007.

[55] A. R. Evans, M. Limp-Foster, M. R. Kelley, *Mutat Res* **2000**, *461*, 83-108.

[56] a) B. Demple, T. Herman, D. S. Chen, *Proc Natl Acad Sci U S A* **1991**, *88*, 11450-11454; b) D. S. Chen, T. Herman, B. Demple, *Nucleic Acids Res* **1991**, *19*, 5907-5914; c) J. H. Hoeijmakers, *Nature* **2001**, *411*, 366-374.

[57] D. S. Daniels, T. T. Woo, K. X. Luu, D. M. Noll, N. D. Clarke, A. E. Pegg, J. A. Tainer, *Nat Struct Mol Biol* **2004**, *11*, 714-720.

[58] K. S. Srivenugopal, X. H. Yuan, H. S. Friedman, F. Ali-Osman, *Biochemistry* **1996**, *35*, 1328-1334.

[59] M. R. Middleton, G. P. Margison, *Lancet Oncol* **2003**, *4*, 37-44.

[60] D. B. Longley, P. G. Johnston, *J Pathol* **2005**, *205*, 275-292.

[61] J. P. Belzile, S. A. Choudhury, D. Cournoyer, T. Y. Chow, *Curr Gene Ther* **2006**, *6*, 111-123.

[62] A. M. Reed, M. L. Fishel, M. R. Kelley, *Future Oncol* **2009**, *5*, 713-726.

[63] a) M. L. Fishel, Y. He, M. L. Smith, M. R. Kelley, *Clin Cancer Res* **2007**, *13*, 260-267; b) M. L. Fishel, M. R. Kelley, *Mol Aspects Med* **2007**, *28*, 375-395.

[64] M. Luo, M. R. Kelley, *Anticancer Res* **2004**, *24*, 2127-2134.

[65] P. Taverna, L. Liu, H. S. Hwang, A. J. Hanson, T. J. Kinsella, S. L. Gerson, *Mutat Res* **2001**, *485*, 269-281.

[66] S. Madhusudan, F. Smart, P. Shrimpton, J. L. Parsons, L. Gardiner, S. Houlbrook, D. C. Talbot, T. Hammonds, P. A. Freemont, M. J. Sternberg, G. L. Dianov, I. D. Hickson, *Nucleic Acids Res* **2005**, *33*, 4711-4724.

[67] a) A. Sabharwal, M. R. Middleton, *Curr Opin Pharmacol* **2006**, *6*, 355-363; b) A. E. Pegg, *Cancer Invest* **1984**, *2*, 223-231; c) M. Belanich, M. Pastor, T. Randall, D. Guerra, J. Kibitel, L. Alas, B. Li, M. Citron, P. Wasserman, A. White, H. Eyre, K. Jaeckle, S. Schulman, D. Rector, M. Prados, S. Coons, W. Shapiro, D. Yarosh, *Cancer Res* **1996**, *56*, 783-788; d) R. S. Foote, S. Mitra, B. C. Pal, *Biochem Biophys Res Commun* **1980**, *97*, 654-659; e) A. E. Pegg, *Cancer Res* **1990**, *50*, 6119-6129.

[68] W. P. Tong, M. C. Kirk, D. B. Ludlum, *Cancer Res* **1982**, *42*, 3102-3105.

[69] L. Yan, J. R. Donze, L. Liu, *Oncogene* **2005**, *24*, 2175-2183.

[70] a) T. P. Brent, P. J. Houghton, J. A. Houghton, *Proc Natl Acad Sci U S A* **1985**, *82*, 2985-2989; b) G. Tagliabue, L. Citti, G. Massazza, G. Damia, R. Giavazzi, M. D'Incalci, *Anticancer Res* **1992**, *12*, 2123-2125; c) R. Pepponi, G. Marra, M. P. Fuggetta, S. Falcinelli, E. Pagani, E. Bonmassar, J. Jiricny, S. D'Atri, *J Pharmacol Exp Ther* **2003**, *304*, 661-668.

[71] a) S. L. Gerson, *J Clin Oncol* **2002**, *20*, 2388-2399; b) G. P. Margison, A. C. Povey, B. Kaina, M. F. Santibanez Koref, *Carcinogenesis* **2003**, *24*, 625-635; c) S. L. Gerson, *Nat Rev Cancer* **2004**, *4*, 296-307.

[72] a) M. E. Hegi, A. C. Diserens, T. Gorlia, M. F. Hamou, N. de Tribolet, M. Weller, J. M. Kros, J. A. Hainfellner, W. Mason, L. Mariani, J. E. Bromberg, P. Hau, R. O. Mirimanoff, J. G. Cairncross, R. C. Janzer, R. Stupp, *N Engl J Med* **2005**, *352*, 997-1003; b) M. Esteller, J. Garcia-Foncillas, E. Andion, S. N. Goodman, O. F. Hidalgo, V. Vanaclocha, S. B. Baylin, J. G. Herman, *N Engl J Med* **2000**, *343*, 1350-1354.

[73] a) A. E. Pegg, K. Swenn, M. Y. Chae, M. E. Dolan, R. C. Moschel, *Biochem Pharmacol* **1995**, *50*, 1141-1148; b) E. Alvino, R. Pepponi, E. Pagani, P. M. Lacal, C. Nunziata, E. Bonmassar, S. D'Atri, *J Pharmacol Exp Ther* **1999**, *291*, 1292-1300.

[74] A. E. Pegg, *Chem Res Toxicol* **2011**, *24*, 618-639.

[75] B. Kaina, G. P. Margison, M. Christmann, *Cell Mol Life Sci* **2010**, *67*, 3663-3681.

[76] A. E. Pegg, S. Kanugula, S. Edara, G. T. Pauly, R. C. Moschel, K. Goodtzova, *J Biol Chem* **1998**, *273*, 10863-10867.

[77] O. Khan, M. R. Middleton, *Expert Opin Investig Drugs* **2007**, *16*, 1573-1584.

[78] N. C. Seeman, *J Theor Biol* **1982**, *99*, 237-247.

[79] P. W. Rothemund, N. Papadakis, E. Winfree, *PLoS Biol* **2004**, *2*, e424.

[80] J. Fu, M. Liu, Y. Liu, H. Yan, *Acc. Chem. Res.* **2012**, *45*, 1215-1226.

[81] E. Winfree, F. Liu, L. A. Wenzler, N. C. Seeman, *Nature* **1998**, *394*, 539-544.

[82] J. H. Chen, N. C. Seeman, *Nature* **1991**, *350*, 631-633.

[83] a) W. M. Shih, J. D. Quispe, G. F. Joyce, *Nature* **2004**, *427*, 618-621; b) Y. S. Zhang, N.C., *J. Am. Chem. Soc* **1994**, *116*, 1661; c) R. P. Goodman, I. A. Schaap, C. F. Tardin, C. M. Erben, R. M. Berry, C. F. Schmidt, A. J. Turberfield, *Science* **2005**, *310*, 1661-1665; d) Y. He, T. Ye, M. Su, C. Zhang, A. E. Ribbe, W. Jiang, C. Mao, *Nature* **2008**, *452*, 198-201.

[84] M. Tintore, R. Eritja, C. Fabrega, *Chembiochem* **2014**, *15*, 1374-1390.

[85] P. W. Rothemund, *Nature* **2006**, *440*, 297-302.

[86] a) R. Chhabra, J. Sharma, Y. Ke, Y. Liu, S. Rinker, S. Lindsay, H. Yan, *J Am Chem Soc* **2007**, *129*, 10304-10305; b) H. T. Maune, S. P. Han, R. D. Barish, M. Bockrath, W. A. Iii, P. W. Rothemund, E. Winfree, *Nat Nanotechnol* **2010**, *5*, 61-66; c) S. Pal, Z. Deng, B. Ding, H. Yan, Y. Liu, *Angew Chem Int Ed Engl* **2010**, *49*, 2700-2704; d) B. Sacca, R. Meyer, M. Erkelenz, K. Kiko, A. Arndt, H. Schroeder, K. S. Rabe, C. M. Niemeyer, *Angew Chem Int Ed Engl* **2010**, *49*, 9378-9383.

[87] a) H. Gu, J. Chao, S. J. Xiao, N. C. Seeman, *Nature* **2010**, *465*, 202-205; b) S. F. Wickham, J. Bath, Y. Katsuda, M. Endo, K. Hidaka, H. Sugiyama, A. J. Turberfield, *Nat*

Nanotechnol **2012**, *7*, 169-173; c) N. V. Voigt, T. Torring, A. Rotaru, M. F. Jacobsen, J. B. Ravnsbaek, R. Subramani, W. Mamdouh, J. Kjems, A. Mokhir, F. Besenbacher, K. V. Gothelf, *Nat Nanotechnol* **2010**, *5*, 200-203.

[88] A. V. Pinheiro, D. Han, W. M. Shih, H. Yan, *Nat Nanotechnol* **2011**, *6*, 763-772.

[89] Y. Ke, S. Lindsay, Y. Chang, Y. Liu, H. Yan, *Science* **2008**, *319*, 180-183.

[90] H. K. Subramanian, B. Chakraborty, R. Sha, N. C. Seeman, *Nano Lett* **2011**, *11*, 910-913.

[91] M. Endo, Y. Katsuda, K. Hidaka, H. Sugiyama, *Angew Chem Int Ed Engl* **2010**, *49*, 9412-9416.

[92] M. Endo, Y. Katsuda, K. Hidaka, H. Sugiyama, *Angew. Chem. Int. Ed. Engl.* **2010**, *49*, 9412-9416.

[93] S. M. Douglas, I. Bachelet, G. M. Church, *Science* **2012**, *335*, 831-834.

[94] M. Langecker, V. Arnaut, T. G. Martin, J. List, S. Renner, M. Mayer, H. Dietz, F. C. Simmel, *Science* **2012**, *338*, 932-936.

[95] a) R. Subbiah, M. Veerapandian, K. S. Yun, *Curr Med Chem* **2010**, *17*, 4559-4577; b) S. Hassan, A. V. Singh, *J Nanosci Nanotechnol* **2014**, *14*, 402-414; c) A. E. Nel, L. Madler, D. Velegol, T. Xia, E. M. Hoek, P. Somasundaran, F. Klaessig, V. Castranova, M. Thompson, *Nat Mater* **2009**, *8*, 543-557.

[96] a) S. K. Ghosh, T. Pal, *Chem Rev* **2007**, *107*, 4797-4862; b) M. C. Daniel, D. Astruc, *Chem Rev* **2004**, *104*, 293-346; c) R. Baron, B. Willner, I. Willner, *Chem Commun (Camb)* **2007**, 323-332; d) E. Katz, I. Willner, *Angew Chem Int Ed Engl* **2004**, *43*, 6042-6108; e) N. L. Rosi, C. A. Mirkin, *Chem Rev* **2005**, *105*, 1547-1562; f) J. J. Storhoff, C. A. Mirkin, *Chem Rev* **1999**, *99*, 1849-1862; g) W. Zhao, M. A. Brook, Y. Li, *ChemBioChem* **2008**, *9*, 2363-2371.

[97] S. Link, M. A. El-Sayed, *Annu Rev Phys Chem* **2003**, *54*, 331-366.

[98] S. Zeng, D. Baillargeat, H. P. Ho, K. T. Yong, *Chem Soc Rev* **2014**, *43*, 3426-3452.

[99] a) J. H. Teichroeb, J. A. Forrest, V. Ngai, L. W. Jones, *Eur Phys J E Soft Matter* **2006**, *21*, 19-24; b) M. Stobiecka, *Biosens Bioelectron* **2014**, *55*, 379-385; c) C. Ge, L. Yu, Z. Fang, L. Zeng, *Anal Chem* **2013**, *85*, 9343-9349; d) H. Dong, Z. Zhu, H. Ju, F. Yan, *Biosens Bioelectron* **2012**, *33*, 228-232; e) C. T. Ng, S. T. Dheen, W. C. Yip, C. N. Ong, B. H. Bay, L. Y. Lanry Yung, *Biomaterials* **2011**, *32*, 7609-7615; f) M. Y. Sha, H. Xu, S. G. Penn, R. Cromer, *Nanomedicine (Lond)* **2007**, *2*, 725-734; g) K. Kneipp, H. Kneipp, J. Kneipp, *Acc Chem Res* **2006**, *39*, 443-450; h) S. Hwang, J. Nam, S. Jung, J. Song, H. Doh, S. Kim, *Nanomedicine (Lond)* **2014**, *9*, 2003-2022; i) W. Zhao, W. Chiuman, M. A. Brook, Y. Li, *Chembiochem* **2007**, *8*, 727-731.

[100] R. Elghanian, J. J. Storhoff, R. C. Mucic, R. L. Letsinger, C. A. Mirkin, *Science* **1997**, *277*, 1078-1081.

[101] http://bionems.cloud.ntu.edu.tw/research1.php

[102] R. Weissleder, *Science* **2006**, *312*, 1168-1171.

[103] http://bme240.eng.uci.edu/students/08s/ykim30/03.htm

[104] a) Y. X. Wang, S. M. Hussain, G. P. Krestin, *Eur Radiol* **2001**, *11*, 2319-2331; b) R. Weissleder, G. Elizondo, J. Wittenberg, C. A. Rabito, H. H. Bengele, L. Josephson, *Radiology* **1990**, *175*, 489-493.

[105] a) A. Z. Wang, V. Bagalkot, C. C. Vasilliou, F. Gu, F. Alexis, L. Zhang, M. Shaikh, K. Yuet, M. J. Cima, R. Langer, P. W. Kantoff, N. H. Bander, S. Jon, O. C. Farokhzad, *ChemMedChem* **2008**, *3*, 1311-1315; b) G. K. Kouassi, J. Irudayaraj, *J Nanobiotechnology* **2006**, *4*, 8; c) G. K. Kouassi, J. Irudayaraj, *Anal Chem* **2006**, *78*, 3234-3241; d) R. Hao, R. Xing, Z. Xu, Y. Hou, S. Gao, S. Sun, *Adv Mater* **2010**, *22*, 2729-2742; e) M. V. Yigit, D. Mazumdar, Y. Lu, *Bioconjug Chem* **2008**, *19*, 412-417.

[106] W. Wu, Q. He, C. Jiang, *Nanoscale Res Lett* **2008**, *3*, 397-415.

[107] L. Y. Zhou, J.; Wei, J., *J. Mater. Chem.* **2011**, *21*, 2823-2840.

[108] a) I. Robinson, D. Tung le, S. Maenosono, C. Walti, N. T. Thanh, *Nanoscale* **2010**, *2*, 2624-2630; b) L. Wang, J. Luo, Q. Fan, M. Suzuki, I. S. Suzuki, M. H. Engelhard, Y. Lin, N. Kim, J. Q. Wang, C. J. Zhong, *J Phys Chem B* **2005**, *109*, 21593-21601.

[109] W. H. De Jong, P. J. Borm, *Int J Nanomedicine* **2008**, *3*, 133-149.

Objectives

OBJECTIVES:

The long term objective of this thesis is the search for inhibitors of hAGT repair activity to be used as adjuvants in chemotherapy treatment. In order to achieve this goal, in this thesis we have evaluated potential inhibitors of hAGT and we have developed several analytical methods to find a robust technique for the *in vitro* evaluation of hAGT activity that will help us to characterize hAGT inhibitors. The specific objectives of this thesis are:

A. Primary screening of the compounds with potential capacity to inhibit hAGT.
   1. Evaluation of the complex formed by hAGT and its potential inhibitors by ESI-MS.
   2. Evaluation of the toxicity and efficacy of the candidate compounds in cell culture.

B. Development of methods for the detection of hAGT repair activity *in vitro*:
   1. Methods based on the conformational change of a G-quadruplex:
      1.1. Fluorescence assay based on the conformational change of a G-quadruplex oligonucleotide.
      1.2. Design of a supramolecular platform that allows the detection of hAGT activity through the direct monitoring of the conformational change of a pair of G-quadruplexes using Atomic Force Microscopy.
   2. New method to detect hAGT activity by transfer of fluorescence from the substrate oligonucleotide to the active site of the protein.

C. Comparative study of the properties of different type of nanoparticles to detect a single methylation that implies a conformational change in a G-quadruplex, to set the bases for a new detection platform for hAGT activity over a nanoparticle system.

Chapter 1

Potential inhibitors of hAGT's DNA repair activity: study of the hAGT-compound complex formation by ESI-MS and toxicity in cell culture.

In this first chapter, we evaluate the potency of small molecules which can be inhibitors of the DNA repair activity of the protein hAGT. A virtual screening was realized in collaboration with the Bioinformatics Unit of the CMBSO. A library of 4 million compounds was screened for shape complementarity to the active site of the protein, assuming that the best candidates could be good hits for hAGT inhibition due to their ability to enter the active site and occupy the space where the alkylated guanine of the DNA needs to enter in order to be repaired, as well as for their interaction with the amino acids implied in the repair. A set of 15 compounds with potential inhibitory activity against hAGT was selected. From these 15 compounds, only 10 were commercially available. These 10 compounds were studied by ESI-MS to pre-establish their ability to form a complex with hAGT *in vitro*, and subsequently, their toxicity was assessed in cell culture by MTT and colony formation assays.

In this chapter, we include as an annex a work we realized related to the search of inhibitors for another DNA repair protein, Ape1, involved in the base excision repair pathway. This paper reports the identification of new compounds as potential Ape1 inhibitors selected by a docking-based virtual screening and characterized following similar techniques as the ones described in chapter 1 for hAGT.

Potential inhibitors of hAGT's DNA repair activity: study of the hAGT-compound complex formation by ESI-MS and its toxicity in cell culture.

Table of contents:

1. Introduction: inhibition of hAGT.

The human O^6-alkylguanine-DNA-alkyltransferase (hAGT)[1] is a DNA repair protein that removes alkyl mutations from the O^6 position of guanines, restoring the DNA which has been damaged by alkylating agents. This group of chemotherapeutic anticancer drugs, alkylating agents, produce their cytotoxic effects by introducing alkyl groups which generate adducts and crosslinks at multiple sites in DNA.[2] For this reason, hAGT represents a relevant pharmacological target in the fight against chemotherapy resistance and patients' survival.[3] Chemotherapy based on alkylating agents, together with the inhibition of hAGT, may result in a higher efficiency of the treatment, due to the blocking in the repair of the alkylated-DNA by hAGT that leads to apoptosis of cancer cells.[3]

hAGT is a suicidal enzyme which repairs alkyl damage from the O^6 position of guanines, and in minor rate, from the O^4 position of thymidines. It has 207 amino acids, a molecular weight of 21645.9 Da and a theoretical isoelectric point of 8.28. Its crystallographic structure was solved by Daniels and coworkers in 2000.[1b] hAGT is a monomer and has 2 domains, the N- and the C-terminal, where the active site cysteine is found (Figure 1).

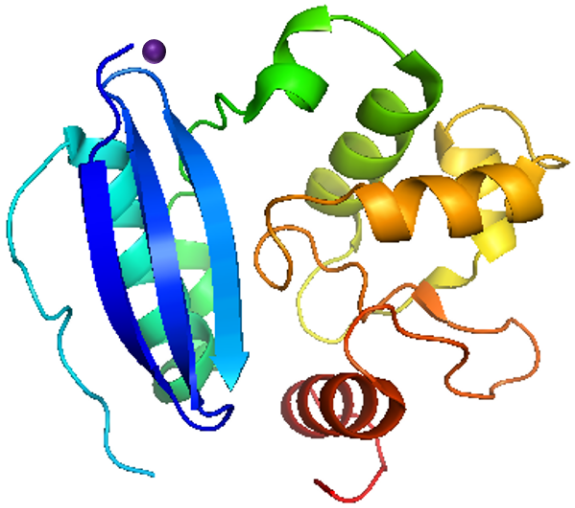

Figure 1. hAGT structure, described by Daniels *et. al.* The two domains are clearly seen. The violet sphere corresponds to a zinc atom present in the N-terminal domain. PBD code 1EH8.

Later on, the same group solved the structure of hAGT together with DNA, enlightening the mechanism of action and the amino acids involved in the repair reaction.[1c] Arginine 128 plays an important role in the dealkylation process, entering the DNA double strand and pulling out the damaged guanine. In this way, the damaged guanine can accommodate in the active site close to cysteine 145 to be repaired (figure 2).

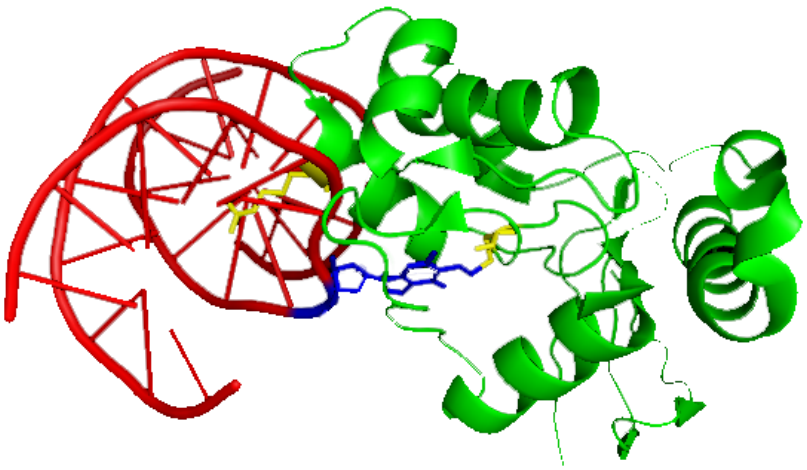

Figure 2. hAGT (green) bound to DNA (red), with Arginine 128 (yellow, left) entering the double helix and pushing outside the alkylated guanine (blue), which interacts with the active site, Cysteine 145 (yellow, right). PDB code 1T39.

The first objective of this thesis is to evaluate the potency of small molecules which can be inhibitors of the repair activity of hAGT. Previously, a virtual screening was realized in collaboration with the Bioinformatics Unit of the CMBSO. A library of 4 million compounds was screened for shape complementarity to the active site of the protein, assuming that the best candidates could be good hits for hAGT inhibition due to their ability to enter the active site and occupy the space where the alkylated guanine of the DNA needs to enter in order to be repaired, as well as for their interaction with the amino acids implied in the repair. A set of 15 compounds with the best free energy of binding with hAGT was selected. We did an exhaustive search for companies that chemically synthesize and sell these compounds and finally, from these 15 compounds, only 10 were commercially available. Table 1 shows the chemical structure and properties of these 10 compounds, which were numbered from 1 to 10.

Compound	Chemical structure	xlogP	HBD	HBA	Charge	Molecular Weight
1	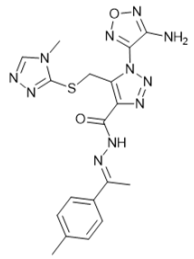	1.78	3	13	0	453.492
2	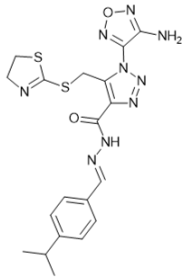	3.68	3	11	0	471.572
3	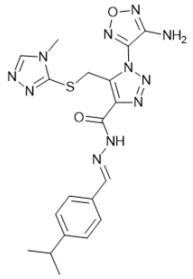	2.93	3	13	0	467.519
4	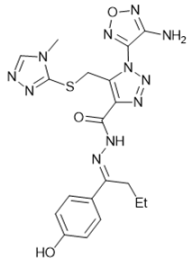	1.91	4	14	0	483.518
5	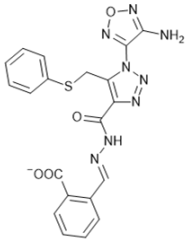	2.93	3	12	-1	463.459

Compound	Chemical structure	xlogP	HBD*	HBA**	Charge	Molecular Weight
6	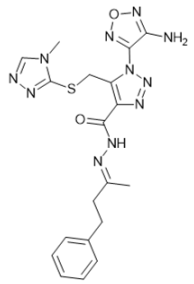	2.05	3	13	0	467.519
7	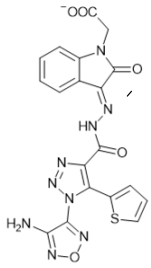	1.15	3	14	-1	478.430
8	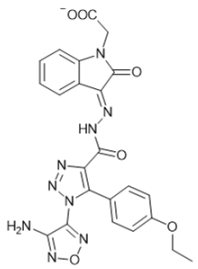	1.79	3	15	-1	516.454
9	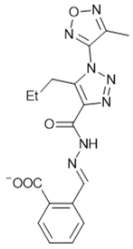	1.96	3	12	-1	383.348
10	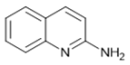	1.90	1	2	0	148.205

Table 1. Chemical structure and properties of the compounds tested in this thesis as potential hits of hAGT activity, found by a virtual screening. *HBD: hydrogen bond donors. **HBA: hydrogen bond acceptors.

In order to confirm the results obtained by the virtual screening about the possible interaction of this set of compounds with hAGT, we undertook a first evaluation of their ability to form a complex with the protein by mass spectrometry, and their toxicity and effectiveness as potential inhibitors was tested in cell culture assays.

2. hAGT: structure, overexpression and purification

Recombinant hAGT full length (FL) (Scheme 1A) was used for the MS study of the complex formation with the potential inhibitors, but here we also describe in full detail the overexpression and purification of a mutant version of hAGT which will be used in the following chapters of this thesis. This inactive mutant of hAGT (hAGT C145S) had a shorter sequence, where 30 amino acids were removed from its C-terminal end without affecting its folding, as represented in scheme 1B. Its active site cysteine was replaced by a serine, causing the loss of its repair activity but maintaining its capacity to recognize and bind alkylguanine-DNA.[4] This hAGT mutant was designed in order to use it as a negative control for the different *in vitro* assays.

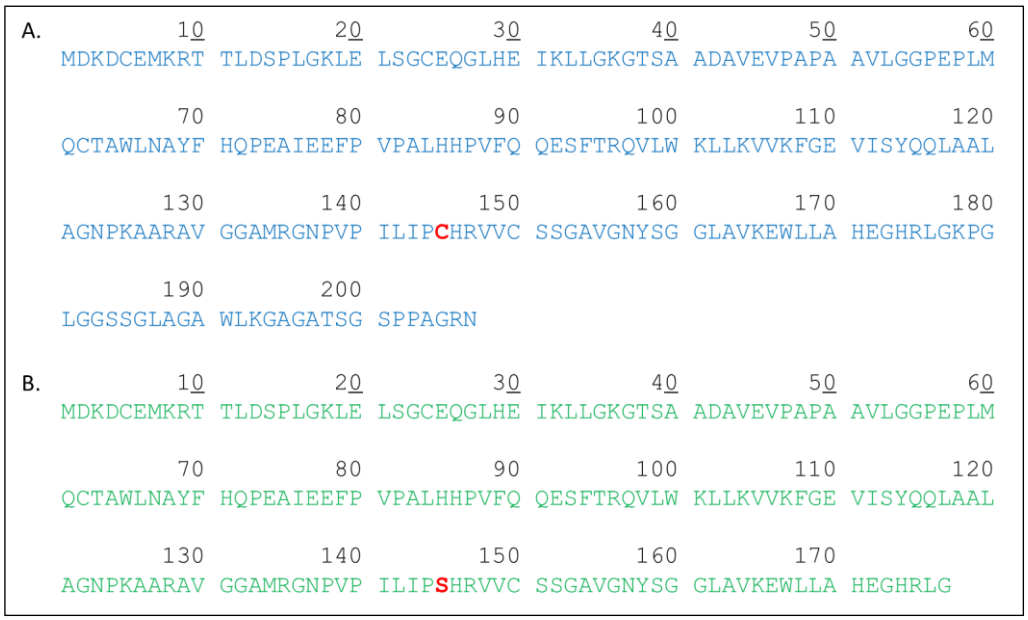

Scheme 1. Amino acid sequence of the hAGT proteins. **1A.** hAGT FL with the active site, cysteine 145, in red. **1B.** hAGT ΔC177 C145S, the shorter version of hAGT FL with a mutation at the active site (serine 145) in red.

The two types of hAGT were overexpressed and purified following the protocol described by Ruiz *et al.*[5] This protocol implied the introduction of a hystidine tag with affinity for nickel at the N terminal end of the sequence of the protein, to enable its purification by a nickel HiTrap chelating column figure 3A. After that, the resulting sample was loaded into a Size exclusion column to further purify the protein and to exchange the buffer used in the chelating column to a more convenient buffer for storing the protein (figure 3B). hAGT FL was obtained in high yield and purity, as shown by polyacrylamide gel electrophoresis (PAGE) which was performed to follow all the purification process (figure 3C).

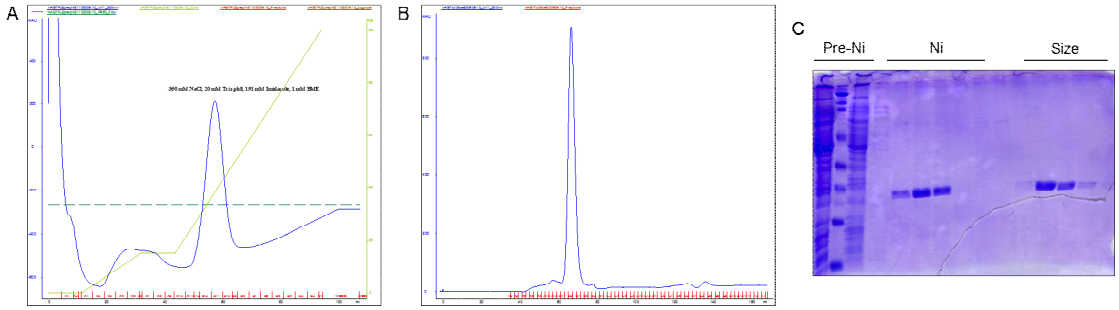

Figure 3. Purification of hAGT full length with Hys-tag. **3A.** Chromatogram of the nickel HiTrap-column purification. **3B.** Chromatogram of the size exclusion column, where a single pure peak can be observed. **3C.** PAGE of the purification process.

In the case of the hAGT C145S, a dyalisis at 4ºC with prescission protease (PrePro) was carried out after the nickel HiTrap column. PrePro is a protease which cuts a specific sequence introduced between the hystidine tag and the N-terminal of hAGT, removing the Hys tag. Finally, a Size exclusion column was used to further purify the protein and to slowly exchange the buffer to the storing buffer.

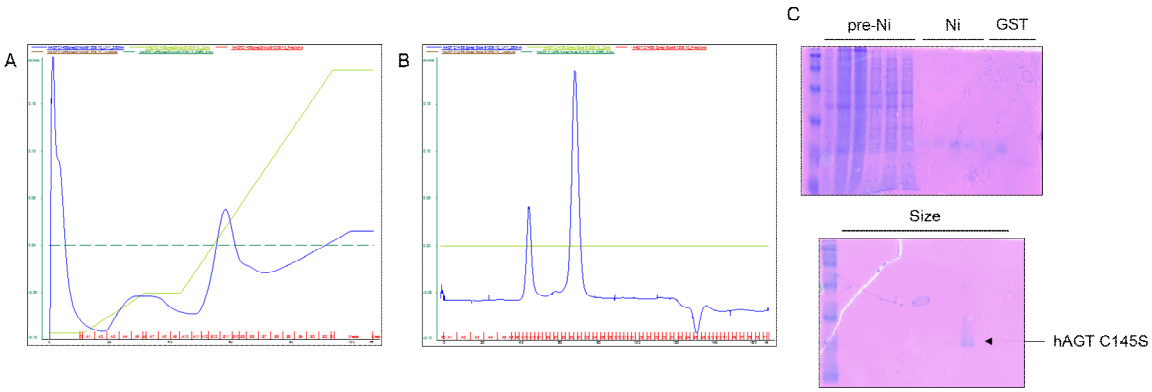

Figure 4. Purification of hAGT C145S with Hys-tag. **4A.** Nickel HiTrap purification chromatogram. **4B.** Size exclusion purification chromatogram. In this case, two peaks are observed: the first and smaller one corresponds to a portion of hAGT which is aggregated and the second one corresponds to the well folded hAGT C145S. **4C.** PAGE of the purification process. The top gel shows the sample preparation prior to the nickel column, the nickel column and the GST column. The bottom gel corresponds to the analysis of the fractions collected from the size exclusion column, showing the pure hAGT C145S.

Both proteins were concentrated in storing buffer and stored in 40% glycerol at -20ºC until further use. All buffers and conditions are detailed in the experimental section of this chapter.

3. Mass Spectrometry analysis of the non-covalent complex between hAGT and the lead compounds.

In order to study the ability of the preselected compounds to form a complex with hAGT and pre-establish that they are molecules with potential capacity to inhibit hAGT, we performed a Mass Spectrometry analysis of their interaction. Mass spectrometry experiments were done using electrospray ionisation, a travelling wave ion mobility cell and a time-of-flight mass analyzer.

This technique allows the detection of an increase in the mass of hAGT when the compound shows a strong interaction with the protein, which may indicate that the active site of hAGT is occupied with the compound. It does not permit to calculate a constant of dissociation nor an inhibitory activity, but is useful to predetermine the disposition of these molecules to be better or worse candidates for hAGT inhibition, based on their chemical structures. The modification of the mass spectra indicates a complexation between hAGT and the studied compounds, but not the nature of this interaction nor the degree of interaction. The presence of several new peaks with a delay corresponding to the addition of the m/z of the compound may indicate that the complex is not specific and more than one molecule can enter the active site of hAGT or interact with its surface instead of entering the active site.

The hAGT buffer was exchanged to 100 mM ammonium acetate pH=7 using BioSpin columns P-6, to prevent buffer interferences in the mass spectrometry experiments. All the compounds are only soluble in DMSO at high concentrations. For this reason, we first realized the mass analysis of hAGT in the presence or absence of DMSO, in order to see how DMSO affects the Mass Spectrometry analysis (figure 5). We observed that a volume of DMSO higher than 1.5% v/v caused the loss of hAGT spectrum and thus determined the maximum concentration of inhibitor which can be used in these experiments, being it 150 µM. This concentration is optimal for our experiments, because it is within a ratio of 1:5 of protein/inhibitor, given that the ideal concentration of hAGT to perform mass experiments was found to be around 30 µM. For inhibitors which require higher concentrations to be active, this technique cannot be used if they are not soluble in aqueous buffer.

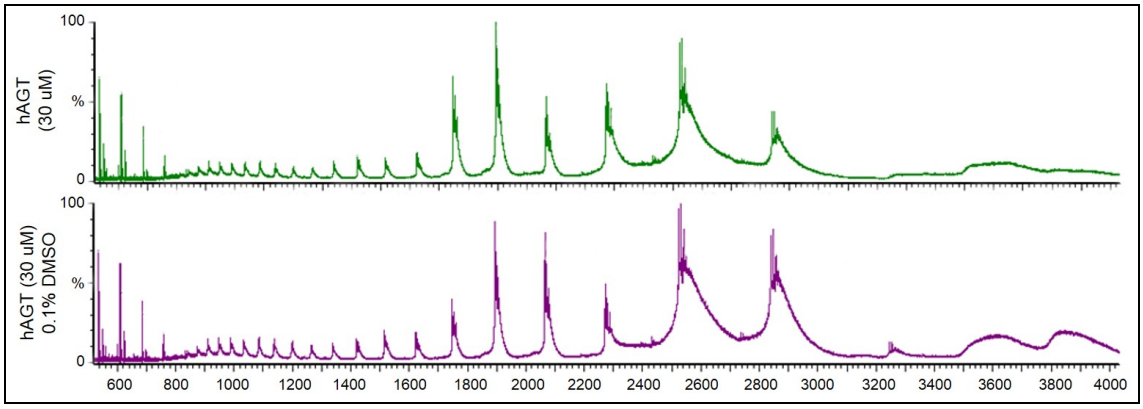

Figure 5. Mass spectra of hAGT 30 μM in absence (green) or presence of DMSO 1.5% v/v (violet).

The mass analysis of hAGT also allowed us also to select the m/z area were the complex formation was observed with clarity, which is from 1800 to 3000. Then, hAGT was mixed with each inhibitor in DMSO on a 1:5 ratio. Figure 6 shows all the results of the mass analysis. Five main peaks of m/z can be observed at 1749.69, 1893.29, 2065.33, 2271.60 and 2530.79. Changes in the chromatogram of hAGT, as the appearance or displacement of the peaks a number of units corresponding to the m/z of the inhibitors, represent an interaction.

Our results show that in the case of compounds 1, 2 and 3, no changes in the chromatogram were observed compared with native hAGT, meaning that these compounds are not able to form a complex with hAGT in these conditions. Compound 4 does not seem to interact with the active site of hAGT, neither, however in this case a variation in the peaks' form is seen in comparison with native hAGT. This replacement of the peaks by a softened curve indicates denaturation of the protein, and we can presume that compound 4 is interacting in some way with hAGT *in vitro*, but it is impossible to determine by these means if the interaction is due to a binding with the active site or with some other amino acids producing its denaturation or unfolding. The chromatogram of hAGT in the presence of compound 10 was not obtained, probably due to a high rate of denaturation of hAGT, which indicates some kind of interaction between compound 10 and hAGT. Smaller concentrations of inhibitor 10 were tested without achieving a stable signal. In contrast, the rest of the compounds (5, 6, 7, 8 and 9) were able to form a complex with hAGT, some of them in a specific way and some others in a non-specific. Compound 9 forms a clearly non-specific complex with hAGT, as various shifts for each peak of the hAGT chromatogram appear. In the case of compounds 5, 6 and 7, it is very difficult to see if the formed complex is specific or non-specific, as two shifts appear for the fourth peak but only one for the rest of the peaks. This probably means that we would be able to see a

non-specific complex formation upon increase of the inhibitor concentration, which is currently impossible to perform due to the constraints in DMSO concentration tolerated. Finally, compound 8 forms a clearly specific complex with hAGT at 150 µM concentration.

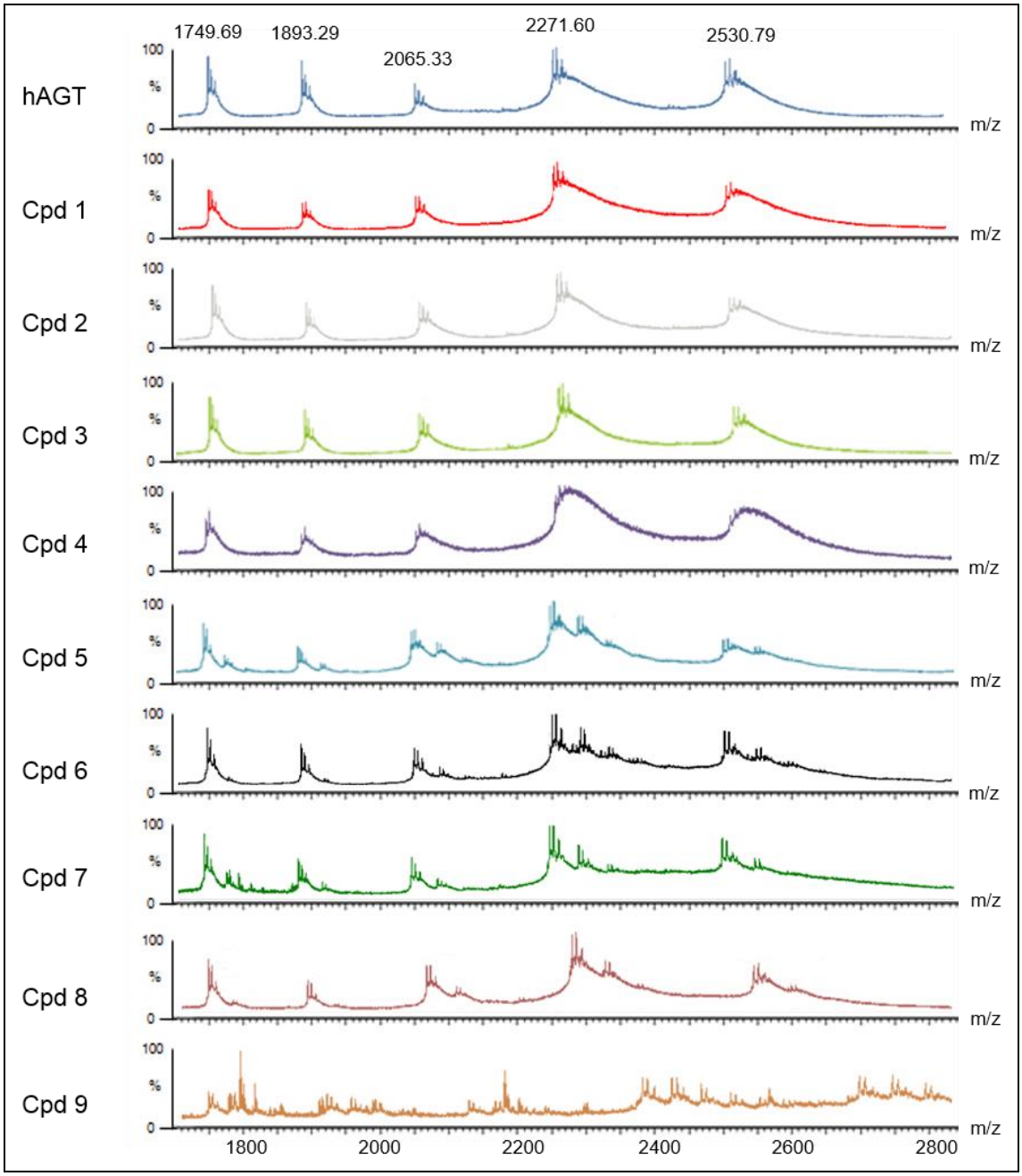

Figure 6. Mass spectra of hAGT and its interaction with the different compounds. hAGT was mixed with each inhibitor in DMSO on a 1:5 ration, being hAGT concentration 30 µM.

4. Cell culture assays: effect of cytotoxicity and enhancement of BCNU on human cancer cells.

All cell culture assays were performed in colon cancer cells (HT-29), described as a cellular line which overexpress hAGT. Carmustine (or BCNU) is a chemotherapeutic drug which alkylates and cross-links DNA during all phases of the cell cycle, resulting in disruption of DNA function, cell cycle arrest, and apoptosis.[6] This agent also carbamoylates proteins, including DNA repair enzymes, resulting in an enhanced cytotoxic effect.[7] Carmustine is highly lipophilic and crosses the blood-brain barrier readily.[8] Inhibition of hAGT in cell culture has been shown to increase sensitivity of human cells to BCNU, and to enhance its efficiency.[9]

These experiments were conducted to establish an IC_{50} value (inhibitory concentration 50%) for all the compounds, which allows to compare its efficiency in enhancing BCNU. According to the FDA, IC_{50} represents the concentration of a drug that is required for 50% inhibition *in vitro*.[10] This quantitative measure indicates how much of a particular drug or other substance (inhibitor) is needed to inhibit a given biological process. In the same line, we have calculated the LD_{50} (lethal dose 50%) for all the compounds, which is the required dose to produce a 50% of cell death.[11] This value was estimated to establish the toxicity of the compounds by themselves.

4.1. MTT assays.

The MTT cytotoxicity assays were performed to evaluate the toxicity of the compounds *per se* or in combination with carmustine. MTT (3-(4,5-Dimethylthiazol-2-yl)-2,5-diphenyltetrazolium bromide) is a bright yellow compound which is reduced to purple formazan in living cells (figure 7). This reduction and change of color allows the detection by UV absorption of the remaining living cells after a certain treatment and is widely used for the toxicity evaluation of new drugs.[12]

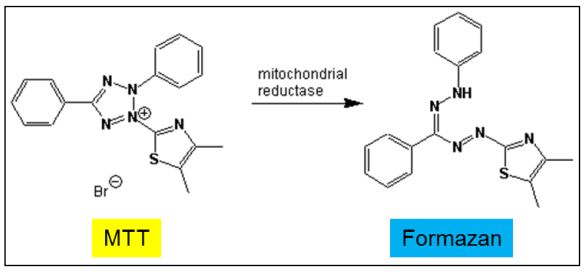

Figure 7. Reduction of MTT (yellow) to formazan (purple blue) by the mitochondrial reductase in living cells.

We first tested the toxicity of carmustine *per se*, observing that BCNU produced around 30% of cell death at 160 µM in 2 hours. This concentration was found to be optimal for our MTT assays, as smaller concentrations of carmustine did not kill the cells and higher concentrations of carmustine did not show a significant increase in cell death. Figure 8 shows the cell survival at different concentrations of BCNU and the optimal concentration of BCNU required for this assay.

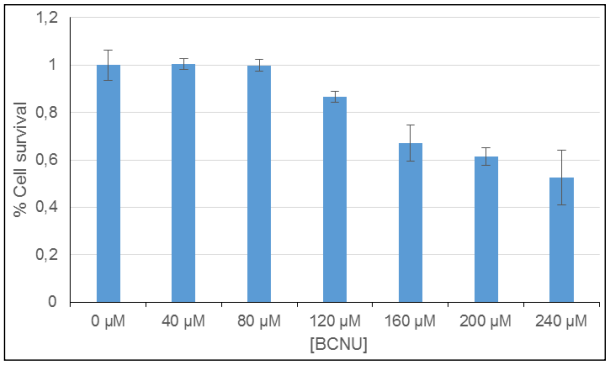

Figure 8. Increasing concentrations of BCNU treatment on cells seeded at 6000 cells/well (2 hours of exposure).

Cells were incubated with the 10 compounds described before, during and after BCNU treatment, to ensure that inhibitors were present during the entire period of time needed for DNA damage to be formed and repaired. As negative controls we evaluated the effect of DMSO and the solvent used as vehicle for BCNU (EtOH:PBS 1:1), which were found to be negligible. Scheme 2 explains the protocol followed for these experiments. Cells incubated with compound alone were used to evaluate its toxicity per se.

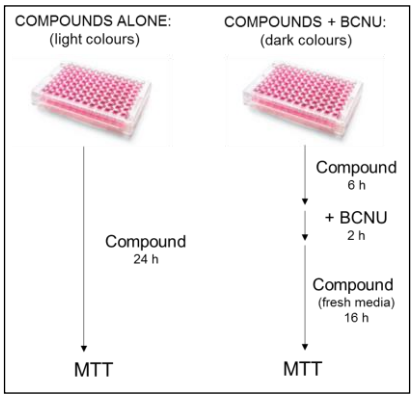

Scheme 2. Schematic representation of the MTT assay for the study of the toxicity of each compound per se (compound + vehicle) or in combination with BCNU (compound + BCNU). Light and dark colours refer to the colour coding of figures 8 and 9.

From the 10 potential inhibitors, compounds 5 and 8 were non-toxic by themselves, as the survival of the cells was not effected in the range of 0 to 100 µM concentrations. The rest of them were toxic, but at different ranges of concentrations (figure 9 and table 2). Compounds 1, 3 and 10 were found to be slightly toxic from 0,1-1 µM concentrations, producing over 20, 30 and 10% of cell death respectively and their LD_{50} was found to be > 100 µM. However, they maintained the level of toxicity constant upon concentration. Compound 2 was slightly toxic at 0.1-1 µM, causing less than 20% of the cell death, but at more than 50 µM it was found to be very toxic, producing a 60% of cell death *per se*. Its LD_{50} was estimated to be around 5 µM. Instead, compound 4 was progressively toxic while increasing its concentrations, reaching a level of 80% of cell death ($LD_{50} \sim 2.5$ µM), and compounds 6 and 7 were toxic from 1 µM but their LD_{50} differed, as compound 6 requires higher concentrations than 100 µM and in contrast the LD_{50} found for compound 7 was around 10 µM. Compound 9 was toxic from 0.1 µM (40% of cell death) but its toxicity was not significantly affected by increasing concentrations. These results suggest that compounds 2, 4 and 7 are clearly toxic by themselves and compounds 1, 3, 6, 9 and 10 were slightly toxic, too. Only compounds 5 and 8 were found to be non-toxic *per se*.

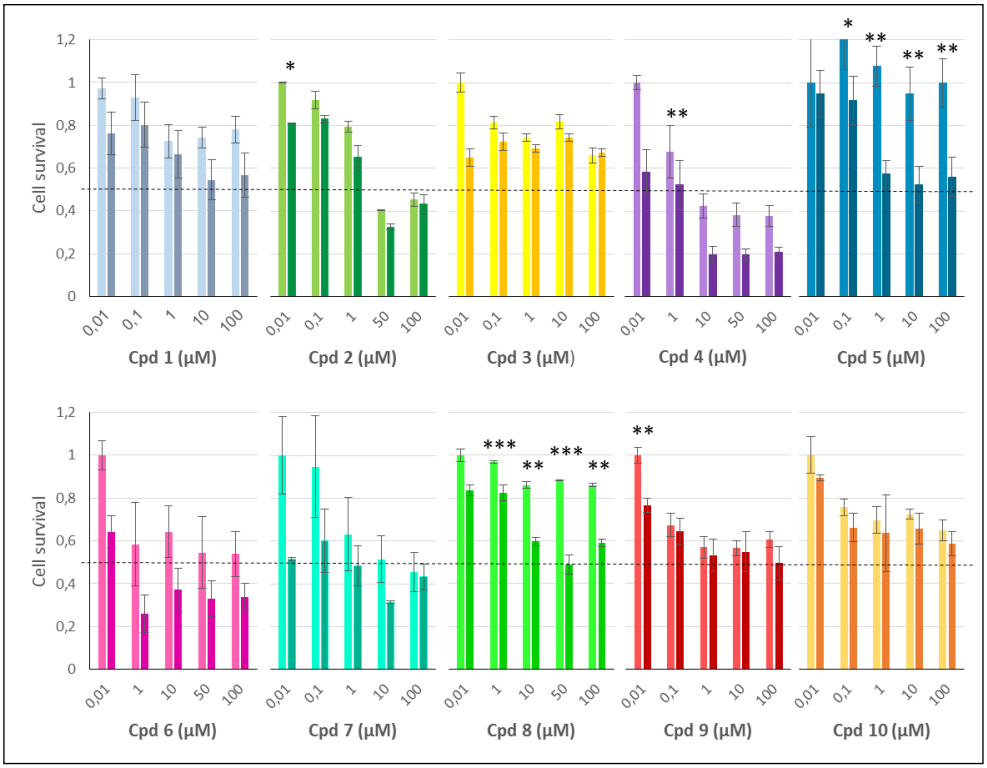

Figure 9. MTT toxicity assays of the different compounds (1-10). Light colours represent the toxicity of the compounds by themselves, while dark colours indicate the toxicity of the different compounds in the presence of 160 µM of Carmustine. The dashed lines indicate the 50% of the cell survival. The *p* values were calculated

using the Student's *t* test comparing cells treated with inhibitor in the absence and presence of BCNU. * $p \leq 0.1$, ** $p \leq 0.05$ and *** $p \leq 0.005$.

Regarding their enhancement of BCNU toxicity, compounds 5 and 8, which were non-toxic *per se*, were found to enhance significantly the effect of carmustine, with IC_{50s} of around 10 and 50, respectively. Compounds 2, 4, 6 and 7 enhanced the effect of carmustine with IC_{50s} around 1 μM, even if they were toxic *per se*. The behaviour of compound 2 at low micromolar concentrations is not toxic while the others presented toxicity by themselves. Compound 1 exhibited a relative capacity to stimulate cell death caused by carmustine, without reaching an IC_{50} at this range of concentrations. Compound 9 showed an increased effect in carmustine toxicity, but this effect is due to its increasing toxicity upon concentrations. In contrast, compounds 3 and 10 were unable to change the effect of carmustine significantly, remaining stable upon increasing concentrations. IC_{50} values were estimated from these results and are shown in table 2. Student's *t* test was performed for all the compounds. The *p* values demonstrate that the enhancement of carmustine toxicity produced by the compounds 5 and 8 were significant.

Compound	LD_{50} (toxicity *per se*)	IC_{50} (enhancement of BCNU)
1	>100 μM	>100 μM
2	5 μM	1.5 μM
3	>100 μM	>100 μM
4	2.5 μM	1 μM
5	NT	~10 μM
6	>100 μM	<1 μM
7	~10 μM	<1 μM
8	NT	~50 μM
9	>100 μM	>1 μM
10	>100 μM	>100 μM

Table 2. Estimated LD_{50} and IC_{50} of the 10 compounds studied by MTT assay. NT = non-toxic.

From these results, we can conclude that compounds 5 and 8 are good candidates to enhance the effect of BCNU in cell culture, as both were non-toxic at 100 μM and they were able to improve the rate of cell death significantly when incubated with carmustine.

4.2. Colony formation assays.

The colony formation assay was used in order to study in more detail the capability of compounds 5, 6, 7 and 8 to enhance BCNU cytotoxicity in colorectal cells. These compounds were selected due to their previous good performance in the MS analysis and MTT toxicity assays. The mass spectrometry analysis points to compounds 5, 6, 7, 8 and 9 as capable of forming a non-covalent complex with hAGT. From this five, compounds 5, 6, 7 and 8 were found to enhance BCNU's toxicity in the MTT assays, and 5 and 8 were non-toxic for the cells by themselves. Compounds 6 and 7 were found to be very toxic for the cells, and will allow us to compare the results obtained.

Cells were incubated with the 4 compounds mentioned above, before, during and after BCNU treatment, to ensure that inhibitors were present during the entire period of time needed for DNA damage to be formed and repaired by hAGT. Then, cells were replated and left to grow for a week with periodic replacement of media. We analysed the colony formation efficiency of HT-29 colorectal cells exposed to inhibitor alone, and in combination with BCNU. In this case, we added 240 μM of carmustine, enough to produce a 50% of cell death (see figure 8). Figure 10 shows the remaining cells stained with crystal violet after treatment with the compounds in absence or presence of carmustine.

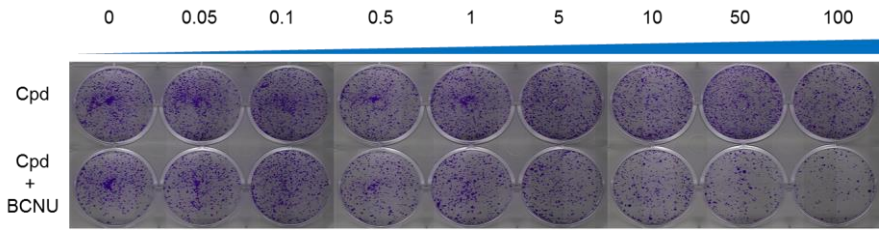

Figure 10. Pictures of a colony formation assay, with the remaining cells after treatment and a week of growth stained with crystal violet.

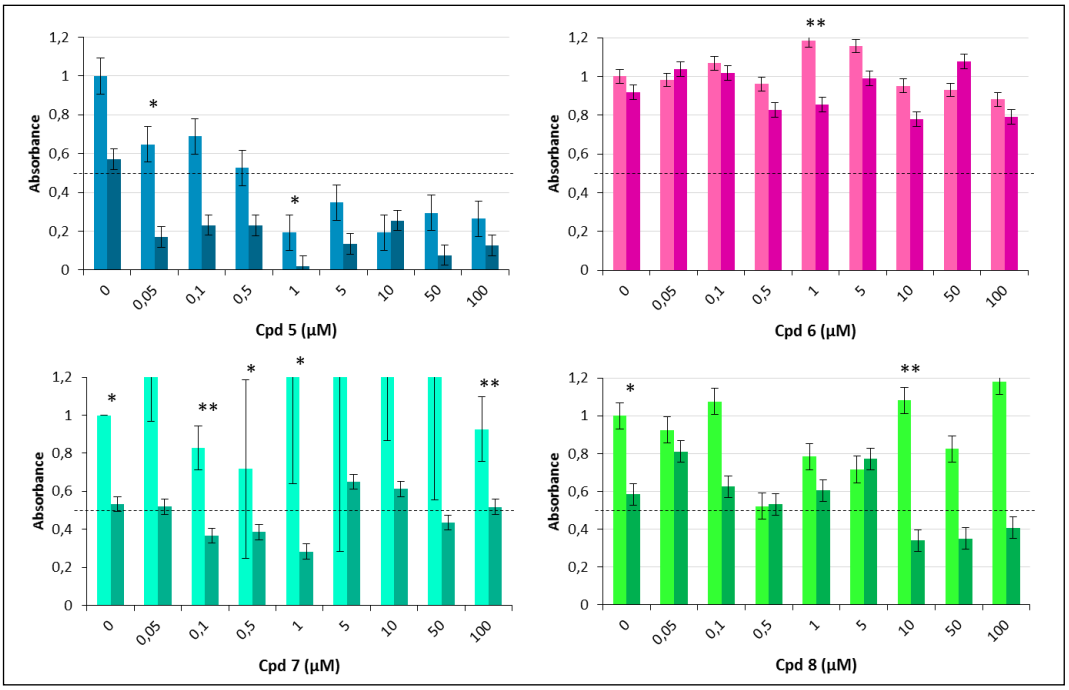

Figure 11. Colony formation assay of compounds 5, 6, 7 and 8. Light colours represent the cell viability of the cells incubated with the compounds alone, while dark colours indicate the survible of the cells in presence of the different compounds and 240 µM of carmustine. The dashed lines indicate the 50% of the cell survival. The *p* values were calculated using the Student's *t* test comparing cells treated with inhibitor in the absence and presence of BCNU. * $p \leq 0.1$, ** $p \leq 0.05$ and *** $p \leq 0.005$.

As shown in Figure 11, all compounds except compound 6 enhanced BCNU cytotoxicity. However, compound 5 reduced cell viability by itself in this case, showing a LD_{50} of around 0.5 µM and enhancing carmustine. The other 3 compounds were found to be non-toxic by these means. Compound 6 seemed not toxic but had little effect in enhancing carmustine. Even though, this results cannot be considered final as the effect of carmustine in this assay was very limited. In contrast, compound 7 is not toxic *per se* but enhances carmustine, showing an IC_{50} around 0.1 µM even if higher concentrations do not seem to potentiate this effect. Compound 8 is slightly more toxic than compound 7 *per se* but strongly enhances BCNU toxicity. IC_{50} values were estimated from these graphical results and are shown in table 3.

Compound	LD_{50} (toxicity *per se*)	IC_{50} (enhancement of BCNU)
5	>0.5 µM	<0.05 µM
6	NT	>100 µM
7	NT	~0.1 µM
8	NT	~7.5 µM

Table 3. Estimated LD_{50} and IC_{50} of the 4 compounds studied by colony formation assays. NT = non-toxic.

5. Conclusions

This set of 10 compounds were selected as candidates for the inhibition of hAGT in a virtual screening. We have tested their complex formation with hAGT by mass spectrometry, and their toxicity to tumoral cells, as well as their capacity to enhance the effect of an alkylating agent, carmustine. Table 1 summarizes the results obtained for the three experiments:

	ESI-MS	MTT assays:		Colony formation assays:	
		Toxicity *per se* (LD_{50})	Enhancement of BCNU (IC_{50})	Toxicity *per se* (LD_{50})	Enhancement of BCNU (IC_{50})
Cpd 1	Non observed	Slightly toxic (>100 μM)	Low (>100 μM)	-	-
Cpd 2	Non observed	Toxic (5 μM)	Low (1.5 μM)	-	-
Cpd 3	Non observed	Slightly toxic (>100 μM)	Low (>100 μM)	-	-
Cpd 4	Denaturation of hAGT	Toxic (2.5 μM)	Significant (1 μM)	-	-
Cpd 5	Complex (Non specific)	Non Toxic (>>100 μM)	Significant (~10 μM)	Toxic (0.5 μM)	Significant (<0.05 μM)
Cpd 6	Complex (Non specific)	Slightly toxic (>100 μM)	Significant (<1 μM)	Non toxic (>>100 μM)	Low (>100 μM)
Cpd 7	Complex (Non specific)	Toxic (10 μM)	Significant (<1 μM)	Non toxic (>>100 μM)	Significant (~0.05 μM)
Cpd 8	Complex (Specific)	Non toxic (>>100 μM)	Significant (>50 μM)	Non toxic (>>100 μM)	Significant (~7.5 μM)
Cpd 9	Complex (Non specific)	Slightly toxic (>100 μM)	None (>100 μM)	-	-
Cpd 10	Precipitation of the sample	Slightly toxic (>100 μM)	None (>100 μM)	-	-

Table 1. Summary and comparison of the results obtained for the mass spectrometry and the cell culture studies.

Combining the results obtained by ESI-MS and by cell culture assays, we can conclude that 2 compounds out of our first ten are able to form a specific (8) or non-specific (5) complex with hAGT and are non-toxic *per se* in MTT toxicity assays. In addition, they seem to enhance the effect of carmustine, both in MTT and in colony formation assays. However, compound 5 showed toxicity *per se* in the colony formation

assays. The differences in toxicity found by MTT and colony formation assays may be due to the fact that the latter studies the cell viability during 10 days, while MTT is applied 24h after the treatment with compounds and BCNU. Even though, the colony formation assays are preliminary and should be reproduced before considering these results conclusive.

Compound 8 represents the best candidate for the study of hAGT inhibition for chemotherapy enhancement, as it formed a specific complex with hAGT, was not found to be toxic *per se* neither by MTT nor by colony formation assays and showed a clear enhancement of carmustine at high concentrations. Following the line of this thesis, these potential inhibitors should be tested by the methods described subsequently to reveal their active concentrations and their suitability to continue preclinical studies in animal models.

6. Experimental details:

1. hAGT overexpression and purification.

hAGT-FL protein cloned in the pet-21a(+) (Novagen) vector was expressed in the *E. coli* strain Rosetta. Once the culture reached an OD_{600} value of 0.98, hAGT was induced by adding 1 mM IPTG (Sigma) and left to grow for 4 h at 30 °C. The pellet from a 1-L culture was disrupted by sonication and centrifuged. The supernatant was filtered, loaded into a HiTrap™ FF column (GE Healthcare) with buffer 350 mM NaCl, 20 mM Tris pH 8, 20 mM imidazole, and 1 mM BME, and then eluted with an imidazole (Fluka) gradient up to 500 mM in the same buffer. Finally, the protein was loaded into a Superdex 75 16/60 column (GE Healthcare) with the following buffer: 200 mM NaCl (Merck), 20 mM Tris pH 8.0 (Merck), 10 mM DTT (Sigma) and 0.1 mM EDTA (Sigma). The protein was concentrated to 2 mg/ml in this buffer and kept at -20 °C in the presence of 40 % glycerol. A similar protocol was used for the purification of the inactive mutant hAGT-C145S, cloned in the pet-28a (+) vector (Novagen) and expressed in the *E. coli* strain BL21. However, in this case the hystidine tag was cut using PrePro during a 4h dyalisis at 4ºC.

2. Compounds.

10 mg of the compounds 1 to 9 were purchase from IBScreen. Compound 10 (2'-aminoquinoline) was obtained from TCI Europe. Their reference numbers are shown in this list.

Compound 1: STOCK5S-10931
Compound 2: STOCK4S-24457
Compound 3: STOCK4S-98799
Compound 4: STOCK4S-90334
Compound 5: STOCK4S-14286
Compound 6: STOCK4S-97010
Compound 7: STOCK4S-94755
Compound 8: STOCK4S-96314
Compound 9: STOCK4S-99868
Compound 10: A0417

All of them were dissolved in DMSO (Sigma) at a final stock concentration of 1 mM and kept at -20°C until used.

3. Mass spectra of the complex with hAGT.

Mass spectrometry experiments were performed on a Waters (Manchester, UK) instrument equipped with electrospray ionisation, a travelling wave ion mobility cell and a time-of-flight mass analyser. Synapt G1 was interfaced to a chip-based nanoESI device, (Advion, Triversa Nanomate). This device contains a 384-well-sample plate, 384 disposable spraying tips and an ESI chip with 100 nozzles in front of the inlet of the mass spectrometer. The instrument was operated in the automatic mode using a contact closure signal. A spraying voltage of +1.76 kV and a sample pressure of 5.80 psi were applied. Each well was loaded with 10µl of sample, from which a total of 4 µl was infused during 10 min. Operating conditions for the Synap G1 mass spectrometer were: cone voltage = 20V; extraction cone = 5.5 V; source temperature = 20 ºC; trap and transfer voltages = 6 V and 4V, respectively. The ion mobility cell was filled with N_2 and an electric field was applied to the cell in the form of waves (wave height = 9.5 V) that passed thought the cell at 300 m/s. The bias voltage for ion introduction into the IMS cell was 15V.

The hAGT buffer was exchanged to 100 mM ammonium acetate pH=7 using BioSpin columns P-6, to prevent buffer interferences in the mass spectrometry experiments. hAGT in the presence of DMSO was used as Mass spectrum control. Different concentrations of DMSO were studied to find the optimal conditions. Once the mass spectrum for the native form of hAGT was confirmed, the non-covalent inhibitor-protein complexes were analyzed. hAGT (30 µM) was mixed with (150 µM of) each inhibitor in ammonium acetate buffer at a final volume of DMSO of 1.5% v/v (1, 2, 3, 4, 5, 6, 7, 8, , 9 and 10) separately and left to equilibrate at rt for one hour. Each study was performed in triplicates.

4. Cell culture assays.

HT-29 colon cancer cells were purchased from ATCC (catalog No. HTB-38) and cultured in RPMI 1640 medium (Gibco) supplemented with 10% fetal bovine serum (Gibco) at 37ºC and 5% CO_2. BCNU (1,3-bis-(2-chloroethyl)- 1-nitrosourea) was obtained from Sigma and dissolved in 50% phosphate-buffered saline buffer (PBS)-50% ethanol at 4 mM (10 mg/ml) stock solution.

4.1. MTT toxicity assays.

The optimal concentration of BCNU was explored using MTT assays. 6000 cells per well (in 100 µL RPMI medium) were seeded in a 96-well plate and left to grow for 24 hours. Then, cells were incubated during 2 h with concentrations of carmustine ranging

from 40 to 240 μM and after that, cells were rinsed with PBS and media was replaced. The day after, 20 μL of MTT (2mg/ml in PBS) were added and left to react for 4 hours. At the end of the reaction blue crystals inside the living cells could be observed at the microscope. The medium + MTT was removed and the crystals resuspended in 200 μL of DMSO and agitated until reaching homogeneity. Absorbance was read at 560 nm using a ELx 800 Universal Microplate Reader (Bio-Tek Instruments INC).

The cytotoxic effects of compounds 1 to 10 in HT-29 human colorectal tumoral cells were analyzed by means of MTT toxicity assay. 6000 cells per well (in 100 μL RPMI medium) were seeded in a 96-well plate and left to grow for 24 hours. The day after, the cells were incubated for 6 hours with different concentrations of compounds 1 to 10 (0, 0.01, 0.1, 1, 10, 50 and 100 μM). Then, enough quantity of BCNU to reach a concentration of 160 μM (or the equivalent volume of the vehicle as negative control) was added and left to react during 2 hours. Afterwards, the medium was replaced by compound-containing RPMI (using the same concentrations as before the treatment) and left overnight. The next morning, the medium was replaced by fresh RPMI and cells were left to grow for 24 hours. Then, 20 μL of MTT (2mg/ml in PBS) were added and left to react for 4 hours. The medium + MTT was absorbed and the crystals resuspended in 200 μL of DMSO and shaked until reaching homogeneity. Absorbance was read at 570 nm using a ELx 800 Universal Microplate Reader (Bio-Tek Instruments INC) and toxicity of the compounds *per se* or in combination with BCNU was determined relative to untreated cells. All these experiments were performed in triplicates and repeated three times. IC_{50} values were estimated from the graphical results. The *p* values were calculated using the Student's *t* test (2 tails, equal variance) comparing cells treated with inhibitor in the absence and presence of BCNU.

4.2. Colony formation assays.

The effect of compounds 6 to 9 on the sensitivity of human colorectal (HT-29) cells to BCNU was determined using colony formation assays as it has been previously described.[5] HT-29 cells were seeded at 10 x 10^3 cells per well density in 24-well, flat-bottomed plates and incubated in a humidified, 5% CO_2 incubator at 37ºC for 48 h. Compound solutions were diluted in the culture medium RPMI at final concentrations of 100, 50, 10, 5, 1, 0.5, 0.1, and 0.05 μM, and were immediately used to treat the cells. Cells were incubated with these compounds' solutions for 6 h and then BCNU (or the equivalent volume of the vehicle as negative controls) was added to a final concentration of 160 μM. After 2 hours of incubation, the medium was replaced with fresh medium containing the same compound concentration, and cells were left to grow for an additional 16 hours. The

cells were then replated at densities of 2000 cells per well in 24-well plates and grown for 1 week until discrete colonies were formed. Colonies were washed twice with PBS and stained with a 0.5% crystal violet - 20% ethanol solution. Cells were rinsed with deionized water and air dried. Stained colonies were counted in a ELx 800 Universal Microplate Reader (Bio-Tek Instruments INC) and clonogenic survival was determined relative to untreated cells. Samples were assayed in triplicates and experiments repeated three times. IC_{50} values were estimated from the graphical results. The *p* values were calculated using the Student's *t* test (2 tails and equal variance), comparing cells treated with inhibitor in the absence and presence of BCNU.

References:

[1] a) D. S. Daniels, J. A. Tainer, *Mutat Res* **2000**, *460*, 151-163; b) D. S. Daniels, C. D. Mol, A. S. Arvai, S. Kanugula, A. E. Pegg, J. A. Tainer, *EMBO J* **2000**, *19*, 1719-1730; c) D. S. Daniels, T. T. Woo, K. X. Luu, D. M. Noll, N. D. Clarke, A. E. Pegg, J. A. Tainer, *Nat Struct Mol Biol* **2004**, *11*, 714-720.

[2] M. R. Middleton, G. P. Margison, *Lancet Oncol* **2003**, *4*, 37-44.

[3] T. P. Brent, P. J. Houghton, J. A. Houghton, *Proc Natl Acad Sci U S A* **1985**, *82*, 2985-2989.

[4] J. J. Rasimas, A. E. Pegg, M. G. Fried, *J Biol Chem* **2003**, *278*, 7973-7980.

[5] F. M. Ruiz, R. Gil-Redondo, A. Morreale, A. R. Ortiz, C. Fabrega, J. Bravo, *J Chem Inf Model* **2008**, *48*, 844-854.

[6] http://pubchem.ncbi.nlm.nih.gov/compound/2578#x291.

[7] E. L. Schaefer, R. I. Morimoto, N. G. Theodorakis, J. Seidenfeld, *Carcinogenesis* **1988**, *9*, 1733-1738.

[8] A. B. Fleming, W. M. Saltzman, *Clin Pharmacokinet* **2002**, *41*, 403-419.

[9] L. Yan, J. R. Donze, L. Liu, *Oncogene* **2005**, *24*, 2175-2183.

[10] http://www.fda.gov/ohrms/dockets/ac/00/slides/3621s1d/sld036.htm

[11] http://www.derangedphysiology.com/php/Pharmacodynamics/Pharmacology---Pharmacodynamics---Definitions-of-median-doses---ED50-LD50-and-TD50.php.

[12] T. Mosmann, *J Immunol Methods* **1983**, *65*, 55-63.

Appendix 1

Receptor-based virtual screening and biological characterization of new inhibitors of Human Apurinic/Apyrimidinic Endonuclease Enzyme (Ape1)

Receptor-based virtual screening and biological characterization of new inhibitors of Human Apurinic/Apyrimidinic Endonuclease Enzyme (Ape1)

Federico M. Ruiz,[1] Sandrea M. Francis,[2] Maria Tintoré,[3] Rubén Ferreira,[3] Rubén Gil-Redondo,[4,5] Antonio Morreale,[4] Ángel R. Ortiz,[4] Ramon Eritja[3] and Carme Fàbrega[3]*

ChemMedChem, (2012) Volume 7, Issue 12, pages 2168–2178.

DOI: 10.1002/cmdc.201200372. Impact factor: **3.046**

[1] Chemical and Physical Biology, CIB (CSIC),

[2] Institute of Biomedicine of Valencia, (IBV-CSIC) Valencia

[3] Institute for Research in Biomedicine of Barcelona, IQAC-CSIC, CIBER-BBN Networking, Centre on Bioengineering Biomaterials and Nanomedicine. Cluster Building, Baldiri i Reixach 10, E-08028 Barcelona

[4] Bioinformatics Unit, CBMSO (CSIC-UAM), Universidad Autónoma de Madrid, Cantoblanco, 28049 Madrid.

[5] SmartLigs Bioinformática S.L., Fundación Parque Científico de Madrid, c/ Faraday, 7. Campus de Cantoblanco UAM, E-28049. Madrid, Spain.

CHEMMEDCHEM

ChemPubSoc Europe

DOI: 10.1002/cmdc.201200372

Receptor-Based Virtual Screening and Biological Characterization of Human Apurinic/Apyrimidinic Endonuclease (Ape1) Inhibitors

Federico M. Ruiz,[a] Sandrea M. Francis,[b] Maria Tintoré,[c] Rubén Ferreira,[c] Rubén Gil-Redondo,[d, e] Antonio Morreale,*[d] Ángel R. Ortiz,[d] Ramon Eritja,[c] and Carmen Fàbrega*[c]

The endonucleolytic activity of human apurinic/apyrimidinic endonuclease (AP endo, Ape1) is a major factor in maintaining the integrity of the genome. Conversely, as an undesired effect, Ape1 overexpression has been linked to resistance to radio- and chemotherapeutic treatments in several human tumors. Inhibition of Ape1 using siRNA or the expression of a dominant negative form of the protein has been shown to sensitize cells to DNA-damaging agents, including various chemotherapeutic agents. Therefore, inhibition of the enzymatic activity of Ape1 might result in a potent antitumor therapy. A number of small molecules have been described as Ape1 inhibitors; however, those compounds are in the early stages of development. Herein we report the identification of new compounds as potential Ape1 inhibitors through a docking-based virtual screening technique. Some of the compounds identified have in vitro activities in the low-to-medium micromolar range. Interaction of these compounds with the Ape1 protein was observed by mass spectrometry. These molecules also potentiate the cytotoxicity of the chemotherapeutic agent methyl methanesulfonate in fibrosarcoma cells. This study demonstrates the power of docking and virtual screening techniques as initial steps in the design of new drugs, and opens the door to the development of a new generation of Ape1 inhibitors.

Introduction

Chemo- and radiotherapy are the two main currently available treatments to improve the outcome in cancer patients. The cytotoxicity of many of these agents is directly related to their propensity to induce genomic DNA damage.[1] The persistence of unrepaired DNA damage results in accumulation of mutations, cell cycle arrest, and apoptosis.[2] However, the ability of cancer cells to recognize this damage and initiate DNA repair is an important mechanism that impacts negatively upon therapeutic efficacy.[3]

The base excision repair (BER) pathway is the major mechanism for dealing with a variety of lesions in DNA produced by alkylating agents. This pathway is initiated by specific DNA glycosylases, which recognize and excise the damaged base to generate an apurinic/apyrimidinic (AP) site. AP endonuclease 1 (Ape1) cleaves the phosphodiester backbone adjacent to the 5′ site of the AP site, generating a 3′-hydroxy and 5′-deoxyribose phosphate termini.[4] Polymerase β removes the 5′-deoxyribose phosphate, fills in the single-nucleotide gap, and the consequent nick is ligated by DNA ligase I or by DNA ligase III/XRCC1.[5] Ape1 is a fundamental protein in this essential repair pathway and it is thought to be responsible for 95% of total AP endonuclease activity in human cell lines.[6] Ape1 also possesses 3′-phosphodiesterase, 3′-phosphatase, RNase H, and 3′→5′ exonuclease functions.[7] In addition to its DNA repair activities, Ape1 acts as a redox factor for a variety of important transcription factors such as NF-κB, p53, c-Fos, and c-Jun.[8] The DNA repair and the redox activities of Ape1 are distinct, both structurally and functionally.

Ape1 protein levels and intracellular distribution have been related to the pathogenesis of several human tumors[5a,9] and its expression pattern appears to have a prognostic significance in cancer cells, including breast,[9b] lung,[10] ovarian,[9e] gastro-esophageal[11] and pancreatic–biliary,[11] and bone[12] tumors. For this reason, several preclinical and clinical studies have suggested that Ape1 may be an attractive target for anticancer drug development. Using either antisense oligonucleotides or RNA interference approaches, different groups have reported that depletion of intracellular Ape1 sensitizes mammalian cells to a variety of DNA-damaging agents.[5a,13] In pancreatic cancer cell lines for example, down-regulation of Ape1 potentiated the cytotoxicity of gemcitabine[14] and

[a] *Dr. F. M. Ruiz*[+]
Chemical and Physical Biology, CIB (CSIC) (Spain)

[b] *S. M. Francis*[+]
Institute of Biomedicine of Valencia, (IBV-CSIC) Valencia (Spain)

[c] *M. Tintoré, R. Ferreira, Prof. R. Eritja, Dr. C. Fàbrega*
Institute for Research in Biomedicine of Barcelona, IQAC-CSIC
CIBER-BBN Networking Centre on Bioengineering Biomaterials and Nanomedicine, Cluster Building, Baldiri i Reixach 10, 08028 Barcelona (Spain)
E-mail: carme.fabrega@irbbarcelona.org

[d] *Dr. R. Gil-Redondo, Dr. A. Morreale, Prof. Á. R. Ortiz*
Bioinformatics Unit, CBMSO (CSIC-UAM)
Universidad Autónoma de Madrid, Cantoblanco, 28049 Madrid (Spain)
E-mail: amorreale@cbm.uam.es

[e] *Dr. R. Gil-Redondo*
SmartLigs Bioinformática S.L., Fundación Parque Científico de Madrid
c/Faraday, 7 Campus de Cantoblanco UAM, 28049 Madrid (Spain)

[+] *These authors contributed equally to this work.*

troxacitabine.[15] Ape1 down-regulation has also been shown to block ovarian cancer cell-growth.[16] In melanoma and colon cell lines, Ape1 down-regulation alone or in combination with bleomycin led to an increase in apoptosis,[2a,17] whereas its overexpression conferred protection from cisplatin- or H_2O_2-induced apoptosis.[17a] Attempts to create Ape1 knockout mice were embryonically lethal, suggesting that Ape1 is crucial for embryonic development.[18] Heterozygous Ape1 mice were viable but abnormally sensitive to oxidative stress and prone to cancer progression.[19]

Recently, there has been a significant effort toward identifying inhibitors of DNA repair proteins in keeping with the emerging concept that sensitizing cancer tissue to core chemotherapeutic regimens by simultaneous targeting DNA repair may result in enhanced treatment outcomes.[20] As a result of the promising therapeutic potential of the inhibition of Ape1 DNA repair activity, several reports have described the identification and characterization of small molecules that inhibit its repair endonuclease activity,[21] including methoxyamine (MX), lucanthone and 7-nitroindole-2-carboxilic acid (NCA). All three compounds were able to enhance the effects of methyl methanesulfonate (MMS) or temozolamida (TMZ) in ovarian,[22] breast,[22b,23] colon,[24] and HT1080 fibrosarcoma cancer cells.[25] In addition, Lucanthone was able to potentiate the effects of radiation therapy in patients with brain metastasis.[26] However, the evidence of lucanthone topoisomerase inhibitory activity raised concerns regarding an off-target effect[27] and the synergistic cell killing effects observed by NCA with TMZ or MMS were unclear, as recent data showed that its specificity for Ape1 is controversial.[22b,28] By using a fluorescence-based high-throughput assay, Kelley and co-workers described the identification of 2,4,9-trimethylbenzo[*b*][1,8]napthyridin-5-amine (AR03), which was found to be active in the low micromolar range in vitro against purified Ape1 and inhibited AP site incision activity and its repair in SF67 glioblastoma cells.[29]

Other research groups using high-throughput screening (HTS) approaches reported Ape1 inhibitors including compounds containing arylstibonic[30] or bis-carboxylic acid,[31] Reactive blue 2, 6-hydroxy-D,L-DOPA, and myricetin.[32] The bis-carboxylic acid derivatives were not tested in cell-based assays,[31] and no information about its in vivo activity can be inferred. The arylstibonic acid compounds effectively inhibited Ape1 in vitro, but were ineffective in vivo due to poor cellular uptake.[30] Moreover, antimony-containing compounds are generally considered from a probe development standpoint due to their possible promiscuity akin to the effect of heavy metal ions and their occasional high toxicity.[33] Reactive blue 2, 6-hydroxy-D,L-DOPA, and myricetin were found to have numerous other targets besides Ape1 in cells; therefore, they lack the selectivity and specificity required for promising Ape1 inhibitors.[32]

We recently developed a flexible, fully automated virtual screening computational platform (VSDMIP)[34] to identify inhibitors of protein targets from libraries of millions of compounds. This computational platform has been successfully applied to the discovery of new inhibitors of the DNA repair protein O^6-alkylguanine DNA alkyltransferase[35] and in the development of small molecules that compete with ubiquitin E2 variant for its interactions with ubiquitin-conjugating enzyme UBC13, inhibiting its enzymatic activity,[36] among others.

Herein we report the identification of new Ape1 inhibitors by using a docking-based virtual screening technique. The activity of these compounds has been experimentally proved both in vitro and in vivo. These molecules are promising lead candidates to establish quantitative structure–activity relationship models for further development of clinically relevant Ape1 inhibitors as co-adjuvants in cancer chemotherapy.

Results and Discussion

Virtual screening (VS)

The virtual screening protocol employed here is summarized in Scheme 1 and briefly described in the Experimental Section. An essential part of the procedure is to characterize the shape

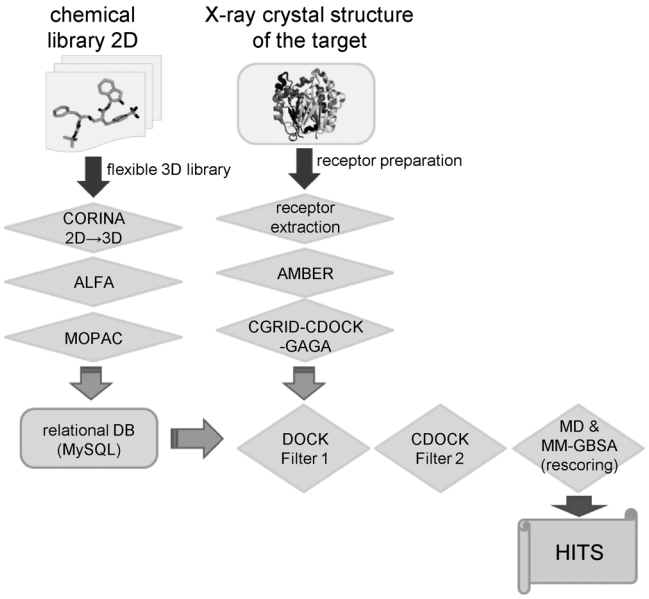

Scheme 1. Flowchart of the virtual screening procedure applied in this study.

of the active site. For this purpose we used GAGA algorithm (see Experimental Section) to obtain a sort of a negative image of the binding site (Figure 1). Overall, the shape of the active site does not undergo significant conformational changes even after binding to the DNA, as very low RMSD values were obtained after superimposing the different Ape1 structures deposited in the PDB (IDs: 1BIX,[37] 1DE9,[38] 1DEW,[38] 1DE8,[38] 1E9N,[39] 2ISI, and 1HD7[39]). This fact is reassuring taking into account that the protein flexibility is not explicitly considered during the docking process. The active site is a well-defined deep V-shaped cleft, with an Mg^{2+} cation located in its "elbow".

Upon characterizing the binding site, the free database of commercially available compounds ZINC[40] was first screened

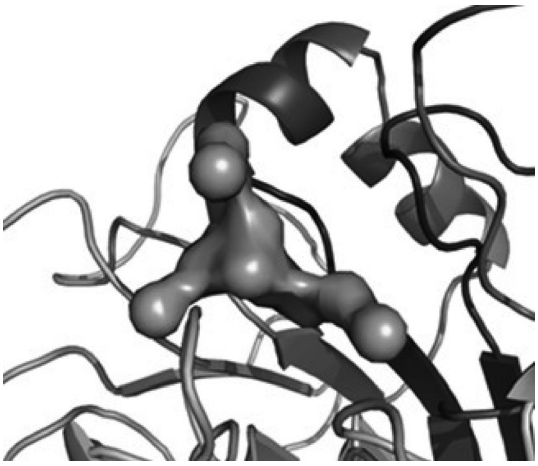

Figure 1. Inside view of the Ape1 active site with the ligand negative spheres image computed with GAGA.

using DOCK[41] and the negative image of the binding site. We applied a *ZScore* (see Experimental Section) cutoff value of 4 on the DOCK-ranked list, and a set of 2288 molecules were taken through to the next step. These molecules were then re-docked with CDOCK[42] and scored with its molecular mechanics energy function, which specifically includes solvent and H-bonding terms. The 100 highest-scoring compounds were submitted to MD simulation in explicit solvent and their binding energies estimated and pairwise decomposed by MM-GBSA[43] calculation over a large collection of snapshots homogenously sampled along the trajectories.

Finally, from the top-scoring compounds, and upon visual examination, a total of 15 candidates were selected, purchased, and tested experimentally. For those showing in vitro activity against Ape1, the MM-GBSA[43] method was used to estimate the binding free-energies from molecular dynamics (MD) trajectories. The physicochemical properties of the molecules as stored in the ZINC database[40] are listed in Table 1.

Table 1. The 15 top-ranked compounds obtained in the virtual screen.[a]

ZINC ID	log *P*	HBD[b]	HBA[c]	Charge	M_r [Da]	IC_{50} [μM][d,f]	EC_{50} [μM][e,f]
1 ZINC08790444	1.57	3	10	0	497.89	1.8 ± 0.5	> 100
2 ZINC09086704	1.82	0	9	0	497.54	6.8 ± 0.5	7.3
3 ZINC00708759	6.37	0	9	−1	543.58	17.3 ± 0.6	> 50
4 ZINC00870176	6.39	0	9	−1	543.58	39.2 ± 0.8	> 100
5 ZINC00730105	4.79	1	8	−1	487.56	52.8 ± 0.9	28.5
6 ZINC02118845	1.97	2	8	−1	473.51	55.7 ± 0.8	> 100
7 ZINC04059809	5.19	0	8	−1	427.48	> 130	ND
8 ZINC08854784	2.61	0	12	0	477.50	> 150	ND
9 ZINC08877288	2.12	3	9	−1	493.58	> 150	ND
10 ZINC04060698	4.63	0	8	−1	413.45	> 150	ND
11 ZINC03583501	3.69	0	9	0	523.95	> 200	ND
12 ZINC08932744	3.48	2	6	0	440.52	> 200	ND
13 ZINC09042551	1.91	3	9	−1	423.45	> 200	ND
14 ZINC04202254	3.97	0	8	−1	456.53	> 200	ND
15 ZINC00706278	2.61	0	8	−1	421.41	> 200	ND

[a] The computed chemical properties (as found in the ZINC database) and the in vitro and in vivo activities of the active compounds are listed. [b] H-bond donors. [c] H-bond acceptors. [d] in vitro IC_{50} value: compound concentration required to decrease Ape1 activity by 50%. [e] in vivo EC_{50} value: compound concentration required to kill 50% of cells in the presence of 300 μM MMS; ND: not determined. [f] Values represent the average ± standard error of the mean (SEM) of three separate experiments.

Ape1 endonuclease in vitro assays

Fifteen top-ranked compounds selected from the VS computations were first dissolved in DMSO. The ability of those 15 candidates to inhibit the recombinant Ape1 activity in vitro was determined by a fluorescence-based assay described by different groups.[25,30] In brief, a double-stranded DNA (dsDNA) substrate was used containing, in one of the strands, an internal ribitol (THF) AP site mimic,[44] and a 5′-6-carboxyfluorescein (FAM) label, whereas the complementary strand was labeled with a 3′-Dabsyl fluorescence-quencher moiety. The close proximity of the fluorophore and the quencher results in a dampened signal upon light excitation. Following DNA-backbone cleavage by Ape1, a short single-stranded DNA fragment 5′-tagged with the FAM group is released from the duplex DNA substrate, resulting in an increase in the fluorescence. Because assay variability is to be expected, as a comparative control we included a compound that was previously described as Ape1 inhibitor (data not shown).[30] Ape1 (at 590 pM concentration) was incubated with the dsDNA at 37 °C for 30 min in the presence of each of the 15 compounds selected during the VS at concentrations of 100 and 200 μM. The results of this first assay showed that compounds **11** to **15** did not exhibit any inhibitory action against Ape1 at these concentrations (Table 1). Compounds **7**–**10** showed an inhibitory effect versus Ape1 at concentration between 150 and 200 μM and therefore they were not evaluated further.

On the other hand, compounds **1**–**6** showed inhibitor activity at concentrations below 100 μM and were further analyzed to determine the concentration dependence for the inhibition of Ape1 endonuclease activity. All of them inhibited Ape1 with IC_{50} values in the low-to-medium micromolar range. Compounds **1** and **2** were identified as the most potent inhibitors of Ape1 with an IC_{50} of 1.8 and 6.8 μM, respectively. These two lead compounds had comparative or slightly higher effects in blocking Ape1 activity than thiolactomycin, methyl 3, 4-dephostatin and better than other compounds found by Simeonov and colleagues.[32] Compounds **3** and **4** had an intermediate effect (IC_{50}: 17–39.5 μM), whereas compounds **5** and **6** were weakly active ($IC_{50} > 50$ μM). The resultant IC_{50} values obtained for all active compounds are listed in Table 1 and in Figure 2. The chemical structures of these compounds are shown in Figure 3, prioritized by low micromolar IC_{50} values.

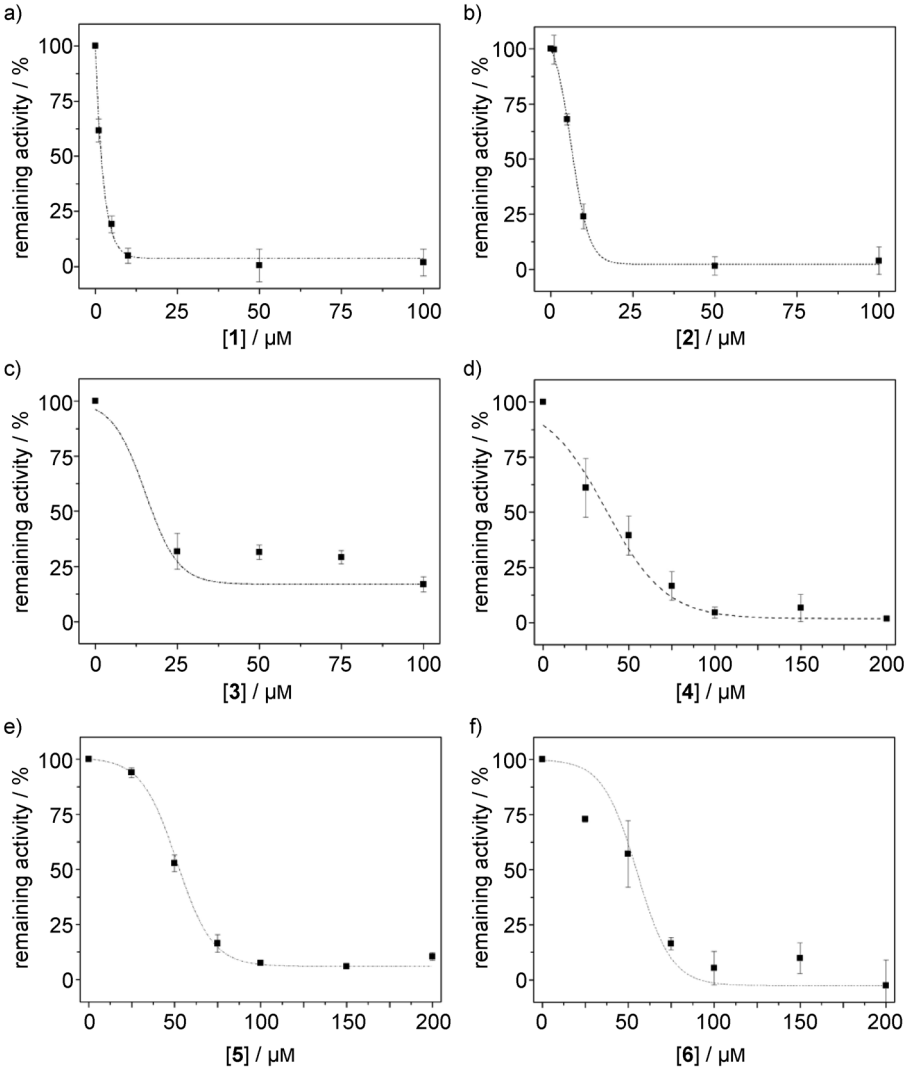

Figure 2. Concentration curves showing the inactivation of human Ape1 by compounds **1**–**6** [panels a)–f), respectively]. Remaining Ape1 activity as a function of compound concentration is plotted relative to untreated control samples. Compounds **1**–**3** show inhibitory effects on Ape1 activity in the low micromolar range, whereas compounds **4**–**6** show inhibitory effects in the mid-micromolar range. Data are the average ± SEM of three separate experiments performed in triplicate.

DNA intercalation binding

To test if these compounds inhibit Ape1 activity through nonspecific DNA binding rather than by direct inhibition of the enzymatic activity, we employed a fluorescent-dye displacement assay.[32,45] Briefly, if a compound acts nonspecifically by association with DNA, it would displace a DNA-bound fluorophore such as thiazole orange (ThO) or ethidium bromide. As these molecules emitted fluorescence upon intercalation to DNA, its displacement should produce a decrease in the fluorescence of the complex dye-DNA when increasing amounts of the compounds were added. We selected ThO, which binds noncovalently to DNA with high affinity instead of ethidium bromide, due to the fact that its fluorescence excitation and emission are red-shifted, which ensures a decreased susceptibility to compound autofluorescence.[32] As shown in Figure 4, compounds **1**–**6** did not displace bound ThO at any range of concentrations starting from 100 pM to 100 μM. This result suggests that these molecules do not inhibit the Ape1 DNA repair activity by a noncompetitive effect such as DNA binding. In contrast, mitoxantrone, described in Simeonov et al.[32] as a DNA binding compound, was able to displace ThO producing a 100% decrease in fluorescence in the same concentration range.

Complex formation detected by MS

Electrospray ionization mass spectrometry (ESIMS) has become an established tool for the investigation of macromolecular complexes.[46] ESI is a gentle ionization method that enables the analysis of proteins without causing internal fragmentation of the molecule. Their typical multiply charged ions result in low mass-to-charge values that allow an accurate mass determination.[47] The noncovalent complex formation of Ape1 with compounds **1**–**6** was analyzed by this means. The mass spectrum of Ape1 alone exhibited a characteristic series of multiply charged positive ions (Figure 5a). A narrow range of charge state is a good indication that Ape1 has retained its folded or native conformation. Moreover, the ion mobility measurements further confirmed that the protein was folded during the nano-ESIMS experiments.

The direct observation of the protein–ligand complex ion can be easily achieved for tight-binding complexes. However, weakly bound complexes, particularly those dependent on hydrophobic effects, are fragile and may dissociate during desolvation,[48] as observed with compounds **2**–**4** (data not shown). The mass spectra of Ape1 in complex with compound **5** (Figure 5a) showed that although the peaks are too complex to be observed in detail, the free-protein peaks shifted to a higher mass-to-charge value and this fact may indicate an inhibitor–protein interaction. In the mass spectrum of Ape1 in presence of compounds **1** and **6**, a clear signal of complex formation was observed. The upper part of Figure 5a shows the ESIMS peaks corresponding to free protein (P) and protein in

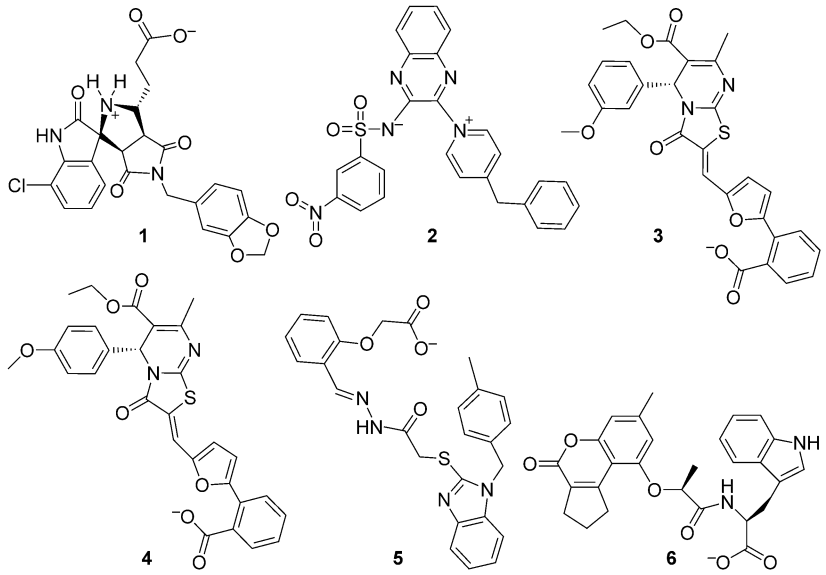

Figure 3. Structures of the six compounds that show Ape1 inhibition in the micromolar range.

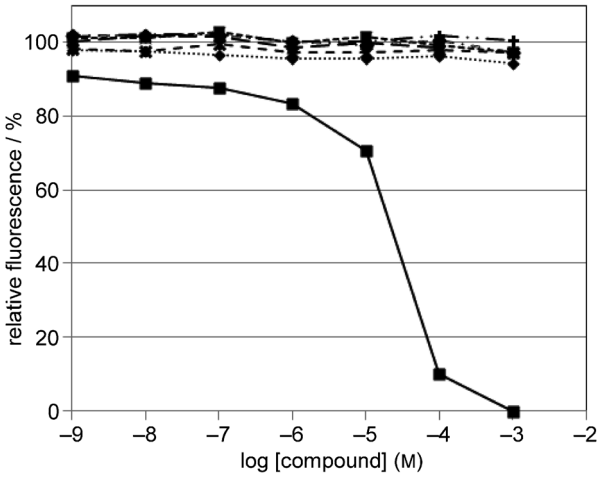

Figure 4. ThO inhibitor displacement assays were used to evaluate the DNA binding ability of all compounds (**1**–**6**) that were active in the Ape1 in vitro assay. No decrease in ThO fluorescence was observed upon addition of the compounds, indicating that they do not bind DNA. Mitoxantrone, a clear DNA binding molecule, was used as positive control (■). The fluorescence signal was normalized against DNA.

complex with inhibitor (PI). The complex peaks are shown in greater detail in Figure 5b. The estimated stoichiometry of the complex between Ape1 and the three studied compounds (**1**, **5** and **6**) respectively was equimolar (1:1).

Docking binding modes

For those compounds showing in vitro activity against Ape1, the binding mode was refined by MD simulations. The binding mode of compound **2** with Ape1 highlights the interaction with the metallic cation, which energetically is the most important. The H-bonding pattern is represented in Figure 6. These interactions were established between: 1) the nitro group of compound **2** and the backbone NH group of residue Asn174; and 2) an oxygen atom from the sulfonyl moiety and the amino group from the side chain of residue Asn212 on the one hand, and the NHε group of residue His309, on the other hand. This binding mode also presented a network of hydrophobic contacts surrounding the quinoxaline core of compound **2** with Phe266, Trp280, and Leu282, and an additional stacking interaction with Tyr269, which stabilizes the benzylpyridinium moiety.

The other five active compounds all have a carboxylic moiety in common, which also presented their main interaction with Ape1 through the Mg^{2+} cation. However, compared with compound **2**, this interaction is somehow skewed. This fact allows a gradual contribution to the stability of the complex from a salt bridge that is formed between the carboxylic moiety and the side chain of residue Lys98, which in turns depends on the position of the Mg^{2+} cation. Nevertheless, rather similar interaction energies were obtained for the contacts of the ligands with the hydrophobic residues Phe266 and Trp280 and polar Asn174 and Asn212. Finally, an important interaction was established between the central core of the ligands and the side chain of residue Lys98, which is mainly hydrophobic except for compound **1** in which a hydrogen bond is formed with one of the oxygen atoms in the succinimide-like central moiety.

Effects of cytotoxicity and enhancement of MMS on human cells

The presented data suggested that the six compounds can potently and selectively inhibit Ape1 in vitro. However, to have a general utility as BER inhibitors, it is important to confirm that they can block Ape1 function in living cells. A colony-forming assay was used to study the capability of compounds **1**–**6** to enhance MMS cytotoxicity in HOS cells.[12,22b,23,25,49] MMS creates base damage by methylation, which is either lost spontaneously or excised by the alkylpurine DNA glycosylase, resulting in a high number of cytotoxic abasic sites.[50] Inhibition of Ape1 in cell culture or the expression of a dominant negative form of the protein has been shown to increase sensitivity of human cells to MMS.[12,22b,23,25,49]

Cells were incubated with the six compounds before, during, and after MMS treatment to ensure that inhibitors were present during the entire period of time required for DNA damage to occur. We analyzed the colony formation efficiency of HOS cells exposed to MMS alone, each inhibitor alone, or the combination of MMS plus inhibitor, relative to an unexposed control. MMS alone decreased the number of colo-

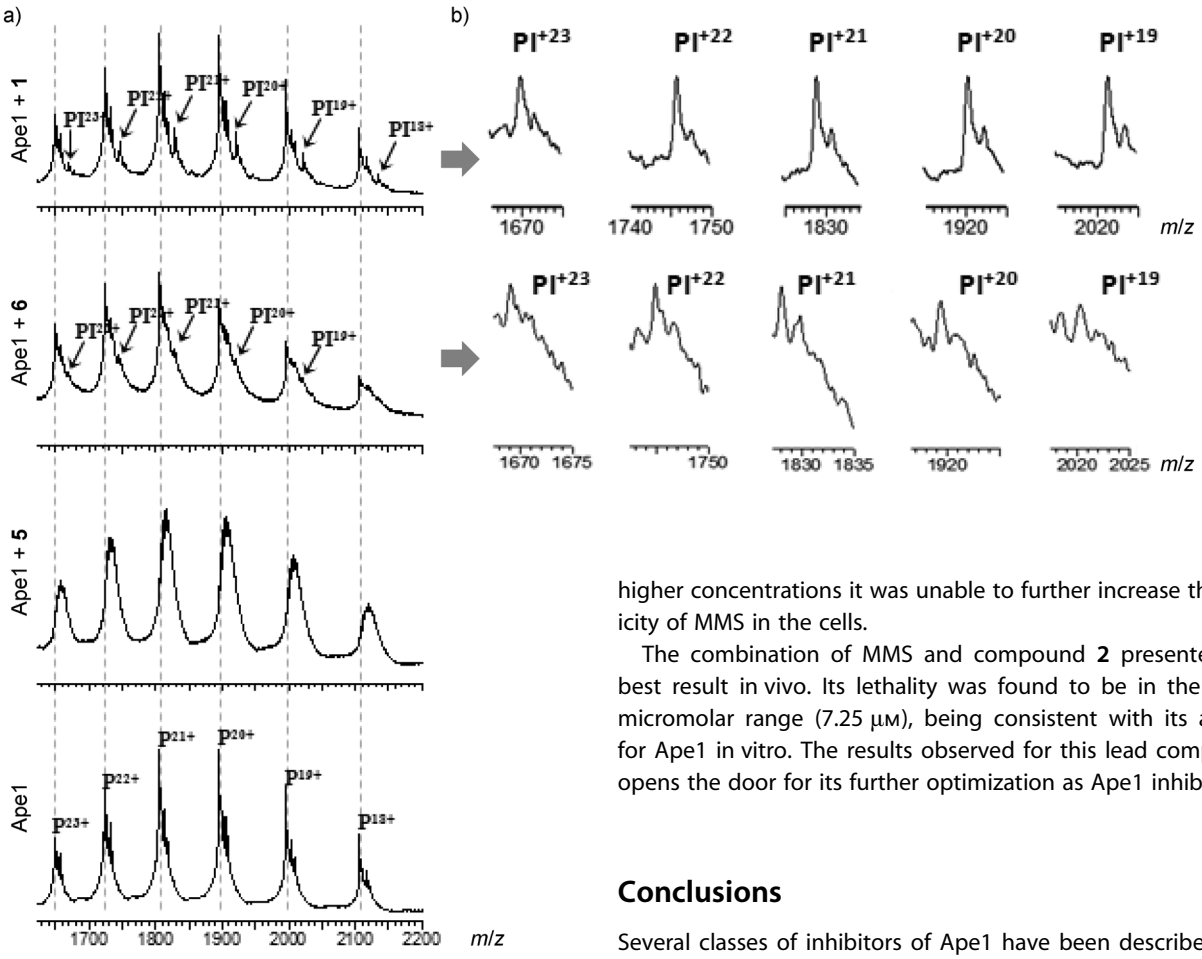

Figure 5. Complex formation identified by mass spectrometry: Ape1 (28 μM) was mixed with each inhibitor (140 μM) in ammonium acetate buffer (100 mM) and allowed to equilibrate at 4 °C for 1 h as described in the Experimental Section. a) ESIMS spectra of Ape1 alone (bottom) or with test compounds as indicated; b) zoom-in of the complex regions for Ape1 with compounds **6** and **1**.

nies by 15%, and, as shown in Figure 7, all six compounds enhance MMS cytotoxicity. However, no significant effect of the compounds alone was observed, indicating that none of them is toxic by itself in the concentrations used. Compounds **1** and **3** are less effective in sensitizing the tumor cell to MMS than the rest, requiring a concentration above 100 μM to obtain a 50% increase in cell death. The lower-sensitizing effect of compound **3** is consistent with its slightly smaller in vitro affinity for Ape1. However, the inefficiency of compound **1** was unexpected on the basis of its high ability to inhibit Ape1 activity in vitro. This observation suggested that it may not be able to cross cell membranes or it could be degraded before reaching its final target. Compound **4** had almost no effect on the cytotoxicity produced by MMS; only a small decrease in cell survival was observed at 50 μM, which was not incremented when cells were incubated with higher concentrations of **4**. Compound **5** exhibited an increasing capability to enhance the killing effect of MMS with an EC_{50} value ~50 μM, which is close to the IC_{50} value obtained in the in vitro experiments. Compound **6** showed a progressive lethal effect (until 50 μM), even if at higher concentrations it was unable to further increase the toxicity of MMS in the cells.

The combination of MMS and compound **2** presented the best result in vivo. Its lethality was found to be in the lower micromolar range (7.25 μM), being consistent with its affinity for Ape1 in vitro. The results observed for this lead compound opens the door for its further optimization as Ape1 inhibitor.

Conclusions

Several classes of inhibitors of Ape1 have been described previously. However, the specificity of some of these compounds for Ape1 remain unclear[27] or slightly controversial.[22b,28] Here, we have applied a docking-based virtual screening technique

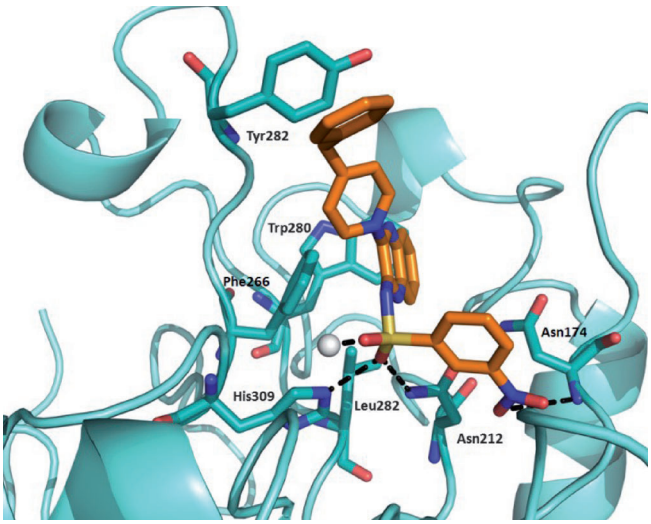

Figure 6. Average minimized structure of the Ape1–compound **2** complex after MD simulations. The protein is represented by the ribbon and loop structure in cyan; side chains of main interacting residues are colored by atom type: C cyan, N blue, and O red. For compound **2**, C atoms are in orange, N in blue, O in red, and S in yellow. Hydrogen atoms have been omitted for clarity. The grey sphere represents the Mg^{2+} cation. Dashed lines correspond to H-bond interactions.

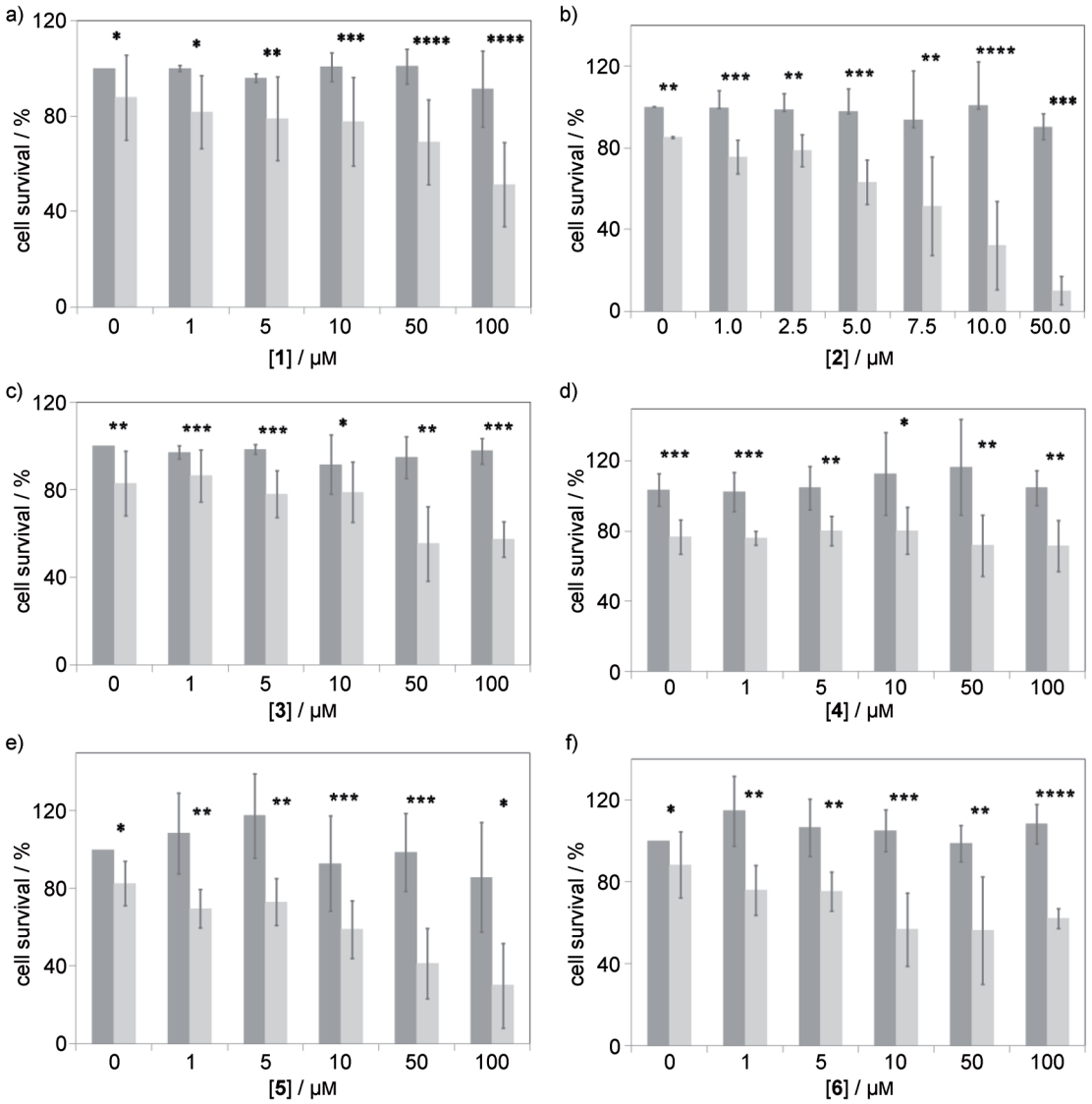

Figure 7. Effect of compounds **1**–**6** [panels a)–f), respectively] on HOS cell survival relative to untreated cells. Dark-grey bars show samples in the presence of various compound concentrations as indicated with no MMS added; light-grey bars show the same experiment in the presence of MMS (300 μM). MMS alone decreased the cell number to an average of 15%. Data represent the average ± SEM of three separate experiments performed in duplicate. Significance was determined by Student's *t* test, comparing cells treated with inhibitor in the absence and presence of MMS: $*p \leq 0.1$, $**p \leq 0.05$, $***p \leq 0.01$, $****p \leq 0.001$.

to select a concrete number of molecules (15 compounds) as hit compounds from a 4 million library, to become new and more potent Ape1 inhibitors. Six of these molecules selected from the ZINC database were found to be active. In particular, two of them are single-digit micromolar inhibitors against purified Ape1 (similar or even more potent than prior reported inhibitors), with the capacity to potentiate the cytotoxicity of a relevant DNA-damaging agent like MMS. The predicted binding modes highlighted the interaction with the metallic cation, which is energetically the most important, the hydrogen bonding with residues Asn174 and Asn212, and a network of hydrophobic contacts of the ligands with the Phe266 and Trp280. In the case of compound **2**, the most important interactions with Ape1 are mainly established through the quinoxaline core.

In summary, new compounds have been identified as potent leads of Ape1 DNA repair inhibition. The binding properties, cellular uptake, and solubility of these compounds can be further optimized to produce a subfamily of candidates with improved pharmacological properties. This new generation of compounds could lead to innovative drugs that may act as co-adjuvants in cancer chemotherapy.

Experimental Section

Materials: The *Ape1* gene (Homo sapiens) inserted into the pOTB7 vector was obtained from the Genomics Unit (Clone ID: IMAGE 2823545) at the Centro Nacional de Investigaciones Oncologicas (CNIO). The pet28a plasmid and the competent *E. coli* strains (DH5α, BL21(DE3), Rosetta) were purchased from Novagen. The en-

zymes and their corresponding buffers for cloning were purchased from Fermentas or New England Biolabs. The chemical reagents used for the expression and purification steps were purchased from Sigma, Merck, Bio-Rad or Fluka, and the SDS-PAGE standards, gels and buffers, from Invitrogen. HiTrap FF and size-exclusion (HiLoad Superdex 75 16/60) columns were purchased from GE Healthcare.

The oligonucleotides 5′-FAM-GAGAA[X]ATAGTCGCG-3′ and 3′-Q-CTCTTGTATCAGCGC-5′ (in which FAM is fluorescein, Q is Dabsyl, and X is ribitol,[51] an abasic (AP) site analogue) were custom-made by Sigma. Candidate compounds were purchased from various sources; in particular, compounds **1**, **5**, and **6** were obtained from IBScreen, compound **2** was obtained from Enamine, and compounds **3** and **4** were obtained from Specs. Stock solutions were prepared by dissolving them in DMSO at a final concentration of 1 mM and kept at −20 °C until further use. The fluorescence assay was carried out on a spectrofluorimeter multi-detection microplate reader BioTek FLx800 and a Jasco FP6200, in optical 96-well reaction plates. Human osteosarcoma cells, (ATCC Number HOS) were cultured in RPMI 1640 medium (Gibco) supplemented with 10% fetal bovine serum (Invitrogen). Methyl methanesulfonate (MMS) was obtained from Sigma.

Virtual screening (VS): All VS calculations were performed within the automated platform VSDMIP[34] (virtual screening data management on an integrated platform), see Figure 1. For clarity, we briefly describe below the main steps of the protocol (Scheme 1).

Receptor preparation: The crystal structure of PDB ID 1HD7[39] was selected as a receptor because no substantial differences were found in the active site amongst the available Ape1 structures and it presented the highest resolution structure (1.95 Å). All atoms other than the receptor were deleted except for the divalent metal (Pb^{2+}) in the active site, which, to resemble in vivo conditions, was replaced by magnesium, the preferred metal cofactor of the human Ape1 enzyme.[52] The AMBER8 ff99[53] force field was then used to assign atom types and charges for each atom in the receptor. Hydrogen atoms were added assuming standard protonation states of titratable groups, except for the key interacting residues, in which the hydrogen atoms were assigned based on the information given from the H++ web server.[54]

For this purpose, the receptor was submitted to the server and a Generalized Born (GB) model was used for the pKa calculation at pH 6.5 with 0.15 M salt concentration and internal and external dielectric constants of 4 and 80, respectively. The histidine residue His309, present in the binding site, was found to be protonated, which is consistent with an NMR study done by Lowry et al.[55]

Binding site definition and characterization: To delimit the binding site PDB codes 1HD7[39] (Ape1 apo form) and 1DEW[38] (Ape1 bound to DNA, subunit A) were superimposed, (RMSD among Cα atoms ≈0.28 Å) selecting a DNA fragment as the core around which to build the docking box by adding a 5.0 Å cushion to its maximum dimensions. This DNA fragment consists of an abasic sugar connected to a cytosine nucleotide residue to its 5′ end and including the following 5′ phosphate. An equally spaced grid of 0.375 Å was then built, and CGRID[42] was used to calculate receptor interaction fields, a 12–6 Lennard–Jones term. The electrostatic term was modeled with a sigmoidal dielectric screening function using typical atom probes (C, H, N, O, S, P, F, Cl, Br, and I) at each grid point. Next benzene, water, and methanol probes were docked with CDOCK[42] to generate intermolecular interaction energy maps aimed to capture the most favorable hydrophobic, hydrophilic, and H-bond interaction areas, respectively. These areas were further compressed into Gaussian functions using GAGA algorithm,[56] producing a sort of a negative image of the interaction site. The putative active ligands in the library must conform to this approximate shape.

Chemical library preparation: Ligands for VS consisted of a library with more than 4 million (4039777) non-redundant molecules, obtained from the publicly available ZINC database[40] in SMILES format.[57] Multiple protonation states and tautomeric forms were considered as implemented by default in ZINC database. The molecules were then processed within VSDMIP[34] as follows: a) conversion from SMILE to 3D MOL2 using CORINA,[58] b) atomic charges calculations with MOPAC[59] (MNDO ESP method) on every single structure provided by CORINA, and c) atom types assignment according to the AMBER ff99[53] force field and conformational analysis with ALFA.[60]

Filter 1: An initial filter was performed with the docking program DOCK[41] to quickly discard those molecules that do not geometrically fit within the binding site. The spheres needed by DOCK were generated previously with GAGA. We used DOCK contact as scoring function, normalizing the score values ($score_i$) by converted them into *ZScore* using mean (average score) and standard deviation (σ) values ($ZScore_i = (score_i - average\ score)/\sigma$). Only molecules with a *ZScore* beyond a cutoff value of 4 were selected and 2500 passed onto the next step.

Filter 2: Selected molecules from filter 1 were studied with the more accurate docking algorithm CDOCK.[42] CDOCK exhaustively docks each molecule within the binding site of the receptor using the interaction energy grids previously calculated with CGRID. This was achieved by an exhaustive exploration of the location and orientation of each molecule by positioning its centers of mass on grid points, where discrete rotations of 27° arc on each axe are performed. Finally, the energy for each pose was evaluated by the molecular mechanism force-field scoring function implemented in CDOCK, which besides including a 12–6 Lennard–Jones term and an electrostatic term modeled with a sigmoidal dielectric screening function, also accounts for ligand and receptor desolvations as well as for H-bonding interactions.[61]

Molecular dynamics simulations: The top ranked 100 molecules (according to the scoring function of CDOCK) were subjected to a more exhaustive binding free-energy estimation by a combination of MD trajectories and MM-GBSA[43] calculation on these trajectories. The 100 complexes were hydrated by using boxes containing explicit water molecules, energy minimized, heated (20 ps), and equilibrated (100 ps). Then, when the equilibration was reached, MD trajectories were continued for 2 ns. Structures were homogenously sampled at each ps and stored for post-processing. All the simulations were performed at constant pressure and temperature (1 atm and 300 K) with an integration time step of 2 fs. SHAKE[62] was used to constrain all the bonds involving H atoms at their equilibrium distances. Periodic boundary conditions and the Particle Mesh Ewald methods were applied to treat long-range electrostatic effects.[63] AMBER ff99[53] and TIP3P[64] force-fields were used in all cases. Finally, the effective binding free energies were qualitatively estimated with the MM-GBSA[43] approach, which calculates the free energy of binding as a sum of a molecular mechanics (MM) interaction term, a solvation contribution thorough a Generalized Born (GB) model and a Surface Area (SA) contribution to account for the nonpolar part of desolvation. A 12–6 Lennard–Jones term was used to model the MM contribution. For GB, the solute dielectric constant was set to 4, whereas that of the solvent was set to 80, and the dielectric boundary was calculated using a sol-

vent probe radius of 1.4 Å. The SA contribution was approximated as a linear relationship to the change in solvent accessible surface area (SASA):

$$\Delta G_{np} = a + b\Delta SASA$$

in which a is 0.092 kcal mol^{-1}, b is 0.00542 kcal mol^{-1} Å^{-2}, ΔG_{np} is the SA contribution, and the change in SASA refers to the complex SASA minus the sum of that of the receptor and the ligand alone. In addition, an interaction energy analysis between the ligands and the more relevant residues in the binding site were computed (with MM-GBSA) and are contained in Table 2. All the trajectories and analysis were performed using the AMBER 8 computer program and associated modules.[65]

Table 2. Interaction energies for compounds **1**–**6** as computed from MD simulations by the MM-GBSA approach.

Residue	E_{int} [kcal mol^{-1}]					
	1	**2**	**3**	**4**	**5**	**6**
Lys98	−1.75	−0.3	−5.97	−1.93	−4.85	−1.94
Tyr128	−0.23	−0.13	−0.16	−0.87	−1.99	−0.53
Asn174	−0.3	−2.45	−2.56	−1.98	−3.23	−0.34
Arg177	−3.91	−0.3	−2.81	−7.47	−4.25	−5.42
Asn212	−0.34	−6.27	−1.85	−0.17	−1.49	−0.23
Phe266	−1.94	−3.04	−3.55	−1.51	−2.94	−1.09
Thr268	−1.2	−0.56	−1.92	−2.51	−1.38	−0.84
Tyr269	−3.38	−3.31	−0.38	−1.44	−0.03	−1.22
Trp280	−2.1	−1.31	−2.2	−1.43	−3.65	−0.04
Leu282	−0.68	−1.4	−1.02	−0.14	−0.78	−0.09
Asp308	−0.04	6.07	2.33	0.54	0.08	−3.46
His309	−0.31	−7.83	−0.66	−0.42	−0.47	−0.5
Mg^{2+}	−59.51	−37.66	−41.01	−56.41	−60.33	−70.59

Selection of candidates: Among the 100 molecules with highest scoring values, a total of 15 were selected upon visual examination. All visualizations were done within the molecular graphics program PyMOL.[66] Averaged structures along the MD trajectories were obtained and minimized in vacuum with the ff99 force field, without periodic boundary conditions and during 1000 steps (the first 500 with the steepest descent method and the rest with the conjugated gradient) solely to alleviate the possible clashes that may be originated by averaging the coordinates. These structures were used for graphical representation and comparison of the binding modes. Finally, those 15 selected compounds were purchased and tested experimentally.

Inhibition of Ape1 activity

Protein production and purification: The in vitro assays were carried out using recombinant Ape1. The cDNA of full-length Ape1 (IMAGE:2823545) was amplified by PCR using primers 5′-CCC GGG **CAT ATG** CCG AAG CGT GGG AAA AAG-3′ and 5′-GCC **CTC GAG** TCA CAG TGC TAG GTA TAG GGT-3′, which incorporated the NdeI and XhoI restriction enzymes sites, respectively. The PCR product was cloned into the pet-28a(+) (Novagen) vector. The resulting construct, Ape1-pet28a, was verified by nucleic acid sequencing. The protein was expressed in the *E. coli* strain BL21 and once the culture reached an OD_{600} value of 0.6 it was induced by adding 1 mM IPTG during 3 h at 30 °C. The pellet from a 2 L culture was disrupted by sonication and centrifuged. The supernatant was filtered, loaded into a HiTrap FF column (GE Healthcare), and eluted with an imidazole gradient. Finally, the protein was loaded into a Superdex 75 16/60 column (GE Healthcare), with buffer NaCl (300 mM), Tris pH 8.0 (20 mM), DTT (1 mM), and glycerol (5% *v/v*).

Ape1 activity assay: The in vitro AP site cleavage assay was carried out by using a modified version of the protocol that had been described previously.[25,30] Briefly, the Ape1 enzyme (590 pM) was incubated with or without compounds (at 100 and 200 μM) in a buffer containing Tris·HCl (50 mM, pH 8.0), $MgCl_2$ (1 mM), NaCl (5 mM) and dithiothreitol (DTT; 2 mM) at room temperature for 30 min. The sequence 5′-FAM-GAGAA[X]ATAGTCGCG-3′ and its complementary oligonucleotide 3′-Q-CTCTTGTATCAGCGC-5′ were annealed to form a double-stranded DNA, and the reaction was initiated by addition of the annealed substrate at 50 nM, considering that this concentration was found to be below the K_M value of Ape1 in the reaction buffer and conditions (data not shown). Fluorescence readings were taken continuously after 30 min incubation at 20 °C, at excitation and emission wavelengths of 485 and 535 nm, respectively. Hits from the initial screen were analyzed further for inhibitory potency using decreasing dilutions of inhibitor. Each compound concentration was assayed in triplicate and experiments repeated three times. The percent of inhibition was calculated relative to DMSO-control samples. Bovine serum albumin (BSA) was used as a negative control (data not shown). The IC_{50} values were determined using OriginPro8 data analysis and graphic software, using the four-parameter equation as follows:

$$y = A_2 + \frac{A_1 - A_2}{1 + \left(\exp\frac{x - x_0}{d_x}\right)}$$

Each value is an average of three independent experiments with their corresponding standard errors.

DNA intercalation assay: A modified version of the ethidium bromide-based DNA binding assay was carried out essentially as described previously.[32,45] In brief, a mixture of labeled double-stranded DNA (500 nM) and ThO (2.5 μM) in Ape1 reaction buffer was prepared to a total volume of 400 μL. Compounds (at concentrations in the range of 100 pM to 100 μM) were added, and the fluorescence signal (excitation 501 nm and emission 530 nm) was measured after 10 min of incubation at room temperature in Tris·HCl (pH 7.5, 50 mM), NaCl (50 mM), $MgCl_2$ (10 mM) and EDTA (1 mM). Each compound concentration was assayed in triplicates. The percentage fluorescence was calculated relative to the total fluorescence acquired with double-stranded DNA and ThO (2.5 μM).

Mass analysis of the noncovalent complex between Ape1 and lead compounds: Mass spectrometry experiments were performed on Waters (Manchester, UK) instrument equipped with electrospray ionization, a travelling wave ion mobility cell and a time-of-flight mass analyzer. The Synapt G1 instrument was interfaced with a chip-based nano-ESI device, (Advion, Triversa Nanomate). This device contains a 96-well sample plate, 96 disposable spraying tips and an ESI chip with 100 nozzles in front of the inlet of the mass spectrometer. The instrument was operated in the automatic mode by using a contact closure signal. A spraying voltage of +1.76 kV and a sample pressure of 5.80 psi were applied. Each well was loaded with 10 μL of sample, from which a total of 4 μL was infused during 10 min. Operating conditions for the Synapt G1 mass spectrometer were as follows: cone voltage = 20 V; extraction cone = 5.5 V; source temperature = 20 °C; trap and transfer voltages = 6 V and 4 V, respectively. The ion mobility cell was filled with N_2, and an electric field was applied to the cell in the form of

waves (wave height = 9.5 V) that passed through the cell at 300 m s^{-1}. The bias voltage for ion introduction into the IMS cell was 15 V.

The Ape1 buffer was exchanged to 100 mM ammonium acetate pH 7 to prevent buffer interferences in the mass spectrometry experiments. Once we confirmed the mass spectrum for the native form of Ape1, we proceeded to analyze the noncovalent inhibitor–protein complexes. Ape1 (28 μM) was mixed with each inhibitor (**1** to **6**; 140 μM) separately and let to equilibrate at 4 °C for 1 h. Ape1 in the presence of DMSO or an inactive molecule (**16**) were used as Mass spectrum controls.

Cell culture cytotoxic assay: The effect of compounds **1**–**6** on the sensitivity of human osteosarcoma cells (HOS) to methyl methanesulfonate (MMS) was determined using colony formation assays as it has been previously described in Ape1 inhibition studies.[30] HOS cells were seeded at 10×10^3 cells per well density in 24-well, flat-bottomed plates and incubated in a humidified, 5% CO_2 incubator at 37 °C for 36 h. Compound solutions were diluted in the culture medium at final concentrations of 100, 50, 30, 20, 5, 2.5, and 1 μM, and were immediately used to treat the cells. Cells were incubated with the drug solutions for 6 h and then MMS (or the equivalent volume of the vehicle as negative controls) was added to a final concentration of 300 μM. After 2 h of incubation, the medium was replaced with fresh medium containing the same compound concentration, and cells were left to grow for an additional 16 h. The cells were then re-plated at densities of 2000 cells per well in 24-well plates and grown for 1 week until discrete colonies were formed. Colonies were washed twice with PBS and stained with a solution of 0.5% crystal violet and 20% ethanol. Cells were rinsed with deionized water and air dried. Stained colonies were counted in a ELx 800 Universal Microplate Reader (BioTek Instruments Inc.) and clonogenic survival was determined relative to untreated cells. Samples were assayed in duplicates and experiments repeated three times.

Acknowledgements

This work was supported by "Fondo de Investigaciones Sanitarias" (grant PI06/1250), by "Ministerio Ciencia e Innovación" (grant CTQ-2010-20541-C03-03), and by "Comunidad de Madrid" (SBIO-0214-2006 [BIPEDD] and S2010-BMD-2457 [BIPEDD2]). C.F. is grateful to Generalitat de Catalunya and Instituto de Salud Carlos III for an SNS Miguel Servet contract. R.G.-R. appreciates the MICINN contract from "Programa de Personal Técnico y de Apoyo 2008". F.M.R. was supported by a Junta de Ampliación de Estudios-Doc contract. A.M. acknowledges financial support from Fundación Severo Ochoa through the AMAROUTO program. We thank Dr. Marta Vilaseca for her advice in the MS experiments. Generous allocation of computer time at the Barcelona Supercomputer Center is gratefully acknowledged. Finally, this work is dedicated to the memory of Ángel Ramírez Ortiz, who has been a great mentor, colleague, and friend.

Keywords: antitumor agents · cancer · DNA repair · drug design · inhibitors

[1] a) M. Christmann, M. T. Tomicic, W. P. Roos, B. Kaina, *Toxicology* **2003**, *193*, 3; b) O. Fleck, O. Nielsen, *J. Cell Sci.* **2004**, *117*, 515; c) T. Lindahl, *Nature* **1993**, *362*, 709.

[2] a) H. Fung, B. Demple, *Mol. Cell* **2005**, *17*, 463; b) L. A. Loeb, B. D. Preston, *Annu. Rev. Genet.* **1986**, *20*, 201.

[3] D. B. Longley, P. G. Johnston, *J. Pathol.* **2005**, *205*, 275.

[4] D. M. Wilson III, M. Takeshita, A. P. Grollman, B. Demple, *J. Biol. Chem.* **1995**, *270*, 16002.

[5] a) A. R. Evans, M. Limp-Foster, M. R. Kelley, *Mutat. Res. DNA Repair* **2000**, *461*, 83; b) A. B. Robertson, A. Klungland, T. Rognes, I. Leiros, *Cell. Mol. Life Sci.* **2009**, *66*, 981.

[6] a) B. Demple, T. Herman, D. S. Chen, *Proc. Natl. Acad. Sci. USA* **1991**, *88*, 11450; b) D. S. Chen, T. Herman, B. Demple, *Nucleic Acids Res.* **1991**, *19*, 5907; c) J. H. Hoeijmakers, *Nature* **2001**, *411*, 366.

[7] a) K. M. Chou, M. Kukhanova, Y. C. Cheng, *J. Biol. Chem.* **2000**, *275*, 31009; b) K. M. Chou, Y. C. Cheng, *J. Biol. Chem.* **2003**, *278*, 18289; c) K. M. Chou, Y. C. Cheng, *Nature* **2002**, *415*, 655; d) D. Suh, D. M. Wilson III, L. F. Povirk, *Nucleic Acids Res.* **1997**, *25*, 2495; e) M. Z. Hadi, K. Ginalski, L. H. Nguyen, D. M. Wilson III, *J. Mol. Biol.* **2002**, *316*, 853.

[8] a) S. Xanthoudakis, G. Miao, F. Wang, Y. C. Pan, T. Curran, *EMBO J.* **1992**, *11*, 3323; b) T. Okazaki, U. Chung, T. Nishishita, S. Ebisu, S. Usuda, S. Mishiro, S. Xanthoudakis, T. Igarashi, E. Ogata, *J. Biol. Chem.* **1994**, *269*, 27855; c) K. K. Bhakat, T. Izumi, S. H. Yang, T. K. Hazra, S. Mitra, *EMBO J.* **2003**, *22*, 6299; d) L. J. Walker, C. N. Robson, E. Black, D. Gillespie, I. D. Hickson, *Mol. Cell. Biol.* **1993**, *13*, 5370.

[9] a) M. S. Bobola, A. Blank, M. S. Berger, B. A. Stevens, J. R. Silber, *Clin. Cancer Res.* **2001**, *7*, 3510; b) S. Kakolyris, L. Kaklamanis, K. Engels, S. B. Fox, M. Taylor, I. D. Hickson, K. C. Gatter, A. L. Harris, *Br. J. Cancer* **1998**, *77*, 1169; c) Y. Xu, D. H. Moore, J. Broshears, L. Liu, T. M. Wilson, M. R. Kelley, *Anti-Cancer Res.* **1997**, *17*, 3713; d) C. J. Herring, C. M. West, D. P. Wilks, S. E. Davidson, R. D. Hunter, P. Berry, G. Forster, J. MacKinnon, J. A. Rafferty, R. H. Elder, J. H. Hendry, G. P. Margison, *Br. J. Cancer* **1998**, *78*, 1128; e) D. H. Moore, H. Michael, R. Tritt, S. H. Parsons, M. R. Kelley, *Clin. Cancer Res.* **2000**, *6*, 602; f) B. Thomson, R. Tritt, M. Davis, M. R. Kelley, *J. Pediatr. Hematol. Oncol.* **2001**, *23*, 234; g) M. I. Koukourakis, A. Giatromanolaki, S. Kakolyris, E. Sivridis, V. Georgoulias, G. Funtzilas, I. D. Hickson, K. C. Gatter, A. L. Harris, *Int. J. Radiat. Oncol. Biol. Phys.* **2001**, *50*, 27; h) G. Fritz, S. Grosch, M. Tomicic, B. Kaina, *Toxicology* **2003**, *193*, 67.

[10] a) S. Kakolyris, A. Giatromanolaki, M. Koukourakis, L. Kaklamanis, P. Kanavaros, I. D. Hickson, G. Barzilay, V. Georgoulias, K. C. Gatter, A. L. Harris, *J. Pathol.* **1999**, *189*, 351; b) F. Puglisi, G. Aprile, A. M. Minisini, F. Barbone, P. Cataldi, G. Tell, M. R. Kelley, G. Damante, C. A. Beltrami, C. Di Loreto, *Anti-Cancer Res.* **2001**, *21*, 4041.

[11] A. Al-Attar, L. Gossage, K. R. Fareed, M. Shehata, M. Mohammed, A. M. Zaitoun, I. Soomro, D. N. Lobo, R. Abbotts, S. Chan, S. Madhusudan, *Br. J. Cancer* **2010**, *102*, 704.

[12] D. Wang, M. Luo, M. R. Kelley, *Mol. Cancer Ther.* **2004**, *3*, 679.

[13] a) L. J. Walker, R. B. Craig, A. L. Harris, I. D. Hickson, *Nucleic Acids Res.* **1994**, *22*, 4884; b) Y. Ono, T. Furuta, T. Ohmoto, K. Akiyama, S. Seki, *Mutat. Res.* **1994**, *315*, 55; c) D. S. Chen, Z. L. Olkowski, *Ann. N. Y. Acad. Sci.* **1994**, *726*, 306; d) J. R. Silber, M. S. Bobola, A. Blank, K. D. Schoeler, P. D. Haroldson, M. B. Huynh, D. D. Kolstoe, *Clin. Cancer Res.* **2002**, *8*, 3008.

[14] J. P. Lau, K. L. Weatherdon, V. Skalski, D. W. Hedley, *Br. J. Cancer* **2004**, *91*, 1166.

[15] D. R. McNeill, W. Lam, T. L. DeWeese, Y. C. Cheng, D. M. Wilson III, *Mol. Cancer Res.* **2009**, *7*, 897.

[16] M. L. Fishel, Y. He, A. M. Reed, H. Chin-Sinex, G. D. Hutchins, M. S. Mendonca, M. R. Kelley, *DNA Repair* **2008**, *7*, 177.

[17] a) S. Yang, K. Irani, S. E. Heffron, F. Jurnak, F. L. Meyskens, Jr., *Mol. Cancer Ther.* **2005**, *4*, 1923; b) H. Fung, B. Demple, *J. Biol. Chem.* **2011**, *286*, 4968.

[18] a) D. L. Ludwig, M. A. MacInnes, Y. Takiguchi, P. E. Purtymun, M. Henrie, M. Flannery, J. Meneses, R. A. Pedersen, D. J. Chen, *Mutat. Res.* **1998**, *409*, 17; b) S. Xanthoudakis, R. J. Smeyne, J. D. Wallace, T. Curran, *Proc. Natl. Acad. Sci. USA* **1996**, *93*, 8919.

[19] L. B. Meira, S. Devaraj, G. E. Kisby, D. K. Burns, R. L. Daniel, R. E. Hammer, S. Grundy, I. Jialal, E. C. Friedberg, *Cancer Res.* **2001**, *61*, 5552.

[20] J. P. Belzile, S. A. Choudhury, D. Cournoyer, T. Y. Chow, *Curr. Gene Ther.* **2006**, *6*, 111.

[21] A. M. Reed, M. L. Fishel, M. R. Kelley, *Future Oncol.* **2009**, *5*, 713.

[22] a) M. L. Fishel, Y. He, M. L. Smith, M. R. Kelley, *Clin Cancer Res.* **2007**, *13*, 260; b) M. L. Fishel, M. R. Kelley, *Mol. Aspects Med.* **2007**, *28*, 375.

[23] M. H. Luo, M. R. Kelley, *Anti-Cancer Res.* **2004**, *24*, 2127.

[24] P. Taverna, L. Liu, H. S. Hwang, A. J. Hanson, T. J. Kinsella, S. L. Gerson, *Mutat. Res. DNA Repair* **2001**, *485*, 269.
[25] S. Madhusudan, F. Smart, P. Shrimpton, J. L. Parsons, L. Gardiner, S. Houlbrook, D. C. Talbot, T. Hammonds, P. A. Freemont, M. J. Sternberg, G. L. Dianov, I. D. Hickson, *Nucleic Acids Res.* **2005**, *33*, 4711.
[26] J. D. Del Rowe, J. Bello, R. Mitnick, B. Sood, C. Filippi, J. Moran, K. Freeman, F. Mendez, R. Bases, *Int. J. Radiat. Oncol. Biol. Phys.* **1999**, *43*, 89.
[27] A. Bapat, M. L. Fishel, M. R. Kelley, *Antioxid. Redox Signaling* **2009**, *11*, 651.
[28] a) J. E. Guikema, E. K. Linehan, D. Tsuchimoto, Y. Nakabeppu, P. R. Strauss, J. Stavnezer, C. E. Schrader, *J. Exp. Med.* **2007**, *204*, 3017; b) T. T. Koll, S. S. Feis, M. H. Wright, M. M. Teniola, M. M. Richardson, A. I. Robles, J. Bradsher, J. Capala, L. Varticovski, *Mol. Cancer Ther.* **2008**, *7*, 1985.
[29] A. Bapat, L. S. Glass, M. Luo, M. L. Fishel, E. C. Long, M. M. Georgiadis, M. R. Kelley, *J. Pharmacol. Exp. Ther.* **2010**, *334*, 988.
[30] L. A. Seiple, J. H. Cardellina II, R. Akee, J. T. Stivers, *Mol. Pharmacol.* **2008**, *73*, 669.
[31] Z. Zawahir, R. Dayam, J. Deng, C. Pereira, N. Neamati, *J. Med. Chem.* **2009**, *52*, 20.
[32] A. Simeonov, A. Kulkarni, D. Dorjsuren, A. Jadhav, M. Shen, D. R. McNeill, C. P. Austin, D. M. Wilson III, *PLoS One* **2009**, *4*, e5740.
[33] F. A. De Wolff, *BMJ* **1995**, *310*, 1216.
[34] R. Gil-Redondo, J. Estrada, A. Morreale, F. Herranz, J. Sancho, A. R. Ortiz, *J. Comput.-Aided Mol. Des.* **2009**, *23*, 171.
[35] F. M. Ruiz, R. Gil-Redondo, A. Morreale, A. R. Ortiz, C. Fàbrega, J. Bravo, *J. Chem. Inf. Model.* **2008**, *48*, 844.
[36] J. Scheper, M. Guerra-Rebollo, G. Sanclimens, A. Moure, I. Masip, D. Gonzalez-Ruiz, N. Rubio, B. Crosas, O. Meca-Cortes, N. Loukili, V. Plans, A. Morreale, J. Blanco, A. R. Ortiz, A. Messeguer, T. M. Thomson, *PLoS One* **2010**, *5*, e11403.
[37] M. A. Gorman, S. Morera, D. G. Rothwell, E. de La Fortelle, C. D. Mol, J. A. Tainer, I. D. Hickson, P. S. Freemont, *EMBO J.* **1997**, *16*, 6548.
[38] C. D. Mol, T. Izumi, S. Mitra, J. A. Tainer, *Nature* **2000**, *403*, 451.
[39] P. T. Beernink, B. W. Segelke, M. Z. Hadi, J. P. Erzberger, D. M. Wilson III, B. Rupp, *J. Mol. Biol.* **2001**, *307*, 1023.
[40] J. J. Irwin, B. K. Shoichet, *J. Chem. Inf. Model.* **2005**, *45*, 177.
[41] I. D. Kuntz, J. M. Blaney, S. J. Oatley, R. Langridge, T. E. Ferrin, *J. Mol. Biol.* **1982**, *161*, 269.
[42] C. Pérez, A. R. Ortiz, *J. Med. Chem.* **2001**, *44*, 3768.
[43] W. Still, A. Tempczyk, R. Hawley, T. Hendrickson, *J. Am. Chem. Soc.* **1990**, *112*, 6127.
[44] D. M. Wilson III, D. Barsky, *Mutat. Res.* **2001**, *485*, 283.
[45] a) W. C. Tse, D. L. Boger, *Curr. Protoc. Nucleic Acid Chem.* **2005**, 8, 8.5; b) D. L. Boger, B. E. Fink, S. R. Brunette, W. C. Tse, M. P. Hedrick, *J. Am. Chem. Soc.* **2001**, *123*, 5878.
[46] a) J. A. Loo, *Mass Spectrom. Rev.* **1997**, *16*, 1; b) B. N. Pramanik, P. L. Bartner, U. A. Mirza, Y. H. Liu, A. K. Ganguly, *J. Mass Spectrom.* **1998**, *33*, 911.
[47] a) M. Karas, U. Bahr, T. Dulcks, *Fresenius J. Anal. Chem.* **2000**, *366*, 669; b) M. Wilm, M. Mann, *Anal. Chem.* **1996**, *68*, 1.
[48] J. L. Benesch, C. V. Robinson, *Curr. Opin. Struct. Biol.* **2006**, *16*, 245.
[49] D. R. McNeill, D. M. Wilson III, *Mol. Cancer Res.* **2007**, *5*, 61.
[50] M. D. Wyatt, D. L. Pittman, *Chem. Res. Toxicol.* **2006**, *19*, 1580.
[51] R. Eritja, P. A. Walker, S. K. Randall, M. F. Goodman, B. E. Kaplan, *Nucleosides Nucleotides* **1987**, *6*, 803.
[52] G. Barzilay, C. D. Mol, C. N. Robson, L. J. Walker, R. P. Cunningham, J. A. Tainer, I. D. Hickson, *Nat. Struct. Biol.* **1995**, *2*, 561.
[53] W. D. Cornell, P. Cieplak, C. I. Bayly, I. R. Gould, K. M. Merz, D. M. Ferguson, D. C. Spellmeyer, T. Fox, J. W. Caldwell, P. A. Kollman, *J. Am. Chem. Soc.* **1995**, *117*, 5179.
[54] a) J. C. Gordon, J. B. Myers, T. Folta, V. Shoja, L. S. Heath, A. Onufriev, *Nucleic Acids Res.* **2005**, *33*, W368; b) J. Myers, G. Grothaus, S. Narayanan, A. Onufriev, *Proteins* **2006**, *63*, 928; c) R. Anandakrishnan, B. Aguilar, A. V. Onufriev, *Nucleic Acids Res.* **2012**, *40*, W537.
[55] D. F. Lowry, D. W. Hoyt, F. A. Khazi, J. Bagu, A. G. Lindsey, D. M. Wilson III, *J. Mol. Biol.* **2003**, *329*, 311.
[56] P. A. Kollman, I. Massova, C. Reyes, B. Kuhn, S. Huo, L. Chong, M. Lee, T. Lee, Y. Duan, W. Wang, O. Donini, P. Cieplak, J. Srinivasan, D. A. Case, T. E. Cheatham III, *Acc. Chem. Res.* **2000**, *33*, 889.
[57] D. Weininger, *J. Chem. Inf. Comput. Sci.* **1988**, *28*, 31.
[58] CORINA, Molecular Networks GmbH, **2000**, Computerchemie Langemarckplatz 1, Erlangen (Germany).
[59] J. J. Stewart, *J. Comput. Aided Mol. Des.* **1990**, *4*, 1.
[60] R. Gil-Redondo, MSc thesis, **2006**, UNED Madrid (Spain).
[61] A. Morreale, R. Gil-Redondo, A. R. Ortiz, *Proteins* **2007**, *67*, 606.
[62] J. Ryckaert, G. Ciccotti, H. Berendsen, *J. Comput. Phys.* **1977**, *23*, 327.
[63] T. Darden, D. York, L. Pedersen, *J. Chem. Phys.* **1993**, *98*, 10089.
[64] W. Jorgensen, J. Chandrasekhar, J. Madura, R. Impey, M. Klein, *J. Chem. Phys.* **1983**, *79*, 926.
[65] S. L. McGovern, E. Caselli, N. Grigorieff, B. K. Shoichet, *J. Med. Chem.* **2002**, *45*, 1712.
[66] W. L. DeLano, DeLano Scientific, Palo Alto, CA (USA) **2002**.

Received: August 2, 2012
Revised: September 26, 2012
Published online on October 25, 2012

F. M. Ruiz, S. M. Francis, M. Tintoré, R. Ferreira, R. Gil-Redondo, A. Morreale, Á. R. Ortiz, R. Eritja, C. Fàbrega**

■■–■■

Receptor-Based Virtual Screening and Biological Characterization of Human Apurinic/Apyrimidinic Endonuclease (Ape1) Inhibitors

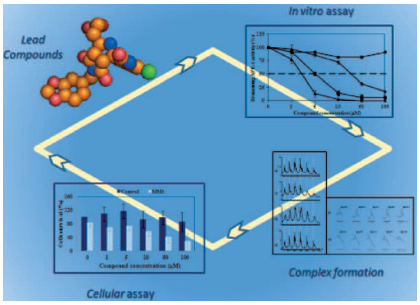

Rational design: Six compounds were identified as potential human apurinic/apyrimidinic endonuclease inhibitors by the use of docking-based virtual screening. The compounds show in vitro inhibitory activity in the low-to-medium micromolar range and also potentiate the cytotoxicity of methyl methanesulfonate in fibrosarcoma cells. This study opens the door to the development of a new generation of Ape1 inhibitors.

Chapter 2

Development of a Novel Fluorescence Assay Based on the Use of the Thrombin Binding Aptamer for the Detection of O^6-alkylguanine–DNA Alkyltransferase Activity

Development of a Novel Fluorescence Assay Based on the Use of the Thrombin Binding Aptamer for the Detection of O^6-alkylguanine–DNA Alkyltransferase Activity

Maria Tintoré,[1] Anna Aviñó,[1] Federico M. Ruiz,[2] Ramón Eritja[1] and Carme Fàbrega[1*]

Journal of Nucleic Acids (2010), Article ID 632041, 9 pages. DOI: 10.4061/2010/632041.

Estimated impact factor: **1.52**

[1] Institute for Research in Biomedicine (IRB Barcelona), IQAC-CSIC, CIBER-BBN Networking Centre on Bioengineering Biomaterials and Nanomedicine, Cluster Building, Baldiri i Reixac 10, E-08028 Barcelona, Spain.

[2] Chemical and Physical Biology CIB (CSIC), Ramiro de Maeztu 9, 28040 Madrid, Spain.

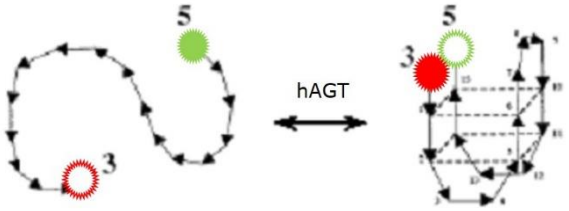

In order to find inhibitors of the repair activity of hAGT to be used as adjuvants in chemotherapy, we developed a real-time fluorescence hAGT activity assay for the *in vitro* evaluation of hAGT activity. This method is based on the detection of the conformational changes of the α-thrombin-binding aptamer (TBA). The quadruplex structure of TBA is disrupted when a central guanine of one of its two tetrads is replaced by an O^6-methyl-guanine. The TBA sequence contains a fluorophore and a quencher attached to the opposite ends. In the unfolded structure, the fluorophore and the quencher are separated. When hAGT removes the methyl group from the alkylated guanine, TBA folds back immediately into its quadruplex structure. Consequently, the fluorophore and the quencher come into close proximity, thereby resulting in a decrease in fluorescence intensity. In this chapter we developed a new method to quantify the hAGT activity without using radioactivity. This new fluorescence resonance energy transfer assay has been designed to detect the conformational change of TBA that is induced by the removal of the O^6-methyl group.

In addition, we include as annex of this chapter a review on the chemical modifications that affect the structure of TBA and its biomedical applications, written by our group.

SAGE-Hindawi Access to Research
Journal of Nucleic Acids
Volume 2010, Article ID 632041, 9 pages
doi:10.4061/2010/632041

Research Article

Development of a Novel Fluorescence Assay Based on the Use of the Thrombin-Binding Aptamer for the Detection of O^6-Alkylguanine-DNA Alkyltransferase Activity

Maria Tintoré,[1] Anna Aviñó,[1] Federico M. Ruiz,[2] Ramón Eritja,[1] and Carme Fàbrega[1]

[1] *Institute for Research in Biomedicine (IRB Barcelona) IQAC-CSIC, CIBER-BBN Networking Centre on Bioengineering Biomaterials and Nanomedicine, Cluster Building, Baldiri i Reixac 10, 08028 Barcelona, Spain*
[2] *Chemical and Physical Biology CIB (CSIC), Ramiro de Maeztu 9, 28040 Madrid, Spain*

Correspondence should be addressed to Carme Fàbrega, carme.fabrega@irbbarcelona.org

Received 11 June 2010; Accepted 17 July 2010

Academic Editor: Ashis Basu

Human O^6-alkylguanine-DNA alkyltransferase (hAGT) is a DNA repair protein that reverses the effects of alkylating agents by removing DNA adducts from the O^6 position of guanine. Here, we developed a real-time fluorescence hAGT activity assay that is based on the detection of conformational changes of the thrombin-binding aptamer (TBA). The quadruplex structure of TBA is disrupted when a central guanine is replaced by an O^6-methyl-guanine. The sequence also contains a fluorophore (fluorescein) and a quencher (dabsyl) attached to the opposite ends. In the unfolded structure, the fluorophore and the quencher are separated. When hAGT removes the methyl group from the central guanine of TBA, it folds back immediately into its quadruplex structure. Consequently, the fluorophore and the quencher come into close proximity, thereby resulting in decreased fluorescence intensity. Here, we developed a new method to quantify the hAGT without using radioactivity. This new fluorescence resonance energy transfer assay has been designed to detect the conformational change of TBA that is induced by the removal of the O^6-methyl group.

1. Introduction

Alkylating agents are chemotherapeutic anticancer drugs that produce their cytotoxic effect by generating adducts at multiple sites in DNA [1]. A subset of alkylating agents, which includes nitrosoureas and temozolamide, have a preference for alkylating guanine at the O^6 position, which is the most relevant in terms of mutagenesis and carcinogenesis [2–9]. In particular, 1,3-bis-(2-chloroethyl)-1-nitrosourea (BCNU) attacks initially at the O^6 guanine position, causing its rearrangement in a cyclic intermediate thus giving rise to N^1,O^6-ethanoguanine [10]. Finally, a cross-link with the opposite cytosine is formed, and, as a consequence, DNA replication is blocked, producing G2/M arrest [11]. In addition to the well-known side effects and limitations of chemotherapeutic agents, these substances also present problems of acquired tumor resistance. In particular, the DNA-repair human O^6-alkylguanine DNA alkyltransferase (hAGT or MGMT) is responsible for removing alkyl adducts from the O^6 position of guanines, thereby blocking the cytotoxic effects of the alkylating agents and making a crucial contribution to the resistance mechanism [12–14]. It is well established that tumor cells show greater expression of this protein than healthy cells. Thus, this increased expression appears to be predictive of a poor response to chemotherapeutic drugs. This effect has been observed in a large number of cancers, ranging from colon cancer, lung tumors, breast cancer, pancreatic tumors, non-Hodgkin's lymphoma, myeloma, and glioblastoma multiforme, among others [15–17]. In addition methylation of the hAGT promoter and consequently the complete depletion of hAGT, it has been associated with longer survival in patients with gliomas undergoing combined radiation-chemotherapy treatment [18, 19]. Therefore, pharmacological inhibition of hAGT has the potential to enhance the cytotoxicity of a diverse range of anticancer agents [20].

hAGT is a 22-kDa (207 AA) DNA-binding protein that contains a highly conserved internal cysteine, which acts as the acceptor site for alkyl groups. The S-alkyl-Cys formed is not regenerated and the protein, which behaves as a suicidal enzyme, inactivates itself in the dealkylation process [21, 22]. This single turnover of hAGT renders it vulnerable to inactivation. On the basis of this observation, intense research effort has been devoted to the identification of small molecules capable of inhibiting hAGT activity and significantly enhancing the cytotoxic effect of BCNU in prostate, breast, colon, and lung tumor cells [20].

Several methods are available to characterize the mechanism of action of hAGT and its activity. Moreover, they also have the capacity to evaluate the capacity of small molecules to inhibit hAGT. Most of these methods are based on radioactivity assays while others are based on multiple-step enzymatic reactions [23–26].

G-quadruplexes are a family of four-stranded DNA structures stabilized by the stacking of guanine tetrads, in which four planar guanines form a cyclic array of hydrogen bonds [27]. These G-rich regions are connected by lateral, central, or diagonal loops of diverse sizes and composition that form base-pairing alignments, which in turn stack with the terminal G-tetrads, thus further stabilizing G-quadruplex structures [28]. Another key element in G-quadruplex formation is the presence of monovalent cations, which stabilize the negative electrostatic potential created by the guanine O^6 oxygen atoms within the quadruplex core [29, 30]. However, most divalent cations have the capacity to induce the dissociation of G-quadruplex structures [31]. Finally, modifications in the base composition of the tetrads are poorly tolerated by these structures. As an example, inosine [32] and O^6-methylguanine [33], both nonnatural bases can form a smaller number of hydrogen bonds and thus destabilize the G-quadruplex.

Given the potential relevance of hAGT as a prognostic marker of cancer and as a therapeutic target, and that its substrate O^6-methylguanine disrupts the formation of G-quadruplex structures [33], here, we developed a new fluorescence activity assay for hAGT. For this purpose, we selected the thrombin-binding aptamer (TBA) as our G-quadruplex model. TBA is a well-known 15 mer that adopts a chair-like structure consisting of two G-tetrads connected by two lateral TT loops and a central TGT loop [34]. The modification of its sequence in positions 5 or 6 by replacing a guanine of the tetrad for an O^6-methylguanine disrupts folding, leaving it in an extended conformation. Giving that the two conformations bring the two ends of TBA together take them further apart, our working hypothesis was that the incorporation of fluorescence probes results in a measurable change in intensity. The final aim of this fluorescence assay was to measure the DNA repair activity of hAGT and thus facilitate the search for new and more potent inhibitors which enhance chemotherapeutic drugs. Although several methods have been described to quantify hAGT activity [23–26], none of them use the conformational change of G-quadruplex for this purpose. Here, we describe the development of a straightforward, rapid, one-step fluorescence resonance energy transfer (FRET) assay.

2. Materials and Methods

2.1. Chemicals. 5′-Fluorescein CE phosphoramidite (6-FAM), 3′-Dabsyl CPG, O^6-methylguanine (O^6-MeG) and G^{dmf} phosphoramidites were purchased from Link technologies (UK) and Glen Research (USA). O^6-methylguanine was protected with the isobutyryl group [35]. Standard phosphoramidites and ancillary reagents were purchased from Applied Biosystems (Europe).

The matrices for MALDI-TOF experiments were 2′,4′,6′-trihydroxiacetophenone monohydrate (THAP) and ammonium citrate dibasic.

Solvents for chromatographic analysis were prepared using triethylamine, acetic acid, and acetonitrile as mobile phase. All other chemicals were of analytical reagent grade and were used as supplied. Ultrapure water (Millipore, USA) was used in all experiments.

2.2. Instrumentation. Semipreparative reverse phase (RP) HPLC was performed on a Waters chromatography system using Nucleosil semipreparative 120 C18 (250 × 8 mm) columns. Analytical RP-HPLC was performed using an XBridge OST C18 2.5 μm column and a Nucleosil Analytical column 120 C18 (250 × 4 mm). Oligonucleotides were detected by UV absorption at 260 nm. Mass spectra were recorded on a MALDI Voyager DE^{TM} RP time-of-flight (TOF) spectrometer (Applied Biosystems, USA) with a nitrogen laser at 337 nm using a 3-ns pulse. Fluorometric measurements were performed on a spectrofluorometer multidetection microplate reader Biotek FL × 800 and a Jasco FP6200. Molecular absorption spectra between 220 and 550 nm were recorded with a Jasco V650 spectrophotometer. The temperature was controlled with a Jasco ETC 272T Peltier device. Hellma quartz cuvettes (0.5 and 1.0 cm path length, 500 or 1000 μL volume) were used.

2.3. Oligonucleotide Synthesis. Oligonucleotide sequences (shown in Table 1) were synthesized on an ABI 3400 DNA Synthesizer (Applied Biosystems, USA) using a 200-nmol scale synthesis and following the standard protocols. We used dimethylformamidino-protected guanine G^{dmf} phosphoramidite for all the syntheses. 5′-Fluorescein CE phosphoramidite (6-FAM), O^6-methylguanine (O^6-MeG) and G^{dmf} phosphoramidites were from commercial sources. The isobutyryl group was used to protect the amino group of O^6-MeG [35]. The quencher group was introduced at the 3′ end using the controlled pore glass functionalized with a 3′-Dabsyl derivative CPG. O^6-MeG-containing oligonucleotides were deblocked using concentrated aqueous ammonia overnight at room temperature following the manufacturer's instructions. The resulting products were desalted by Sephadex G-25 (NAP-10, GE Healtcare, USA) and purified by reversed-phase HPLC using Nucleosil columns. The yields and purities obtained for the products were around 85% for 5-O^6-MeG-TBA and 6-O^6-MeG-TBA, and >98% for the rest of the sequences. The length and homogeneity of the oligonucleotides were checked by MALDI-TOF.

Table 1: Sequences of TBA oligonucleotide derivatives used in the development of the hAGT fluorescence assay. ^{Me}**G** represents O^6-methylguanine. MB represents the fluorophore group (FAM), labelled in the 5′ end, and the quencher group (Dabsyl), labelled in the 3′ end of the sequence.

Abbreviation	Sequence
TBA	5′-GGT TGG TGT GGT TGG-3′
5-O^6-MeG-TBA	5′-GGT T ^{Me}**G**G TGT GGT TGG-3′
6-O^6-MeG-TBA	5′-GGT TG ^{Me}**G**TGT GGT TGG-3′
C-TBA	5′-CCA ACC ACA CCA ACC-3′
MB-TBA	5′-FAM-GGT TGG TGT GGT TGG-Dabsyl-3′
MB-5-O^6-MeG-TBA	5′-FAM-GGT T ^{Me}**G**G TGT GGT TGG- Dabsyl-3′
MB-6-O^6-MeG-TBA	5′-FAM-GGT TG ^{Me}**G** TGT GGT TGG- Dabsyl-3′
3-HP-TBA	5′-A CCT TTT GGT TGG TGT GGT TGG-3′
6-HP-TBA	5′-C CAA CCT TTT GGT TGG TGT GGT TGG-3′
9-HP-TBA	5′-A CAC CAA CCT TTT GGT TGG TGT GGT TGG-3′

5-O^6-MeG-TBA [M] = 4731.7 (expected 4737.8), **6-O^6-MeG-TBA** [M] = 4729.9 (expected 4737.8), **MB-5-O^6-MeG-TBA** [M] = 5828.49 (expected 5826.0), **MB-6-O^6-MeG-TBA** [M] = 5826.80 (expected 5826.0).

The DNA-strand concentration was determined by absorbance measurements (260 nm) by calculating extinction coefficients. Oligonucleotide samples were kept at 4°C until further use. Double-stranded O^6-MeG-TBA was formed by annealing equimolar concentrations of complementary oligonucleotide strands at 72°C for 5 min and then allowed to slowly cool to room temperature.

2.4. Melting Temperature Studies. Melting curves were measured by monitoring the absorbance hyperchromicity at 295 and 495 nm in a JASCO V650 spectrophotometer equipped with a Peltier temperature-controlling unit. UV/Vis absorption spectra were recorded at 1°C/min intervals, with a 1-min equilibration time at each temperature; the sample was heated over the range 20–80°C. The buffer solutions used were 10 mM sodium cacodylate pH 7.0 and 100 mM KCl. Sample concentration was around 4 μM. Each sample was allowed to equilibrate at the initial temperature without any external control of temperature for 5 min before the melting experiment began. The melting temperatures (Tm) are the average value of at least one pair of Tm experiments.

2.5. CD Spectra. Samples were prepared as described for the melting experiments by UV spectroscopy. Measurements were conducted in 10 mM sodium cacodylate pH 7.0 and 100 mM KCl. Sample concentration was between 1–4 μM. The CD spectra were recorded on a Jasco J-810 spectropolarimeter attached to a Julabo F/25HD circulating water bath in 1 cm path-length quartz cylindrical cells. Spectra were recorded at room temperature using a 100 nm/min scan rate, a spectral band width of 1 nm and a time constant of 4 s. All the spectra were corrected with the buffer blank and plotted using Origin software.

2.6. Human Recombinant hAGT Protein. Full-length hAGT was overexpressed and purified as previously described [36]. Briefly, hAGT protein cloned in the pet-21a (+) (Novagen) vector was expressed in the *E. coli* strain Rosetta. Once the culture reached an OD_{600} value of 0.98, hAGT was induced by adding 1 mM IPTG (Sigma) and left for 4 h at 30°C. The pellet from a 1-L culture was disrupted by sonication and centrifuged. The supernatant was filtered, loaded into a HiTrap FF column (GE Healthcare) with buffer 350 mM NaCl, 20 mM Tris pH 8, 20 mM imidazole, and 1 mM BME, and then eluted with an imidazole (Fluka) gradient up to 500 mM in the same buffer. Finally, the protein was loaded into a Superdex 75 16/60 column (GE Healthcare) with the following buffer: 200 mM NaCl (Merck), 20 mM Tris pH 8.0 (Merck), 10 mM DTT (Sigma) and 0.1 mM EDTA (Sigma). The protein was concentrated to 2 mg/mL in this buffer and kept at −20°C in the presence of 40 % glycerol. The same protocol was used for the purification of the inactive mutant hAGT-C145S, cloned in the pet-28a (+) vector (Novagen), and expressed in the *E. coli* strain BL21.

2.7. HPLC hAGT Assay. Assays were conducted using double-stranded 5-O^6-MeG and 6-O^6-MeG TBA paired with TBA complementary sequence or using single-stranded 5-O^6-MeG and 6-O^6-MeG TBA.

In order to measure the dealkylation of O^6-MeG, 50 pmol of the O^6-MeG-TBA substrates were incubated with a range of concentration of hAGT (16 nM to 1.6 μM) to a final volume of 120 μL in a reaction buffer (200 mM NaCl, 50 mM Tris pH 8.0, 1 mM DTT, and 5 mM EDTA). Several incubation times were tested (30, 60, 90, 120, 360, and 1440 min) at 37°C and the reaction was stopped by heating the samples at 72°C for 5 min. The reaction products were analyzed by HPLC on a Nucleosil analytical column at 60°C or room temperature, depending on the substrates used in the experiment (double- or single-stranded TBA). The HPLC flow rate was 1 mL/min, and a gradient of 10%–40% acetonitrile for 20 min was used.

2.8. Fluorescence Assay for hAGT Activity. The fluorescence assay was performed in a multidetection microplate reader biotek FLx800 in optical 96-well Optical btm reaction plates

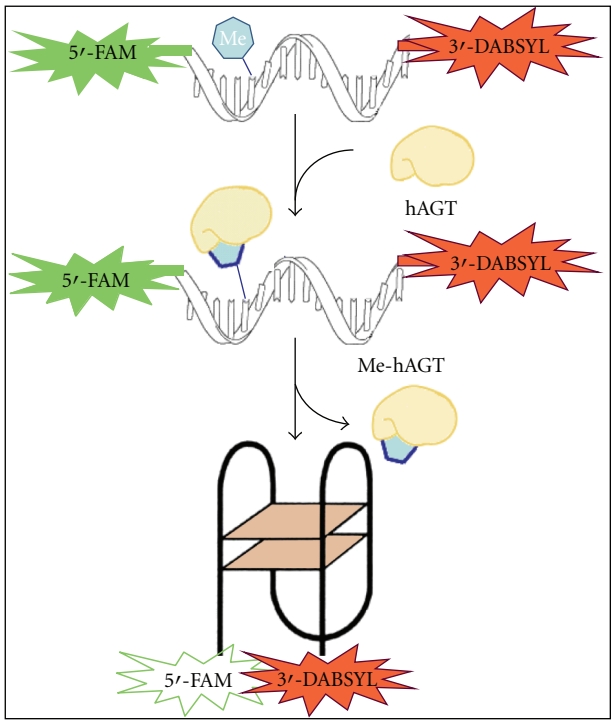

Figure 1: Scheme of fluorescence-based hAGT assay. The substrate is the thrombin-binding aptamer modified by an O^6-methylguanine (Me) in extended conformation, with a fluorophore and quencher in the opposite ends of the sequence. The refold of the G-quadruplex structure of TBA is dependent on the removal of the methyl adduct by alkyl-guanine-DNA-O^6-alkyltransferase (hAGT). This repair moves the quencher and the fluorophore molecules in close proximity and blocks fluorescence.

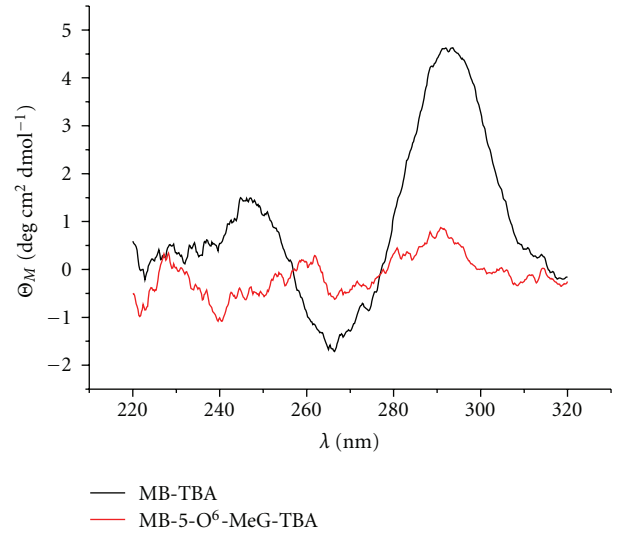

Figure 2: CD spectra of MB-TBA and MB-5-O^6-MeG-TBA at 25°C. Buffer conditions: 10 mM sodium cacodylate pH 7.0 and 100 mM KCl, sample concentration 1 μM.

(Nunc, USA). Full-length hAGT recombinant protein (207 amino acids) was used for the assay and the hAGT-C145S inactive mutant was used as a negative control. The reaction was performed in a total volume of 50 μL in each well, incubating increasing concentrations of hAGT (5, 10, 20, 40, 60, and 80 nM) enzyme in reaction buffer (200 mM NaCl, 50 mM Tris pH 8.0, 1 mM DTT, 5 mM EDTA, and 20 mM KCl). The assay of hAGT was then initiated by the addition of 5 μL of different concentrations (5, 10, 25, and 50 nM) of fluorescently labelled MB-O^6-MeG-TBA substrate and this solution was then placed in a microplate reader system. Fluorescence was measured every minute for 20 min or 40 min at excitation and emission wavelengths of 485 and 535 nm, respectively. Averages over three readings were taken for each condition tested. Each experiment was performed in triplicate.

3. Results and Discussion

The aim of this study was to develop a real-time hAGT activity assay based on the detection of differences between extended and folded conformations of TBA. Our working hypothesis was that the quadruplex structure of TBA is disrupted when a central guanine is replaced by an O^6-methylguanine. The TBA sequence also contains a fluorophore and a quencher group attached to 5′ or 3′ end, respectively. In the presence of O^6-methylguanine, methylated TBA unfolds and the fluorophore and the quencher become physically separated beyond the Förster distance. When the repair protein hAGT is added to the methylated aptamer, the enzyme removes the methyl group from the mutated guanine, thus allowing TBA to fold back into its chair-like conformation. As a result, the quencher comes closer to the fluorophore and blocks its fluorescence, as illustrated in Figure 1. This loss of fluorescence is quantified as a direct measurement of hAGT activity.

3.1. Synthesis of Modified G-Quadruplex Sequences. The G-quadruplex sequences used in this study are shown in Table 1. Oligonucleotide synthesis was performed by the solid-phase 2′-cyanoethyl-phosphoramidite method [37]. Ammonia treatment was performed at room temperature overnight to minimize decomposition of O^6-methylguanine. For the same reason, the dimethylformamidino group was selected for the protection of 2′-deoxyguanosine [38]. The sequences were characterized by HPLC and mass spectrometry, which provided the expected molecular weights. The yields of the isolated molecular beacon oligonucleotides after HPLC purification and desalting were in the range of those obtained for unmodified oligonucleotides.

3.2. Thermal Stability of Methylguanine-Modified TBA. In order to induce the unfolding of the quadruplex structure of TBA, we introduced an O^6-methyl-guanine at position 5 or 6 of TBA. Melting curves of the modified sequences were performed by UV spectroscopy and compared with the unmodified sequence. These experiments were carried

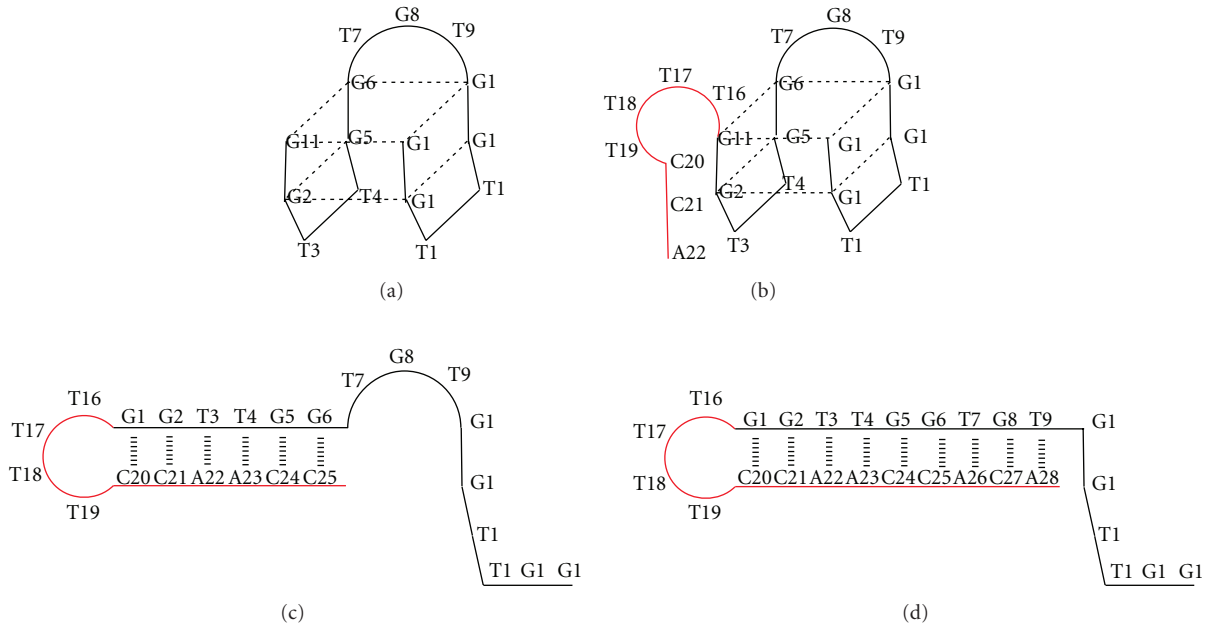

Figure 3: Schematic representation of the structure of several derivatives of thrombin-binding aptamers (TBAs) prepared in this study. TBA sequence is shown in black, and T4 loop with different sizes of the complementary sequences are shown in red. (a) Native TBA; (b) TBA-hairpin containing three overhanging complementary nucleotides (3-HP-TBA); (c) TBA-hairpin containing six overhanging complementary nucleotides (6-HP-TBA); (d) TBA-hairpin containing nine overhanging complementary nucleotides (9-HP-TBA). Between 3–6 complementary nucleotides are required to disrupt the intramolecular quadruplex to form an intramolecular duplex.

out at pH 7 in buffer containing 10 mM sodium cacodylate and 100 mM KCl, which is predicted to stabilize G-quadruplexes structures. We did not observe a melting temperature at 295 nm for 5-O^6-MeG-TBA or 6-O^6-MeG-TBA and the corresponding molecular beacons (see Figures S1–S4 in Supplementary Data Material available online at doi: 10.4061/2010/632041). The absence of this transition is consistent with the disruption of the quadruplex structure. These results contrast with the melting temperature of native TBA (Tm 48°C) and MB-TBA (Tm 46°C). Moreover, circular dicroism of methylated-TBA derivatives did not show the presence of the maximum at 295 nm, which is characteristic of the antiparallel quadruplex of TBA (Figure 2 and Figure S5). These results confirmed that methylation of guanine in either of the two positions of the TBA sequence prevents the formation of the chair structure. This observation confirms our working hypothesis.

Given that the DNA repair activity exerted by hAGT is higher in double-stranded DNA than single-stranded DNA [39], we studied the stability and the quadruplex formation of elongated self-complementary TBA derivatives (see Table 1). We designed several TBA oligonucleotides elongated in their 3′ end with a subset of self-complementary sequences of diverse sizes. The purpose of these elongations was to check whether the extended sequences have the capacity to form a double strand helix of different lengths and strengths with themselves without disrupting the chair-like structure. For 6-HP-TBA and 9-HP-TBA, we found that the corresponding Tm at 260 nm were 63°C and 71.8°C, respectively. This observation confirms our hypothesis of a double helix structure that increases in strength as the sequence length increases. However, we did not detect a melting temperature of these two sequences at 295 nm. The absence of a transition at 295 nm is consistent with the absence of an antiparallel quadruplex structure. In contrast, 3-HP-TBA, corresponding to an overhang of only 3 nucleotides, gave a melting temperature of 46°C at 295 nm, which is slightly but similar to that obtained for natural TBA. This result indicates that 3-HP-TBA forms an antiparallel quadruplex instead of a duplex because the overhang is too short to break the chair-like structure. Circular dichroism confirms the quadruplex structure of 3-HP-TBA and the absence of quadruplex structure in 6-HP-TBA and 9-HP-TBA (Figure S6). Models of all these structures are shown in Figure 3.

3.3. HPLC Analysis of DNA Repair Activity of hAGT. In order to observe the efficiency of hAGT to remove alkyl groups from single-stranded oligonucleotides, we performed several assays to determine the optimal conditions of the reaction.

For this purpose, the full-length hAGT was first over-expressed and purified as described previously [36]. Increasing concentrations of the protein were incubated with double-stranded 5-O^6-MeG and 6-O^6-MeG TBA, annealed with its complementary sequence. Figure 4(a) shows the HPLC profile of the final product of the reaction with double-stranded 5-O^6-MeG-TBA. In order to separate the two strands of the TBA substrate (Figure 4(a) top right panel), HPLC analyses were done at 60°C. After incubation with hAGT, we detected a peak with a shorter retention time, which corresponds to the restored TBA sequence caused by

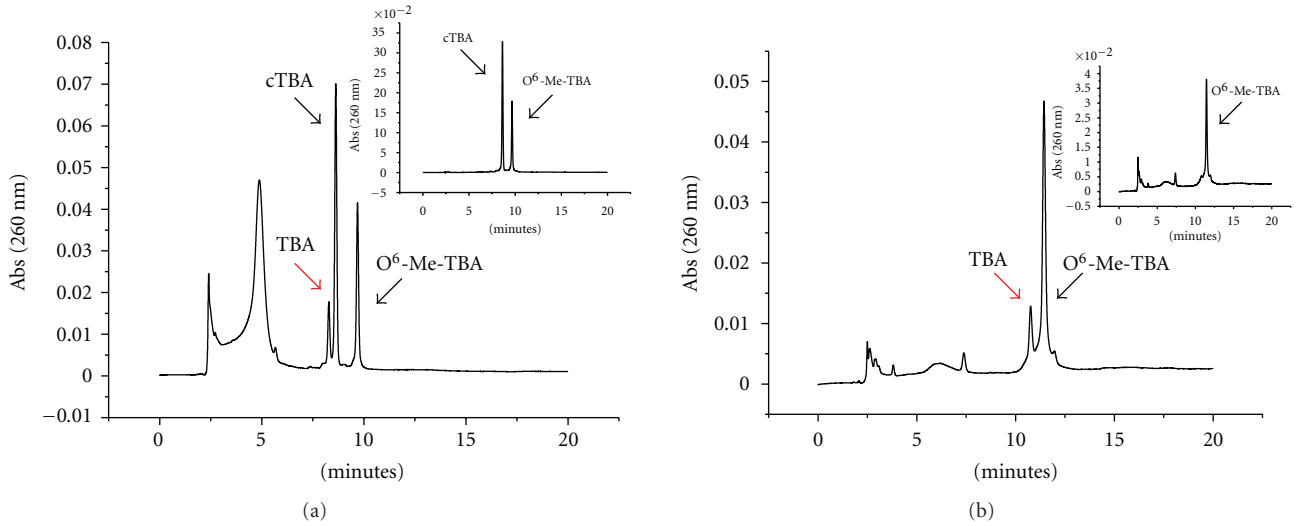

Figure 4: HPLC analysis of hAGT activity over double- and single-stranded TBA before and after incubation with hAGT. (a) Repair of double-stranded 5-O^6-MeG-TBA by hAGT. The peak labelled as cTBA corresponds to the complementary sequence of 5-O^6-MeG-TBA. The top right panel shows HPLC chromatogram in absence of hAGT. The gradient was from 10%–40% acetonitrile for 20 min at 60°C. (b) Repair of single- stranded 5-O^6-MeG-TBA by hAGT. The inserted panel shows HPLC chromatogram in the absence of hAGT. Gradient used: 10%–40% acetonitrile, 20 min at room temperature.

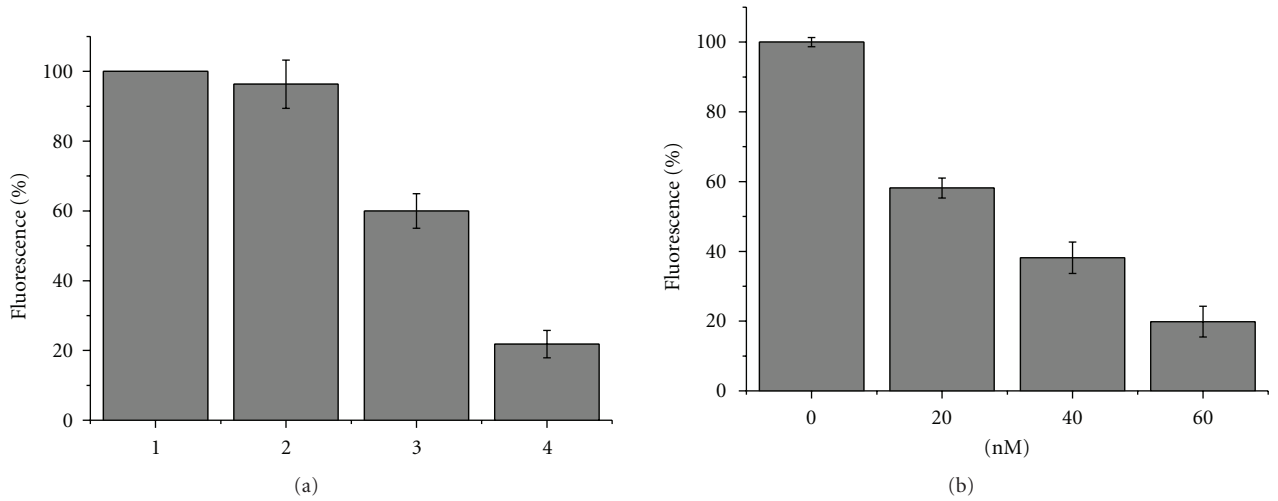

Figure 5: Fluorescence intensity of the real-time hAGT assay, measured at excitation and emission wavelengths of 485 nm and 535, respectively. (a) Illustration of the different controls with 5 nM MB-5-O^6-MeG-TBA: (1) Positive control of MB-5-O^6-MeG-TBA in the absence of hAGT; (2) Intensity in presence of the inactive mutant hAGT-C145S; (3) Decrease in fluorescence when adding 40 nM active hAGT; and (4) basal fluorescence of 5 nM of MB-TBA. (b) Decrease in intensity caused by the activity of hAGT at a range of concentrations (0, 20, 40, and 60 nM), in all of them the basal fluorescence of MB-TBA was subtracted.

the removal of the methyl group. We obtained the same results when we used double-stranded 6-O^6-MeG-TBA as a substrate (data not shown). As expected, hAGT activity was not affected by the position of the alkyl group within the sequence. We then tested hAGT activity over single-stranded methylated TBA in the previously optimized conditions and obtained similar results to those shown in Figure 4(b). The top right panel shows the HPLC chromatogram in the absence of hAGT. In this case, the HPLC analyses were performed at room temperature because the substrate was single-stranded TBA. Our results confirmed that hAGT has the capacity to remove methyl groups from single- or double-stranded TBA with the same efficacy. Therefore, we selected single-stranded TBA as substrate for the development of our fluorescence assay.

3.4. Fluorescence hAGT Activity Assay. On the basis of the results obtained in the melting temperature and the HPLC experiments, we tested the effectiveness of our proposed model to the DNA repair activity of hAGT by means of fluorescence. First of all, we determined the minimum amount of TBA required to achieve a detectable and reliable

difference in intensity compared to the background. As expected, the negative control natural TBA quadruplex gave low background fluorescence, because of the proximity of the fluorophore and the quencher groups in the chair-like structure (Figure 5(a)). Although the fluorescence of MB-TBA was low, this fluorescence was subtracted from the fluorescence value in each experiment. The concentration of 5 nM of fluorescently labelled MB-O^6-MeG-TBA was considered the optimal concentration as the fluorescence signal was intense and only a small amount of hAGT protein was required to achieve a substantial decrease in fluorescence in 20–40 min. In the optimal conditions, the presence of hAGT produced a remarkable decrease in fluorescence intensity, caused by the demethylation of the O^6 position of guanines, thereby allowing the TBA to form its typical quadruplex structure, which brings together the fluorophore and the quencher groups, as occurred in the negative control. The rate of decrease in fluorescence intensity correlated directly with the amount of hAGT in the reaction mixture (Figure 5(b)). Moreover, the inactive mutant hAGT-C145S did not exhibit any decrease in fluorescence (Figure 5(a)). This result was expected because of the inability of this mutated protein to repair the modified TBA. Figure 5(b) shows the fluorescence intensities for the real time hAGT assay. All these observations are consistent with the hypothesis and design of our FRET method.

4. Conclusion

Although radioactivity has been widely used in the search of potential inhibitors of hAGT [23, 24], this technique does not allow real-time data acquisition and, in addition, requires radioactive materials. Here, we developed a sensitive fluorescence method that allows the quantification of hAGT activity in a single step and in a straightforward manner. Although another fluorescence method has already been developed for this purpose [25], it requires the addition of a restriction enzyme, followed by the addition of an exonuclease after the hAGT activity reaction. Consequently, although it is a real-time assay, a three-step reaction is required before observing an increase in fluorescence. In contrast, in our assay, a change in fluorescence is detected in a single step (homogeneous), and this method does not depend on the activity of two additional enzymes.

Our assay is based on the detection of conformational changes of TBA in the presence or absence of O^6-methylguanines in its structure. The quadruplex structure of TBA is disrupted when a central guanine is replaced by an O^6-methylguanine. Fluorophore groups can be added to the modified sequence in order to detect the conformational changes by fluorescence. The variation in fluorescence can be quantified as a direct measurement of hAGT activity. In addition, this technique requires lower amounts of substrate and does not call for the use of radioactive materials. Furthermore, this method can be easily transferred to a high throughput experiment for the evaluation of small molecules as potential hAGT inhibitors [36]. Research in this direction is currently underway in the laboratory.

Abbreviations

BME: 2-mercaptoethanol
Dabsyl: 3-(N-4′-sulfonyl-4-(dimethylamino)-azobenzene)-3-aminopropyl
dmf: Dimethylformamidino group
DTT: Dithiothreitol
EDTA: Ethylenediaminetetraacetic acid
FAM: Fluoresceine
AGT: O^6-alkylguanine-DNA alkyltransferase
hAGT: Human AGT
HPLC: High performance liquid chromatography
IPTG: Isopropyl β-D-1-thiogalactopyranoside
MB: Molecular Beacon
O^6-MeG: O^6-methylguanine
TBA: Thrombin-binding aptamer
cTBA: Complementary TBA
TEAA: Triethylammonium acetate
TFA: Trifluoroacetic acid
Tris: Tris(hydroxymethyl)aminomethane
Tm: Melting temperature
UV: Ultraviolet.

Acknowledgments

This work was supported by the Fondo de Investigaciones Sanitarias (Grant PI06/1250), by the Dirección General de Investigación Científica y Técnica (Grant BFU2007-63287, CTQ2010-20541), the Generalitat de Catalunya (2009/SGR/208), the COST project (G4-net, MP0802), the Instituto de Salud Carlos III (CIBER-BNN, CB06_01_0019), and a SNS Miguel Servet contract from the Instituto de Salud Carlos III. The authors thank Tanya Yates for editing the paper and the reviewer for the detailed revision of the paper. This work is dedicated to the memory of Ángel Ramírez Ortiz who was a great mentor, colleague, and friend.

References

[1] M. R. Middleton and G. P. Margison, "Improvement of chemotherapy efficacy by inactivation of a DNA-repair pathway," *Lancet Oncology*, vol. 4, no. 1, pp. 37–44, 2003.

[2] A. Sabharwal and M. R. Middleton, "Exploiting the role of O^6-methylguanine-DNA-methyltransferase (MGMT) in cancer therapy," *Current Opinion in Pharmacology*, vol. 6, no. 4, pp. 355–363, 2006.

[3] A. E. Pegg and B. Singer, "Is O^6-alkylguanine necessary for initiation of carcinogenesis by alkylating agents?" *Cancer Investigation*, vol. 2, p. 18, 1984.

[4] R. Saffhill, G. P. Margison, and P. J. O'Connor, "Mechanisms of carcinogenesis induced by alkylating agents," *Biochimica et Biophysica Acta*, vol. 823, no. 2, pp. 111–145, 1985.

[5] B. Singer, "O-Alkyl pyrimidines in mutagenesis and carcinogenesis: occurrence and significance," *Cancer Research*, vol. 46, no. 10, pp. 4879–4885, 1986.

[6] K. A. Jaeckle, H. J. Eyre, J. J. Townsend et al., "Correlation of tumor O^6 methylguanine-DNA methyltransferase levels with survival of malignant astrocytoma patients treated with bischloroethylnitrosourea: a Southwest Oncology Group study," *Journal of Clinical Oncology*, vol. 16, no. 10, pp. 3310–3315, 1998.

[7] M. Belanich, M. Pastor, T. Randall et al., "Retrospective study of the correlation between the DNA repair protein alkyltransferase and survival of brain tumor patients treated with carmustine," *Cancer Research*, vol. 56, no. 4, pp. 783–788, 1996.

[8] R. S. Foote, S. Mitra, and B. C. Pal, "Demethylation of O^6-methylguanine synthetic DNA polymer by an inducible activity in Escherichia coli," *Biochemical and Biophysical Research Communications*, vol. 97, no. 2, pp. 654–659, 1980.

[9] A. E. Pegg, "Mammalian O^6-alkylguanine-DNA alkyltransferase: regulation and importance in response to alkylating carcinogenic and therapeutic agents," *Cancer Research*, vol. 50, no. 19, pp. 6119–6129, 1990.

[10] W. P. Tong, M. C. Kirk, and D. B. Ludlum, "Formation of the cross-link 1-[N3-deoxycytidyl],2-[N1-deoxyguanosinyl]ethane in DNA treated with N,N'-bis(2-chloroethyl)-N-nitrosourea," *Cancer Research*, vol. 42, no. 8, pp. 3102–3105, 1982.

[11] L. Yan, J. R. Donze, and L. Liu, "Inactivated MGMT by O^6-benzylguanine is associated with prolonged G2/M arrest in cancer cells treated with BCNU," *Oncogene*, vol. 24, no. 13, pp. 2175–2183, 2005.

[12] T. P. Brent, P. J. Houghton, and J. A. Houghton, "O^6-alkylguanine-DNA alkyltransferase activity correlates with the therapeutic response of human rhabdomyosarcoma xenografts to 1-(2-chloroethyl)-3-(trans-4-methylcyclohexyl)-1-nitrosourea," *Proceedings of the National Academy of Sciences of the United States of America*, vol. 82, no. 9, pp. 2985–2989, 1985.

[13] G. Tagliabue, L. Citti, G. Massazza, G. Damia, R. Giavazzi, and M. D'Incalci, "Tumour levels of O^6-alkylguanine-DNA-alkyltransferase and sensitivity to BCNU of human xenografts," *Anticancer Research*, vol. 12, no. 6B, pp. 2123–2125, 1992.

[14] R. Pepponi, G. Marra, M. P. Fuggetta et al., "The effect of O^6-alkylguanine-DNA alkyltransferase and mismatch repair activities on the sensitivity of human melanoma cells to temozolomide, 1,3-bis(2-chloroethyl)1-nitrosourea, and cisplatin," *Journal of Pharmacology and Experimental Therapeutics*, vol. 304, no. 2, pp. 661–668, 2003.

[15] S. L. Gerson, "Clinical relevance of MGMT in the treatment of cancer," *Journal of Clinical Oncology*, vol. 20, no. 9, pp. 2388–2399, 2002.

[16] G. P. Margison, A. C. Povey, B. Kaina, and M. F. Santibáñez Koref, "Variability and regulation of O^6-alkylguanine-DNA alkyltransferase," *Carcinogenesis*, vol. 24, no. 4, pp. 625–635, 2003.

[17] S. L. Gerson, "MGMT: its role in cancer aetiology and cancer therapeutics," *Nature Reviews Cancer*, vol. 4, no. 4, pp. 296–307, 2004.

[18] M. E. Hegi, A.-C. Diserens, T. Gorlia et al., "MGMT gene silencing and benefit from temozolomide in glioblastoma," *The New England Journal of Medicine*, vol. 352, no. 10, pp. 997–1003, 2005.

[19] M. Esteller, J. Garcia-Foncillas, E. Andion et al., "Inactivation of the DNA-repair gene MGMT and the clinical response of gliomas to alkylating agents," *The New England Journal of Medicine*, vol. 343, no. 19, pp. 1350–1354, 2000.

[20] A. E. Pegg, K. Swenn, M.-Y. Chae, M. E. Dolan, and R. C. Moschel, "Increased killing of prostate, breast, colon, and lung tumor cells by the combination of inactivators of O^6-alkylguanine-DNA alkyltransferase and N,N'-bis(2-chloroethyl)-N-nitrosourea," *Biochemical Pharmacology*, vol. 50, no. 8, pp. 1141–1148, 1995.

[21] K. S. Srivenugopal, X.-H. Yuan, H. S. Friedman, and F. Ali-Osman, "Ubiquitination-dependent proteolysis of O^6-methylguanine-DNA methyltransferase in human and murine tumor cells following inactivation with O^6-benzylguanine or 1,3-bis(2-chloroethyl)-1-nitrosourea," *Biochemistry*, vol. 35, no. 4, pp. 1328–1334, 1996.

[22] M. Xu-Welliver and A. E. Pegg, "Degradation of the alkylated form of the DNA repair protein, O^6-alkylguanine-DNA alkyltransferase," *Carcinogenesis*, vol. 23, no. 5, pp. 823–830, 2002.

[23] B. D. Wilson, M. Strauss, B. J. Stickells, E. G. Hoal-van Helden, and P. D. Van Helden, "An assay for O^6-alkylguanine-DNA alkyltransferase based on restriction endonuclease inhibition and magnetic bead separation of products," *Carcinogenesis*, vol. 15, no. 10, pp. 2143–2148, 1994.

[24] M. E. Dolan, D. Schicchitiano, and A. E. Pegg, "Use of oligodeoxynucleotides containing O^6-alkylguanine for the assay of O^6-alkylguanine-DNA-alkyltransferase activity," *Cancer Research*, vol. 48, no. 5, pp. 1184–1188, 1988.

[25] A. M. Moser, M. Patel, H. Yoo, F. M. Balis, and M. E. Hawkins, "Real-time fluorescence assay for O^6-alkylguanine-DNA alkyltransferase," *Analytical Biochemistry*, vol. 281, no. 2, pp. 216–222, 2000.

[26] R. S. Wu, S. Hurst-Calderone, and K. W. Kohn, "Measurement of O^6-alkylguanine-DNA alkyltransferase activity in human cells and tumor tissues by restriction endonuclease inhibition," *Cancer Research*, vol. 47, no. 23, pp. 6229–6235, 1987.

[27] J. L. Huppert, "Four-stranded nucleic acids: structure, function and targeting of G-quadruplexes," *Chemical Society Reviews*, vol. 37, no. 7, pp. 1375–1384, 2008.

[28] S. Neidle, "The structures of quadruplex nucleic acids and their drug complexes," *Current Opinion in Structural Biology*, vol. 19, no. 3, pp. 239–250, 2009.

[29] N. V. Hud, F. W. Smith, F. A. L. Anet, and J. Feigon, "The selectivity for K^+ versus Na^+ in DNA quadruplexes is dominated by relative free energies of hydration: a thermodynamic analysis by 1H NMR," *Biochemistry*, vol. 35, no. 48, pp. 15383–15390, 1996.

[30] S. Burge, G. N. Parkinson, P. Hazel, A. K. Todd, and S. Neidle, "Quadruplex DNA: sequence, topology and structure," *Nucleic Acids Research*, vol. 34, no. 19, pp. 5402–5415, 2006.

[31] S. W. Blume, V. Guarcello, W. Zacharias, and D. M. Miller, "Divalent transition metal cations counteract potassium-induced quadruplex assembly of oligo(dG) sequences," *Nucleic Acids Research*, vol. 25, no. 3, pp. 617–625, 1997.

[32] A. G. Petrovic and P. L. Polavarapu, "Quadruplex structure of polyriboinosinic acid: dependence on alkali metal ion concentration, pH and temperature," *Journal of Physical Chemistry B*, vol. 112, no. 7, pp. 2255–2260, 2008.

[33] C. S. Mekmaysy, L. Petraccone, N. C. Garbett et al., "Effect of O^6-methylguanine on the stability of G-quadruplex DNA," *Journal of the American Chemical Society*, vol. 130, no. 21, pp. 6710–6711, 2008.

[34] R. F. Macaya, P. Schultze, F. W. Smith, J. A. Roe, and J. Feigon, "Thrombin-binding DNA aptamer forms a unimolecular quadruplex structure in solution," *Proceedings of the National Academy of Sciences of the United States of America*, vol. 90, no. 8, pp. 3745–3749, 1993.

[35] O. S. Bhanot and A. Ray, "The in vivo mutagenic frequency and specificity of O^6-methylguanine in φX174 replicative form DNA," *Proceedings of the National Academy of Sciences of the United States of America*, vol. 83, no. 19, pp. 7348–7352, 1986.

[36] F. M. Ruiz, R. Gil-Redondo, A. Morreale, Á. R. Ortiz, C. Fábrega, and J. Bravo, "Structure-based discovery of novel non-nucleosidic DNA alkyltransferase inhibitors: virtual screening and in vitro and in vivo activities," *Journal of Chemical Information and Modeling*, vol. 48, no. 4, pp. 844–854, 2008.

[37] M. H. Caruthers, A. D. Barone, S. L. Beaucage et al., "Chemical synthesis of deoxyoligonucleotides by the phosphoramidite method," *Methods in Enzymology*, vol. 154, pp. 287–313, 1987.

[38] H. Vu, C. McCollum, C. Lotys, and A. Andrus, "New reagents and solid support for automated oligonucleotide synthesis," *Nucleic Acids Symposium Series*, no. 22, pp. 63–64, 1990.

[39] J. J. Rasimas, A. E. Pegg, and M. G. Fried, "DNA-binding mechanism of O^6-alkylguanine-DNA alkyltransferase: effects of protein and DNA alkylation on complex stability," *Journal of Biological Chemistry*, vol. 278, no. 10, pp. 7973–7980, 2003.

Supplementary data

Development of a Novel Fluorescence Assay Based on the Use of the Thrombin Binding Aptamer for the Detection of O^6-alkylguanine–DNA Alkyltransferase Activity

Maria Tintoré, Anna Aviñó, Federico M. Ruiz, Ramón Eritja and Carme Fàbrega*

CONTENTS:

Figure S1. UV spectra of MB-TBA (5'-FAM-GGT TGG TGT GGT TGG-Dabsyl-3') at 20 and 80 ºC.

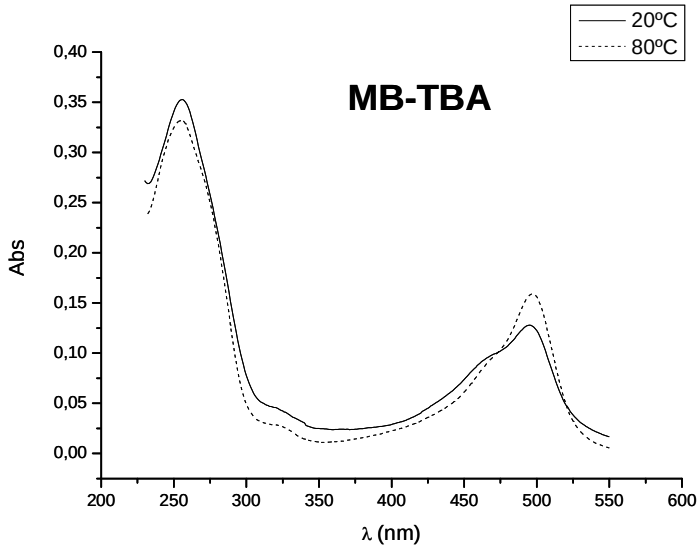

Figure S2. UV spectra of MB-5-O^6-MeG-TBA (5'-FAM-GGT T**^{Me}G**G TGT GGT TGG-Dabsyl-3') at 20 and 80 ºC.

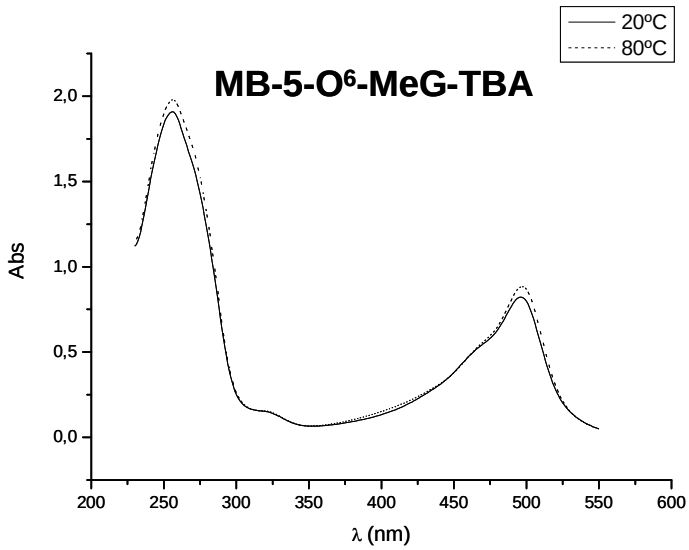

Figure S3. Melting curves of MB-TBA and MB-5-O^6-MeG-TBA recorded at 295 nm. A quadruplex-to-random-coil transition is observed for the MB-TBA (Tm = 46 ºC). No transition was observed for MB-5-O^6-MeG-TBA.

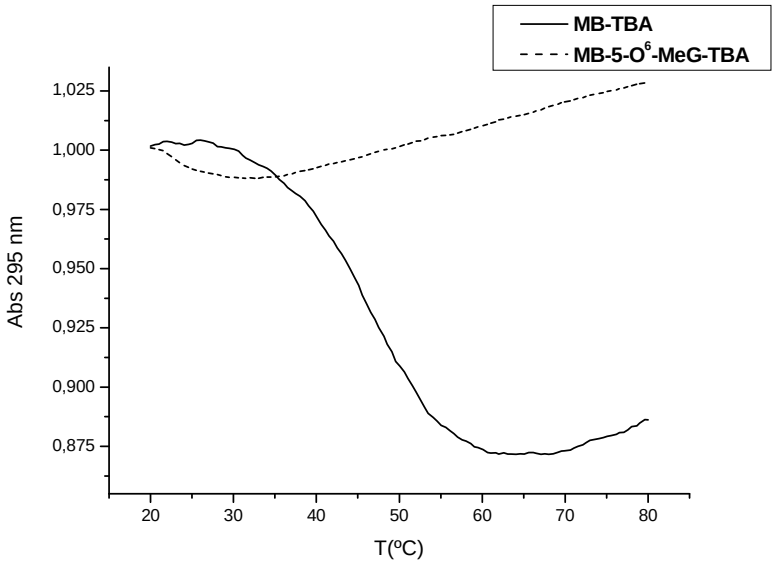

Figure S4. Melting curves of MB-TBA and MB-5-O^6-MeG-TBA recorded at 495 nm. A quadruplex-to-random-coil transition is observed for the MB-TBA (Tm = 46 ºC). No transition was observed for MB-5-O^6-MeG-TBA.

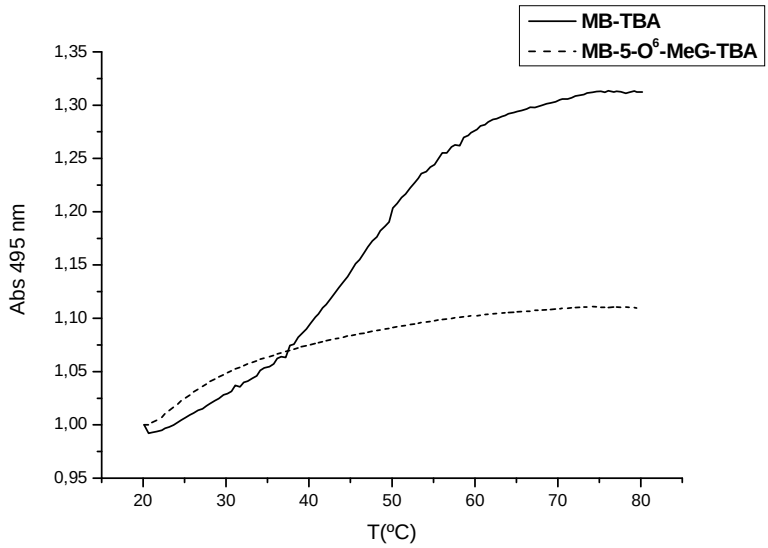

Figure S5. CD spectra of TBA, 5-O^6-MeG-TBA and 5-O^6-MeG-TBA recorded at 25 ºC. Conditions 10 mM sodium cacodylate pH 7.0 and 100 mM KCl., sample concentration 4 μM.

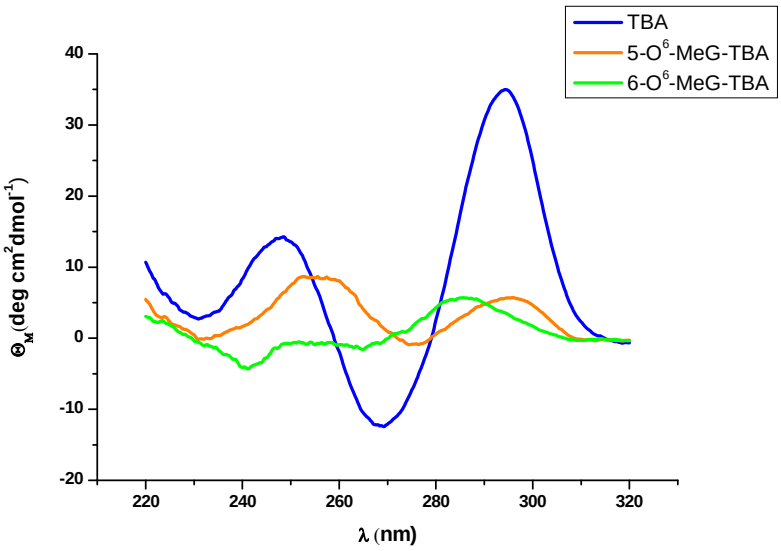

Figure S6. CD spectra of TBA, 3HP-TBA, 6HP-TBA and 9HP-TBA recorded at 25 ºC. Conditions 10 mM sodium cacodylate pH 7.0 and 100 mM KCl., sample concentration 4 μM.

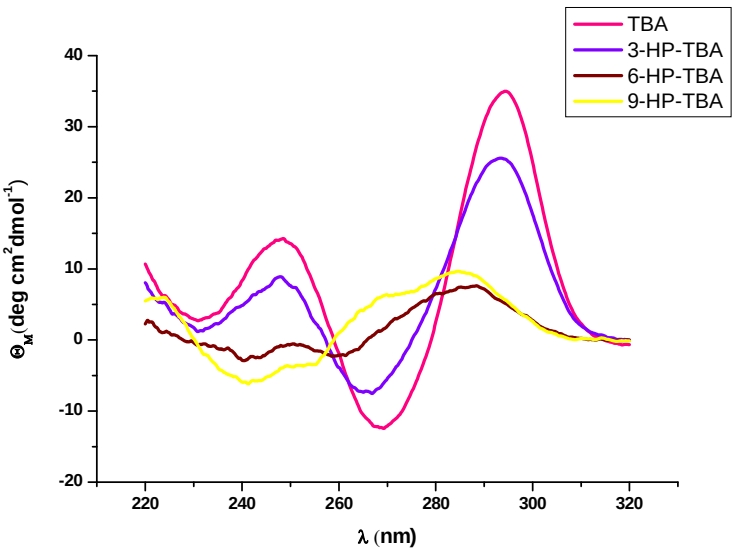

Appendix 2

Thrombin binding aptamer, more than a simple aptamer: chemically modified derivatives and biomedical applications.

Thrombin binding aptamer, more than a simple aptamer: chemically modified derivatives and biomedical applications.

Anna Aviñó,[1] Carme Fàbrega,[1] Maria Tintoré,[1] and Ramon Eritja[1]

Current Pharmaceutical Design (2012) Volume 18, Issue 14, pages 2036-2047.

DOI: 10.2174/138161212799958387. Impact factor: **3.288**

[1] Institute for Research in Biomedicine of Barcelona, IQAC-CSIC, CIBER-BBN Networking, Centre on Bioengineering Biomaterials and Nanomedicine. Cluster Building, Baldiri i Reixach 10, E-08028 Barcelona

Thrombin Binding Aptamer, More than a Simple Aptamer: Chemically Modified Derivatives and Biomedical Applications

Anna Aviñó, Carme Fàbrega, María Tintoré and Ramon Eritja*

Institute for Research in Biomedicine, IQAC-CSIC, CIBER-BBN Networking Centre on Bioengineering, Biomaterials and Nanomedicine, Edifici Helix, Baldiri Reixac 10, E-08028 Barcelona, Spain

Abstract: The thrombin binding aptamer (TBA) is a well characterized chair-like, antiparallel quadruplex structure that binds specifically to thrombin at nanomolar concentrations and therefore it has interesting anticoagulant properties. In this article we review the research involved in the development of new TBA derivatives with improved anticoagulant properties as well as the use of the TBA as a model compound for the study of quadruplex structures. Specifically, we describe the impact of modified nucleosides and non-natural backbones in the guanine tetrads or in the loops and the introduction of pendant groups at the 3' or 5'-ends. The modified oligonucleotides are shown to be excellent tools for the understanding of the molecular structure of the TBA and its folding properties. Finally, we review the use of the TBA-Thrombin recognition system for the development of analytical tools based on the TBA folding.

Keywords: Thrombin binding aptamer, TBA, G-quadruplex, thrombin, anticoagulant, oligonucleotide synthesis, DNA, aptamer.

INTRODUCTION

Aptamers are oligonucleotides that were originally derived from an *in vitro* selection and polymerase chain reaction process known as SELEX (systematic evolution of ligands by exponential enrichment) [1-4] which selects them on the basis of their specific and tight binding affinity to a target of choice from a library of sequences including proteins. Through this approach, a large number of aptamers with very high affinity have been developed for diagnostics, therapeutics and other technical applications [5], but there is still room for improvement in terms of increasing their binding properties and their pharmacokinetic properties [6].

The thrombin binding aptamer (TBA) is the first example of a potential nucleic acid therapeutic agent, targeted to a protein that does not physiologically bind nucleic acids with the following consensus sequence: 5'-$G^1G^2T^3T^4G^5G^6T^7G^8T^9G^{10}G^{11}T^{12}T^{13}G^{14}G^{15}$-3' [7]. This 15-base-long oligonucleotide binds specifically to thrombin at 10 nM concentrations and therefore, it has interesting anticoagulant properties. It inhibits specifically clot-bound thrombin and reduces arterial thrombus formation. In addition, it does not compete with other known active site inhibitors of thrombin [7-10]. Nevertheless, TBA binding to other serum proteins or proteolytic enzymes is essentially undetectable.

In an effort to identify the region of thrombin with which the TBA aptamer interacts, the inhibition of fibrinogen-clotting activity was studied using recombinant mutagenesis of anion-binding exosite of thrombin (exosite I) [10]. The results suggested that the single-stranded DNA binding site is located in the thrombin exosite I and overlaps the thrombin platelet receptor and thrombomodulin binding sites. The TBA binding site on thrombin was also examined by solid-phase plate binding assays [11] and by chemical modifications studies [12]. These studies showed that the TBA aptamer binds specifically to α-thrombin but not to γ-thrombin, which is a proteolytic cleavage product of α-thrombin in the fibrinogen-binding exosite. Both results suggest again that the thrombin exosite I is important for the aptamer-thrombin interaction.

The awareness of the folded structure of this aptamer, both free in solution or bound to thrombin, is essential to understand its biological activity and useful in the future development of oligonucleotide-based therapeutics or drug design. The TBA has been characterized by NMR spectroscopy [12-15] and X-ray crystallography [16-18]. These studies have led to the description of its compact and symmetrical chair-like, unimolecular antiparallel quadruplex structure. This structure consists of two G-tetrads connected by three edge-wise loops: two TT loops (T^3T^4 and $T^{12}T^{13}$) at one end and a single $T^7G^8T^9$ loop in the other end Fig. (**1A**). The conformational distribution of the four co-planar 2'-deoxyguanosines in the G-quartets of the TBA aptamer is well defined and they are stabilized by cyclic Hoogsteen hydrogen bounding Fig. (**1B**). All sugar puckers are predominantly *South (S)* while the guanines on the same G-quartet plane display alternating 5'-*syn-anti-syn-anti-3'* conformations with respect to the glycosyl torsion angle (*syn*-G at positions G^1, G^5, G^{10} and G^{14}; *anti*-G at positions G^2, G^6, G^{11} and G^{15}, Fig. (**1**)), except for the G^8 and the thymines in the loops which are all *anti*. The two TT loops, both at one end of the quadruplex, span a narrow groove, while the TGT loop, placed at the other end, spans a wide groove.

It has been known for several years that not only the primary nucleotide sequence, but also environmental conditions and in particular cations, play an important role in the formation, topology and stability of G-quadruplexes [19-25]. In the case of the thrombin binding aptamer, it was believed that the presence of K^+ in the medium was necessary to shift the equilibrium toward the quadruplex conformation, subsequently favouring thrombin binding, its ionic size fitting into the free space existing in the center of each quartet. Preliminary studies with Mn^{2+} suggested that it can bind strongly in two sites with one in the each narrow groove [26]. Both Mn^{2+} ions are released when the aptamer is complexed with thrombin, indicating that both narrow grooves are involved in the TBA-thrombin interactions. Some authors have used a combination of temperature-dependent UV spectroscopy, calorimetry, NMR and electrospray ionization mass spectrometry techniques to evaluate the effect in the stability, hydration and thermodynamics of the monovalent and divalent metal ions in the formation of 3D structures of the TBA complexes [26-34]. Divalent ions (Pb^{2+}, Ba^{2+} and Sr^{2+}) and NH_4^+ bind and stabilize the quadruplex structure with even higher efficiency than K^+ while Li^+, Na^+, Cs^+, Mg^{2+} and Ca^{2+} form weaker complexes only at very low temperatures. These results have been rationalized in terms of their radii; cations with an ionic radius in the range 1.3-1.5 Å fit well within the two G-quartets of the complex while the other cations do not. The divalent cations like Pb^{2+}, Ba^{2+} and Sr^{2+} efficiently occupy the region between the two quar-

*Address correspondence to this author at the Institute for Research in Biomedicine, IQAC-CSIC, CIBER-BBN Networking Centre on Bioengineering, Biomaterials and Nanomedicine, Edifici Helix, Baldiri Reixac 10, E-08028 Barcelona, Spain; Tel: +34(93)4039942; Fax: +34(93)2045904;
E-mail: recgma@cid.csic.es; ramon.eritja@irbbarcelona.org

1381-6128/12 $58.00+.00

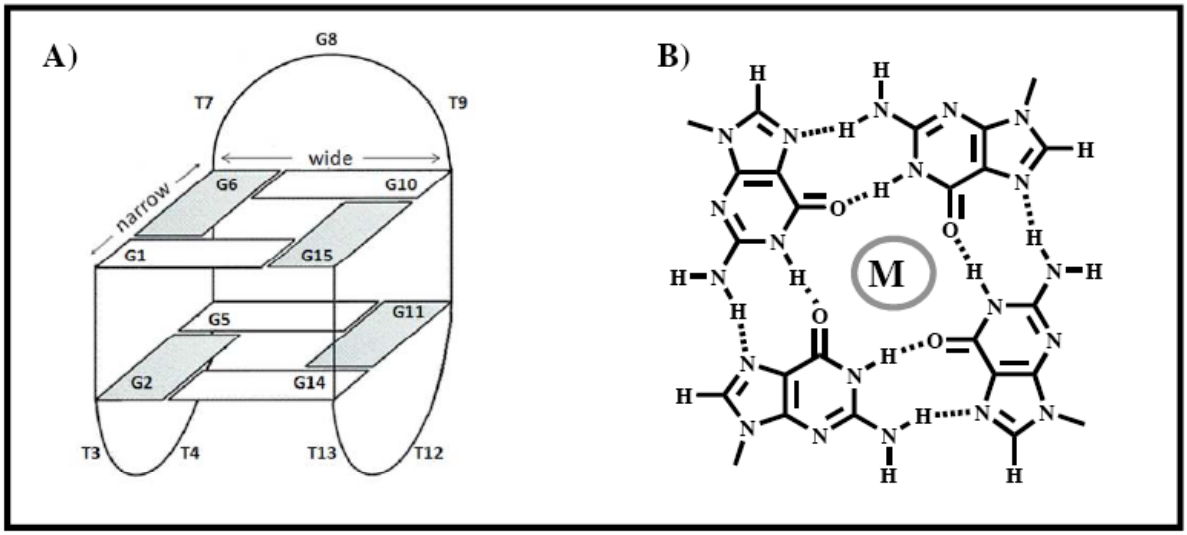

Fig. (1). A) Folding topology of the intramolecular quadruplex adopted by the d($G^1G^2T^3T^4G^5G^6T^7G^8T^9G^{10}G^{11}T^{12}T^{13}G^{14}G^{15}$) thrombin-binding DNA aptamer containing three edge-wise loops. **B**) Structure of the G-quartet with cyclic array of four guanines formed by Hoogsteen-type H-bonds, M indicates a metal ion.

tets in the TBA-ion complex in a 1:1 stoichiometry [27, 29, 33]. The aptamer complex with monovalent and divalent ions unfolds in a monophasic transition [30].

Hong *et al*. have determined the alkali metal binding site and constant by electrospray ionization (ESI) and infrared multiphoton dissociation (IRMPD) respectively [35]. The binding constant of potassium is 5-8 times greater than those for other alkali metal ions and the K^+ binding site is different from other metal binding sites. In a 1:1 TBA-metal complex, potassium coordinated between the bottom G-quartet and the two adjacent TT loops of the TBA. In a 1:2 ratio TBA-metal complex, the second potassium ion binds at the distant TGT loop. In the other hand, Na^+, Rb^+ and Cs^+ bind at the lateral TGT loop in both 1:1 and 1:2 complexes, presumably due to the formation of ion-pair adducts.

By contrast, some published works provide evidence that the TBA is able to bind thrombin in the absence of divalent and monovalent ions [24, 25, 36-37], which suggests that the binding to thrombin promotes the TBA folding to its 3D structure, even in the absence of salts.

Several groups have studied and suggested that molecular crowding causes a structural transition from an antiparallel to a parallel DNA G-quadruplex and they are an important factor to control the formation of G-quadruplex [38-39]. Miyoshi *et al*. have shown that different molecular crowding promotes and stabilizes the G-quadruplex structure of the TBA by a favourable enthalpic contribution that exceeds an unfavourable entropic contribution. Moreover, the thermodynamic effect correlates with the number of hydroxyl groups of the molecular crowding cosolute [39].

It is worth noting that despite the robust stability of the intramolecular quadruplex structure, alternative intermolecular quadruplexes are possible at high aptamer concentration, as detected by CD and electrophoresis migration experiments [40]. The crystal structure of the TBA-thrombin complex solved by Padmanabhan *et al*. [16] at 2.9 Å resolution differs in the aptamer quadruplex topology with the NMR structure. Indeed, the core of the two G-tetrads is the same in the two models, although structural differences exist in the way the central bases are connected. A difference concerning the disposition of the two TT and the TGT loops with respect to the grooves. In an effort to resolve this ambiguity, the structure of the TBA-thrombin complex has been determined at 2.8 Å, built on the basis of the NMR structure of the aptamer [17]. The results confirmed that both structures fit the crystallographic data equally well, thus leaving the doubt on which binding model is the correct one. In both models, the TBA is sandwiched between two symmetry-related thrombin molecules and interacts with the exosite I of a thrombin molecule and exosite II of the second one. In particular, the two TT loops in the NMR structure interact with the fibrinogen-recognition site (exosite I) of the thrombin molecule and the TGT loop interacts with the heparin-binding site (exosite II) of the neighbouring thrombin, whereas in the X-ray structure the opposite occurs [16-17]. The structure of the complex between thrombin and TBA is shown in Fig. (**2**).

The uncertainty between the two models was caused by the absence or poor electron density in the region of the TT loops and in the G^{10} for the X-ray structure and in the G^{14} and in the TGT loop for the NMR structure. In a more systematic analysis [18], eight orientations of the NMR aptamer were evaluated in an effort to reconcile the NMR and X-ray data [16-17]. The resulting crystallographic R-factors and the analysis of the aptamer-protein complexes clearly distinguished between the two possible oligonucleotides backbone directionalities. However, due to the missing density in the connecting loops of the aptamer, the details of the ligand protein interactions could not be properly addressed. Moreover, even recent papers still discuss modified aptamer-thrombin interactions on the bases of both models [39].

The recent solved high resolution structure of the complex of thrombin with a modified TBA (mTBA), which contains a 5'-5' inversion between T^3 and T^4, clarifies several questions regarding thrombin-aptamer interaction [41]. The aptamer tightly binds to thrombin exosite I by its TT loops, through a mix of hydrophobic and polar interactions in agreement with the results obtained in the systematic analysis [18]. However, the interaction details are different for the two aptamers due to the chain inversion of the mTBA. This chain inversion allows the formation of a great number of contacts with the enzyme and lead to an increase in shape complementarity. In addition, the quadruplex structure is efficiently stabilized by a potassium ion, which is sandwiched between the two quartets.

The antiparallel quadruplex structure of the TBA has a distinctive denaturation-renaturation profile that is reversible and observ-

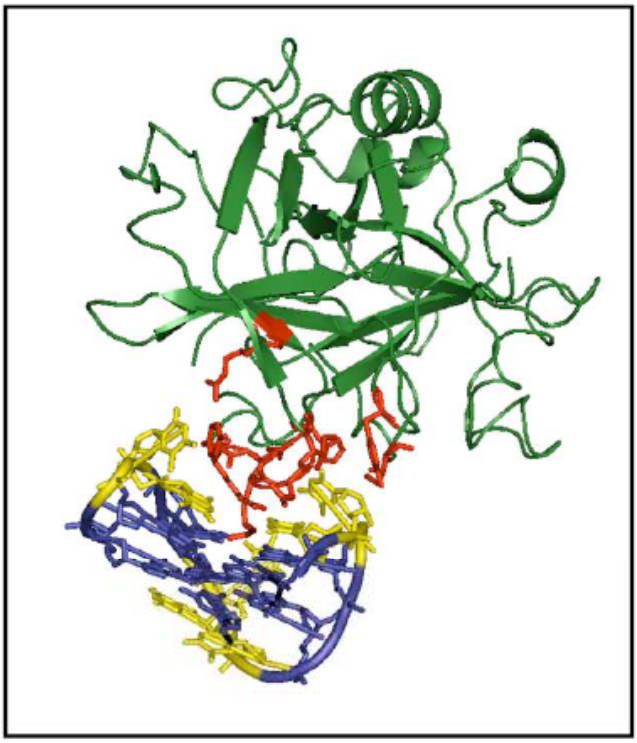

Fig. (2). Structure of the complex formed by thrombin and the thrombin binding aptamer (TBA). Thrombin is coloured in green with the amino acid residues that contact the TBA in red (cartoon representation). The TBA is coloured in blue except the residues involved in the TT and TGT loops that are highlighted in yellow (stick representation).

able by different techniques, particularly by NMR experiments, which suggest that the denaturation of the quadruplex occurs by the opening of the G-G base pairs that are not protected by a loop, followed by the opening of the TGT loop [42].

1. CLINICAL TRIALS WITH THE THROMBIN-BINDING APTAMER

The anticoagulant properties of TBA were first evaluated on cynomolgus monkeys, and sheeps [8]. The rapid onset and the short half-life of TBA ($t_{1/2}$: 2 min) *in vivo* lead to an interest for the use of TBA for certain acute clinical settings such as surgical interventions where regional anticoagulation is required. TBA was able to inhibit clot-bound thrombin and platelet thrombus formation in an ex vivo whole-artery angioplasty model [9]. Moreover, when TBA was administered by infusion in a short-term canine cardiopulmonary bypass model it was shown that TBA could be used as anticoagulant safely and as efficiently as heparine [43]. Clinical trials evaluating TBA (ARC-183, HD1, Archemix Corporation) as anticoagulant during coronary artery bypass graft surgery were halted after phase I due to suboptimal dosing profiles, primarily caused by the restricted binding affinity of the aptamer [44]. A more potent second-generation DNA aptamer (NU172, Archemix Coorp., Nuvelo Inc.) was developed showing clear inhibition of clot formation [45].

2. MODIFICATIONS ON THE THROMBIN-BINDING APTAMER

In recent years, several attempts to improve pharmacological properties of the TBA have been described, such as stability, higher thrombin affinity, longer life time *in vivo* etc. These modifications have included substitutions in the nucleosides [46], LNA [47-48], UNA [49], RNA [50-51] or 2'-*O*-methyl-RNA [50, 52], methylphosphonate or phosphorothioate internucleoside linkages [50, 52], partial inversion of the TBA polarity with and 5'-5' internucleoside linkage or change in the loop size and sequence [28]. In some cases, the modifications introduced are evaluated in different positions of the aptamer in order to increase the knowledge of the interactions between thrombin and the TBA which are critical for the biological activity. Besides these modifications, thrombin binding aptamer has been functionalized with different derivatives such as fluorescein, biotin or thiol groups to be incorporated in biosensors for the detection of thrombin. These derivatives will be described in section 7. Herein, we have classified the modifications of the TBA depending on the location: G-tetrads, loops or changes of the overall quadruplex structure.

2.1. Modifications of the Guanine Tetrad

Several modifications have been introduced in the G-tetrads, some of which are analogues of the guanine base. Other modifications are related with the sugar structure or with the internucleotide phosphate bonds in the guanine tetrad. The guanine analogues that have been introduced in the TBA are summarized in Fig. (**3**). Hypoxanthine, 7-deazaguanine and C^8-methylguanine were the first guanine analogues to be introduced into the TBA to understand its structure by NMR. These guanine derivatives are unable to form the hydrogen bond required for the formation of the G-tetrad and consequently cause significant disruption to the chair-like structure [12]. He and co-workers studied the N^2 and C^8-alkyl substituted of the G residues forming G-tetrads [53]. These positions are not forming the H-bonding of the tetrads and are available for attaching one or more groups pointing away from the chair-like structure. This is the main reason why these substitutions caused relatively small perturbation on the quadruplex structure. However, they can produce different effects on the thrombin activity. The increased activities for the substitutions on C^8 positions may be explained by the stabilization of *syn* conformation of the G residues, while the increased activities for the substitutions on N^2 positions may be due to the interaction with thrombin.

6-Thioguanine reduced the quadruplex formation due to the increased radius and decreased electronegativity of the sulphur [54]. This modification caused a destabilization of the Hoogsteen hydrogen bonding of guanine tetrads. Moreover, the thiol group at position 6 disrupted the interactions with water molecules and with cations, becoming a weaker hydrogen bond acceptor than the oxo group. 8-Aminoguanine did not significantly alter the structure of the TBA quadruplex but it has a small destabilization effect on the TBA quadruplex. A detailed study of this modification in the G^2 position was carried out by molecular dynamics simulations, NMR, UV spectroscopy and circular dichroism. The presence of 8-aminoguanine did not affect hydrogen bonding or purine-ion interaction, but clearly reduced the strength of stacking interactions [55]. Nallagatla *et al.* prepared a library of all possible substitutions of guanine by isoguanine in the TBA by split and mix synthesis [56]. The library was screened for binding to human thrombin and selected sequences were individually resynthesized and their affinities were assayed by isothermal titration calorimetry. Three modified aptamers carrying one single isoguanine were found to have higher binding affinity for thrombin than the unmodified TBA. The thermal stability of these modified TBAs was not analysed although it is presumed that the effect of the modification will depend on the position of the aptamer.

Finally, the effect of adding a third tetrad on the TBA aptamer has also been explored [28]. This modified thrombin binding aptamer is more stable than the native TBA due to the enthalpic contribution of the extra guanine tetrad.

2.2. Modification of the 2'-deoxyribose of the Guanine Tetrad

Several modifications in the TBA have been applied to the sugar moiety of the guanine tetrad. The structures of the modified 2'-deoxyribose incorporated in the TBA are summarized in Fig. (**4**).

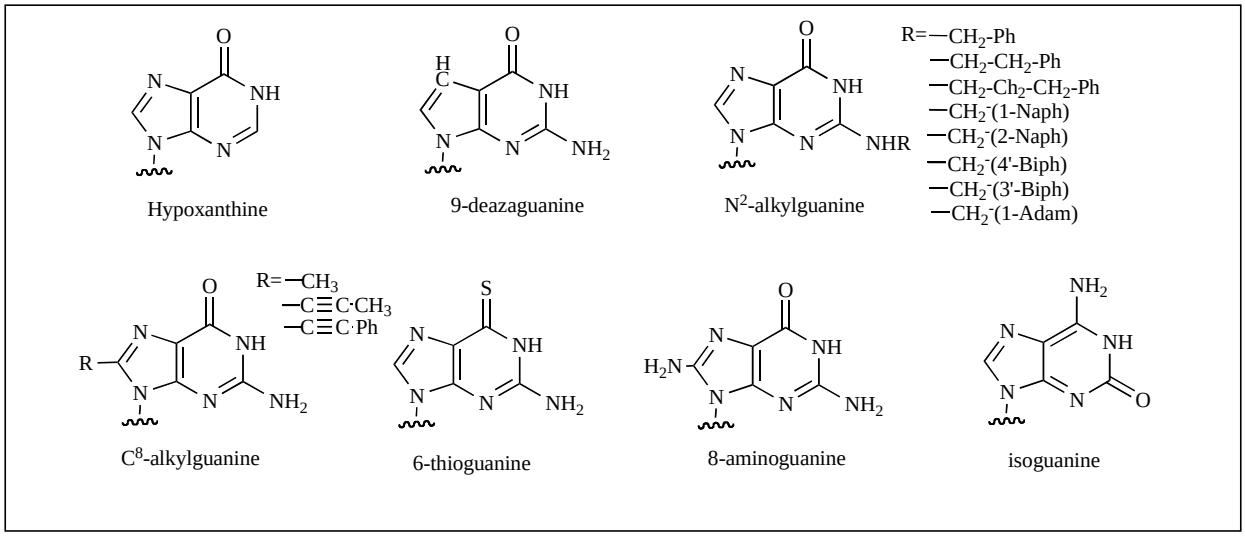

Fig. (3). Chemical structure of the modified guanines in the TBA tetrads.

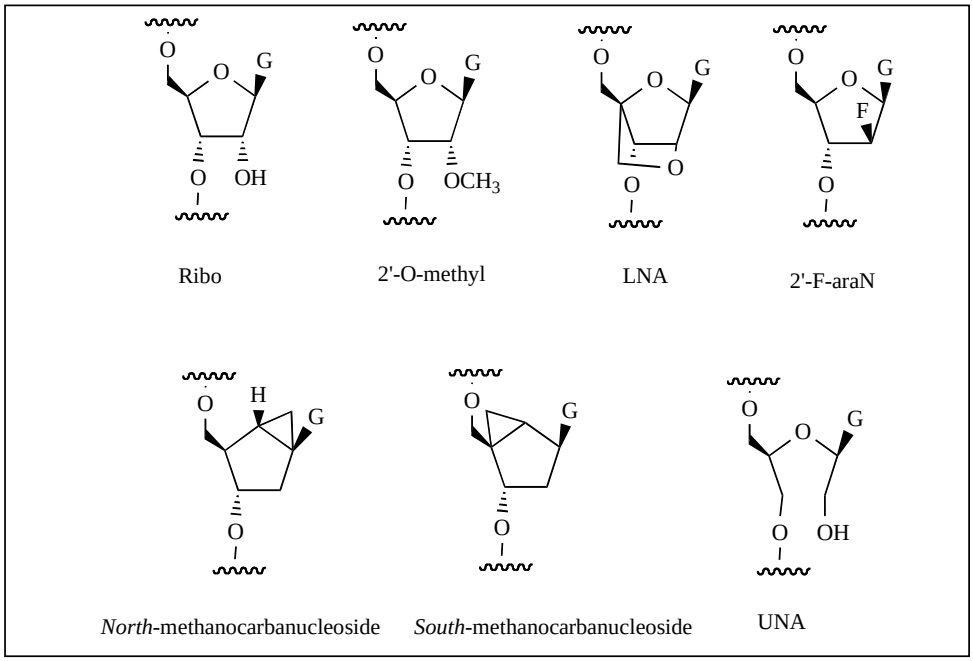

Fig. (4). Chemical structure of the modified carbohydrate moiety in the guanine TBA tetrads. LNA: locked nucleic acid, UNA: unlocked nucleic acid.

In some of them, the 2'-deoxyribose moiety was replaced by a non carbohydrate structure. On the contrary, other modifications are based on the addition of different groups in the 2'-position. These groups may influence sugar puckering and glycosidic bond conformation of the G-tetrad.

In a very interesting work, Shafer's group [51] examined the influence of individual nucleoside conformation on the overall folding topology by selective replacement of deoxyG by riboG. The unimolecular antiparallel TBA is reversed to bimolecular parallel quadruplex by a specific ribonucleotides substitutions. The parallel quadruplex conformation implies that all nucleosides are in the *anti* conformation. The strong preference of guanine ribonucleosides for the *anti* conformation is the driving force for the change in topology and also impact in quadruplex molecularity.

The denaturation behaviour of the TBA derivatives carrying ribonucleotides was also described by Mergny's group [50]. The authors prepared a TBA analogue with all the G of the two tetrads replaced by riboG. In this case, the modified TBA presented a complex behaviour with a non-superimposable and multi-phasic response upon heating and cooling (hysteresis). The same authors also described the same TBA analogues with 2'-O-Me guanosine substitutions. This analogue, instead, showed reversible transitions with concentration independent of the melting temperature (Tm). In fact, substitution of the ribose 2'-H with a methoxy group destabilized the quadruplex structure.

LNA are 2'-O-4'-C-methylene-linked ribonucleotide nucleic acids analogues that bind with increased affinity to DNA and RNA. The bicyclic structure of DNA forces the sugar to be in the C3'-*endo* conformation, and nucleotides with a C3'-*endo* conformation

prefer the glycosidic bond to be in the *anti* configuration. Three different works were addressed to study the effect of LNA in the TBA quadruplex [47-48, 57]. Mayol's group prepared four different TBA-based oligonucleotides containing LNA residues [47, 57]. The first analogue was fully substituted by LNA residues. This oligonucleotide was unstructured most probably due to the decreased flexibility of the oligomer. Oligonucleotides containing G-LNA in the eight positions of the tetrads or in the first G^1 position (*syn* configuration) gave mixtures of several structures. On the other hand, the oligonucleotide containing G-LNA in the last guanine G^{15} (*anti* configuration) folded in the same TBA chair-like quadruplex. Bonifacio *et al.* also studied the effect of single LNA substitutions on different positions of the TBA [48]. The LNA substitutions had either a moderate stabilizing or destabilizing effect on the folded structure, depending on the position of the LNA in the TBA. The thermal stability of the substituted aptamers did not correlate to thrombin inhibition.

Damha and co-workers studied the impact of 2'-deoxy-2-fluoroarabinonucleoside residues (2'-F-araN) on the thrombin binding aptamer [58]. 2'-Deoxy-2'-fluoro-D-arabinonucleic acids (2'F-araN) confer DNA-like (*South*/*East*) conformation to oligonucleotides while rendering them more nuclease resistant. It was found that incorporation of 2'-F-araN G or T residues into the TBA stabilizes the complex (ΔTm + 3ºC /2'-F-araN modification). Oligonucleotides with all nucleotides replaced by 2'-F-araN in the G-*syn* positions or in the G-tetrads showed a moderated increase of the melting temperature compared to the unmodified TBA. The CD spectrum and the hysteresis observed in the heating and cooling processes of these analogues supported a parallel structure with all *anti*-dG and the existence of multimeric G-quadruplex structures. On the contrary, when the 2'-F-araN are replaced in the G-*anti* positions, in the loops or in both the resulted quadruplex structures correspond to antiparallel quadruplex with alternating *syn-anti* Gs. The lack of concentration dependence in the Tm data and the lack of hysteresis in the heating/cooling processes support a unimolecular G-quadruplex structure. Moreover, nuclease resistance of this modified TBA was increased up to 48-fold in 10 % fetal bovine serum (FBS).

Carbacyclic bicyclo [3.1.0] hexane locked nucleoside analogues are a different "locked" nucleoside from the previously presented LNA [52]. An advantage of this methanocarba nucleoside system over LNAs is that both *North (N)*- and *South (S)*-locked platforms can be prepared by shifting the position of the fused cyclopropane ring. It has been described the effects of replacing a single 2'-deoxyguanosine residue at the 3'-end of the TBA (positions dG^{14} and dG^{15}) with methanocarba nucleosides locked in either the *N*- or *S*-conformation [59]. These positions were selected to explore the combined effects of a constrained sugar pucker (*N* or *S*) and the corresponding biased glycosyl torsion angle (*anti* or *syn*) associated with a particular pseudosugar conformation. Experimental and theoretical results indicated that a *N*-pseudosugar conformation favours the *anti* glycosyl orientation, whereas the *S*-pseudosugar conformation favours the *syn* disposition of the base. The introduction of methanocarba nucleosides at positions G^{14} and G^{15} with locked-*N*(*anti*) and locked-*S* (*syn*) conformations fixed the conformational state of these nucleosides and helped to understand the impact of conformational restrictions on the antiparallel, G-quartet DNA structure of the TBA. These results indicated that the glycosyl conformation is more restrictive for the TBA stability than the sugar puckering.

Wengel's group examined the influence of unlocked nucleic acid (UNA) on the thermodynamic stability, binding affinity and biological activity of the quadruplex TBA [49]. UNA is an acyclic RNA mimic, which misses the bound between the C2' and C3' atoms of the ribose ring. The modified variants are aptamers singly substituted with a UNA monomer in every possible position. UNA modified TBAs in positions U^3, U^7 and U^{12} showed an antiparallel folding topology. In contrast, modifications of any of the guanine monomers forming G-tetrads resulted in significant destabilization of the quadruplex structure. The modified TBA with UNA in position 7 resulted in the highest thrombin binding affinity. Recently, the same authors have also evaluated the effects of the modification of 2'-C-piperazino-UNA monomer [60]. This monomer is characterized by more efficient stabilization of quadruplexes structures in comparison to regular UNA and increases thermodynamic stability of TBA by 0.28-0.44 kcal/mol in a position depending manner with retained quadruplex topology and molecularity.

2.3. Modifications in the Internucleotide Phosphates of the Guanosine Tetrad

The TBA has been modified with three different phosphate linkers, phosphorothioate, methylphosphonate and formacetal. The structures of these linkages are summarized in Fig. (**5**). The modified TBA oligonucleotides containing thiophosphoryl substitutions at different internucleotide sites were studied. It was found that these linkages do not disrupt the antiparallel ntramolecular quadruplex [52]. The substitutions placed between planes of G-quartets led to a drop in formation free energy, and the stability decreases linearly with the number of these modifications. The TBA containing phosphorothioate linkages have more resistance to various nucleases. In this way, the *in vivo* half-life of the modified TBAs are increased. Mergny's group also studied the introduction of phosphorothioate bonds in all of G-forming tetrads [50]. The resulting modified TBA was less stable than the unmodified TBA. It also had an intramolecular G-quadruplex structure with concentration independent melting temperatures showing a reversible quadruplexes to random coil transitions. The same group studied the modified TBA carrying backbone methylphosphonate in the two G- tetrads [50]. The methylphosphonate TBA variant suffered a loss of negative charge at the level of the phosphate backbone that led to a strong destabilization. Non observable melting transition was detected. The negative charge of the oxygen atoms in the phosphate groups was found to be involved in a complex pattern of water bridges with the sugar group and the edges of the guanine units. A series of TBA analogues were synthesized containing one or more phosphodiester linkages replaced by a natural formacetal group [61]. The formacetal group is achiral and the incorporation of these moieties into oligonucleotides decreased the tissue uptake and increased the *in vivo* half-life. Unfortunately, no structural studies were carried out with these TBA analogues.

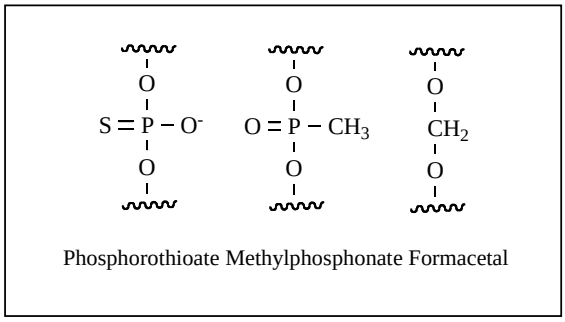

Fig. (5). Chemical structure of the modified internucleotide phosphate bonds in the guanine TBA tetrads.

In summary, several G-tetrad modifications of the TBA have been studied. Some of them have destabilized or disrupted the quadruplex structure because the introduced modification have changed directly the H-bonding tetrad arrangement, sugar puckering or glycosidic guanine orientation. In addition, some modifications have destabilized the antiparallel quadruplex to form a more undefined multimer quadruplex structures.

3. MODIFICATION OF THE LOOPS

The TBA is formed by two guanine tetrads connected by three edge-wise-loops: a central TGT loop and two TT loops as it is shown in the Fig. (**1A**). The loops are important in the folding of the aptamer and in the interactions with the thrombin. Most of the modifications are based in changes of the composition or in the length of the loops. Thymine bases in the loop region exclusively prefer the *anti* orientation. The literature reports that G^8 shows base stacking interactions with the first tetrad, but the conformation of the nucleoside is not mentioned.

3.1. Modifications of the Loop Composition by Natural Nucleosides

Shafer's group has undertaken a systematic examination of the thermodynamic stability of thrombin aptamer analogues containing sequence modifications in one or more loops [28]. The results indicated that changes in loop sequences had a significant impact on the aptamer stability. Most of the changes in the central loop led to a decrease in thermodynamic stability, indicating that, at least among the sequences explored, the TGT loop sequence is optimal for stability. These effects may involve changes in both stacking interactions and cation binding. The impact of replacing single Ts in the external loops with Cs provide evidence for hydrogen bond formation between these loops, as observed in the NMR structures. The stability of aptamers containing a C in position 3 or 12 was similar or slightly higher than the unmodified TBA. A recent paper has examined the stability of the G-quadruplex of TBA in which thymine residues were substituted by adenine. The G-quadruplexes formed by T^4A and $T^{13}A$ were more stable and T^3A, T^7A, T^9A and $T^{12}A$ were more unstable than that of the wild-type [62].

3.2. Modifications of the Loop Composition by Non-natural Nucleosides

Replacement of *anti* thymines in the loops with *anti* conformationally biased 2'-F-araT increased the thermal stability to different degrees depending on the number and position of the modification. In addition, the modification of G^8 with 2'-F-araG resulted in an increase of the stability. Overall, 2'-F-araN modifications in the loops stabilizes the formation of a unimolecular G-quadruplex [58]. LNA substitutions in the loops demonstrate a position dependent effect on the stability of the TBA. The substitution of G^8 for G-LNA increased the stability, but the substitution of T^7 decreased the stability. Nevertheless, substitution of T^4 disrupted the aptamer [48]. On the other hand, single UNA modification of the TBA in U^3, U^7 and U^{12} positions did not affect the stability of the unimolecular antiparallel structure. However, these same modifications in positions U^4, G^8, U^9 and U^{13} resulted in significant destabilization of the quadruplex structure [49].

Borbone's group modified the different positions of the TBA with flexible acyclic thymidines [63]. They obtained the same pattern of thermodynamic stabilities than UNA modifications. These analogues were able to fold into a bimolecular or monomolecular quadruplex structure depending on the nature of the monovalent cations (sodium or potassium) coordinated in the quadruplex core. Thermal stability was in agreement with the structural model in which T^9, T^4 and T^{13} are stacked on the adjacent G-quartet. These interactions were totally or partially disrupted by the introduction of the acyclic nucleotide at these positions. The TBA analogues containing an acyclic residue at positions T^3, T^7 or T^{12} resulted in a similar stability than the observed for the unmodified TBA, thus suggesting a marginal role of these positions on the structural stability [63].

Modifications of the TBA loops by thiophosphoryl internucleotide bonds were evaluated [52]. No destabilization was observed in each of the loop regions, although the stability against nuclease was increased in comparison to that of the native TBA. Finally, a new TBA aptamer modified with 4-thio-2'-deoxyuridines replacing some Ts in the loops was described [64]. This substitution was based on previous experiments showing that oligonucleotides with 4-thio-2'-deoxyuridines showed high-affinity binding to HIV-1 reverse transcriptase [65]. No thermodynamic data were performed but TBA modified with 4-thio-2'-deoxyuridines has an increased anticoagulant and antithrombotic properties [64].

3.3. Modification of the Loop Length

Loop length plays an important role in intramolecular quadruplex formation. When the central loop was replaced by four nucleotides, the resulting aptamer had a lower stability compared to unmodified TBA [28]. The thermodynamic analysis indicated that the central loop sequence in the parent aptamer is optimal for stability. Reduction of the two external TT loops to a single T led to a complete disruption of the quadruplex structure. This was expected due to the difficulty of forming a single base loop. On the contrary, extension to TTT loops had the same stability as the unmodified TBA. Addition of a single G at the 5'-end decreased the stability of the aptamer while addition of a G at the 3'-end increased the stability [28].

4. SYNTHESIS OF DIFFERENT CONSTRUCTS BASED ON THE TBA

In an effort to select more potent and selective DNA ligands to thrombin, several authors have synthesized different constructs. Most of them have modified the TBA structure itself or others have incorporated additional structures or molecules to the TBA. The first approach was comprised of an unimolecular quadruplex motif and complementary flanking sequences capable of forming an additional Watson-Crick duplex motif [66]. After that, following the same approach, a new 29 nucleotide single stranded oligonucleotide based on a quadruplex/duplex structure was described to bind the heparin-binding exosite of thrombin [67]. Seela's group proposed a new construct arising by replacement of the TGT loop of the TBA by a mini-hairpin 5'-GCGAAGC-3'. This fused oligonucleotide exhibited a two-phase thermal transition indicating the presence of the two unaltered moieties [68].

A new interesting architecture demonstrated that the combination of bivalent TBA aptamers, which simultaneously targeted and accordingly inhibited the regulatory exosites I and II of thrombin [69]. This approach turned out to be a combination of features of the individual aptamers in one molecule: high affinity binding and anticoagulant activity. A new quadruplex structure was studied in the $d(G^2T^4G^2CAG^2GT^4G^2T)$ sequence, which differs from the TBA in having longer first (T^4) and third (GT^4) loop and a shorter (CA) middle loop. This oligonucleotide has different strand directionalities, loop connectivities and *syn*/*anti* G-tetrad distribution [70]. Circularization is an attractive alternative to chemical modification for improving aptamer stability. This new approach was used in the design and construction of a TBA aptamer. The new construct has increased target binding affinity and much improved stability in biological fluids [71].

Mayol and co-workers described a new topology of the TBA that consists of a series of oligonucleotides containing 3'-3' or 5'-5' inversion of polarity sites [72]. The oligonucleotide d(3'-GGT-5'-5'-TGGTGTGGTTGG-3') was characterized by an unusual folding, three strands parallel to each other and only one strand oriented in an opposite manner. This led to an *anti-anti-anti-syn* and *syn-syn-syn-anti* arrangement of the Gs in the two tetrads. The thermal stability of the modified oligonucleotide was higher than the corresponding for the unmodified TBA.

Several intercalating agents have been conjugated to the 3'-end of the TBA and they have been found to stabilize the aptamer. Moreover, the hydrophobicity and fluorescent properties may be used to enhance the bioavailability of these conjugates [73]. Finally, the capping of the 3'-end of the TBA with bridged nucleosides was described. The bridged nucleosides increased the nuclease resis-

tance 36-27 fold and the stability in serum 1.5-4 fold without affecting the binding affinities of the aptamers to thrombin [74].

5. BINDING ACTIVITY OF MODIFIED THROMBIN BINDING APTAMERS

The reported bibliography concerning the modified TBAs might give an insight into the variables involved in the mode of action of the TBA. Nevertheless, the mode of action of the TBAs actually requires a more wide recognition process that involves even locally a single residue. Several assays are described to study the binding or interaction of the modified TBAs to thrombin such as nitrocellulose filter binding assay [58], isothermal tritation calorimetry [53, 56, 62, 75], surface plasmon resonance [49] or by non-equilibrium capillary electrophoresis of equilibrium mixtures (NECEEM) [74]. Recently, the interaction of the TBA with thrombin was evaluated by differential pulse voltammetry at a glassy carbon electrode and atomic force microscopy at a highly oriented pyrolytic graphite electrode [76].

Thrombin binding affinity of the modified TBAs in the tetrads was studied by different researchers. The thrombin binding of a TBA containing 2'-deoxyinosine or 7-deaza-2'-deoxyguanosine was significantly decreased as the residues were unable to form the hydrogen bonds required for the formation of the G-tetrad [77]. On the contrary, the TBA containing isoguanine showed an enhanced binding activity to human α-thrombin compared to the unmodified TBA determined by isothermal titration calorimetry [56]. The effect of 2'-F-araN modifications was conducted using nitrocellulose filter binding assay. The binding of 2'-F-araN aptamers to thrombin was always adversely affected when the modification was on G tetrads themselves. Some loop modifications with 2'-F-araN also reduced thrombin binding. However, the two loop modified aptamers in positions 7, 9, 12, 13 or 3, 4 , 7, 9 showed a 4-5 fold enhancement in thrombin binding affinity [58].

On the other hand, real-time measurements of the interaction between thrombin and the TBA containing UNA modifications were performed by surface plasmon resonance. The modification of the G^1 position showed similar affinities to the unmodified TBA. The rest of the Gs involved in the tetrads showed a higher dissociation constant or were not measurable, presumably due to a lack of significant affinity towards thrombin after the incorporation of UNA in these positions. The U^7 UNA modification located in the central loop was the only UNA modified aptamer that showed small but significant improvement in affinity [49]. Similar results were obtained with 2'-C-piperazino-UNA-U monomer, but in this case the presence of a positively charge decreased the thrombin affinity [60].

Another interesting work has focused on the replacement of thymine loop residues by adenine. Isothermal titration calorimetry (ITC) measurements indicated that the binding constant of the interactions between $T^{13}A$, T^7A, T^9A and $T^{12}A$ aptamers and thrombin was close to that of the unmodified TBA, whereas $T^{13}A$ was significantly lower and T^4A did not appear to bind thrombin [62]. The binding energy of the modified TBA containing a 5'-5'-site of polarity inversion to thrombin was characterized by means of ITC. The equilibrium constant for the interaction of the modified TBA was about one order of magnitude higher than that for the TBA. The binding process was enthalpically driven with a larger favorable enthalpy for the modified aptamer [75]. The construct formed by a quadruplex core of the TBA and a duplex interacted with a 20 to 50 –fold higher affinity to the heparin-binding exosite than the unmodified TBA by nitrocellulose filter [67]. Finally, thrombin binding affinities of capped TBAs with 2',4'-bridged nucleotides were measured using non-equilibrium capillary electrophoresis of equilibrium mixtures (NECEEM) [74]. The binding abilities were almost the same level than the native TBA.

According to the different strategies used to measure the thrombin binding, we can conclude that no important binding changes are observed when the modification does not disrupt the quadruplex structure. In addition, some modifications in the loops or in the overall construct structure do not affect or increase the binding affinity.

6. THROMBIN INHIBITION BY MODIFIED THROMBIN BINDING APTAMERS

Prothrombin Time (PT) is the more used assay to study the inhibition of thrombin. PT assay is a routine diagnostic assay that evaluates *in vitro* the activation of extrinsic pathway of the coagulation cascade. This ultimately measures the conversion of fibrinogen in fibrin by thrombin, with the consequent formation of a solid gel clot. When this assay is performed in presence of the aptamer TBA, the binding of fibrinogen to the thrombin is inhibited and a longer time is required to form a clot. Moreover, other important assays are fibrinopeptide A release assay, platelet aggregation and thrombus growth.

The effects of the substitutions at N^2 and C^8 of the G residues which form the G-tetrad on the thrombin inhibitory activity measured by PT were relatively small. The introduction of a benzyl group into N^2 of G^6 and G^{11} and naphthylmethyl groups into N^2 of G^6 increased the thrombin inhibitory activity, whereas other substituents in these positions had almost no effect or decreased the activity. Particularly, the oligonucleotides carrying a 1–naphthylmethyl group in the N2 position of G^6 showed an increase in activity by about 60% *in vitro* and *in vivo*. The introduction of a relatively small group such as methyl and propynyl, into the C8 positions of G^1, G^5, G^{10} and G^{14} increased the activity, presumably due to the stabilization of the quadruplex, whereas the introduction of a large substituent group, decreased the activity, probably due to steric hindrance [53]. The 2'-C-piperazino-UNA-U monomer modification showed an unfavorable impact of the piperazino moiety on the inhibition with thrombin [60]. The biological effect of the UNA-modified TBAs was tested in a prothrombin time assay. The TBA modified with UNA-U^7 showed an increased inhibitory effect relative to the unmodified TBA, while inhibition of coagulation by G^1, U^3, G^8, U^9 and U^{12} was near two fold decreased, and U^4, U^{13} and G^{15} showed no influence on fibrin-clot formation [49].

The TBA modified with LNA showed a different thrombin inhibition according the position of the modification. Stable aptamers with LNA in positions G^5, T^7 or G^8 showed a decreased thrombin inhibition measured by fibrin clotting assay. Nevertheless, a less stable aptamer with LNA at G^2 was as active as the unmodified aptamer [48]. In addition, Mayol's group described that the TBA modified by LNA in the G^{15} position displayed a prolonged PT [47]. The modification of the phosphate linkages by formacetal [61] or thiophosphoryl [52] groups exhibited a similar prothrombin time to the one found for the unmodified TBA. The effect of the modified loops on the thrombin inhibitory activity was also studied using acyclic nucleosides. In this case, the analysis of PT assays confirmed that the highest PT value was obtained for a modified TBA containing an acyclic thymidine in position 7 [63]. On the other hand, the TBA modified with four 4-thiodeoxyuridine showed a 2-fold increased inhibition of thrombin catalyzed fibrin clot formation, fibrinopeptide A release and thrombus formation [46].

The structural changes in the overall structure that have been described do not seem to affect too much the thrombin inhibition [75]. The TBA containing a 5'-5' inversion of polarity site affected sensibly the biological inhibition. Cook and co-workers presented a series of constrained unimolecular quadruplex/duplex molecules with increased thrombin inhibition using clot formation assay and release of fibrinopeptide A [66]. Moreover, Steiner also described a quadruplex/duplex molecule construct that binds the heparin-binding exosite with 20-50 fold higher affinity measured by clotting time [67].

Finally, the new construct assembled by two distinct aptamers that targets thrombin combines features of the individual aptamer

subdomains with enhanced activities regarding both functionalities; these are probably due to an enhanced affinity of the bivalent fusion aptamer. This structure displayed enhanced anticoagulant activity when compared to the TBA, however, affinities were improved only two to three fold compared to those of the individual precursors [69].

Similar conclusions could be obtained for the thrombin inhibition of the modified TBA. It is important to mention that T^7 position seems very sensitive to different modifications in terms of increasing the thrombin inhibition. Moreover, the addition of different constructs with improved pharmacokinetic properties to the TBA could be a reasonable idea that probably would not compromise the inhibitory activity.

7. NOVEL APPLICATIONS USING THROMBIN BINDING APTAMER.

In addition to the anticoagulant properties, a large number of analytical tools based on the folding and refolding of the TBA have been developed. In the following section some of these new developments are reviewed.

7.1. The TBA as Model for the Analysis of Binding Mode of Drugs with Affinity to G-Quadruplex

G-quadruplexes have become structures of special interest for drug development due to their possible implications in anticancer research. The potential role of G-quadruplexes has been highlighted with the development of strategies designed to stabilize telomere ends as G-quadruplex structures using specific small molecules, which can destabilize telomere maintenance in tumour cells [78]. G-quadruplexes are also found in transcriptional regulatory sequences of critical oncogenes such as *c-myc* and *c-kit* [79, 80]. Ligands that selectively bind and stabilize these structures were studied as potential anticancer drugs of interest [81]. The TBA was used as a model for the analysis of the interaction of several drugs with G-quadruplex structures. In one of the first studies, Joachimi *et al*. described the potential role of porphyrins in the modulation of the anticoagulant properties of the TBA [82]. Later, Del Toro *et al*. confirmed the formation of an interaction complex with a stoichiometry 1:1 between the porphyrin (TmPyP4) and the TBA [83]. Ultraviolet melting and circular dichroism data reflected that the initial G-quadruplex structure of the TBA was stabilized in the interaction complex: being slightly disordered by the presence of the ligand. The interaction between the porphyrin (TmPyP4) and the TBA was also studied by time-resolved fluorescence anisotropy. Based on the anisotropic decay curves, a sandwich-type binding mode was proposed in which both terminal G-quartet and T-T base pairs stack on the porphyrin ring [84]. The interaction between the TBA and the bipyridinium salts was studied by cyclic voltammetry. A strong interaction between G-quadruplex forming DNA sequences and viologens was observed [85].

7.2. TBA as Sensing Element for Thrombin and Metal Ions

The conformational change of the TBA during the folding /unfolding process was exploited for building sensors for metal ions and for detection of thrombin. This work together with the use of other aptamers as sensors has been summarized in several recent reviews [86-90]. One of the most relevant studies is the development of probes for the detection of intracellular potassium concentration [91-92]. Oligonucleotides containing the TBA sequence functionalized with a fluoresceine derivative as fluorophore and a rhodamine dye as quencher at the 3' and 5'-ends were prepared. Upon binding of potassium, the TBA probes folded in the intramolecular quadruplex. The quadruplex folding induced by potassium was observed by a decrease of fluorescence due to fluorophore-quencher interaction [91-92]. The development of quadruplex DNA-based FRET probes with special emphasis on the TBA quadruplexes were reviewed [93].

A similar FRET experiment was adapted recently for the detection of the activity of human O^6-alkylguanine-DNA alkyltransferase (hAGT) [94]. The modified TBA probe contained one O^6-methylguanine residue that prevented quadruplex formation. Upon removal of the O^6-methyl group in the guanine by hAGT, the natural TBA sequence is formed and it folds into the quadruplex, inducing a decrease of fluorescence due to fluorophore-quencher interaction [94]. A colorimetric assay for the determination of mercury (II) using the TBA was also reported [95]. The binding of mercury to the TBA induced the folding of the molecule that triggered salt-induced gold nanoparticle aggregation [95].

The folding/unfolding of the TBA can also be regulated by light. The incorporation of *o*-nitrobenzyl thymidine derivatives (caged nucleosides) in the TBA sequence did not allow the folding of the TBA, preventing thrombin binding. Photoremoval of the nitrobenzyl groups on thymidines generated the native aptamer which now is capable of binding thrombin, which prevented blood clotting [96]. Also, the effect of a photoactive nitrobenzyl group on a guanine residue of TBA has been studied using classical molecular simulations [97]. Theoretical calculations are able to describe the change in the structure when the modified residue is incorporated in the TBA as well as the formation of the quadruplex after photolysis [97]. The photodeprotection of the nitrobenzyl groups is irreversible and for this reason, Ogazawara *et al.* [98] developed a guanine derivative carrying a fluorenylvinyl group at position 8. The fluorenylvinyl guanine derivative may undergo to *cis-trans* photoisomerization that is reversible. The *cis-trans* isomerization affected the formation of the quadruplex structure and subsequently the binding of thrombin. In this way, the binding of thrombin to the TBA derivatives carrying guanines with the fluorenylvinyl group can be reversibly modulated by light [97].

The conjugation of several derivatives of the TBA to gold nanoparticles was studied [99]. Some of the TBA-gold nanoparticles are highly efficient as anticoagulants [99]. Moreover, the functionalization of iron oxide nanoparticles with TBA has described [100]. The TBA magnetic nanoparticles conjugates showed a clear magnetic resonance imaging (MRI) signal when binding to thrombin [100].

Several electrochemical sensing platforms based on the TBA quadruplex were developed for the detection of thrombin. A label-free electronic detection system for the direct detection of thrombin based on electrochemical impedance spectroscopy was developed [101]. The TBA carrying an amino group was covalently linked to multi walled carbon nanotube disposable screen-printed carbon electrodes by amide formation and the resulting electrodes were able to sense thrombin at a detection limit of 105 pM [101]. The incorporation of ferrocene to the TBA increased the sensitivity of the detection reaching a detection limit for thrombin to 0.5 pM [102]. Conjugation of the TBA to silver nanoparticles and to gold nanoshells allowed the detection of thrombin by surface-enhanced Raman spectroscopy [103-106]. The interaction of thrombin with the TBA was also studied on quantum dots and in surface plasmon resonance [107].

The absorption and redox behavior of the TBA and the complex thrombin-TBA was evaluated by differential pulse voltammetry at a glassy carbon electrodes [76, 108]. The TBA guanine oxidation peak was found to be sensitive to G-quadruplex formation and to thrombin binding, showing a higher oxidation potential [76, 108]. Recently, the excellent binding properties of a 29-base-long thrombin-binding aptamer linked to gold nanoparticles were used for the development of a sensitive detection of DNA that relied on the modulation of the thrombin activity on the surface of the nanoparticles [109].

7.3. Single-molecule Experiments on the TBA

One of the first single-molecule experiments using the TBA-thrombin interaction was performed by atomic force microscopy

(AFM) [110]. An AFM gold-coated tip was functionalized with the thiolated TBA. The thrombin was linked covalently to a gold-coated glass slide. The rupture force for a single aptamer/thrombin complex was determined as 4.45 pN. The analysis of the system revealed that the rupture forces corresponded to the melting of the G-quadruplex of the aptamer bound to the thrombin and subsequent dissociation of the complex [110].

Recently, the TBA folding and unfolding induced by ions was studied using nanopores encapsulated with single molecules. The TBA quadruplex was formed rapidly in the presence of potassium ions and had a slow unfolding reaction. The sodium and lithium complex of the TBA were similar but the folding and unfolding of the sodium complex was faster than the folding and unfolding of the lithium complex [111].

The excellent molecular recognition properties of DNA were exploited to incorporate functionalities in molecular constructs and for the design of 2-dimensional arrays with well defined structures [112-113]. A remarkable development in this field was the use of stable DNA Holliday junctions with addressable sticky ends to form two-dimensional DNA crystals [113]. The so-called DNA tile system was used for the assembly of bidimensional DNA arrays, containing thrombin binding aptamer sequences [114-115]. The DNA arrays templated the formation of ordered thrombin arrays that were visualized by AFM [114-117]. Origami DNA is a new method for the rational organisation of structures that uses a circular viral single stranded DNA (M13 DNA) and about two hundred oligonucleotides (staple strands) that are designed to fold the viral DNA into a rationally designed shape [118]. The TBA sequences were also introduced in DNA origamis, showing a nanometric control of the deposition of thrombin molecules on the origami [119-120].

CONCLUSIONS

Aptamers are a novel class of nucleic acids with affinity to proteins that may be used for therapeutic or diagnostic purposes. The thrombin-binding aptamer was one of the first aptamers developed by SELEX and probably one of the most studied aptamer. The TBA is a relatively short sequence, easy to synthesize with a well-defined structure and has a good affinity for thrombin. For all these reasons, it can be considered a paradigm of the potential applications of the aptamers. During the last 20 years, several authors have defined the structural facets of the TBA molecule exploring several potential variables such as sugar puckering, glycosidic bond conformation, H-bonding groups, backbone modifications, etc… Some of the modified TBA derivatives have a good affinity for thrombin, as well as a large stability in physiological conditions, which has led to the setting of some clinical assays. The lessons learned in this process are important not only for the anticoagulant properties of the TBA but also to improve the understanding of G-quadruplex structures present in telomeres and some promoter regions of oncogenes.

An important development in the last years has been the conjugation of the TBA to nanomaterials such as gold and iron oxide nanoparticles, which may increase the stability in plasma as well as it may open the opportunity of adding receptor-mediated systems for efficient *in vivo* targeting. Moreover, the TBA-thrombin recognition system is already being used for the development of sensors based on both electrical and optical methods, and more recently for the DNA-templated directed assembly of nanomaterials. As the time goes on, the potential applications of this relatively simple DNA molecule are increasing exponentially. This intense activity will help to further develop the aptamer field and it may also span the knowledge about other useful nucleic acids for therapeutic or diagnostic purposes.

ACKNOWLEDGEMENT

This study was supported by the European Communities (FUNMOL, FP7-NMP-213382-2), Spanish Ministry of Education (MOL2MED, CTQ2010-20541), the Generalitat de Catalunya (2009/SGR/208), IRB Barcelona, COST (G4net, MP0802) and CIBER-BBN (VI National R&D&i Plan 2008-2011, Iniciativa Ingenio 2010, Consolider Program, CIBER Actions, Instituto de Salud Carlos III with assistance from the European Regional Development Fund.

REFERENCES

[1] Irvine D, Tuerk C, Gold L. SELEXION. Systematic evolution of ligands by exponential enrichment with integrated optimization by non-linear analysis. J Mol Biol 1991; 222: 739-61.

[2] Ellington AD, Szostak JW. *In vitro* selection of RNA molecules that bind specific ligands. Nature 1990; 346: 818-22.

[3] Tuerk C, Gold L. Systematic evolution of ligands by exponential enrichment: RNA ligands to bacteriophage T4 DNA polymerase. Science 1990; 249: 505-10.

[4] Szostak JW. *In vitro* genetics. Trends Biochem Sci, 1992; 17: 89-93.

[5] Brody EN, Gold L. Aptamers as therapeutic and diagnostic agents. J Biotechnol 2000; 74: 5-13.

[6] Kusser W. Chemically modified nucleic acid aptamers for *in vitro* selections: evolving evolution. J Biotechnol 2000; 74: 27-38.

[7] Bock LC, Griffin LC, Latham JA, Vermaas EH, Toole JJ. Selection of single stranded-DNA molecules that bind and inhibit human thrombin. Nature 1992; 355: 564-566.

[8] Griffin LC, Tidmarsh GF, Bock LC, Toole JJ, Leung LL. *In vivo* anticoagulant properties of a novel nucleotide-based thrombin inhibitor and demonstration of regional anticoagulation in extracorporeal circuits. Blood 1993; 81: 3271-6.

[9] Li WX, Kaplan AV, Grant GW, Toole JJ, Leung LL. A novel nucleotide-based thrombin inhibitor inhibits clot-bound thrombin and reduces arterial platelet thrombus formation. Blood 1994; 83: 677-82.

[10] Wu Q, Tsiang M, Sadler JE. Localization of the single-stranded DNA binding site in the thrombin anion-binding exosite. J Biol Chem, 1992; 267: 24408-12.

[11] Paborsky LR, McCurdy SN, Griffin LC, Toole JJ, Leung LLK. The single-stranded-DNA aptamer-binding site of human thrombin. J Biol Chem 1993; 268: 20808-20811.

[12] Wang KY, Krawczyk SH, Bischofberger N, Swaminathan S, Bolton PH. The tertiary structure of a DNA aptamer which binds to and inhibits thrombin determines activity. Biochemistry 1993; 32: 11285-92.

[13] Macaya RF, Schultze P, Smith FW, Roe JA, Feigon J. Thrombin-binding DNA aptamer forms a unimolecular quadruplex structure in solution. Proc Natl Acad Sci USA 1993; 90: 3745-9.

[14] Wang KY, McCurdy S, Shea RG, Swaminathan S, Bolton PH. A DNA Aptamer which binds to and inhibits thrombin exhibits a new structural motif for DNA. Biochemistry 1993; 32: 1899-904.

[15] Schultze P, Macaya RF, Feigon J. 3-Dimensional solution of the thrombin-binding-DNA aptamer d-(GGTTGGTGTGGTTGG). J Mol Biol 1994; 235: 1532-47.

[16] Padmanabhan K, Padmanabhan KP, Ferrara JD, Sadler JE, Tulinsky A. The structure of alpha-thrombin inhibited by a 15-mer single-stranded-DNA aptamer. J Biol Chem 1993; 268: 17651-4.

[17] Padmanabhan K, Tulinsky A. An ambiguous structure of a DNA 15-mer thrombin complex. Acta Cryst 1996; 52: 272-82.

[18] Kelly JA, Feigon J, Yeates TO. Reconciliation of the X-ray and NMR structures of the thrombin-binding aptamer d(GGTTGGTGTGGTTGG). J Mol Biol 1996; 256: 417-22.

[19] Bouaziz S, Kettani A, Patel DJ. A K cation-induced conformational switch within a loop spanning segment of a DNA quadruplex containing G-G-G-C repeats. J Mol Biol 1998; 282: 637-52.

[20] Guschlbauer W, Chantot JF, Thiele D. Four-stranded nucleic acid structures 25 years later: from guanosine gels to telomer DNA. J Biomol Struct Dyn 1990; 8: 491-511.

[21] Sen A, Gilbert A. The structure of telomeric DNA: DNA quadruplex formation. Nucleic Acids Res 1991; 1: 435-8.

[22] Kettani A, Bouaziz S, Gorin A, Zhao H, Jones RA, Patel DJ. Solution structure of a Na cation stabilized DNA quadruplex containing G.G.G.G and G.C.G.C tetrads formed by G-G-G-C repeats observed in adeno-associated viral DNA. J Mol Biol 1998; 282: 619-36.

[23] Marathias VM, Wang KY, Kumar S, Pham TQ, Swaminathan S, Bolton PH. Determination of the number and location of the

manganese binding sites of DNA quadruplexes in solution by EPR and NMR in the presence and absence of thrombin. J Mol Biol 1996; 260: 378-94.

[24] Nagatoishi S, Tanaka Y, Tsumoto K. Circular dichroism spectra demonstrate formation of the thrombin-binding DNA aptamer G-quadruplex under stabilizing-cation-deficient conditions. Biochem Biophys Res Comm 2007; 352: 812-7.

[25] Hianik T, Ostatná V, Sonlajtnerova M, Grman I. Influence of ionic strength, pH and aptamer configuration for binding affinity to thrombin. Bioelectrochem 2007; 70: 127-33.

[26] Marathias VM, Bolton PH. Determinants of DNA quadruplex structural type: sequence and potassium binding. Biochemistry 1999; 38: 4355-64.

[27] Smirnov I, Shafer RH. Lead is unusually effective in sequence-specific folding of DNA. J Mol Biol 2000; 296: 1-5.

[28] Smirnov I, Shafer RH. Effect of loop sequence and size on DNA aptamer stability. Biochemistry 2000; 39: 1462-8.

[29] Smirnov IV, Kotch FW, Pickering IJ, Davis JT, Shafer RH. Pb EXAFS studies on DNA quadruplexes: identification of metal ion binding site. Biochemistry 2002; 41: 12133-9.

[30] Kankia BI, Marky LA. Folding of the thrombin aptamer into a G-quadruplex with Sr2+: Stability, heat, and hydration. J Am Chem Soc 2001; 123: 10799-804.

[31] Vairamani M, Gross ML. G-quadruplex formation of thrombin-binding aptamer detected by electrospray ionization mass spectrometry. J Am Chem Soc 2003; 125: 42-3.

[32] Marathias VM, Bolton PH. Structures of the potassium-saturated, 2:1, and intermediate, 1:1, forms of a quadruplex DNA. Nucleic Acids Res 2000; 28: 1969-77.

[33] Mao X, Marky LA, Gmeiner WH. NMR structure of the thrombin-binding DNA aptamer stabilized by Sr2+. J Biomol Struct Dyn 2004; 22: 25-33.

[34] Trajkovski M, Sket P, Plavec J. Cation localization and movement within DNA thrombin binding aptamer in solution. Org Biomol Chem 2009; 7: 4677-84.

[35] Hong ES, Yoon HJ, Kim B, Yim YH, So HY, Shin SK. Mass Spectrometric Studies of Alkali Metal Ion Binding on Thrombin-Binding Aptamer DNA. J Am Soc Mass Spectrom 2010; 21: 1245-55.

[36] Baldrich E, Restrepo A, O'Sullivan CK. Aptasensor development: Elucidation of critical parameters for optimal aptamer performance. Anal Chem 2004; 76: 7053-63.

[37] Ho HA, Leclerc M. Optical sensors based on hybrid aptamer/conjugated polymer complexes. J Am Chem Soc 2004; 126: 1384-7.

[38] Li J, Correia JJ, Wang L, Trent JO, Chaires JB. Not so crystal clear: the structure of the human telomere G-quadruplex in solution differs from that present in a crystal. Nucleic Acids Res 2005; 33: 4649-59.

[39] Miyoshi D, Karimata H, Sugimoto N. Hydration regulates thermodynamics of G-quadruplex formation under molecular crowding conditions. J Am Chem Soc 2006; 128: 7957-63.

[40] Fialova M, Kypr J, Vorlickova M. The thrombin binding aptamer GGTTGGTGTGGTTGG forms a bimolecular guanine tetraplex. Biochem Biophys Res Comm 2006; 344: 50-54.

[41] Russo Krauss I, Merlino A, Giancola C, Randazzo A, Mazzarella L, Sica F. Thrombin-aptamer recognition: a revealed ambiguity. Nucleic Acids Res 2011, in press, doi: 10.1093/nar/gkr522.

[42] Mao X, Gmeiner WH. NMR study of the folding-unfolding mechanism for the thrombin-binding DNA aptamer d(GGTTGGTGTGGTTGG). Biophys Chem 2005; 113: 155-60.

[43] DeAnda A, Coutre SE, Moon MR, *et al*. Pilot study of the efficacy of a thrombin inhibitor for use during cardiopulmonary bypass. Ann Thorac Surg 1994, 58:344-50.

[44] Schwienhorst A. Direct thrombin inhibitors - a survey of recent developments. Cell Mol Life Sci 2006; 63: 2773-91.

[45] Lancellotti S, De Cristofaro R. Nucleotide-derived thrombin inhibitors: a new tool for an old issue. Cardiovasc Hematol Agents Med Chem 2009; 7: 19-28.

[46] Mendelboum Raviv S, Horvath A, Aradi J, *et al*. 4-thio-deoxyuridylate-modified thrombin aptamer and its inhibitory effect on fibrin clot formation, platelet aggregation and thrombus growth on subendothelial matrix. J Thromb Haemost 2008; 6: 1764-71.

[47] Virno A, Randazzo A, Giancola C, Bucci M, Cirinoc G, Mayol L. A novel thrombin binding aptamer containing a G-LNA residue. Bioorg Med Chem 2007; 15: 5710-8.

[48] Bonifacio L, Church FC, Jarstfer MB. Effect of locked-nucleic acid on a biologically active G-quadruplex. A structure-activity relationship of the thrombin aptamer. Int J Mol Sc 2008; 9: 422-33.

[49] Pasternak A, Hernandez FJ, Rasmussen LM, Vester B, Wengel J. Improved thrombin binding aptamer by incorporation of a single unlocked nucleic acid monomer. Nucleic Acids Res 2011; 39: 1155-64.

[50] Sacca B, Lacroix L, Mergny JL. The effect of chemical modifications on the thermal stability of different G-quadruplex-forming oligonucleotides. Nucleic Acids Res 2005; 33: 1182-92.

[51] Tang CF, Shafer RH. Engineering the quadruplex fold: Nucleoside conformation determines both folding topology and molecularity in guanine quadruplexes. J Am Chem Soc 2006; 128: 5966-73.

[52] Zaitseva M, Kaluzhny D, Shchyolkina A, Borisova O, Smirnov I, Pozmogova G. Conformation and thermostability of oligonucleotide d(GGTTGGTGTGGTTGG) containing thiophosphoryl internucleotide bonds at different positions. Biophys Chem 2010; 146: 1-6.

[53] He GX, Krawczyk SH, Swaminathan S, *et al*. N-2- and C-8-substituted oligodeoxynucleotides with enhanced thrombin inhibitory activity *in vitro* and *in vivo*. J Med Chem 1998; 41: 2234-42.

[54] Marathias VM, Sawicki MJ, Bolton PH. 6-Thioguanine alters the structure and stability of duplex DNA and inhibits quadruplex DNA formation. Nucleic Acids Res 1999; 27: 2860-7.

[55] de la Osa JP, Gonzalez C, Gargallo R, *et al*. Destabilization of quadruplex DNA by 8-aminoguanine. Chembiochem 2006; 7: 46-8.

[56] Nallagatla SR, Heuberger B, Haque A, Switzer C. Combinatorial synthesis of thrombin-binding aptamers containing iso-guanine. J Comb Chem 2009; 11: 364-9.

[57] Randazzo A, Esposito V, Ohlenschlager O, Ramachandran R, Virgilio A, Mayol L. Structural studies on LNA quadruplexes. Nucleosides Nucleotides Nucleic Acids 2005; 24: 795-800.

[58] Peng CG, Damha MJ. G-quadruplex induced stabilization by 2'-deoxy-2'-fluoro-D-arabinonucleic acids (2'F-ANA). Nucleic Acids Res 2007; 35: 4977-88.

[59] Saneyoshi H, Mazzini S, Avino A, *et al*. Conformationally rigid nucleoside probes help understand the role of sugar pucker and nucleobase orientation in the thrombin-binding aptamer. Nucleic Acids Res 2009; 37: 5589-601.

[60] Jensen TB, Henriksen JR, Rasmussen BE, *et al*. Thermodynamics and biological evaluation of a thrombin binding aptamer modified with several unlocked nucleic acids (UNA) monomers and a 2'-C-piperazino-UNA-monomer). Bioorg Med Chem 2011; 19: 4739-45.

[61] He GX, Williams JP, Postich MJ, *et al*. *In vitro* and *in vivo* activities of oligodeoxynucleotide-based thrombin inhibitors containing neutral formacetal linkages. J Med Chem 1998; 41: 4224-31.

[62] Nagatoishi S, Isono N, Tsumoto K, Sugimoto N. Loop residues of thrombin-binding DNA aptamer impact G-quadruplex stability and thrombin binding. Biochimie 2011, 93: 1231-8.

[63] Coppola T, Varra M, Oliviero G, *et al*. Synthesis, structural studies and biological properties of new TBA analogues containing an acyclic nucleotide. Bioorg Med Chem 2008; 16: 8244-53.

[64] Raviv SM, Horvath A, Aradi J, *et al*. 4-thio-deoxyuridylate-modified thrombin aptamer and its inhibitory effect on fibrin clot formation, platelet aggregation and thrombus growth on subendothelial matrix. J Thromb Haemost 2008; 6: 1764-71.

[65] Horvath A, Tokes S, Hartman T, *et al*. Potent inhibition of HIV-1 entry by (s4dU)35. Virology 2005; 334: 214-23.

[66] Macaya RF, Waldron JA, Beutel BA, *et al*. Structural and functional-characterization of potent antithrombotic oligonucleotides possessing both quadruplex and duplex motifs. Biochemistry 1995; 34: 4478-92.

[67] Tasset DM, Kubik MF, Steiner W. Oligonucleotide inhibitors of human thrombin that bind distinct epitopes. J Mol Biol 1997; 272: 688-98.

[68] Rosemeyer H, Moskrosch V, Jawalekar A, Becker EM, Seela F. Single-stranded DNA: Replacement of canonical by base-modified nucleosides in the mini hairpin 5'-d(GCGAAGC)-3' and constructs with the aptamer 5'-d(GGTTGGTGTGGTTGG)-3'). Helv Chim Acta 2004; 87: 536-53.

[69] Muller J, Wulffen B, Potzsch B, Mayer G. Multidomain targeting generates a high-affinity thrombin-inhibiting bivalent aptamer. Chembiochem 2007; 8: 2223-6.

[70] Kuryavyi V, Majumdar A, Shallop A, *et al*. A double chain reversal loop and two diagonal loops define the architecture of a unimolecular DNA quadruplex containing a pair of stacked G(syn)-G(syn)-G(anti)-G(anti) tetrads flanked by a G-(T-T) Triad and a T-T-T triple. J Mol Biol 2001; 310: 181-94.

[71] Di Giusto DA, King GC. Construction, stability, and activity of multivalent circular anticoagulant aptamers. J Biol Chem 2004; 279: 46483-9.

[72] Martino L, Virno A, Randazzo A, *et al*. A new modified thrombin binding aptamer containing a 5 '-5' inversion of polarity site. Nucleic Acids Res 2006; 34: 6653-62.

[73] Aviño A, Mazzini S, Ferreira R, Eritja R. Synthesis and structural properties of oligonucleotides covalently linked to acridine and quindoline derivatives through a threoninol linker. Bioorg Med Chem 2010; 18: 7348-56.

[74] Kasahara Y, Kitadume S, Morihiro K, *et al*. Effect of 3 '-end capping of aptamer with various 2 ',4 '-bridged nucleotides: Enzymatic post-modification toward a practical use of polyclonal aptamers. Bioorg Med Chem Lett 2010; 20: 1626-9.

[75] Pagano B, Martino L, Randazzo A, Giancola C. Stability and binding properties of a modified thrombin binding aptamer. Biophys J 2008; 94: 562-9.

[76] Diculescu VC, Chiorcea-Paquim AM, Eritja R, Oliveira-Brett AM. Evaluation of the structure-activity relationship of thrombin with thrombin binding aptamers by voltammetry and atomic force microscopy. J Electroanal Chem 2011; 656: 159-66.

[77] Krawczyk SH, Bischofberger N, Griffin LC, Law VS, Shea RG, Swaminathan S. Structure-activity study of oligonucleotides which inhibit thrombin. Nucleosides Nucleotides 1995; 14: 1109-16.

[78] Patel DJ, Phan AT, Kuryavyi V. Human telomere, oncogenic promoter and 5'-UTR G-quadruplexes: diverse higher order DNA and RNA targets for cancer therapeutics. Nucleic Acids Res 2007; 35: 7429-55.

[79] Huppert JL. Hunting G-quadruplexes. Biochimie 2008; 90: 1140-8.

[80] Hurley LH. Secondary DNA structures as molecular targets for cancer therapeutics. Biochem Soc Trans 2001; 21: 136-42.

[81] Han H, Hurley LH. G-quadruplex DNA: a potential target for anti-cancer drug design. Trends Pharmacol Sci 2000; 21: 136-42.

[82] Joachimi A, Mayer G, Hartig JS. A new anticoagulant-antidote pair: control of thrombin activity by aptamers and porphyrins. J Am Chem Soc 2007; 129: 3036-7.

[83] del Toro M, Gargallo R, Eritja R, Jaumot J. Study of the interaction between the G-quadruplex-forming thrombin-binding aptamer and the porphyrin 5,10,15,20-tetrakis-(N-methyl-4-pyridyl)-21, 23H-porphyrin tetratosylate. Anal Biochem 2008; 379: 8-15.

[84] Jia G, Feng Z, Wei C, Zhou J, Wang X, Li C. Dynamic insight into the interaction between porphyrin and G-quadruplex DNAs: time-resolved fluorescence anisotropy study. J Phys Chem B 2009; 113: 16237-45.

[85] Asaftei S, Rosemeyer H, Walder L. Interaction of viologens with nucleic acid G-tetrades. Langmuir 2008; 24: 5641-3.

[86] Mairal T, Ozalp VC, Lozano Sanchez P, Mir M, Katakis I, O'Sullivan CK. Aptamers: molecular tools for analytical applications. Anal Bioanal Chem 2008; 390: 989-1007.

[87] Liu J, Cao Z, Lu Y. Functional nucleic acid sensors. Chem Rev 2009; 109: 1948-98.

[88] Lee JO, So HM, Jeon EK, Chang H, Won K, Kim YH. Aptamers as molecular recognition elements for electrical nanobiosensors. Anal Bioanal Chem 2008; 390: 1023-32.

[89] Bini A, Minunni M, Tombelli S, Centi S, Mascini M. Analytical performances of aptamer-based sensing for thrombin detection. Anal Chem 2007; 79: 3016-9.

[90] Li N, Ho CM. Aptamer-based optical probes with separated molecular recognition and signal transduction modules. J Am Chem Soc 2008; 130: 2380-1.

[91] Nagatoishi S, Nojima T, Juskowiak B, Takenaka S. A pyrene-labeled G-quadruplex oligonucleotide as a fluorescent probe for potassium ion detection in biological applications. Angew Chem Int Ed Engl 2005; 44: 5067-70.

[92] Nagatoishi S, Nojima T, Galezowska E, Juskowiak B, Takenaka S. G quadruplex-based FRET probes with the thrombin-binding aptamer (TBA) sequence designed for the efficient fluorometric detection of the potassium ion. Chembiochem 2006; 7: 1730-7.

[93] Juskowiak B. Analytical potential of the quadruplex DNA-based FRET probes. Anal Chim Acta 2006; 568: 171-80.

[94] Tintoré M, Aviñó A, Ruiz FM, Eritja R, Fàbrega C. Development of a novel fluorescence assay based on the use of the thrombin-binding aptamer for teh detection of O6-alkylguanine-DNA alkyltransferase activity. J Nucl Acids 2010; 2010: 1-9.

[95] Wang Y, Yang F, Yang XR. Colorimetric biosensing of mercury(II) ion using unmodified gold nanoparticle probes and thrombin-binding aptamer. Biosen Bioelectron 2010; 25: 1994-8.

[96] Heckel A, Mayer G. Light regulation of aptamer activity: an anti-thrombin aptamer with caged thymidine nucleobases. J Am Chem Soc 2005; 127: 822-3.

[97] Jayapal P, Mayer G, Heckel A, Wennmohs F. Structure-activity relatioships of a caged thrombin DNA aptamer: Insight gained from molecular dynamics simulation studies. J Struct Biol 2009; 166: 241-50.

[98] Ogasawara S, Maeda M. Reversible photoswitching of a G-quadruplex. Angew Chem Int Ed Engl 2009; 48: 6671-4.

[99] Shiang YC, Huang CC, Wang TH, Chien CW, Chang HT. Aptamer-conjugated nanoparticles based efficiently probes and thrombin-binding aptamer. Biosen Bioelectron 2010; 25: 1994-8.

[100] Yigit MV, Mazumdar D, Lu Y. MRI detection of thrombin with aptamer functionalized superparamagnetic iron oxide nanoparticles. Bioconjug Chem 2008; 19: 412-7.

[101] Kara P, de la Escosura-Muniz A, Maltez-da Costa M, Guix M, Ozsoz M, Merkoci A. Aptamers based electrochemical biosensor for protein detection using carbon nanotubes platforms. Biosen Bioelectron 2010; 26: 1715-8.

[102] Liu X, Li Y, Zheng J, Zhang J, Sheng Q. Carbon nanotube-enhanced electrochemical aptasensor for the detection of thrombin. Talanta 2010; 81: 1619-24.

[103] Pagda CV, Lane SM, Cho H, Wachsmann-Hogiu S. Direct detection of aptamer-thrombin binding *via* surface-enhanced Raman spectroscopy. J Biomed Optics 2010; 15: 047006/1-8.

[104] Ochsenkuehn MA, Campbell CJ. Probing biomolecular interactions using enhanced Raman spectroscopy: label-free protein detection using a G-quadruplex DNA aptamer. Chem Comm 2010; 46: 2799-801.

[105] Cho H, Baker BR, Wachsmann-Hogiu S, *et al*. Aptamer-Based SERRS Sensor for Thrombin Detection. Nano Lett 2008; 8: 4386-90.

[106] Pagda CV, Lane SM, Wachsmann-Hogiu S. Raman and surface-enhanced Raman spectroscopic studies of the 15-mer DNA thrombin binding aptamer. J. Raman Spec 2009; 41: 241-7.

[107] Balamurugan S, Obubuafo A, McCarley RL, Soper SA, Spivak DA. Effect of Linker Structure on Surface Density of Aptamer Monolayers and Their Corresponding Protein Binding Efficiency. Anal Chem 2008; 80: 9630-4.

[108] Diculescu VC, Chiorcea-Paquim AM, Eritja R, Oliveira-Brett AM. Thrombin-binding aptamer quadruplex formation: AFM and voltammetric characterization. J Nucl Acids 2010; 2010: 1-8.

[109] Jian JW, Huang CC. Colorimetric Detection of DNA by Modulation of Thrombin Activity on Gold Nanoparticles. Chem-Eur J 17: 2374-80.

[110] Basnar B, Elnathan R, Willner I. Following aptamer-thrombin binding by force measurements. Anal Chem 2006; 78: 3638-42.

[111] Shim JW, Tan Q, Gu LQ. Single-molecule detection of folding and unfolding of the G-quadruplex aptamer in a nanopore nanocavity. Nucleic Acids Res 2009; 37: 972-82.

[112] Aldaye FA, Palmer AL, Sleiman HF. Assembling materials with DNA as the guide. Science 2008; 321: 1795-9.

[113] Winfree E, Liu F, Wenzler LA, Seeman NC. Design and self-assembly of two-dimensional DNA crystals. Nature 1998; 394: 539-44.

[114] Lin C, Katilius E, Liu Y, Zhang J, Yan H. Self-assembled signaling aptamer DNA arrays for protein detection. Angew Chem Int Ed Engl 2006; 45: 5296-301.

[115] Liu Y, Lin C, Li H, Yan H. Aptamer-directed self-assembly of protein arrays on a DNA nanostructure. Angew Chem Int Ed Engl 2005; 44: 4333-8.

[116] Li H, LaBean TH, Kenan DJ. Single-chain antibodies against DNA aptamers for use as adapter molecules on DNA tile arrays in nanoscale materials organization. Org Biomol Chem 2006; 4: 3420-6.

[117] Hansen MN, Zhang AM, Rangnekar A, *et al*. Weave tile architecture construction strategy for DNA nanotechnology. J Am Chem Soc 2010; 132: 14481-6.

[118] Rothemund PW. Folding DNA to create nanoscale shapes and patterns. Nature 2006; 440: 297-302.
[119] Chhabra R, Sharma J, Ke Y, Liu Y, Rinker S, Lindsay S, Yan H. Spatially addressable multiprotein nanoarrays templated by aptamer-tagged DNA nanoarchitectures. J Am Chem Soc 2007; 129: 10304-5.
[120] Rinker S, Ke Y, Liu Y, Chhabra R, Yan H. Self-assembled DNA nanostructures for distance-dependent multivalent ligand-protein binding. Nat Nanotechnol 2008; 3: 418-22.

Received: October 19, 2011 **Accepted: November 28, 2011**

Chapter 3

DNA Origami as DNA Repair Nanosensor at the Single-Molecule Level.

DNA Origami as DNA Repair Nanosensor at the Single-Molecule Level.

Maria Tintoré,[*1] Isaac Gállego,[*2] Brendan Manning,[3] Ramon Eritja[1] and Carme Fàbrega[1]

Angewandte Chemie International Edition, (2013), Volume 52, Issue 30, pages 7747–7750

DOI: 10.1002/anie.201301293. Impact factor (2013): **11.336**

[1] IRB Barcelona, IQAC-CSIC, CIBER-BBN Networking Centre on Bioengineering Biomaterials and Nanomedicine. c/ Jordi Girona 18-26. 08034 Barcelona (Spain).

[2] School of Chemistry and Biochemistry, Georgia Institute of Technology, Atlanta, GA 30332-0400 (USA).

[3] Biokit, S.A. 08186 Lliçà d'Amunt, Barcelona (Spain).

[*] These authors contributed equally to this work.

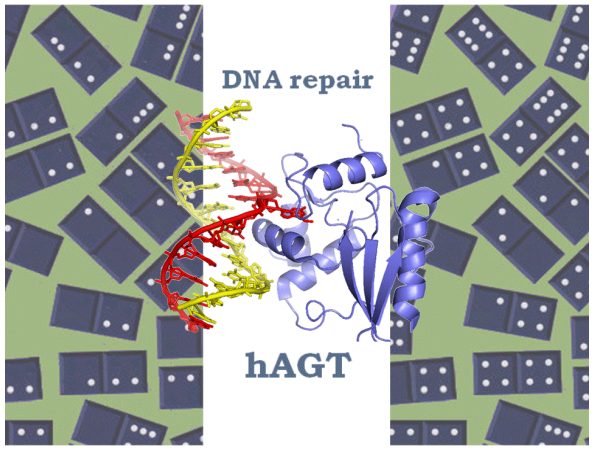

The self-assembly of DNA molecules provides an attractive route towards the formation of complex structures at the nanoscale. In particular, the DNA origami uses hundreds of nucleotides “staples” to fold a long single-stranded DNA scaffold of 7-kilobase, the M13 phage genome, in a rational and desired shape. It represents a versatile tool for the self-assembly of other molecular species and constitutes an excellent platform to create a variety of new nanoscale devices with great potential and applications. In this chapter, we describe the use of the DNA origami as a nanosensor to analyze the enzymatic DNA repair activity of hAGT via TBA conformational changes that condition α-thrombin interaction with DNA aptamers. As this structural change can be caused by a single methylation in the central guanines of the tetrads of the aptamers, it can be utilised to detect the DNA repair activity of hAGT, given that methylguanine is the substrate of this protein. These findings illustrate the potential use of the DNA origami as a protein recognition biosensor, and open the door to the development of a method for the evaluation of potential inhibitors of hAGT.

As a result of the high impact achieved by the publication of this work, we were invited to write a review on the state of the art of DNA nanotechnology, and this work is included as an annex of this chapter. In this review we examine recent progresses towards the potential use of DNA nanostructures for molecular and cellular biology.

Biosensors

DOI: 10.1002/anie.201301293

DNA Origami as a DNA Repair Nanosensor at the Single-Molecule Level**

*Maria Tintoré, Isaac Gállego, Brendan Manning, Ramon Eritja, and Carme Fàbrega**

The development of DNA origami[1] has been one of the most important advances for structural DNA nanotechnology.[2] This method uses hundreds of nucleotide staples to fold a long single-stranded DNA scaffold of 7-kilobase, the M13 phage genome in a rational and desired shape. DNA origami is a versatile method for the self-assembly of other molecular species[3] and is an excellent way to create a variety of new nanoscale devices[4] with great potential and applications.[5] Yan and co-workers have used the DNA origami as an addressable support for label-free detection of RNA hybridization;[6] more recently, Seeman and co-workers have developed a nanosensor to detect single nucleotide polymorphism (SNP).[7] Both strategies are an innovative way to use the DNA origami method to create a nanosensor for biomedical applications at the single-molecule level using atomic force microscopy (AFM).

Advances in the molecular biology of cancer have identified key mechanisms involved in the DNA repair pathways induced by chemotherapeutic drugs, as for example alkylating agents. Adducts formed at the O^6 position of guanine are of major importance in both the initiation of mutations and in the cytotoxic effects of these agents. Human O^6-alkylguanine-DNA alkyltransferase (hAGT) is a DNA-binding protein responsible for the repair of the O^6-methylguanine, contributing to the resistance to chemotherapeutic agents. For these reasons, hAGT is considered relevant as a prognosis marker of cancer and is a potential therapeutic target.[8] Intense research efforts have been devoted to the identification of small molecules capable of inhibiting hAGT activity and enhancing the cytotoxic effect of the alkylating agents in tumor cells.[9] Several methods are available to characterize the mechanism of action of hAGT, its activity, and its inhibition by small molecules. However, most of these methods are based on radioactivity assays, while others are based on multiple-step enzymatic reactions.[10] Our research group developed a new fluorescence method using a DNA G-quadruplex, the thrombin binding aptamer (TBA), as a molecular beacon for the detection of hAGT activity and the development of new inhibitor compounds.[11]

G-quadruplexes are a family of four-stranded DNA structures stabilized by the stacking of guanine tetrads in which four planar guanines form a cyclic array of hydrogen bonds stabilized by the presence of monovalent cations.[12] Modifications in the base composition of the tetrads are poorly tolerated by these structures. As an example, O^6-methylguanine can form a smaller number of hydrogen bonds and consequently destabilize the G-quadruplex, provoking the loss of its conformation (Supporting Information, Figure S1).[13]

Herein, we exploit the spatial addressability of DNA origami in combination with the change of conformation of a DNA G-quadruplex to visually detect by AFM the change in its binding affinity to α-thrombin. As this structural change is caused by a single methylation in the central guanines, it can be utilized to detect the DNA repair activity of hAGT, given that methylguanine is the substrate of this protein. To attain this goal, we have used the specific binding properties of the TBAs (aptamers with anticoagulant properties) to α-thrombin, their natural substrate.[14] The two TBA sequences used in this work (see the Supporting Information, Table S1, for sequences) are known to bind specifically and cooperatively to two specific and almost opposite epitopes of α-thrombin.[15] TBA1 (primarily fibrinogen-recognition exosite binding)[14] is a 15 mer nucleotide composed of two G-tetrads that are connected by three edge-wise loops, forming a well-characterized intramolecular chair-like, antiparallel quadruplex. In contrast, TBA2 (29mer nucleotide, heparin-binding exosite) forms a combined quadruplex/duplex structure.[15]

Previous studies provide evidence that the TBAs are able to bind α-thrombin in the absence of monovalent cations promoting the TBA folding to its 3D structure, following the typical chaperone-macromolecule system.[16]

Previously, to study the interaction between TBA1 and α-thrombin, fluorescence quenching experiments and electrophoresis mobility shift assays were performed (Supporting Information, Figures S2 and S3). Both results confirmed that the introduction of a methylated guanine prevented α-thrombin interaction, and furthermore that a 10-fold concen-

[*] M. Tintoré,[+] Dr. I. Gállego,[$] [+] Dr. B. Manning, Dr. R. Eritja, Dr. C. Fàbrega
IRB Barcelona, IQAC-CSIC, CIBER-BBN Networking Centre on Bioengineering Biomaterials and Nanomedicine
c/Jordi Girona 18-26, 08034 Barcelona (Spain)
E-mail: carme.fabrega@irbbarcelona.org
Dr. B. Manning
Biokit, S.A.
08186 Lliçà d'Amunt, Barcelona (Spain)
[$] Present address: School of Chemistry and Biochemistry
Georgia Institute of Technology
Atlanta, GA 30332-0400 (USA)
[+] These authors contributed equally to this work.

[**] This work was supported by European Communities FUNMOL, "Fondo de Investigaciones Sanitarias" (grant PI06/1250) and by "Ministerio Ciencia e Innovación" (grant CTQ-2010-20541-C03-03). C.F. is grateful to Generalitat de Catalunya and Instituto de Salud Carlos III for a SNS Miguel Servet contract. We acknowledge Gerard Oncins from Scientific and Technological Centers of the University of Barcelona (CCiTUB) for his help and advice regarding AFM.

Supporting information for this article is available on the WWW under http://dx.doi.org/10.1002/anie.201301293.

tration of α-thrombin can be sufficient to appreciate a different pattern of union of this protein to the TBAs and methyl-TBA-containing origami.

Based on these preliminary studies, we designed a DNA origami in which some of the staple strands were modified by the insertion of TBA1 and TBA2 in the middle, protruding from the DNA origami surface[17] (see the Supporting Information, Table S1, for sequences). The staple strands were arranged asymmetrically along the length of the origami in a way that allowed the differentiation between methylated/non-methylated, to enable the observation and quantification of α-thrombin interaction with the aptamers. For this purpose, we built a dual-aptamer system composed of two lines of five TBA1 and TBA2 doublets placed at a distance of about 5.8 nm from each other, increasing the recognition probabilities by at least 10-fold as reported by Rinker et al.[17] The right double line corresponds to the unmodified dual system, and the left dual-aptamer line consists of 15 mer methylated-TBAs and non-modified 29 mer TBAs (Supporting Information, Scheme S1). The formation of the DNA origami with the modified TBA staple strands was performed successfully, confirming that the addition of a methylated sequence does not affect its assembly (Supporting Information, Figure S4).

Afterwards, the complex formation between α-thrombin and the non-methylated/methylated TBA modified origami was studied. In Figure 1, the asymmetric interaction can be

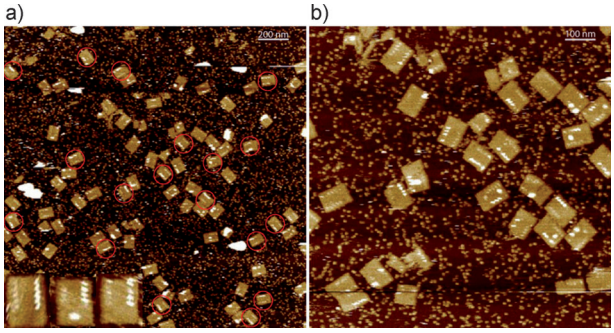

Figure 1. a),b) AFM images (scale bars 200 nm (a), 100 nm (b)) of the interaction of α-thrombin with the origami. The interaction can be observed as white aligned dots deposited over the origami surfaces. The complex was only formed with the native TBAs (right line; see inserts in (a) for more details), whereas in the left line, in which the 15mer TBA carried an O^6-methylguanine, no interaction was observed.

observed. As expected (Scheme 1 a), the complex was only formed with the native TBAs, whereas in the left line no interaction was reported, confirming that α-thrombin is not able to bind the disrupted quadruplex. The study of the profiles and pixel distribution (Figure 3 b) confirms that the height of the dots in the dual-aptamer is in agreement with the expected size of α-thrombin (ca. 4 nm in diameter) in comparison with the height of the origami control (Figure 3 a). We observed that more than 95 % of the chemically modified origami tiles faced pointing towards the solution, in agreement with data reported by Voigt et al.[4c]

This result is a clear confirmation that the complex between the dual-aptamer system and α-thrombin is only formed with the non-methylated TBA, and confirms the

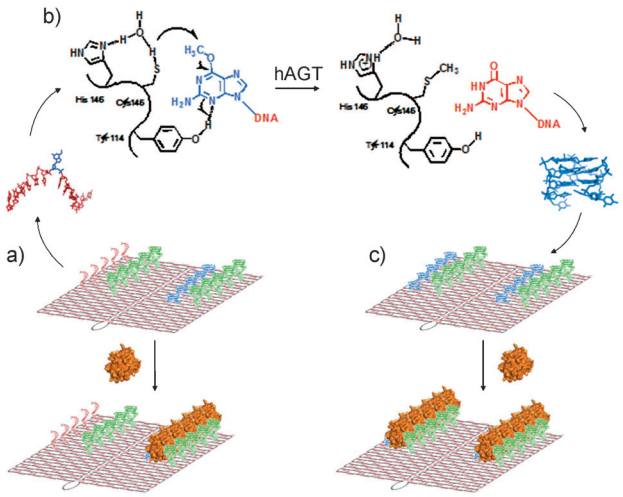

Scheme 1. a) Representation of the asymmetric binding of α-thrombin to TBA aptamers of methylated DNA origami. b) Methyl-TBA repair by hAGT, thus allowing G-quadruplex formation. c) Representation of the symmetric binding of α-thrombin to the repaired DNA origami quadruplexes.

ability of our design to discern between the methylated and non-methylated state.

To explore the efficiency of our design, we performed a quantitative study of the binding location of α-thrombin. From the 160 well-formed DNA origami studied, around 20 % of them contained all five α-thrombin molecules in positions coinciding with unmodified TBA and almost none in the methylated line. In all, more than 93 % of the DNA arrays contained at least 1 α-thrombin attached to the unmodified TBAs (see the Supporting Information).

We then intended to repair the O^6-methylguanine of the TBA-containing staple strands by hAGT. For this purpose, the methyl-TBA-staple strands were incubated with hAGT. hAGT was removed and the resulting strands were used to assemble the DNA origami (see Materials and Methods in the Supporting Information). The recovery of the chair-like structure of the now demethylated 15mer was expected, leading to the binding of α-thrombin to both dual-aptamers, as the two of them contain the native 15 and 29mer TBAs.

The binding of α-thrombin in both dual-aptamers is shown in Figure 2, confirming the repair of the alkylated guanine by hAGT. Upon quantitative exploration of the binding, we can conclude that α-thrombin binds with equal contingency in both lines of the origami, with no significant tendency ($p < 0.5$) for any of the dual systems composed by TBA1 and TBA2. The study of the height profiles corroborated the theoretical height of the α-thrombin on both dual-aptamers (Figure 3 c). Furthermore, we titrated hAGT (0 to 10-fold origami:hAGT; see the Supporting Information) against methyl-TBA staples and incorporated these staples into the DNA origami. The results showed that α-thrombin binding to the methylated/repair side was clearly dependent on hAGT concentration (Supporting Information, Figures S10 and S11).

In summary, we have developed a new method to study the DNA repair activity of hAGT. To the best of our

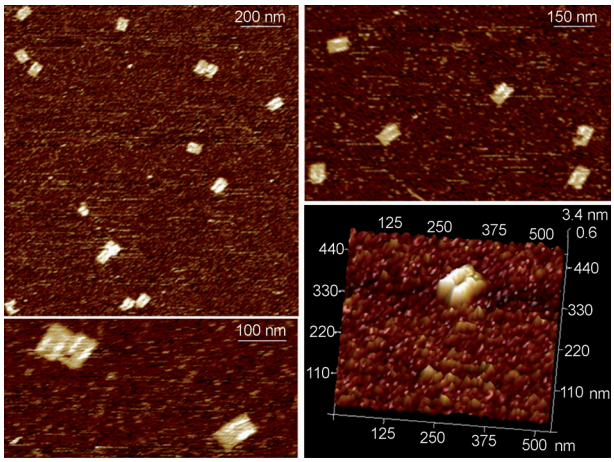

Figure 2. Symmetric binding of α-thrombin to the origami after the repair of the methylation in the TBA1 (left line). The bottom-right panel shows the 3D profile of an origami with all its binding positions occupied by α-thrombin.

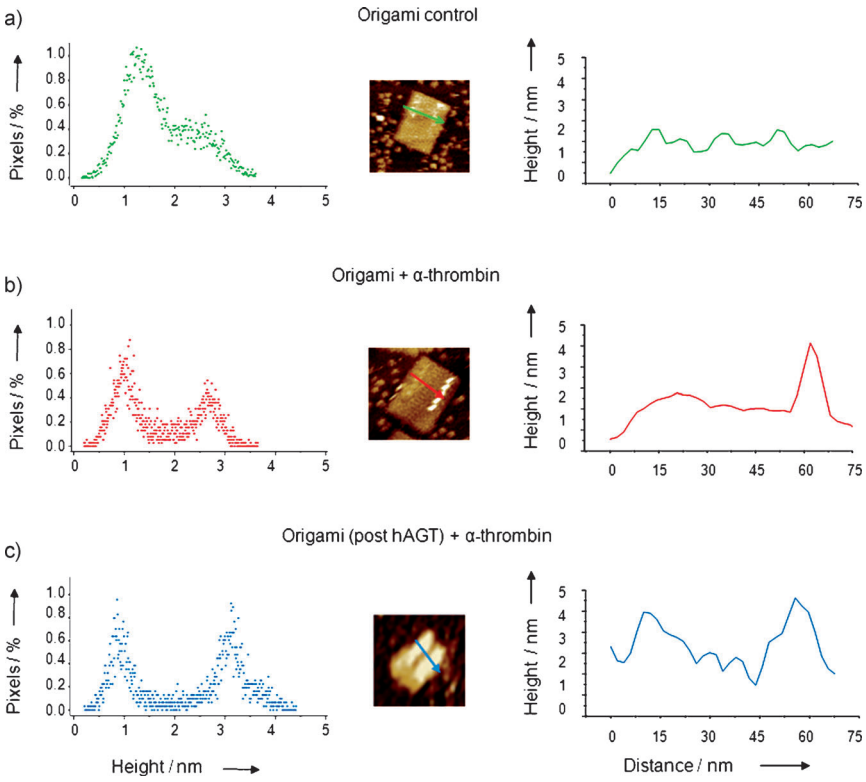

Figure 3. Distribution of heights, corresponding AFM images, and their cross-sections. a) TBA-origami. b) α-thrombin methyl-TBA origami complex. c) α-thrombin complex with demethylated TBA origami.

knowledge, this is the first time the enzymatic activity of hAGT has been visualized on an origami platform. This study combines the capabilities of the α-thrombin recognition/binding to TBA and the single-molecule features of the DNA origami applied to the detection of DNA repair. The system appears to be extremely effective and reliable, and the results are clearly visualized by AFM. Their consistency suggests that our system could be further evolved to design hAGT activity assays for the identification of potential inhibitors as chemotherapy enhancers and for the study of other DNA repair enzymes. The application of the DNA origami as a platform for single-molecule recognition opens the door for the development of new biosensors for the detection of a variety of complexes and the activity of other proteins. Finally, it can also contribute to the study of other DNA lesions that affect G-quadruplexes. This in turn would increase our knowledge on the effect of DNA damage in biologically relevant G-quadruplex structures.[18]

Experimental Section

Standard oligonucleotides were purchased from Sigma. Modified staple strands were synthesized on a DNA synthesizer following standard methods. All of the oligonucleotides sequences are detailed in the Supporting Information. Full-length hAGT was overexpressed and purified as previously described.[10e] A mixture of the modified staple strands containing the methylated 15-mer TBA sequence were left to react with hAGT. DNA origami tiles were assembled following the method developed by Rothemund.[1] A sufficient amount of α-thrombin was added and left to equilibrate before imaging. Images were acquired in tapping mode in liquid environment using triangular-shaped AFM probes and their analysis was performed using NanoScope Analysis Version 1.40. All of the experiments were performed in triplicate. Statistical comparisons of the binding performance were done according to Student's *t* distribution.

Received: February 13, 2013
Revised: April 12, 2013
Published online: June 13, 2013

Keywords: biosensors · DNA origami · DNA repair · G-quadruplexes · hAGT

[1] P. W. Rothemund, *Nature* **2006**, *440*, 297.
[2] N. C. Seeman, *Annu. Rev. Biochem.* **2010**, *79*, 65.
[3] a) R. Chhabra, J. Sharma, Y. Ke, Y. Liu, S. Rinker, S. Lindsay, H. Yan, *J. Am. Chem. Soc.* **2007**, *129*, 10304; b) H. T. Maune, S. P. Han, R. D. Barish, M. Bockrath, W. A. Iii, P. W. Rothemund, E. Winfree, *Nat. Nanotechnol.* **2010**, *5*, 61; c) S. Pal, Z. Deng, B. Ding, H. Yan, Y. Liu, *Angew. Chem.* **2010**, *122*, 2760; *Angew. Chem. Int. Ed.* **2010**, *49*, 2700; d) B. Saccà, R. Meyer, M. Erkelenz, K. Kiko, A. Arndt, H. Schroeder, K. S. Rabe, C. M. Niemeyer, *Angew. Chem.* **2010**, *122*, 9568; *Angew. Chem. Int. Ed.* **2010**, *49*, 9378.
[4] a) H. Gu, J. Chao, S. J. Xiao, N. C. Seeman, *Nature* **2010**, *465*, 202; b) S. F. Wickham, J. Bath, Y. Katsuda, M. Endo, K. Hidaka, H. Sugiyama, A. J. Turberfield, *Nat. Nanotechnol.* **2012**, *7*, 169; c) N. V. Voigt, T. Torring, A. Rotaru, M. F. Jacobsen, J. B. Ravnsbaek, R. Subramani, W. Mamdouh, J. Kjems, A. Mokhir, F. Besenbacher, K. V. Gothelf, *Nat. Nanotechnol.* **2010**, *5*, 200.
[5] A. V. Pinheiro, D. Han, W. M. Shih, H. Yan, *Nat. Nanotechnol.* **2011**, *6*, 763.

[6] Y. Ke, S. Lindsay, Y. Chang, Y. Liu, H. Yan, *Science* **2008**, *319*, 180.
[7] H. K. Subramanian, B. Chakraborty, R. Sha, N. C. Seeman, *Nano Lett.* **2011**, *11*, 910.
[8] R. Pepponi, G. Marra, M. P. Fuggetta, S. Falcinelli, E. Pagani, E. Bonmassar, J. Jiricny, S. D'Atri, *J. Pharmacol. Exp. Ther.* **2003**, *304*, 661.
[9] A. E. Pegg, *Chem. Res. Toxicol.* **2011**, *24*, 618.
[10] a) B. D. Wilson, M. Strauss, B. J. Stickells, E. G. Hoal-van Helden, P. van Helden, *Carcinogenesis* **1994**, *15*, 2143; b) M. E. Dolan, A. E. Pegg, N. K. Hora, L. C. Erickson, *Cancer Res.* **1988**, *48*, 3603; c) A. M. Moser, M. Patel, H. Yoo, F. M. Balis, M. E. Hawkins, *Anal. Biochem.* **2000**, *281*, 216; d) R. S. Wu, S. Hurst-Calderone, K. W. Kohn, *Cancer Res.* **1987**, *47*, 6229; e) F. M. Ruiz, R. Gil-Redondo, A. Morreale, A. R. Ortiz, C. Fabrega, J. Bravo, *J. Chem. Inf. Model.* **2008**, *48*, 844.
[11] M. Tintore, A. Avino, F. M. Ruiz, R. Eritja, C. Fabrega, *J. Nucleic Acids* **2010**, DOI: 10.4061/2010/632041.
[12] a) I. Smirnov, R. H. Shafer, *Biochemistry* **2000**, *39*, 1462; b) B. I. Kankia, L. A. Marky, *J. Am. Chem. Soc.* **2001**, *123*, 10799.
[13] M. Trajkovski, P. Sket, J. Plavec, *Org. Biomol. Chem.* **2009**, *7*, 4677.
[14] L. C. Bock, L. C. Griffin, J. A. Latham, E. H. Vermaas, J. J. Toole, *Nature* **1992**, *355*, 564.
[15] D. M. Tasset, M. F. Kubik, W. Steiner, *J. Mol. Biol.* **1997**, *272*, 688.
[16] a) H. A. Ho, M. Leclerc, *J. Am. Chem. Soc.* **2004**, *126*, 1384; b) E. Baldrich, A. Restrepo, C. K. O'Sullivan, *Anal. Chem.* **2004**, *76*, 7053.
[17] S. Rinker, Y. Ke, Y. Liu, R. Chhabra, H. Yan, *Nat. Nanotechnol.* **2008**, *3*, 418.
[18] G. Biffi, D. Tannahill, J. McCafferty, S. Balasubramanian, *Nat. Chem.* **2013**, *5*, 182.

Supporting Information

DNA Origami as DNA repair nanosensor at the single-molecule level.

Maria Tintoré[ψ], Isaac Gállego[ψ], Brendan Manning, Ramon Eritja and Carme Fàbrega[*]

Table of contents:

1. Materials and Methods

1.1. Abbreviations.

3’-Dabsyl CPG: 1-Dimethoxytrityloxy-3-[O-(N-4'-sulfonyl-4-(dimethylamino)-azobenzene)-3-aminopropyl]-propyl-2-O-succinoyl-long chain alkylamino-CPG

6’-FAM: 6-[(3’,6’-dipivaloylfluoresceinyl)-carboxamido]-hexyl-1-O-[(2-cyanoethyl)-(*N*,*N*-diiso propyl)]-phosphoramidite

AFM: atomic force microscopy

BCNU: bis-chloroethylnitrosourea or carmustine

CPG: controlled pore glass

dmf: N,N-dimethylamino methylidene

hAGT: human O^6-alkylguanine-DNA alkyltransferase

MALDI: matrix-assisted laser disorption/ionization

O^6-MeG: O^6-methylguanine

PAGE: Polyacrylamide gel electrophoresis

RP-HPLC: reverse phase high pressure liquid chromatography

TEAA: triethylammonium acetate

THAP: trihydroxyacetophenone monohydrate

TOF: time of flight

UV: ultraviolet

1.2. Chemicals

The standard phosphoramidites and ancillary reagents used during oligonucleotide synthesis were obtained from Applied Biosystems and Link Technologies Ltd. 5'-Fluorescein CE phosphoamidite (6'-FAM) was acquired from Link Technologies, 3'-Dabsyl CPG, O^6-methylguanine (O^6-MeG) and G^{dmf} phosphoramidites were from Glen Research. Matrix for MALDI-TOF experiments were 2',4',6'-trihydroxiacetophenone monohydrate (THAP, Aldrich) and ammonium citrate dibasic (Fluka). Solvents for HPLC analysis were prepared using triethylammonium acetate (TEAA) and acetonitrile (Merck) as mobile phase. The rest of the chemicals are analytical reagent grade from commercial sources as specified. Ultrapure water (Millipore) was used in all experiments. The 10 % non denaturing PAGE were prepared from the stock solution acrylamide/bis-acrylamide solution 40% (Sigma).

1.3. Instrumentation

Modified staple strands were synthesized on an ABI 3400 DNA Synthesizer (Applied Biosystems). Semipreparative RP-HPLC was performed on a Waters chromatography system using Symmetry Nucleosil Semipreparative 120 C18 (250x8mm) column. Analytical RP-HPLC was performed using an XBridge OST C18 2.5 μm column. Mass spectra were recorded on a MALDI Voyager DE RP time-of-flight (TOF) spectrometer (Applied Biosystems). Molecular absorption spectra between 220 and 550 nm were recorded with a Jasco V650 spectrophotometer. The temperature was controlled with an 89090A Agilent Peltier device. Hellma quartz cuvettes (0.5 and 1.0 cm path length, 500 or 1000 μl volume) were used. The CD spectra were recorded on a Jasco J-810 spectropolarimeter attached to a Julabo F/25HD circulating water bath in 1 cm path-length quartz cylindrical cells. Fluorometric measurements were performed on a spectrofluorometer Jasco FP6200 at 25ºC. Set temperature was controlled with an 89090A Agilent Peltier device and Hellma quartz cuvettes were used (100 μL volume). Non-denaturing PAGE was run on an AA Hoefer SE 600 standard vertical electrophoresis device, using an Apelex Electrophoresis Power Supply PS 3002. Gels were imaged with a Gene Genius Bioimaging system (Syngene). AFM imagenes were obtained by liquid tapping on a Nanoscope 3A Multimode 4 AFM, using Bruker SNL-10 silicon tips.

1.4. Oligonucleotides Synthesis

Standard staple strand oligonucleotides were purchased to Sigma. Modified staple strands were synthesized on an ABI 3400 DNA Synthesizer (Applied Biosystems), using the 200-nmol scale synthesis and the standard protocols. The more labile dmf grup was used for the protection of all guanines. For strands containing O^6-MeG or FAM, these phosphoramidites were site-specifically inserted into the oligonucleotide. In the case of the fluorescent probes, the quencher group was introduced at the 3' end using the controlled pore glass functionalized with a 3'-Dabsyl derivative CPG. O^6-MeG-containing oligonucleotides were deblocked according to the manufacturer's instructions (ammonia deprotection was performed overnight at room temperature and followed by 1h at 55ºC). The resulting products were desalted by Sephadex G-25 (NAP-10, Amersham Biosciences) and purified by RP-HPLC using Nucleosil columns. The length and homogeneity of the oligonucleotides were checked by MALDI-TOF. The DNA-strand concentration was determined by absorbance measurements (260 nm) and their extinction coefficient. Oligonucleotide samples were kept at 4 ºC until further use. All the oligonucleotides sequences are detailed in Table 1.

1.5. CD spectra.

Measurements were conducted in 10 mM sodium cacodylate pH 7.0 and 100 mM KCl. Sample concentration was between 1-4 μM. Each sample was allowed to equilibrate at the initial temperature without any external control of temperature for 5 min before the melting experiment began. Spectra were recorded at room temperature using a 100 nm/min scan rate, a spectral band width of 1 nm and a time constant of 4 s. All the spectra were corrected with the buffer blank and plotted using Microsoft Office Excel 2007 software.

1.6. Fluorescence assay

Binding between human α-thrombin (Haematologic Technologies Inc.) and TBA, 5-O^6-MeG-TBA and 6-O^6-MeG-TBA molecular beacons (MB) was monitored by measuring changes in fluorescence intensity of the MB solution over time. 150 μL of a 1μM solution of MB-TBA in MB buffer (20 mM Tris pH 7.4, 140 mM NaCl, 5 mM KCl, 1 mM $CaCl_2$, 1 mM $MgCl_2$, 5% v/v). Each time, 1.5 μL of α-thrombin were added and after a quick manual mix, the fluorescence intensity was measured at excitation wavelength of 485 nm and emission wavelength of 520 nm. The measurements were performed until reaching a molar ratio of 3:1 between α-thrombin and the molecular beacon MB-TBA. This same experiment was repeated using the modified MB-5-O^6-MeG-TBA and MB-6-O^6-MeG-TBA sequences. All the experiments were performed in triplicates.

1.7. EMSA assay

In these experiments TBA sequences with an overhang of 5 thymines were used, to make the DNA longer and easier to manipulate. $TBA(T)_5$ and 5-O^6-MeG-$TBA(T)_5$ (1μM) were incubated with specified amounts of α-thrombin for 1 hour at room temperature. The reaction buffer was 250 mM Tris pH 7.4, 150 mM acetic acid, 15 mM EDTA and 37.5 mM magnesium acetate. The reaction was stopped by adding the loading buffer and a non-denaturing 10% PAGE was run at constant 160 V for 3 hours at 20 ºC. The gels were stained with SybrGold (Invitrogen, 1× dye in 100 mL water) or SybrGreen (Invitrogen, 1× dye in 100 mL water).

1.8. hAGT expression and purification

Full-length human AGT was overexpressed and purified as previously described.[1] Briefly, hAGT protein (pet-21a(+) vector, Novagen) was overexpressed in the E. coli strain Rosetta and once the culture reached an OD_{600} value of 0.8, it was induced by adding 1 mM IPTG during 4 h at 30 °C. The pellet from a 1 L culture was disrupted by sonication and centrifuged. The supernatant was filtered, loaded into a HiTrapTM FF column (GE Healthcare) and eluted with an imidazole gradient. Finally the protein was loaded into a Superdex 75 16/60 column (GE Healthcare), being the buffer 200 mM NaCl, 20 mM Tris pH 8.0, 10 mM DTT and 0,1 mM EDTA. The protein was concentrated to 2 mg/ml in hAGT reaction buffer (200 mM NaCl, 50 mM Tris pH 8.0, 1 mM DTT and 5 mM EDTA) and kept at -20 °C in presence of 40 % glycerol.

1.9. hAGT repair of the methylated TBA strands

1.9.1 Repair of the methylated TBAs in the origami

hAGT was incubated directly with the methylated origami adsorbed over the mica surface, (for origami formation details, see AFM imaging section1.10). Sufficient amount of hAGT to reach a concentration 10 fold bigger than the origami was added to the solution and left to react for one hour in hAGT reaction buffer. Then, the mica surface was washed three times with 40 μL of TAE-Mg^{+2} buffer (40 mM Tris pH 8.0, 12.5 magnesium acetate, 2.5 mM EDTA and 20 mM acetic acid). Afterwards, 10 fold concentration of α-thrombin was added to the solution and left to equilibrate for some minutes before imaging.

1.9.2 Reaction of hAGT with the methylated TBA staple strands

A mixture of the five modified staple strands containing the methylated 15-mer TBA sequence was dried under vacuum and resuspended in hAGT reaction buffer to reach a concentration of 35 μM. Then, increasing concentrations (0, 70, 175 and 350 μM) of hAGT were added, and the resulting mixtures were incubated during one hour at 37 ºC. In order to purify the demethylated staple strands, the reaction mixtures were loaded into a Niquel His SpinTrap column (GE Healthcare) and washed out with water three times to allow the oligonucleotides to elute. Recovered samples were quantified, concentrated to 10 μM and stored until further use.

1.10. AFM imaging

Tall rectangle DNA origami tiles were assembled following the method developed by Rothemund[2]. Helper strands modified with different TBA sequences and unmodified helper strands were mixed with the viral DNA M13 at molar ratio of 10:5:1. In the case of the demethylated origami, helper strands modified with TBA sequences, hAGT-demethylated TBA staple strands and unmodified helper strands were mixed with the viral DNA M13 at molar ratio of 10:50:5:1. The origami was assembled using a Biorad Termocycler starting at 90ºC and decreased to 20ºC at -1ºC per minute. Two methodologies were used to bind α-thrombin to the origami surface with equal success. Firstly, arrays were mixed with α-thrombin (1:10 ratio origami:thrombin) and incubated during 1 hour before imaging. 1 μL of sample was deposited on a mica surface and left to adsorb for 1 minute before 40 μL of TAE-Mg^{+2} buffer was added. In the second case, 1 μL of plain origami was deposited on a mica surface and left to adsorb for 1 minute, and then 60 μL of TAE-Mg^{+2} buffer (40 mM tris pH 8.0, 12.5 magnesium acetate, 2.5 mM EDTA and 20 mM acetic acid) were added. Sufficient amount of α-thrombin to reach a concentration 10 fold bigger than the origami was added to the solution and left to equilibrate for some minutes before imaging. To perform the measurements shown in this study, an Extender Multimode AFM attached to a Nanoscope III electronics (Bruker) was used. Images were acquired in tapping mode in liquid environment using triangular-shaped AFM probes (SNL-10, Bruker) with a nominal spring constant of 0.35nN/nm. 30 minutes were laged before acquiring topographic images so as to thermically equilibrate the sample and the probe and to ensure a stable environment. The cantilevers are made of silicon nitride, while the tip pyramid is made of silicon for maximum sharpness and resolution. In order to maintain the sample integrity while scanning, free amplitude was maintained as low as possible (typically between 0.2 and 0.4V) and amplitude setpoint was maximized for these conditions. Scan rate was set between 1.5 and 3 Hz depending on the softness of the sample and image resolution was set to 512x512 pixels.

Comparison of averages of the two types of binding (right line and left line) was performed using Student's t model.

1. TBA staple strands, helper strands sequences and DNA origami design.

ODN	**Sequence (5' to 3')**
TBA1*	GGTTGGTGTGGTTGG
5-O^6-MeG-TBA1*	GGTTG^{Me}GTGTGGTTGG
6-O^6-MeG-TBA1*	GGTTGG^{Me}TGTGGTTGG
TBA2	AGTCCGTGGTAGGGCAGGTTGGGGTGACT
Fluorescence assays	
MB-TBA1*	FAM-GGTTGGTGTGGTTGG-Dabsyl
MB-5-O^6-MeG-TBA1*	FAM-GGTTG^{Me}GTGTGGTTGG-Dabsyl
MB-6-O^6-MeG-TBA1*	FAM-GGTTGG^{Me}TGTGGTTGG-Dabsyl
EMSA assays	
TBA1(T)$_5$*	GGTTGGTGTGGTTGGTTTTT
5-O^6-MeG-TBA1(T)$_5$*	GGTTG^{Me}GTGTGGTTGGTTTTT
Origami assembly	
t-5r4e-5-O^6-MeG-TBA1*	AAAGGCCGCTCCAAAATTTT**GGTTG^{Me}GTGTGGTTGG**TTTT GGAGCCTTAGCGGAGT
t-5r8e-5-O^6-MeG-TBA1*	CCAAATCATTACTTAGTTTT**GGTTG^{Me}GTGTGGTTGG**TTTTC CGGAACGTACCAAGC
t-5r12e-5-O^6-MeG-TBA1*	TAAATATTGAGGCATATTTT**GGTTG^{Me}GTGTGGTTGG**TTTTG TAAGAGCACAGGTAG
t-5r16e-5-O^6-MeG-TBA1*	TTTCATTTCTGTAGCTTTTT**GGTTG^{Me}GTGTGGTTGG**TTTTC AACATGTTTAGAGAG
t-5r20e-5-O^6-MeG-TBA1*	CATGTCAAAAATCACCTTTT**GGTTG^{Me}GTGTGGTTGG**TTTTA TCAATATAACCCTCA
t3r4e-TBA1	GTTTGCCACCTCAGAGTTTT**GGTTGGTGTGGTTGG**TTTTCC GCCACCGCCAGAAT
t3r8e-TBA1	ATACCCAAACACCACGTTTT**GGTTGGTGTGGTTGG**TTTTGA ATAAGTGACGGAAA
t3r12e-TBA1	AGGTTTTGGCCAGTTATTTT**GGTTGGTGTGGTTGG**TTTTCA AAATAAACAGGGAA
t3r16e-TBA1	ACGCTCAACGACAAAATTTT**GGTTGGTGTGGTTGG**TTTTGG TAAAGTATCCCATC
t3r20e-TBA1	TTGAATTATTGAAAACTTTT**GGTTGGTGTGGTTGG**TTTTAT AGCGATTATAACTA
t5r2f-TBA2	AATGCCCCATAAATCCTTTT**AGTCCGTGGTAGGGCAGGTT GGGGTGACT**TTTTTCATTAAAAGAACCAC
t5r6f-TBA2	AGCACCGTAGGGAAGGTTTT**AGTCCGTGGTAGGGCAGGTT GGGGTGACT**TTTTTAAATATTTTATTTTG
t5r10f-TBA2	GCAATAGCAGAGAATATTTT**AGTCCGTGGTAGGGCAGGTT GGGGTGACT**TTTTACATAAAAACAGCCAT
t5r14f-TBA2	TCATTACCGAACAAGATTTT**AGTCCGTGGTAGGGCAGGTT GGGGTGACT**TTTTAAAATAATAATTCTGT
t5r18f-TBA2	AGGCGTTAGGCTTAGGTTTT**AGTCCGTGGTAGGGCAGGTT GGGGTGACT**TTTTTTGGGTTAAGCTTAGA
t-3r2f-TBA2	TGTAGCATAACTTTCATTTT**AGTCCGTGGTAGGGCAGGTT GGGGTGACT**TTTTACAGTTTCTAATTGTA
t-3r6f-TBA2	TTTCATGATGACCCCCTTTT**AGTCCGTGGTAGGGCAGGTT GGGGTGACT**TTTTAGCGATTAAGGCGCAG
t-3r10f-TBA2	TTTCAACTACGGAACATTTT**AGTCCGTGGTAGGGCAGGTT GGGGTGACT**TTTTACATTATTAACACTAT
t-3r14f-TBA2	TCAGAAGCCTCCAACATTTT**AGTCCGTGGTAGGGCAGGTT GGGGTGACT**TTTTGGTCAGGATTTAAATA
t-3r18f-TBA2	CAAAATTAGGATAAAATTTT**AGTCCGTGGTAGGGCAGGTT GGGGTGACT**TTTTATTTTTAGGATATTCA

Table 1. Modified oligonucleotides used in this work. All the strands used for the G-quadruplex disruption studies and for α-thrombin interaction studies were synthesized in the laboratory, as well as the staple strands containing methylated-TBA (*). Bold remarks the sequence of TBA1 and TBA2 and red identifies the position of the O^6-methylguanine. The rest of the staple strands with TBA1 and TBA2 sequences inserted were purchased from commercial sources.

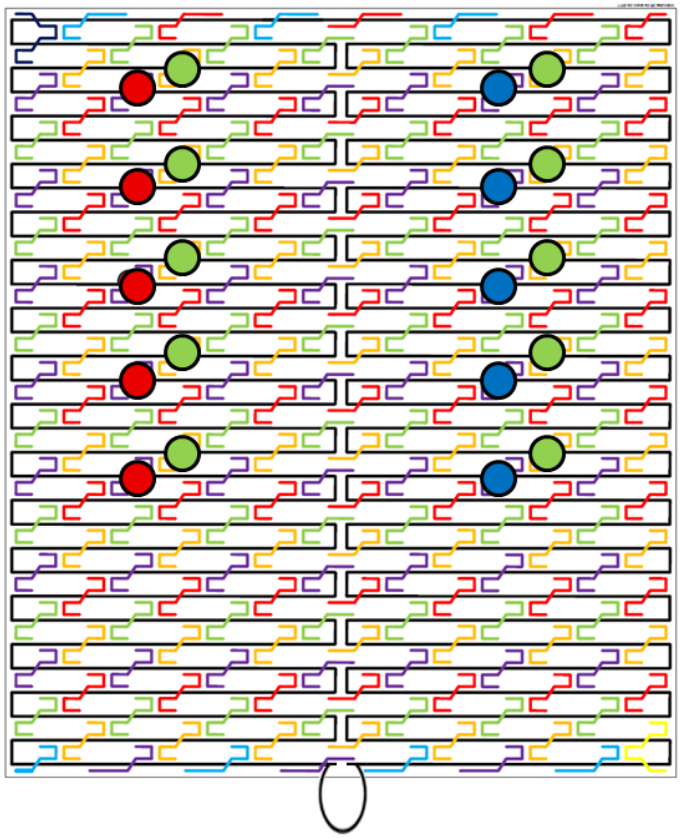

Scheme S1. Sketch of the DNA origami design, showing the right and left dual-aptamer system formed by TBA1 (blue), TBA2 (green) and 5-O^6-Methylguanine-TBA1 (red). The loop indicates the direction of the origami.

List of the helper strands used to build the DNA origami. All these oligonucleotides were purchased from commercial sources:

t1r0g	AGGGTTGATATAAGTATAGCCCGGAATAGGTG
t1r2e	TAAGCGTCGGTAATAAGTTTTAACCCGTCGAG
t1r2f	AGTGTACTATACATGGCTTTTGATCTTTCCAG
t1r4e	AACCAGAGACCCTCAGAACCGCCACGTTCCAG
t1r4f	GAGCCGCCCCACCACCGGAACCGCTGCGCCGA
t1r6e	GACTTACGTAAAGGTCGCAACATACCGTCACC
t1r6f	AATCACCACCATTTGGGAATTAGACCAACCTA
t1r8e	TTATTACGTAAAGGTCGCAACATACCGTCACC
t1r8f	TACATACACAGTATGTTAGCAAACTGTACAGA
t1r10e	TGAACAAAGATAACCCACAAGAATAAGACTCC
t1r10f	ATCAGAGAGTCAGAGGGTAATTGAACCAGTCA

t1r12e	TATTTTGCACGCTAACGAGCGTCTGAACACCC
t1r12f	TCTTACCAACCCAGCTACAATTTTAAAGAAGT
t1r14e	ATCGGGCTGACCAAGTACCGCACTCTTAGTTGC
t1r14f	GGTATTAATCTTTCCTTATCATTCATATCGCG
t1r16e	CATATTTATTTCGAGCCAGTAATAAATCAATA
t1r16f	AGAGGCATACAACGCCAACATGTATCTGCGAA
t1r18e	ACAAAGAAAATTTCATCTTCTGACAGAATCGC
t1r18f	TTTTAGTTCGCGAGAAAACTTTTTTTATGACC
t1r20e	AAATCAATCGTCGCTATTAATTAAATCGCAAG
t1r20f	CTGTAAATATATGTGAGTGAATAAAAAGGCTA
t1r22e	TTTAACGTTCGGGAGAAACAATAACAGTACAT
t1r22f	CTTTTACACAGATGAATATACAGTGCCATCAA
t1r24e	TTATTAATGAACAAAGAAACCACCTTTTCAGG
t1r24f	ATTTTGCGTTTAAAAGTTTGAGTACCGGCACC
t1r26e	CTAAAGCAAATCAATATCTGGTCACCCGAACG
t1r26f	AAACCCTCTCACCTTGCTGAACCTAGAGGATC
t1r28e	CTAAAAGCAAATCAATATCTGGTCACCCGAACG
t1r28f	GCGTAAGAAGATAGAACCCTTCTGAACGCGCG
t1r30e	GTTGTAGCCCTGAGTAGAAGAACTACTTCTG
t1r30f	ATCACTTGAATACTTCTTTGATTAGTTGTTCC
t1r32h	TACAGGGCGCGTACTATGGTTGCTAATTAACC
t3r0g	TGCTCAGTACCAGGCGGATAAGTGGGGGTCAG
t3r2e	GGAAAGCGGTAACAGTGCCCGTATCGGGGTTT
t3r2f	TGCCTTGACAGTCTCTGAATTTACCCCTCAGA
t3r4f	GCCACCACTCTTTTCATAATCAAATAGCAAGG
t3r6e	TTATTCATGTCACCAATGAAACCATTATTAGC
t3r6f	CCGGAAACTAAAGGTGAATTATCATAAAAGAA
t3r8f	ACGCAAAGAAGAACTGGCATGATTTGAGTTAA
t3r10e	GCGCATTAATAAGAGCAAGAAACAATAACGGA
t3r10f	GCCCAATAGACGGGAGAATTAACTTTCCAGAG
t3r12f	CCTAATTTAAGCCTTAAATCAAGAATCGAGAA
t3r14e	CTAATTTACCGTTTTTATTTTCATCTTGCGGG
t3r14f	CAAGCAAGCGAGCATGTAGAAACCAGAGAATA
t3r16f	TAAAGTACCAGTAGGGCTTAATTGCTAAATTT
t3r18e	TATGTAAAGAAATACCGACCGTGTTAAAGCCA
t3r18f	AATGGTTTTGCTGATGCAAATCCATTTTCCCT
t3r20f	TAGAATCCCCTTTTTTAATGGAAACGGATTCG
t3r22e	ACAGAAATCTTTGAATACCAAGTTAATTTCAT
t3r22f	CCTGATTGAAAGAAATTGCGTAGAAGAAGGAG
t3r24e	CGACAACTTCATCATATTCCTGATCACGTAAA

t3r24f	CGGAATTACGTATTAAATCCTTTGGTTGGCAA
t3r26e	GCCACGCTTTGAAAGGAATTGAGGAAACAATT
t3r26f	ATCAACAGGAGAGCCAGCAGCAAAATATTTTT
t3r28e	GTCACACGATTAGTCTTTAATGCGGCAACAGT
t3r28f	GAATGGCTACCAGTAATAAAAGGGCAAACTAT
t3r30e	GTAAAAGACTGGTAATATCCAGAAATTCACCA
t3r30f	CGGCCTTGGTCTGTCCATCACGCATTGACGAG
t3r32h	CACGTATAACGTGCTTTCCTCGTTGCCACCGA
t5r0g	CCTCAAGAGAAGGATTAGGATTAGAAACAGTT
t5r2e	ACAAACAACTGCCTATTTCGGAACCTGAGACT
t5r4e	TCGGCATTCCGCCGCCAGCATTGATGATATTC
t5r4f	CACCAGAGTTCGGTCATAGCCCCCTCGATAGC
t5r6e	ATTGAGGGAATCAGTAGCGACAGACGTTTTCA
t5r8e	GAAGGAAAAATAGAAAATTCATATTTCAACCG
t5r8f	TCACA ATCCC GAGGA AACGC AATAA TGAAATA
t5r10e	CTTTACAGTATCTTACCGAAGCCCAGTTACCA
t5r12e	GAGGCGTTTCCCAATCCAAATAAGATAGCAGC
t5r12f	ATTATTTATTAGCGAACCTCCCGACGTAGGAA
t5r14e	TAAGTCCTGCGCCCAATAGCAAGCAAGAACGC
t5r16e	GCGTTATACGACAATAAACAACATACAATAGA
t5r16f	CCAGACGACAAATTCTTACCAGTAGATAAATA
t5r18e	TAACCTCCAATAAGAATAAACACCTATCATAT
t5r20e	AAAACAAACTGAGAAGAGTCAATATACCTTTT
t5r20f	TTAAGACGATTAATTACATTTAACACAAAATC
t5r22e	AACCTACCGCGAATTATTCATTTCACATCAAG
t5r22f	GCGCAGAGATATCAAAATTATTTGTATCAGAT
t5r24e	GGATTTAGTTCATCAATATAATCCAGGGTTAG
t5r24f	GATGGCAAAAGTATTAGACTTTACAAGGTTAT
t5r26e	AGGCGGTCTCTTTAGGAGCACTAAACATTTGA
t5r26f	CTAAAATAAGTATTAACACCGCCTCGAACTGA
t5r28e	GAAATGGAAAACATCGCCATTAAACAGAGGTG
t5r28f	TAGCCCTATTATTTACATTGGCAGCAATATTA
t5r30e	AGAAGTGTCATTGCAACAGGAAAAAATCGTCT
t5r30f	CCGCCAGCTTTTATAATCAGTGAGAGAATCAG
t5r32h	AGCGGGAGCTAAACAGGAGGCCGAGAATCCTG
t-1r0g	TATCACCGTACTCAGGAGGTTTAGATAGTTAG
t-1r2e	ACGTTAGTTCTAAAGTTTTGTCGTGATACAGG
t-1r2f	CGTAACGAAAATGAATTTTCTGTAGTGAATTT
t-1r4e	CAATGACAGCTTGATACCGATAGTCTCCCTCA

t-1r4f	CTTAAACAACAACCATCGCCCACGCGGGTAAA
t-1r6e	AAACGAAATGCCACTACGAAGGCAGCCAGCAA
t-1r6f	ATACGTAAGAGGCAAAAGAATACACTGACCAA
t-1r8e	CCAGGCGCGAGGACAGATGAACGGGTAGAAAA
t-1r8f	CTTTGAAAATAGGCTGGCTGACCTACCTTATG
t-1r10e	GGACGTTGAGAACTGGCTCATTATGCGCTAAT
t-1r10f	CGATTTTAGGAAGAAAAATCTACGGATAAAAA
t-1r12e	TTTGCCAGGCGAGAGGCTTTTGCAATCCTGAA
t-1r12f	CCAAAATAAGGGGGTAATAGTAAAAAAAGATT
t-1r14e	TTTTAATTGCCCGAAAGACTTCAACAAGAACG
t-1r14f	AAGAGGAACGAGCTTCAAAGCGAAAGTTTCAT
t-1r16e	CGAGTAGAACAGTTGATTCCCAATATTTAGGC
t-1r16f	TCCATATATTTAGTTTGACCATTAAGCATAAA
t-1r18e	CTGTAATAGGTTGTACCAAAAACACAAATATA
t-1r18f	GCTAAATCCTTTTGCGGGAGAAGCCCGGAGAG
t-1r20e	TCAGGTCATTTTTGAGAGATCTACCCTTGCTT
t-1r20f	GGTAGCTATTGCCTGAGAGTCTGGTTAAATCA
t-1r22e	AAATAATTTTTAACCAATAGGAACAACAGTAC
t-1r22f	GCTCATTTCGCGTCTGGCCTTCCTGGCCTCAG
t-1r24e	GCTTCTGGCACTCCAGCCAGCTTTACATTATC
t-1r24f	GAAGATCGTGCCGGAAACCAGGCAGTGCCAAG
t-1r26e	CCCGGGTACCTGCAGGTCGACTCTCAAATATC
t-1r26f	CTTGCATGCCGAGCTCGAATTCGTCCTGTCGT
t-1r28e	GGGAGAGGCATTAATGAATCGGCCACCTGAAA
t-1r28f	GCCAGCTGCGGTTTGCGTATTGGGAATCAAAA
t-1r30e	AGTTTGGACGAGATAGGGTTGAGTGTAATAAC
t-1r30f	GAATAGCCACAAGAGTCCACTATTAAGCCGGC
t-1r32h	GAACGTGGCGAGAAAGGAAGGGAATGCGCCGC
t-3r0g	CCCTCAGAACCGCCACCCTCAGAAACAACGCC
t-3r2e	TGCTAAACTCCACAGACAGCCCTCTACCGCCA
t-3r4e	ATATATTCTCAGCTTGCTTTCGAGTGGGATTT
t-3r4f	TCGGTTTAGGTCGCTGAGGCTTGCAAAGACTT
t-3r6e	CTCATCTTGGAAGTTTCCATTAAACATAACCG
t-3r8e	AGTAATCTTCATAAGGGAACCGAACTAAAACA
t-3r8f	ACGGTCAATGACAAGAACCGGATATGGTTTAA
t-3r10e	ACGAACTATTAATCATTGTGAATTTCATCAAG
t-3r12e	ACTGGATATCGTTTACCAGACGACTTAATAAA
t-3r12f	CATAACCCGCGTCCAATACTGCGGTATTATAG
t-3r14e	GAAGCAAAAAAGCGGATTGCATCAATGTTTAG
t-3r16e	TCGCAAATAAGTACGGTGTCTGGACCAGACCG

t-3r16f	TGCAACTAGGTCAATAACCTGTTTAGAATTAG
t-3r18e	CAACGCAAAGCAATAAAGCCTCAGGATACATT
t-3r20e	AGAGAATCAGCTGATAAATTAATGCTTTATTT
t-3r20f	ACCGTTCTGATGAACGGTAATCGTAATATTTT
t-3r22e	CTTTCATCTCGCATTAAATTTTTGAGCAAACA
t-3r22f	GTTAAAATAACATTAAATGTGAGCATCTGCCA
t-3r24e	TTCGCCATGGACGACGACAGTATCGTAGCCAG
t-3r24f	GTTTGAGGTCAGGCTGCGCAACTGTTCCCAGT
t-3r26e	TCATAGCTTGTAAAACGACGGCCAAAGCGCCA
t-3r26f	CACGACGTGTTTCCTGTGTGAAATTTGCGCTC
t-3r28e	TGGTTTTTCTTTCCAGTCGGGAAAAATCATGG
t-3r28f	ACTGCCCGCTTTTCACCAGTGAGATGGTGGTT
t-3r30e	TGGACTCCGGCAAAATCCCTTATACGCCAGGG
t-3r30f	CCGAAATCAACGTCAAAGGGCGAAAAGGGAGC
t-3r32h	CCCCGATTTAGAGCTTGACGGGGAAAAGAACG
t-5r0g	CTCAGAGCCACCACCCTCATTTTCCGTAACAC
t-5r2e	GAGAATAGGTCACCAGTACAAACTCCGCCACC
t-5r2f	TGAGTTTCAAAGGAACAACTAAAGATCTCCAA
t-5r4f	AAAAAAGGCTTTTGCGGGATCGTCGGGTAGCA
t-5r6e	GCGAAACAAGAGGCTTTGAGGACTAGGGAGTT
t-5r6f	ACGGCTACAAGTACAACGGAGATTCGCGACCT
t-5r8f	GCTCCATGACGTAACAAAGCTGCTACACCAGA
t-5r10e	AAAGATTCTAAATTGGGCTTGAGATTCATTAC
t-5r10f	ACGAGTAGATCAGTTGAGATTTAGCGCCAAAA
t-5r12f	GGAATTACCATTGAATCCCCCTCACCATAAAT
t-5r14e	TACCTTTAAGGTCTTTACCCTGACAATCGTCA
t-5r14f	CAAAAATCATTGCTCCTTTTGATAATTGCTGA
t-5r16f	ATATAATGGGGGCGCGAGCTGAAATTAACATC
t-5r18e	TATATTTTCATACAGGCAAGGCAAAGCTATAT
t-5r18f	CAATAAATAAATGCAATGCCTGAGAAGGCCGG
t-5r20f	AGACAGTCTCATATGTACCCCGGTTTGTATAA
t-5r22e	ACCCGTCGTTAAATTGTAAACGTTAAAACTAG
t-5r22f	GCAAATATGATTCTCCGTGGGAACCGTTGGTG
t-5r24e	GGCGATCGCGCATCGTAACCGTGCGAGTAACA
t-5r24f	TAGATGGGGTGCGGGCCTCTTCGCGCAAGGCG
t-5r26e	GCTCACAAGGGTAACGCCAGGGTTTTGGGAAG
t-5r26f	ATTAAGTTTTCCACACAACATACGCCTAATGA
t-5r28e	AGCTGATTACTCACATTAATTGCGTGTTATCC
t-5r28f	GTGAGCTAGCCCTTCACCGCCTGGGGTTTGCC
t-5r30e	TATCAGGGCGAAAATCCTGTTTGACGGGCAAC

t-5r30f	CCAGCAGGCGATGGCCCACTACGTGAGGTGCC
t-5r32h	GTAAAGCACTAAATCGGAACCCTAAAACCGTC

3. Disruption of the G-quadruplex

G-quadruplexes are a family of four-stranded DNA structures stabilized by the stacking of guanine tetrads, in which four planar guanines form a cyclic array of hydrogen bonds.[3] Modifications in the base composition of the tetrads are poorly tolerated by these structures. As an example, O^6-methylguanine[4], a non-natural base, can form a smaller number of hydrogen bonds and consequently destabilize the G-quadruplex.

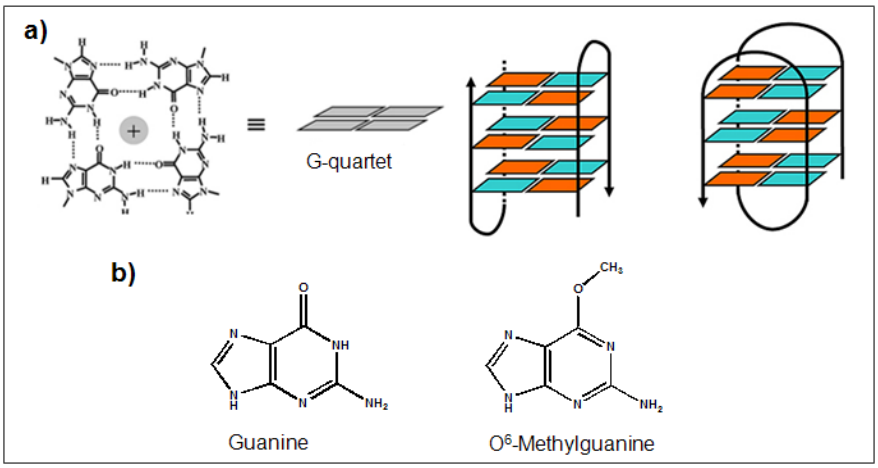

Scheme S2. a) Schematic representation of a G-tetrad and a G-quadruplex. **b)** Chemical structure of guanine and it variant, O^6-methylguanine.

To determine the disruption of the quadruplex structure, its circular dichroism spectrum was recorded. As shown in Figure S1, the circular dichroism spectra of methylated derivatives of TBA1 did not show the presence of the maximum at 295 nm, characteristic of antiparallel quadruplexes as TBA.

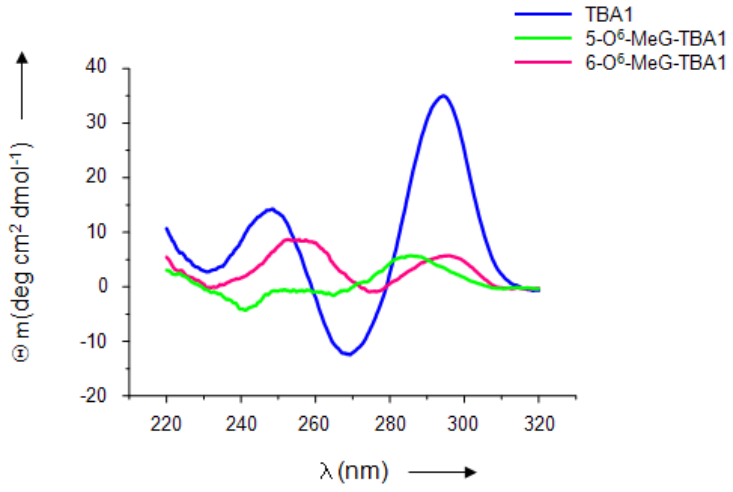

Figure S1. Circular dichroism of the methylated derivatives of TBA1 (in pink and green), contrasted with the profile of the unmodified TBA1 (in blue).

4. Fluorescence assays to study α-thrombin-TBA binding.

A fluorescence quenching assay was intended to evaluate the variation in the binding between α-thrombin and native or modified TBA. This experiment was designed on the basis of our previous work in the development of a fluorescent TBA probe to detect the activity of the DNA repair protein hAGT.[5] There, we demonstrated that the introduction of a methylated guanine in the tetrads of the TBA prevents its folding, leaving it in an extended conformation. Given that the two conformations bring the two ends of TBA together or take them further apart, we incorporated fluorescence probes at each ends, to be able to measure the changes in intensity.

A TBA1 sequence and its equivalents with the 5th and 6th guanine replaced by O^6-methylguanine were synthesized, containing a fluorophore (6'-FAM) and a quencher group (Dabsyl) attached to their 5' or 3' ends respectively. A conformational change in the MB-TBA occurs when α-thrombin binds the aptamer, due to its capability of folding the random coiled oligonucleotide into its chair-like quadruplex structure. This rearrangement brings close the fluorophore and the quencher group attached to the ends, and thus reduces the intensity of its emitted fluorescence. It is expected that O^6-methylguanine-modified MB-TBAs will not be recognized nor folded by α-thrombin and the fluorophore and the quencher will remain physically separated beyond the Förster distance, not allowing a significant decrease in the fluorescence intensity.

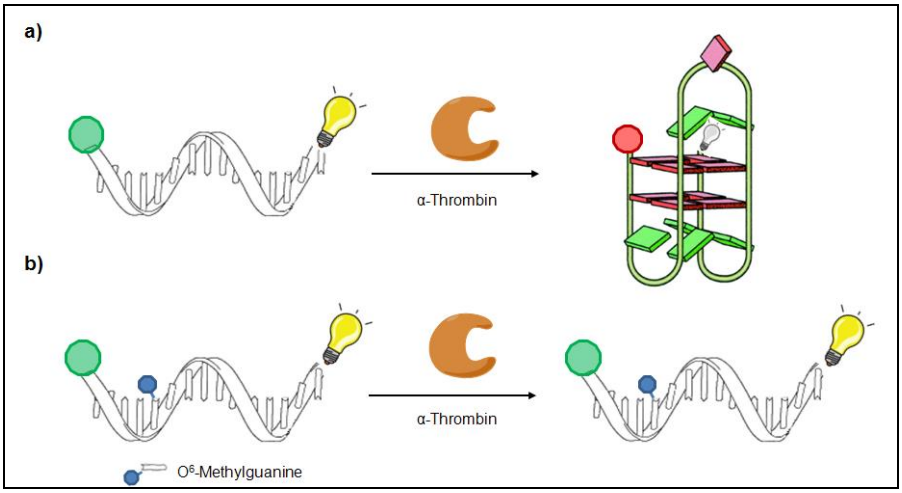

Scheme S3. Schematic representation of the bases of the fluorescence assay. **A.** Fluorescence is blocked when TBA1 is incubated with thrombin, which is able to fold it into a quadruplex and thus reduce its emission. **B.** By contrast, methylated TBA1 cannot be folded and therefore it is not able to adopt its quadruplex structure and the fluorescence emitted remains almost unchanged.

Titration of the modified MB-TBAs was carried out in physiological buffer at 25 ºC. Figure S2 shows the titration curves for the unmodified molecular beacon TBA and the two modified TBAs, either in position 5 or 6. As predicted, the fluorescence of the MB-TBA was decreased almost in a continuous way when an excess of α-thrombin was added, until reaching stabilization, indicating that α-thrombin was folding the MB-TBA back into its quadruplex structure. The stoichiometric binding ratio obtained from the titration curve was 1:1-1:1.5, as described previously[6].

By contrast, the interaction between α-thrombin and the methylated MB-TBAs was clearly smaller. Although the fluorescence intensity decreased smoothly at the beginning, it reached rapidly a plateau without reducing fluorescence's intensity significantly. These

observations indicated that α-thrombin is almost unable to fold the TBA typical structure. The variation in the slope of the schuss proved that the interaction of α-thrombin with TBA depends on the capability of the aptamer in adopting its quadruplex structure. In addition, this difference seemed to apply for both methylated TBAs, indicating that modifications in both tetrads are evenly efficient in disrupting the chair-like structure[5] and hence, making it impossible for α-thrombin to interact.

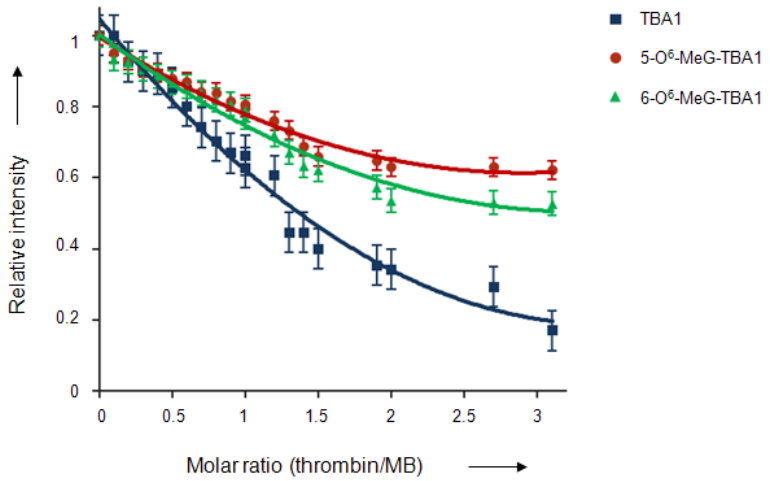

Figure S2. Titration of MB-TBAs in physiological buffer at 25ºC. The diamond red graph represents the titration of the unmodified MB-TBA, triangle green plot shows the interaction of α-thrombin with the 5-O^6-methylated derivative of MB-TBA and the squared blue one the interaction with 6-O^6-MeG-TBA molecular beacon. In the three cases, the concentration of MB is 1μM. The experiments were performed in triplicates.

5. EMSA assay to explore α-thrombin-TBA binding.

To confirm the fluorescence results, gel-mobility shift assays were performed to analyze the interaction between α-thrombin and the modified TBAs. Increasing concentrations of human α-thrombin were incubated with a constant TBA concentration, as shown in figure S3.

When non-modified TBA$(T)_5$ sequence was incubated with α-thrombin, a clear migration of the bands could be appreciated from 10 μM concentration, representing that a population of the DNA was binding α-thrombin at 1:10 ratio. However, when increasing concentrations of α-thrombin were incubated with 5-O^6-MeG-TBA$(T)_5$, no complex formation could be observed, even at a molar ratio of 1:15 and 1:20. These results confirmed that the methylation of the aptamer prevents its quadruplex structure formation and thus makes it impossible for α-thrombin to recognize and bind to it, at least at these concentration ratios. From this EMSA assay, the apparent K_D value for TBA: α-thrombin is estimated to be 15 nM and for 5-O^6-MeG-TBA, >120 nM.

Considering that 6-O^6-MeG-TBA and 5-O^6-MeG-TBA behaved similarly in the fluorescence assays, EMSA experiments were decided to be done only for 5-O^6-MeG-TBA, as only one of the sequences will be required to design the origami modified staple strands.

From these results, we could presume that a concentration of 10 fold of α-thrombin can be sufficient to appreciate a different pattern of union of this protein to the TBA and O^6-MeG-TBA-containing origami.

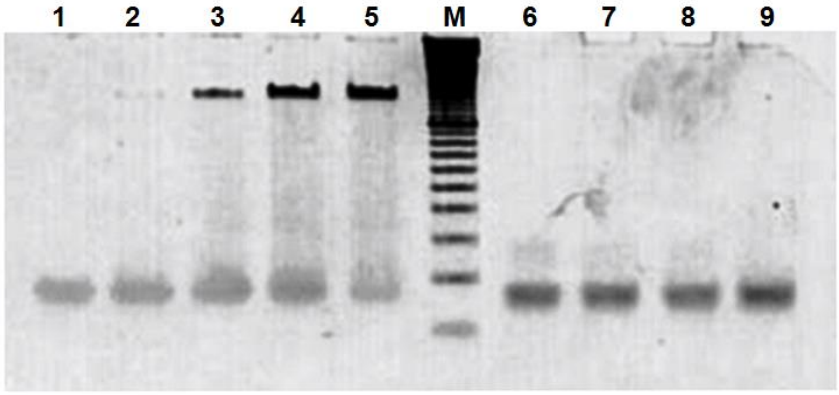

Figure S3. Gel-mobility shift assays. Non-denaturing (10% polyacrylamide) PAGE image of the titration experiment for TBA$(T)_5$ (lanes 1 to 5) and 5-O^6-MeG-TBA$(T)_5$ (lines 6 to 9). Lane M corresponds to a 10 bp double stranded DNA ladder. TBA$(T)_5$ (1) and 5-O^6-MeG-TBA$(T)_5$ (6) served as controls, and were loaded at 1 μM concentration, which was the same for all the samples. Lanes 1, 2, 3, 4 and 5 correspond to TBA with increasing concentrations of α-thrombin. TBA: α-thrombin ratios were the following: 1:0, 1:5, 1:10, 1:15 and 1:20. Lanes 6, 7, 8 and 9 correspond to the same increasing concentration of α-thrombin incubated with the methylated TBA (1:0, 1:10, 1:15 and 1:20).

6. Origami formation control

The formation of the tall rectangle origami where several staple strands were modified by the insertion of TBA1, 5-O^6-MeG-TBA1 and TBA2 was performed successfully, as it is shown in figure S4. The protruding TBAs can be clearly seen by means of AFM as two parallel lines as it was intended in the design of the array.

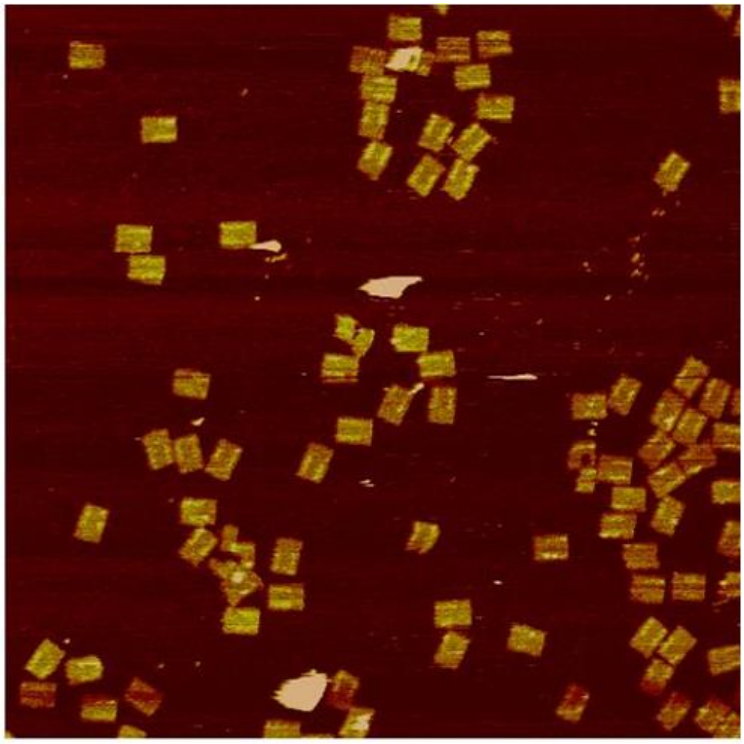

Figure S4. AFM image of the DNA origami carrying the modified TBA staple strands. The origami was formed correctly, showing that the introduction of the modified tiles did not affect to its assembly. The protruding TBA sequences can be observed as white lines of up to 3 nm height above mica, while the plannar unmodified origami protrudes 1.5 nm from mica.[2] Image height: -2.0 nm to 2.7 nm.

7. Additional AFM images of α-thrombin-DNA origami interaction

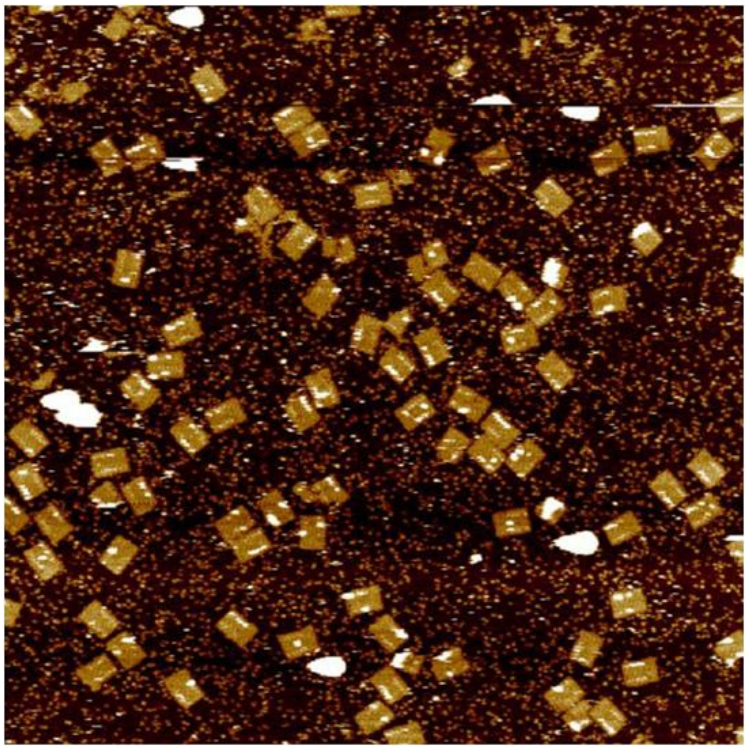

Figure S5. AFM images of the origami containing methylated TBA staple strands in the left line, incubated with α-thrombin. Image size: 3 μm x 3 μm. In this case, the height represents an increase up to 3-4 nm, due to the α-thrombin molecules attached to the origami surface. Image height: -2.0 nm to 2.7 nm.

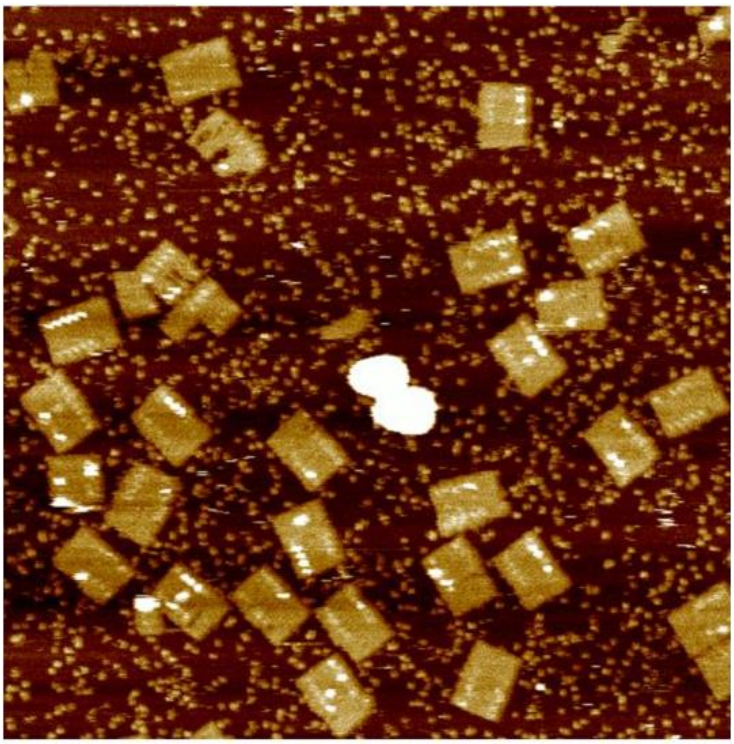

Figure S6. AFM images of the origami containing methylated TBA staple strands in the left line, incubated with α-thrombin. Image size: 1 μm x 1 μm. Image height: -2.0 nm to 2.7 nm.

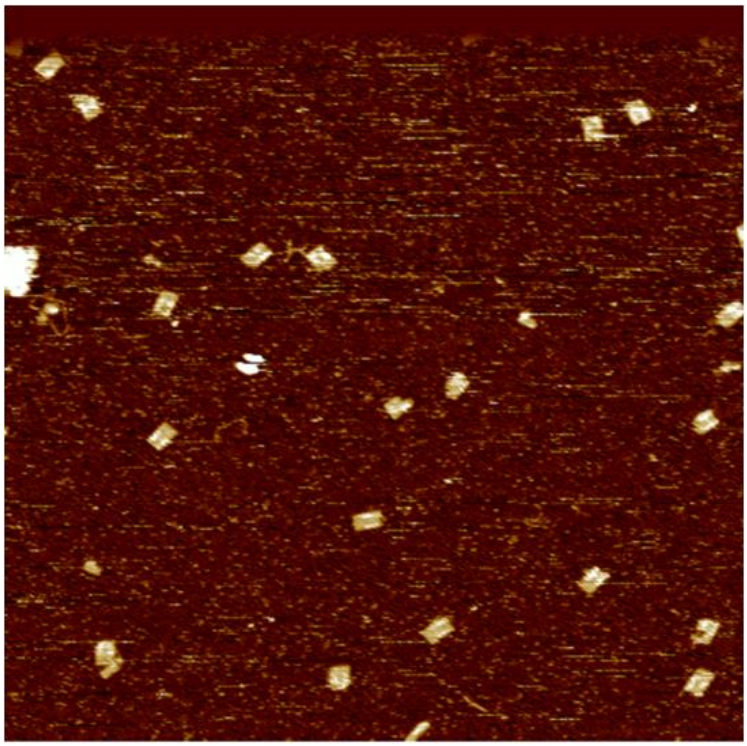

Figure S7. AFM images of the origami containing demethylated TBA staple strands, incubated with α-thrombin. Images size: 3 μm x 3 μm. Image height: -2.0 nm to 2.7 nm.

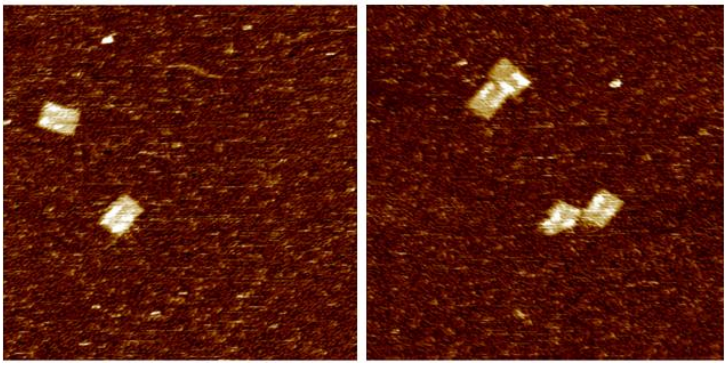

Figure S8. AFM images of the origami containing demethylated TBA staple strands, incubated with α-thrombin. Images size: 1 μm x 1 μm. Images height: -2.0 nm to 2.7 nm.

8. Section analysis of the AFM images.

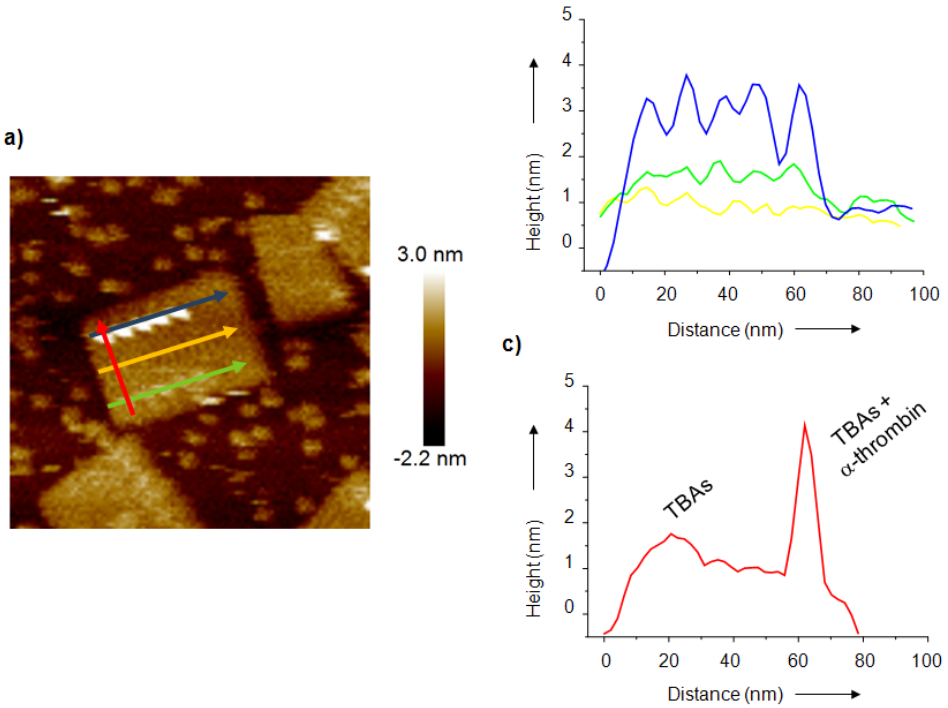

Figure S9. Line section of the methylated origami: a) AFM images of the methylated origami binding α–thrombin. b) Horizontal section of the origami, in yellow, origami surface; in green, protruding methylated TBAs; in blue five α–thrombin molecules interacting with the natives TBAs. C) Cross-section of the origami.

9. Titration of the hAGT repair activity.

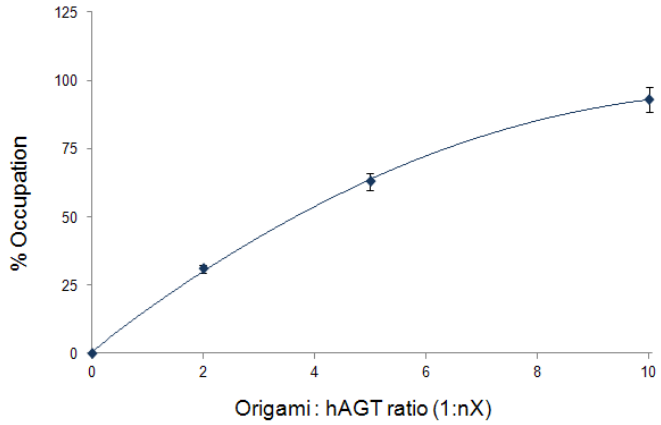

Figure S10. Titration of hAGT activity in the origami. Repair of the methylTBAs with increasing concentrations of hAGT (0x, 2x, 5x and 10x).

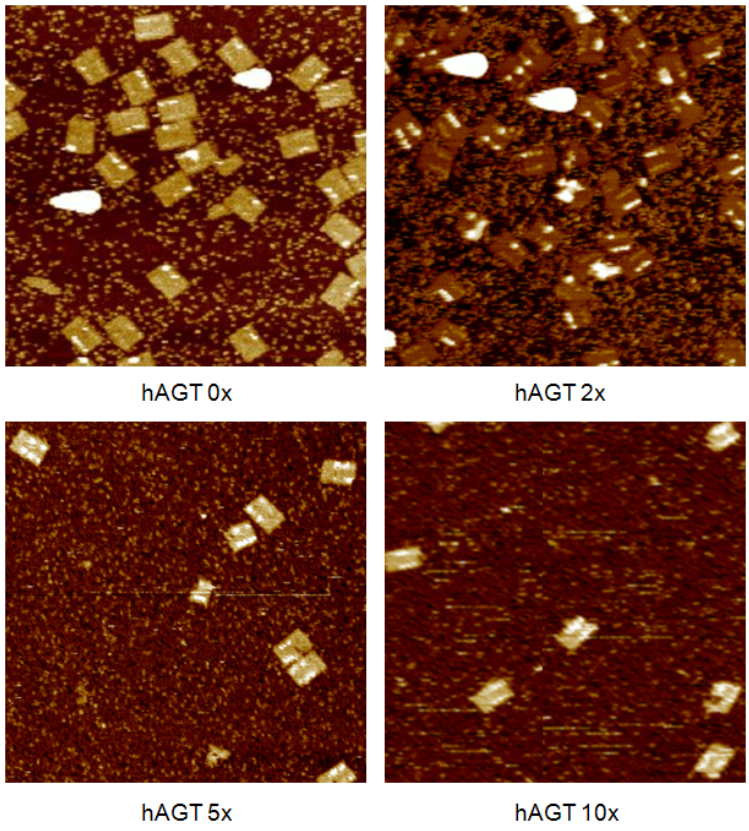

Figure S11. AFM images of the demethylated origami binding α–thrombin, showing improving occupation due to the increase in TBA repair by hAGT.

10. Quantitative and statistic studies of α-thrombin-TBA binding on DNA origami

10.1. Quantitative studies of TBA- α-thrombin binding on the methylated origami.

To explore the binding reactions quantitatively, all α-thrombin molecules on the well-shaped two-dimensional origami templates were counted according to their position, and of the 160 well-formed DNA origami structures investigated, around 20% of them contained all five α-thrombin molecules in positions coinciding with the unmodified TBAs. If we consider those origamis that were found to contain more than 4 α-thrombin molecules attached to the TBA overhangs, more than the 40% are to fit in this group. Accordingly, the counting reveals that almost the 60% of the well-shaped origamis contained more than 3 out of 5 possible positions occupied, and almost 80% considering more than 2 occupied positions. In all, more than 93% of the DNA arrays contained almost 1 α-thrombin attached to the unmodified TBAs.

10.2. Statistic studies to validate the α-thrombin binding models

Comparison of averages of the two types of binding (right line and left line) was performed using Student's t distribution. Right line corresponded to the TBA2 and TBA1 staple strands, the later methylated and subsequently repaired by hAGT, and the left one consisted of TBA1 and TBA2 staple strands, both unmodified. Binding of α-thrombin was supposed to happen similarly in both lines after hAGT demethylation. Comparison of averages resulted in an insignificant difference between them ($p < 0.5$), which confirmed that binding was occurring equally, without any preference for any line.

10. References

Main text references:

[4] c) N. V. Voigt, T. Torring, A. Rotaru, M. F. Jacobsen, J. B. Ravnsbaek, R. Subramani, W. Mamdouh, J. Kjems, A. Mokhir, F. Besenbacher, K. V. Gothelf, *Nat Nanotechnol* **2010**, 5, 200.

[18] M. Stolz, R. Gottardi, R. Raiteri, S. Miot, I. Martin, R. Imer, U. Staufer, A. Raducanu, M. Duggelin, W. Baschong, A. U. Daniels, N. F. Friederich, A. Aszodi, U. Aebi, *Nat Nanotechnol* **2009**, 4, 186.

SI references:

[1] F. M. Ruiz, R. Gil-Redondo, A. Morreale, A. R. Ortiz, C. Fabrega, J. Bravo, *J Chem Inf Model* **2008**, *48*, 844.
[2] P. W. Rothemund, *Nature* **2006**, *440*, 297.
[3] I. Smirnov, R. H. Shafer, *Biochemistry* **2000**, *39*, 1462.
[4] M. Trajkovski, P. Sket, J. Plavec, *Org Biomol Chem* **2009**, *7*, 4677.
[5] M. Tintore, A. Avino, F. M. Ruiz, R. Eritja, C. Fabrega, *J Nucleic Acids* **2010**, *2010*.
[6] J. J. Li, X. Fang, W. Tan, *Biochem Biophys Res Commun* **2002**, *292*, 31.

Appendix 3

DNA nanoarchitectures: steps towards biological applications.

DNA nanoarchitectures: steps towards biological applications.

Maria Tintoré,[1] Ramon Eritja[1] and Carme Fàbrega[1]*

ChemBioChem (2014) Volume 15, Issue 10, pages 1374–1390.
DOI: 10.1002/cbic.201402014. Impact factor: **3.06**

[1] IQAC-CSIC, CIBER-BBN Networking, Centre on Bioengineering Biomaterials and Nanomedicine. Cluster Building, Baldiri i Reixach 10, E-08028 Barcelona

ChemPubSoc Europe

DOI: 10.1002/cbic.201402014

DNA Nanoarchitectures: Steps towards Biological Applications

Maria Tintoré, Ramon Eritja, and Carmen Fábrega*[a]

Dedicated to the memory of Dr. Francisco Sánchez Baeza

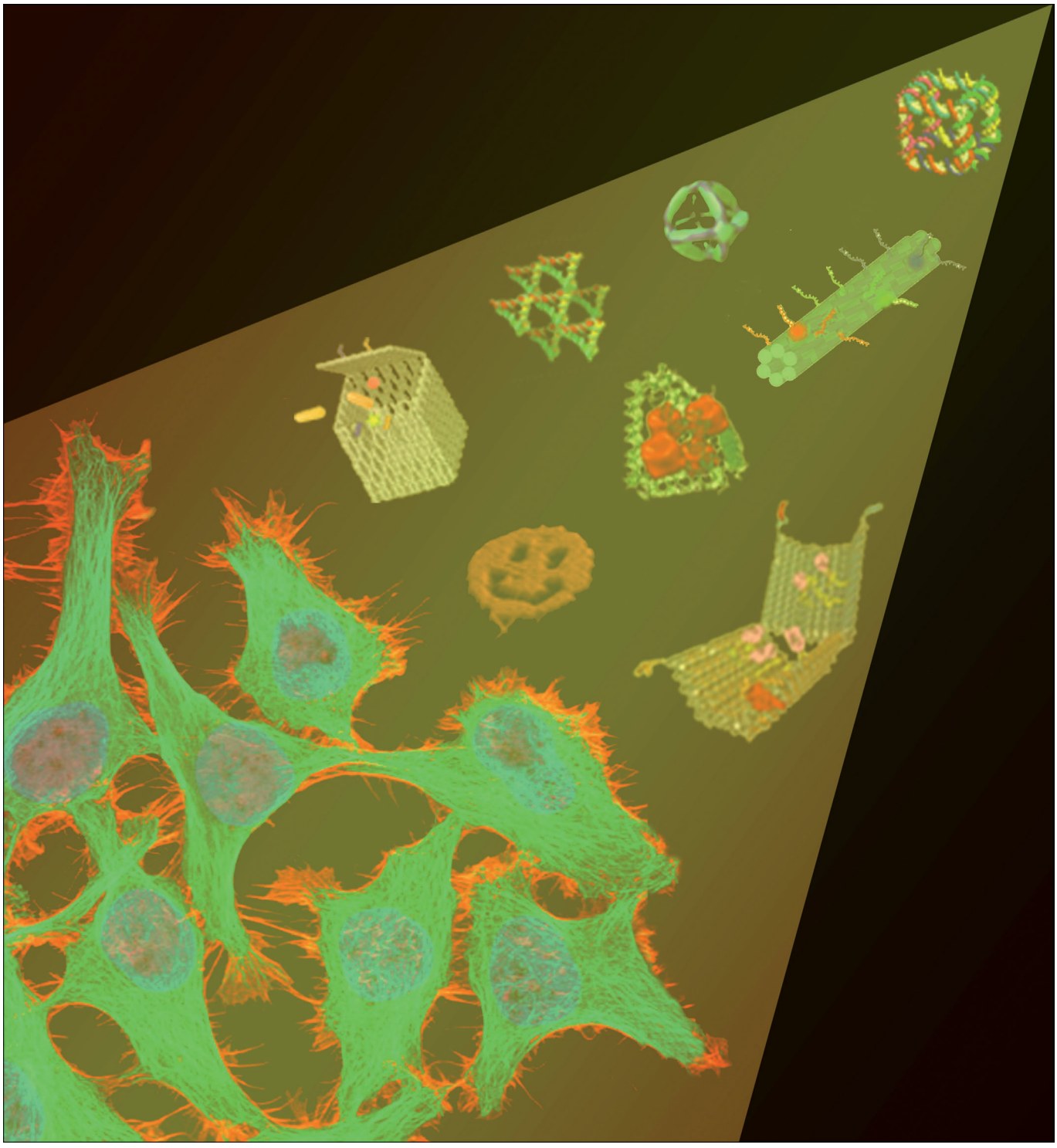

DNA's remarkable molecular recognition properties, flexibility, and structural features make it one of the most promising scaffolds to design a variety of nanostructures. During recent decades, two major methods have been developed for the construction of DNA nanomaterials in a programmable way; both generate nanostructures in one, two, and three dimensions. The tile-based assembly process is a useful tool to construct large and simple structures; the DNA origami method is suitable for the production of smaller, more sophisticated and well-defined structures. Proteins, nanoparticles and other functional elements have been specifically positioned into designed patterns on these structures. They can also act as templates to study chemical reactions, help in the structural determination of proteins, and be used as platform for genomic and drug delivery applications. In this review we examine recent progresses towards the potential use of DNA nanostructures in molecular and cellular biology.

Introduction

Last year saw the sixtieth anniversary of the DNA double-helix model of Watson and Crick.[1] The advances in the field since then have been prodigious and far beyond expectations in areas as diverse as medicine, basic biology, genetics, forensics, and archeology, and culminated in the sequencing of the human genome.[2]

Deoxyribonucleic acid is a self-assembling biopolymer that forms double helices directed by canonical Watson–Crick base pairing and is stabilized by hydrogen bonds, π–π stacking, and hydrophobic interactions. The B-form of these double-helical molecules have well-defined structures, which are repeated along the strands: the helical turn measures ~3.4 nm, the diameter is ~2.0 nm, and the twist angle between base pairs in solution is ~34.3°.[1] The remarkable specificity of the molecular recognition between complementary nucleotides has made DNA an attractive molecule for scientists and engineers interested in micro- and nanofabrication. Its predictability, rigidity, and precise structural control, as well as the creation of algorithms for de novo design of new self-assembled structures,[3] make it a useful building material to develop different kinds of nanotechnological platforms. Compared to other self-assembling molecules, DNA nanostructures offer programmable interactions and surface features for the precise positioning of other nanoparticles and biomolecules.[4]

The field of DNA nanotechnology was pioneered by Ned Seeman, who set the basis for the use of DNA as a scaffold for nanoscale building.[5] Seeman's original goal was the creation of regular 3D lattices of DNA that could be used as scaffolding for the rapid, orderly binding of biological macromolecules, in order to speed the formation of suitable crystals for 3D protein–structure elucidation in X-ray diffraction studies.[5] This gave rise to the tile-based assembly method, which has been used to synthesize two-dimensional periodic lattices[6] and three-dimensional architectures (e.g., a cube in solution,[7] and a solid-phase truncated octahedron).[8] In both cases a strategy that relies on repeated enzymatic treatment and purification was used.

[a] M. Tintoré, Dr. R. Eritja, Dr. C. Fábrega
Biomaterials and Nanomedicine
IQAC-CSIC, CIBER-BBN Networking Centre on Bioengineering
c/Jordi Girona 18–26. 08034 Barcelona (Spain)
E-mail: carme.fabrega@iqac.csic.es

Another important breakthrough in the field of structural DNA nanotechnology has been the development of DNA "origami" by Paul Rothemund,[9] where a long scaffold strand is folded with the help of hundreds of short "staples" to create the desired 2D shape. Since then, various 2D and 3D DNA motifs have been designed, and extensive studies are currently ongoing to apply these nanostructures to a large range of biomedical, computational, and molecular motor purposes.

In this review, we outline the evolution of DNA nanotechnology from simple to sophisticated, complex systems, with the aim of providing insights into the applications of the DNA-based nanostructures for the study of biological systems.

1. Basic Considerations in DNA Nanotechnology

The design and construction of DNA-based nanoarchitectures involves several major considerations. The design of the construct and its potential applications should be identified, and concerns, such as flexibility or rigidity of the scaffold, and static or dynamic devices, should be defined. It must be considered whether symmetric or non-symmetric patterns of the array are required, and whether the growth is to be limited or infinite. The periodicity and growth dimensions of the scaffold are also important. All these requirements of the scaffold architecture determine the DNA motif, as well as the building blocks design, which can comprise junctions, loops, crossovers, and single-strand binding sites. These motifs can be chemically modified to enable the attachment of non-nucleic-acids, such as proteins and nanoparticles. In addition, particular properties, such as length, specific hybridization of complementary strands, minimization of undesired hybridization, different binding sites for proteins, and restriction sites for characterization, need to be studied to achieve the final nanostructure with the best yield.

Seeman developed the first program, SEQUIN, to facilitate the design of oligonucleotides for the preparation of arrays.[10] Since then, several automated software packages have been described.[11] An overview of the concepts and algorithmic approaches of some programs was presented by Brenneman and Codon.[12]

Finally, the designed DNA oligonucleotides have to be assembled in vitro, and it can be as easy as following a typical self-assembly process by simple mixing components. However, sometimes more complex protocols are needed, such as the

assembly of single building blocks, different kinds of purification, structural integrity characterization by biochemical methods like electrophoresis,[13] digestion and/or fragmentation analysis,[14] and visualization techniques such as atomic force microscopy (AFM),[6] transmission electron microscopy (TEM), and cryo-electron microscopy.[15]

Major DNA motifs

In the early 1980s, Seeman conducted pioneering work on the construction of artificial nucleic acid architectures by using branched DNA junctions containing three or four arms of double-stranded DNA helices with sticky ends (Figure 1 A).[5] Variants with five and six arms were less stable.[16] Sticky ends at the junction arms enabled self-assembly into 2D lattices (by enzymatic or chemical coupling).[5] Three-dimensional "dendritic" structures labeled with different fluorescent dyes[17] have been generated with these junctions motifs, but they are considered inappropriate for the assembly of regular architectures because of their high flexibility.[18] A study by Malo and coworkers demonstrated that the presence of a DNA-binding protein in the process of assembling a four-armed junction resulted in a grid of squares rather than hexagon–triangle lattices (Kagome-lattices).[19a] One-dimension "railroad track" and two-dimensional lattices have been assembled with four arm junctions despite the high flexibility of these building blocks.[19b]

The generation of "4×4 tile" motifs (containing four-armed junctions with T4 loops at their arms) facilitated assembly as linear ribbons and two-dimensional arrays. He et al. assembled larger two-dimensional arrays from this motif by applying two new concepts (Figure 1 B).[20] First, the motif was designed to be symmetric, and second, it followed a "corrugation strategy", consisting of two adjacent building blocks facing opposite directions in such a way that the small curvatures of the individual motifs are canceled (by each other) instead of accumulating throughout the structure. This system has been used to template streptavidin (STV) into periodic protein arrays, by in-

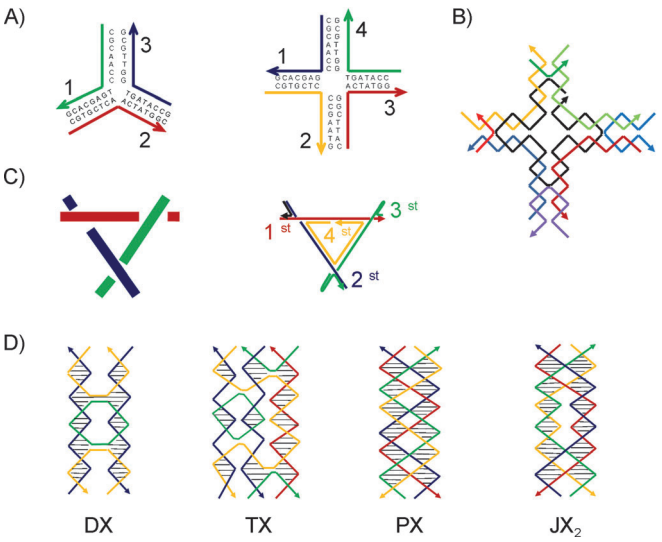

Figure 1. Major motifs in DNA nanotechnology. Arrows indicate the 3′-ends of DNA strands. A) Branched DNA junctions containing three or four arms/strands. Double-helix arms form between strand pairs. B) A 4×4 DNA tile of nine unique strands. C) A DNA triangle contains three DNA duplexes, shown as rods (left) or as thin lines for single DNA strands ("st" right). D) A DX molecule results from double exchange between double helices. A TX molecule results from two successive double reciprocal exchanges. Both molecules contain exchanges between strands of opposite polarity. A PX molecule is formed when two double helices exchange strands at every point where helices come into contact. A JX_2 molecule differs from PX in that it lacks the two central crossovers. The exchanges in PX and JX_2 are between strands of the same polarity.

Maria Tintoré received her B.Sc. in Pharmacy at the University of Barcelona in 2009. She then obtained a Master in Molecular Biotechnology at the University of Barcelona in 2011. She is currently working on her Ph.D. thesis in the laboratory of Dr. R Eritja under the supervision of Dr. Fábrega at the IQAC-CSIC Institute, where she focuses on the design and biological evaluation of inhibitors of alkyl-transferases as potential enhancers in cancer therapy, by using DNA nanotechnology tools.

Ramon Eritja received his Ph.D. in Chemistry from the University of Barcelona in 1983. In 1990, after two postdoctoral positions, he became a group leader at CSIC, and in 1994 he transferred to EMBL as a group leader. He returned in 1999 as a Research Professor at IQAC-CSIC leading the Nucleic Acid Chemistry Group. In 2012 he was appointed director of the IQAC-CSIC. His research focuses on oligonucleotide and peptide synthesis for biomedical and nanotechnological applications.

Carmen Fábrega completed her Ph.D. on the incorporation of mutated bases in oligonucleotides at the University of Barcelona in 1997. After postdoctoral studies on aminoacyl tRNA synthetase and mRNA capping enzymes, she was appointed Tenure-Track Scientist at CNIO in 2003, where she researched inhibition of DNA repair enzymes. Since 2009 she has been a Senior Scientist in Dr. Eritja's group developing new biosensing methods for the study of DNA repair mechanisms and its application to cancer.

serting a biotin group into the T4 loops at the tile center.[21] A step toward versatile, size-controlled, and programmable DNA-based nanoarrays was reported with cross-shaped tiles, by using a stepwise hierarchical assembly technique.[22]

DNA triangles are promising candidates for the fabrication of "tensegrity" structures. These are constructs of rigid rods connected by short "tendons" (here, branch points of DNA junction motifs) that are connected by short tensegrity segments (Figure 1 C).[23] As mentioned above, DNA junctions are rather flexible, and assembly does not often yield a regular structure. Seeman and co-workers solved this problem by creating the most fundamental motif in DNA nanotechnology: the double crossover (DX) motif (Figure 1 D). This consists of two double-stranded helices that interchange single strands at two crossover points.[24] DX motifs with sticky ends allow the constructions of 2D arrays.[6] Rinker demonstrated that it is possible to replace DNA strands in a DX motif with locked nucleic acid (LNA) strands in the formation of 2D arrays.[25] After the success of the DX motif, triple-crossover (TX) tiles were designed; these consist of three helices lying in a plane, connected at crossover points (Figure 1 D),[26] as found in linear lattices, 2D arrays,[26] and DNA tubes.[27] Various other tiles (other than square and rectangular) have been prototyped. At least three versions of triangular tiles have been described: in one the plane is tiled entirely with triangles,[23] and in the other two hexagonal patterns are formed.[28] Three-point[29] and six-point star[30] motifs have also been self-assembled into two dimensional arrays.

Another important class of DNA motif is the paranemic crossover (PX) motif,[31] which is composed of two parallel helices with crossovers at every possible site (Figure 1 D). This motif can be topoisomerased to form the JX_2 motif, where the relative positions of the two ends of the motif are rotated 180° relative to PX (Figure 1 D).[32] Extensive information about DNA major motifs, self-assembled DNA nanostructures and mechanical devices is found in several reviews.[33]

1.2. Polyhedra

One of the major goals in DNA nanotechnology is the construction of three-dimensional DNA structures. However, 3D constructs have proved to be more difficult to build than 2D constructs.[34] The first 3D structures to be assembled were a cube[7] and a truncated octahedron[35] (Figure 2 A and B), but these were obtained with low yield and were not suitable for biological applications. Seeman successfully engineered crystals with altered lattice dimensions in 2004,[36] thus pursuing his initial idea to generate 3D crystals for X-ray crystallographic study of "guest" molecules, such as proteins.[37] A remarkable achievement was the design and synthesis of an octahedron with DX-like edges and PX motifs:[38] a 1.7-kb, ssDNA molecule amplified by polymerase and folded with five 40-mer synthetic oligodeoxynucleotides (Figure 2 D).[15] Later, a chiral tetrahedral unit with short double helix edges was constructed in higher yield (Figure 2 C).[39] By this approach, it was found that adding programmable linkers confers structural stability and resistance to deformation. The robustness of the structure was studied by AFM.[40] One of the edges of the tetrahedron was examined for mechanical movement by exchanging the DNA strands, thereby producing a reconfiguration of the DNA tetrahedral shape in a precise and reversible manner.[41] Covalently closed octahedral DNA cages were reported to be resistant to thermal and chemical denaturation, and could thus represent a step towards to the use of these devices as delivery systems.[42] More

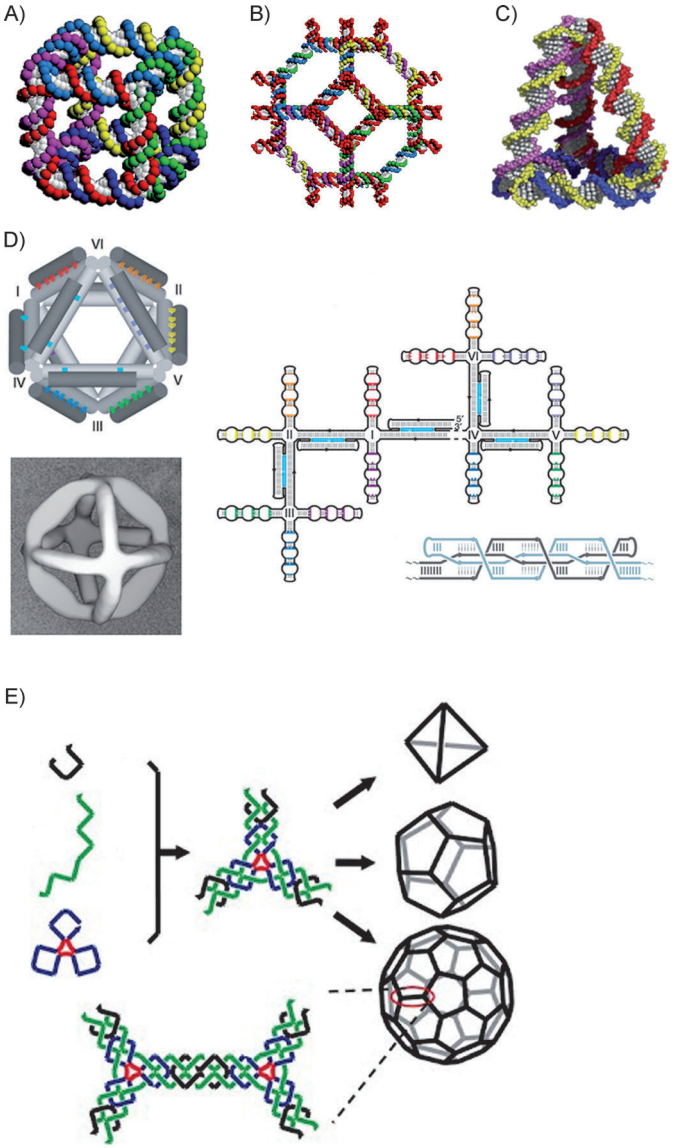

Figure 2. A) Cube formed from twelve equal-length double-helical edges arranged around eight vertices. B) Double-helical representation of an ideal truncated octahedron. Reprinted with permission from ref. [35]. Copyright 1994, American Chemistry Society. C) DNA tetrahedron. Reprinted with permission from ref. [40]. Copyright 2005, American Association for the Advancement of Science. D) 3D model of an octahedron. Secondary structures consist of five DX and seven PX motifs; hybridization of PX motifs for 3D formation. Reprinted with permission from ref. [15]. Copyright 2004, Nature Publishing Group. E) Polyhedral structures: tetrahedron, dodecahedron and buckyball, assembled from three-point star building blocks. Adapted with permission from ref. [45]. Copyright 2008, Nature publishing Group.

complex and modified polyhedra were also created in a single step.[43]

Sleiman reported a new method to increase the range of 3D structures to include a prism, a cube, pentameric and hexameric prisms, a heteroprism, and a biprism.[44] Mao took advantage of the "sequence symmetry"[20] to generate three-point star motifs or tiles. By controlling the flexibility and the concentration of the tiles and adapting the length of central single-stranded loop, his group synthesized a tetrahedron, a dodecahedron, and a buckyball from a minimal set of building blocks (Figure 2E).[45] By the same strategy, a five point start motif was designed and self-assembled into icosahedra.[46] Strategies to restrict polyhedral faces to those with an even number of vertices were used to assemble DNA cubes.[47] Trisoligonucleotides with an organic vertex (C_{3h} linker) were employed to assemble a DNA dodecahedron, thus demonstrating the usability of this construct for multimodular machines by the introduction of extension arms that allow overhanging with other sequence.[48]

Chirality is an essential feature in nature.[49] Enzymes and cell receptors have the ability to distinguish different substrates stereoisomers, thus leading to highly efficient and stereoselective reactions and binding. Understanding and control of chirality is crucial for drug design,[50] encapsulation,[51] and other processes.[52] The chirality of DNA duplexes is indisputable; however, its extension to building stereoisomeric pure DNA nanostructures has been a challenge. Mitchell et al. described the self-assembly of chiral nanotubes,[53] and subsequently, He et al. reported a well-defined chiral octahedron.[54] The assembly of both structures was relatively straightforward, and their chiral features might enable the use of this type of structures for all the applications mentioned above.

Another important tool in 3D DNA nanotechnology is "tensegrity": the balance between components that are in pure compression and those in pure tension for stability. The Shih group reported nanoscale prestressed 3D tensegrity structures in which rigid bundles of DNA resist compressive forces exerted by single-stranded DNA segments that act as tension-bearing cables.[55] These tensile structural elements could be used to study molecular forces, cellular mechanotransduction and other fundamental processes.

1.3. DNA origami

The implementation of DNA computing by Winfree's group in 2004[3] formed the basis for the development of what would be one of the most important breakthroughs in the field: DNA origami, as reported by Rothemund in 2006.[9] This involves the folding of a long, circular, single-stranded DNA scaffold into arbitrary 2D shapes, directed by a collection of various (hundreds of) shorter single-stranded oligonucleotides that are complementary to different regions of the scaffold (Figure 3A). The specific matching of the scaffold and "staple" strands leads to well-shaped nanostructures, with high yield and reproducibility (Figure 3B). In addition, it avoids stoichiometric dependence, thus eliminating the need for purification and exact determination of the concentration of the oligonucleotides, and thereby reducing the time and effort required for its assembly. One of the most attractive features of this technique is the addressability of the surface, thus permitting the attachment of different biomolecules or nanoscale objects by the modification of specific staple strands at desired positions.[4]

The origami approach was further developed for the construction of 3D nanostructures. Gothelf's group assembled a box with a controllable lid from a combination of six origami sheets;[56] at the same time, Kuyuza and Komiyana designed another box-shaped origami by selective closing of a preformed motif.[57] A scaffold DNA origami of a closed DNA tetrahedron was designed by Ke et al.; this resembled the icosahedral structure of many viral particles.[58] Shih and co-workers introduced a strategy to generate 3D nanostructures by honeycombing (or square packing) scaffolded DNA[59] (Figure 3D). This group also described the insertion of twists and curves into 3D nanoconstructs, through addition or deletion of base pairs at specific positions within the helical layers.[60] The Yan group developed a method based on the organization of concentric DNA rings of different radii to build DNA shapes with complex curvatures (Figure 3E).[61] They also reported the design of quasi-2D origami tiles with a Mobius topology, which implies a certain degree of twist and curvature, as well as flexibility and strength.[62] These novel 3D structures further demonstrate the robustness and potential of the origami technique in different kinds of application.

An important limitation of this technique is that it results in a relatively small area, limited by the length of the standard scaffold. In many cases, the origami surface might not be sufficient for the precise positioning of functional molecules or for other applications. For this reason, other efforts in the field are focused on assembling larger structures, including approaches such as algorithmic assembly from origami seeds,[63] origami oligomerization[64] and polymerization,[65] the use of eight-helix bundles as staples,[66] long single-stranded PCR amplification products,[67] and double-stranded viral genomes[68] as scaffolds. An example of this oligomerization is given in Figure 3C.[64b] A more detailed description of these methodologies can be found in a review by Tørring et al.[69]

A novel approach by Sugiyama's group was to design RNA-templated DNA origami structures that were folded to form seven-helix, bundled rectangular shapes. These nanoconstructs were composed of an RNA transcript (as scaffold) with DNA staple strands, and have been exploited for specific applications such as catalysis and RNA interference.[70]

Recently, DNA origami technology is becoming more accessible to researchers from different fields because of the development of several computational tools for the design of diverse structures, for example SARSE-DNA,[71] caDNAno,[72] and CanDo.[73] These software tools facilitate the sketching and patterning of the nanoconstructs and broaden the scope in terms of time, cost and need for researcher experience. Today, a few hours and basic computation fluency is sufficient to design origami tiles for a wide variety of applications.

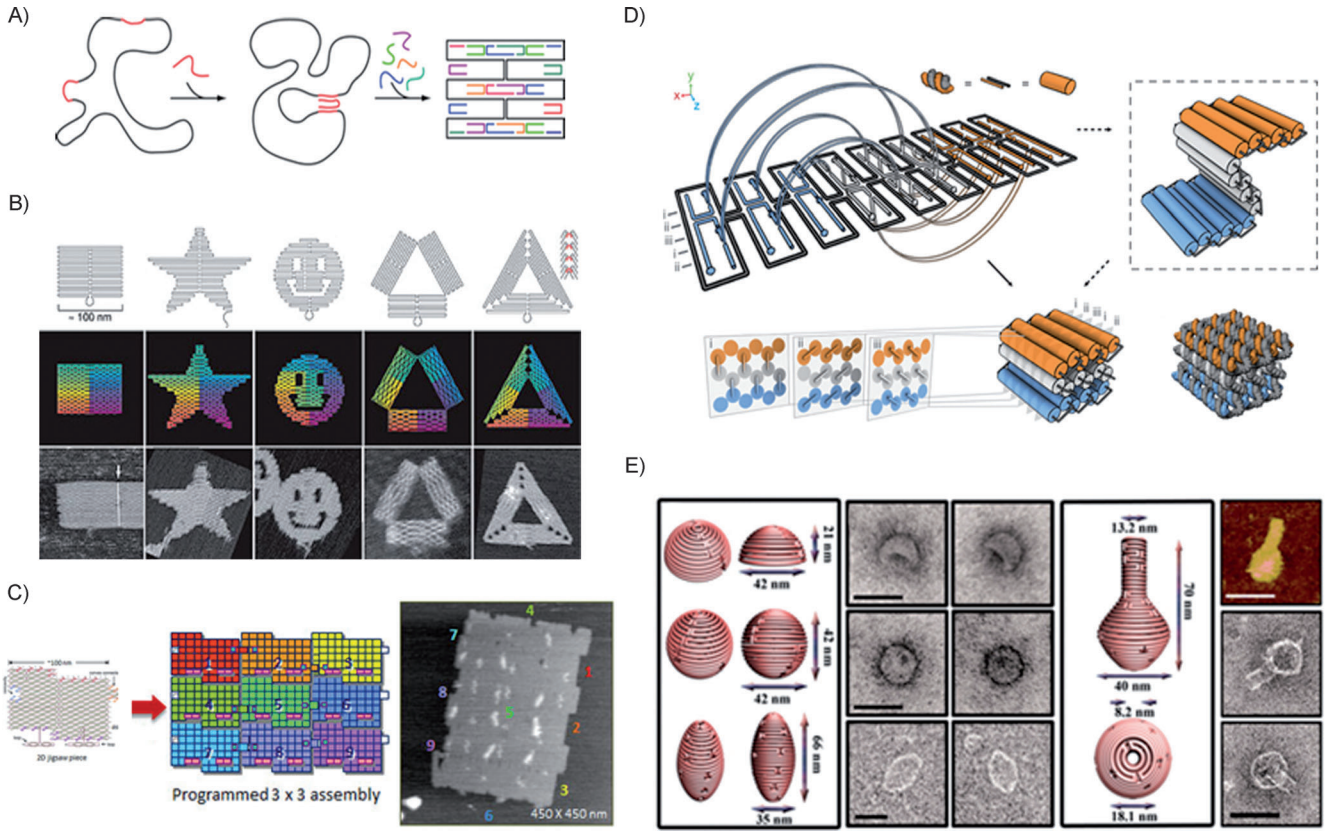

Figure 3. A) Formation of DNA origami. B) Example DNA origami nanostructures and their AFM images described by Paul Rothemund. Reprinted with permission from ref. [9]. Copyright 2006, Nature Publishing Group. C) Example strategy for enlargement of DNA origami dimensions, by the union of "jigsaw" pieces. Adapted with permission from ref. [64b]. Copyright 2011, American Chemistry Society. D) Strategy to generate 3D nanostructures by honeycomb or square packing of the scaffolded DNA. Reprinted with permission from ref. [59a]. Copyright 2009, Nature Publishing Group. E) Method to build DNA shapes with complex curvatures, based on the organization of concentric DNA rings of different radii. Adapted with permission from ref. [61]. Copyright 2011, American Association for the Advancement of Science.

2. Biochemical Applications

The advent of nanotechnology and the expansion of computational algorithms has led to an explosion in the number of DNA scaffolds that can be created, and for a wide variety of applications, including nanomaterial assembly, biosensors,[41] molecular computation,[33d,74] biomolecular actuation, drug delivery, and nanodevices.[33d]

2.1. Tiles and Polyhedra

One great challenge in engineering functional materials and devices has been how to integrate and assemble them into hierarchical arrays with minimal defects. However, innovative methods by Mirkin[75] and Alivisatos[76] demonstrated that gold particles and surfaces are generally easily modified with oligonucleotides, and assembled into different packing densities and arrangements for a variety of applications. The design and generation of more-complex DNA tile motifs have been used for the assembly of lattices, particularity for allowing the incorporation of components that protrude from the plane,[26] such as gold nanoparticles[77] of different size[78] (Figure 4 A), and combinations of streptavidin and gold nanoparticles.[79] All these developments open the door to extensive work for the creation of nanoelectronic, nanophotonic, and optoelectronic devices, which are beyond the scope of this review.

Mirkin[80] and Gang[81] demonstrated that DNA can be used to control the crystallization of nanoparticle–oligonucleotide conjugates; different DNA sequences guide the assembly of the same type of inorganic nanoparticles into different crystalline states, thereby controlling distance and packing dynamics.

Nanostructures for the sensitive detection of biomolecules have been reported by Niemeyer and co-workers by using DNA–streptavidin conjugates. Such DNA–protein conjugates could be versatile molecular tools in immunoassays, nanoscale biosensor elements, microstructural biochips, and supramolecular devices.[82] The streptavidin–biotin interaction has been the most explored method in the creation of molecular networks.[21,22,83] Efficient assembly into 2D DNA arrays of other ligands such as DNA aptamers[84] with target proteins such as thrombin or antibodies has been accomplished (Figure 4 B).[85] In a similar approach, Krishnan and co-workers designed the I-switch, a DNA nanosensor that maps spatial and temporal pH changes inside living cells by FRET.[86] Organic and inorganic linkage connecting multiple DNA strands has been extended to include dendrimers,[84a,87] macrocycles,[88] multibranched

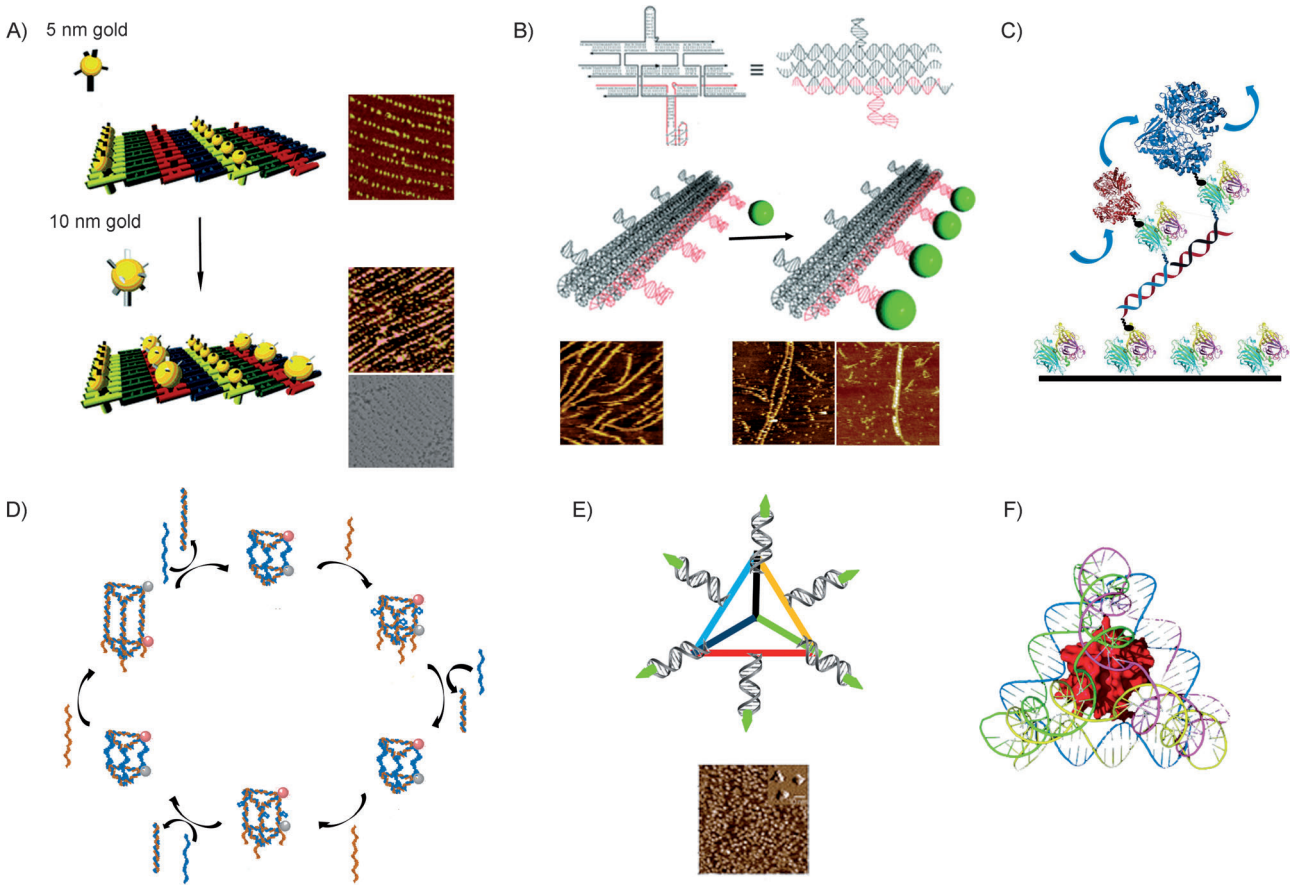

Figure 4. A) DNA scaffold deposited on mica combined with DNA-encoded nanocomponents of two sizes, and AFM and TEM images. Adapted with permission from ref. [78a]. Copyright 2005, American Chemical Society. B) Aptamer-directed self-assembly of thrombin protein (green spheres) on a 2D DNA tile generates a linear protein arrays. AFM images prior to and after thrombin binding. Adapted with permission from ref. [84a]. Copyright 2005, Wiley. C) DNA-directed organization. Biotinylated recombinant enzymes are coupled to covalent DNA-streptavidin conjugates. D) Dynamic structural changes upon hybridization of a specific complementary strand in a prism structure. E) Tetrahedral delivery system for siRNA conjugated to cancer-targeting ligands. AFM image shows tetrahedron nanoparticles on mica. AFM image show the three upper edges of the tetrahedral. Adapted with permission from ref. [99c]. Copyright 2012 Nature Publishing Group. F) Tetrahedron containing a molecule of cytochrome *c*. Adapted with permission from ref. [100a]. Copyright 2006, Wiley.

structures,[89] and linear arrays containing functional molecules.[90]

Many biochemical systems in biology require more than just one catalytic reaction by a single enzyme; for instance, with multienzyme reaction complexes,[91] the substrate is passed directly from one catalytic site to the next. A benefit of special arrangements of enzymes is concerted action of several complementary enzymes to cooperatively perform a complex task. Artificial co-localization of enzymes (to improve reaction flux) has been attempted by a variety of approaches, such as with solid matrices, by chemical connections, by recombinant engineering, or by using protein–protein interaction domains.[92]

In recent decades, there have been several attempts to apply DNA scaffolding for the creation of artificial multienzyme systems. Niemeyer and co-workers[93] demonstrated for the first time that DNA-directed assembly of two proteins could be the initial step for the efficient generation of artificial multienzyme complexes (Figure 4C). Later, they also reported the covalently linkage of enzymes like glucose oxidase (GOX) or horseradish peroxidase (HRP) to DNA to generate supramolecular complexes.[94] In both cases, improved performance was observed when the proximity of the cooperative enzymes was constrained.[93,94] The first example of enzyme systems arranged on a larger supramolecular DNA scaffold was demonstrated by Wilner et al.[95] Again with the GOX/HRP system, they reported a significant increase in overall activity when the two enzymes were held in close proximity by a hexagon-type DNA scaffold. In addition, they immobilized glucose dehydrogenase and its tethered cofactor NAD^+ on the scaffold, and observed different activities for different tether lengths and distances. More recently, the same multienzyme system was incorporated into a switchable DNA scaffold to dynamically control a diffusion distance of intermediate products.[85c] In this way, the system reversibly regulated the reaction in situ.[96] Another impressive achievement was the control of spatial organization of a multienzymatic complex by using RNA molecules that are sequence-programmed to be isothermally assembled into predefined discrete, 1D and 2D structures in vivo. The reaction was optimized as a function of scaffold architecture.[97] Further studies could be useful for the development of novel catalysts for enzymatic processes or to perform multistep

chemical transformations of cheap precursors into drugs and fine chemicals.

DNA nanostructures are also promising candidates for drug delivery, as they possess a combination of features. Firstly, they have a great flexibility in size and shape, thus offering a variety of parameters for optimization in order to improve cellular internalization.[84b, 98] Sleiman has reported a new method for the construction of the first dynamic 3D DNA capsules whose size is able to switch between three different lengths. These 3D switchable capsules can be used for drug delivery and dynamic DNA structures (Figure 4D).[44] In addition, DNA can be functionalized with different molecules as cargos, by covalent modification,[98a] self-assembly of DNA polyhedral nanoparticles with a well-defined size which can deliver small molecules, siRNAs and antisense oligodeoxynucleotides into cells and silence target genes in tumors,[99] and encapsulation (Figure 4E and F).[100] Recently, Wollman et al. created a DNA molecular motor that performs a wide range of tasks, including self-organization, capture, and concentration of cargoes transport signals for release and track or follow disassembly.[101] Moreover, these structures are stable under physiological conditions[102] and, as natural material in living creatures, possess excellent biocompatibility.[98a]

2.2. DNA origami

Since Rothemund's original report,[9] a large number of research groups have adopted the DNA origami technique in several novel applications, from all type of chemical or enzymatic single-molecule reactions to applications in photonics,[103] nanorobotics,[104] and nanomechanics.[105] Here we provide a brief list of these applications. Gold nanoparticles have been selectively positioned and patterned on origami structures.[103b, 106] Yan and co-workers connected gold nanoparticles to DNA origami nanotubes, a development which represents progress towards the goal of combining origami self-assembly and lithographic methods to design patterns on surfaces.[107] Precise DNA sequences with sugar moieties covalently attached were used for the site-specific immobilization of fluorescent silver nanoclusters at predefined positions on the nanoscaffold;[108] the resulting high density array of emissive nanoclusters could have potential applications in the nanofabrication of semiconductor nanostructures. A methodology combining gold and silver nanoparticles using a predetermined pattern was developed by Pal et al.[103c] A general method for arranging single-walled carbon nanotubes (SWNT) in two dimensions by using DNA origami was reported by the Winfree group; it has potential use in the synthesis of multi-SWNT logic gates or memory circuits.[109] As a final example, Stein et al.[110] achieved a combination of multistep energy transfer in a photonic wire-like origami structure using fluorophores that undergo an energy-transfer cascade. This work demonstrates the wide and multidisciplinary potential of DNA origami nanotechnology for the above-mentioned applications. Given that the field is so extensive, here we focus on the biological and biochemical applications of DNA origami and their pros and cons for specific uses; we do not review the more mechanical and computational approaches, which have been covered in many excellent reviews.[4, 111]

2.2.1. Material organization: There is almost no limitation in attaching functional biomolecules to DNA origami, as chemically modified sequences can be incorporated to staple strands, or specifically modified DNA can be readily attached by hybridization to staples strands.[112]

Several research groups have demonstrated the possibility of displaying nucleic acids on the origami surface: when mRNA probes are attached to DNA origami structures, they can be used for the detection of gene expression at the single-molecule level.[113] These findings open the door for using the origami technique for a great variety of diagnostic applications. By using the same basic concept, the complete sequence of a synthetic oligonucleotide can also be tracked down over an origami surface by using complementary probes, with broad applications for the recognition of unknown DNA sequences.[114]

In addition, a huge number of proteins have been programmed over DNA nanoconstructs. Niemeyer and co-workers decorated DNA origami with three types of proteins by using coupling systems orthogonal to the biotin–streptavidin interaction (Figure 5A).[115] This study raised the question over preference for face-down or face-up orientation of the origami structures when deposited over mica; this was found to depend principally on the method used for the binding of the proteins to the origami tile.

A possible application of the origami technique is the study and control of the binding distances between DNA and the protein partners. For example, Rinker et al. studied the multivalent interactions of α-thrombin and its two α-thrombin binding aptamers (TBA), and the distance dependence for simultaneous binding (Figure 5B).[116] By taking advantage of the spatial accuracy of this platform, it was found that α-thrombin binds the dual system with a tenfold better recognition than with a single aptamer, and it was shown for the first time that 5.3 nm between the two aptamers is optimal for bivalent binding. This group used a similar strategy to study the distance-dependent kinetic processes associated with the GOX/HRP enzyme pair. The distance between enzymes was systematically increased from 10 to 65 nm, thereby revealing strongly enhanced activities for these enzymes when closely spaced, whereas the activity dropped dramatically when as little as 20 nm apart. They also observed that strong activity enhancement was not simply achieved by reducing the inter-enzyme distance but also by restricting the diffusion of intermediates to the 2D surface connecting the enzymes.[117] These results further demonstrate the high resolution and spatial accuracy of the technique, and the possibility of using it for the visualization and characterization of single-molecule events.

A new method was reported to direct protein nanopatterning over origami nanoconstructs, by using nitrilotriacetic acid and histidine-tag metal-linked interactions. This report describes a new way of selectively binding a staple strand to the target protein—highly relevant in protein immobilization on DNA origami.[118] Although it provided a novel way of attaching proteins to the DNA origami surface, this method needs to be extended to other tags, as the histidine tag is not well tolerat-

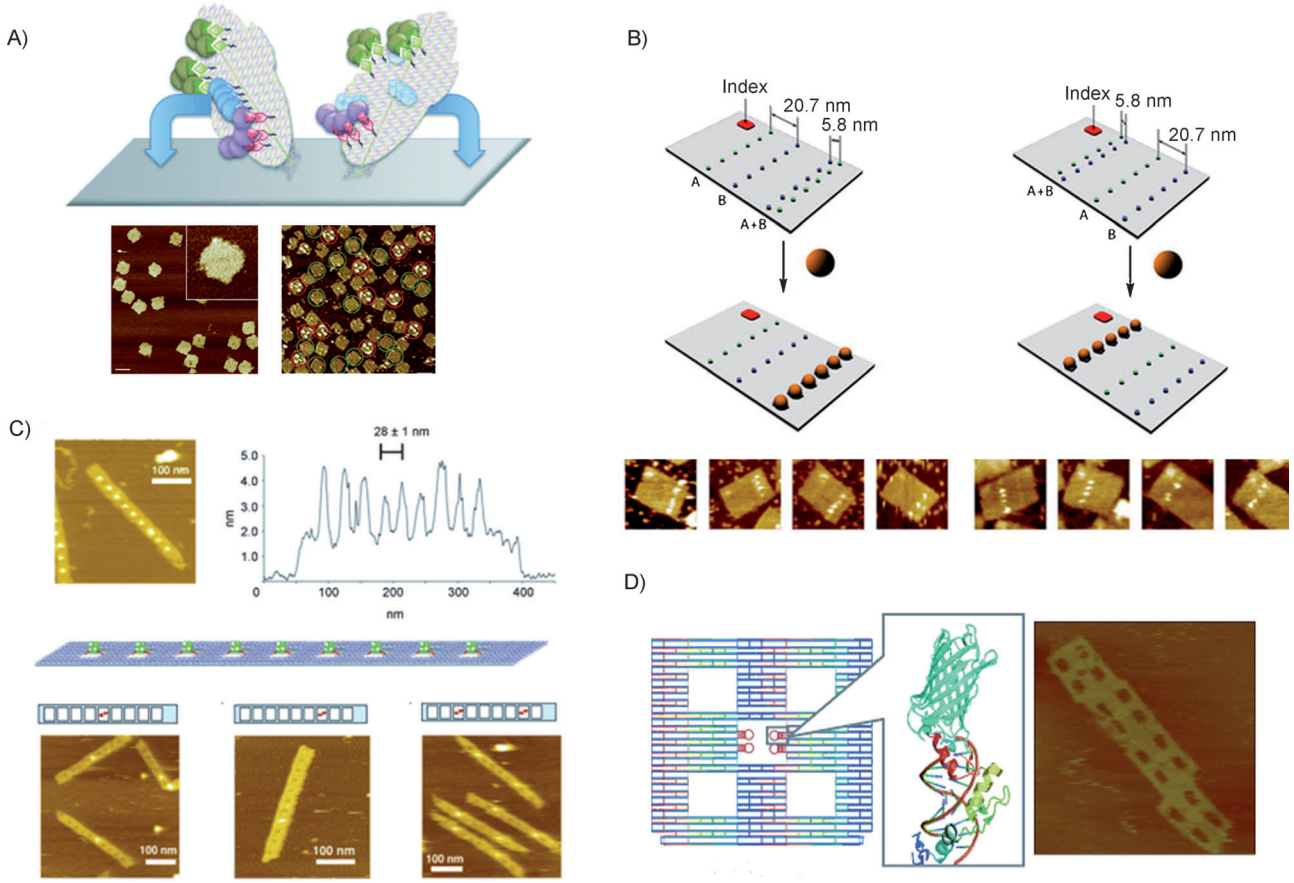

Figure 5. Examples of precise material organization on DNA origami surfaces. A) Orthogonal decoration of DNA origami, raising the controversy of face-up or face-down disposition of the nanostructures over mica surfaces for visualization. Reprinted with permission from ref. [115]. Copyright 2010, Wiley. B) Distance-dependence study of multivalent interactions of α-thrombin with two binding aptamers (TBA) on an origami platform. Adapted with permission from ref. [116]. Copyright 2008 Nature Publishing Group. C) Construction of a streptavidin nanoarray on a DNA origami, by size-selective capture of one streptavidin tetramer in each well. Adapted with permission from ref. [119]. Copyright 2009, Wiley. D) Assembly of zinc-finger proteins (ZFP) on DNA origami structures, to enable placement of multiple engineered proteins at different locations. Reprinted with permission from ref. [121a]. Copyright 2012, Wiley.

ed by all proteins, and can prevent folding and/or activity. The chemical functionalization of the target molecules could be also be a drawback, so will need further development to extend this method to a broader range of proteins.

Streptavidin nanoarrays were created by using periodical nanometer-scale wells embedded in DNA origami in which single streptavidin molecules could be held (Figure 5C).[119] This represents an innovation because all in previous attachments nanomaterials were anchored to DNA origami at the surface of the array. In this design, gold nanoparticles were nanopatterned, by selectively capturing a single nanoparticle in each well of the punched DNA origami. Subsequently, they combined alternating organic (streptavidin) and inorganic (gold nanoparticle) materials in a defined pattern.[120]

Recently, zinc-finger proteins (ZFP) were assembled on an origami scaffold (Figure 5D).[121] Orthogonal targeting of the specific locations in the structures was demonstrated by using two adaptors, and *Escherichia coli* lysate containing the adaptor-fused proteins successfully afforded the expected protein–DNA assembly. The diversity of target DNA sequences and the semi-programmable design of ZFPs offers orthogonal adaptors, thus enabling the placement of multiple engineered proteins at different locations on DNA-origami structures. Nature uses multiple enzymes in close proximity to efficiently carry out chemical reactions and signal transduction. Such assemblies of multiple proteins could be realized in vitro by using DNA origami structures that have predefined binding sites and various kinds of ZFP adaptor-fused proteins.

2.2.2. Single-molecule reaction: Single-molecule studies are crucial to understand the trajectories of molecules as they undergo reactions. For this reason, considerable effort has been made in this area, and the application of the origami technique has given the opportunity to solve many spatial and isolation problems because of its nanometric resolution and addressability. In addition, any functionality that can be conjugated with DNA can be placed on the origami surface, thereby serving as a molecular recognition probe. Some of the applications described in the above could be also considered single-molecule reactions, for example RNA hybridization assays or the distance-dependent thrombin-aptamers binding.

One of the first reports to show the possibility of detecting single molecule reactions in real time at positions of an origa-

mi platform was conducted by Voigt et al.[122] They performed three successive cleavage and bond-forming reactions with high yield and chemoselectivity, and they demonstrated the feasibility of post-assembly chemical modification of DNA nanostructures, as well as their potential use as locally addressable solid supports. Furthermore, they gave a different perspective to the face-up/face-down discussion by finding that in their case almost all of the constructs had the chemical modifications pointing towards the solution, thus keeping the question raised by Niemeyer and co-workers[115] open to debate.

Several methods exist for the detection of single-nucleotide polymorphism (SNPs),[123] as these differences are the major basis for phenotypic individuality and genetic variation. The ability of DNA nanotechnology to detect SNP unimolecularly is straightforward, as probes for the polymorphism can be placed over the origami sequence with full control of the location of each probe. Seeman and co-workers employed the effectiveness of kinetic methods based on branch migration[124] to detect single molecule polymorphisms by AFM over an origami surface (Figure 6 A).[113b] However, these methodologies are still far from feasible as diagnostics, as they require AFM, which is neither quick to use nor affordable for many labs. In addition, DNA microarrays are extensively used for the same purpose, with good efficiency and simpler manipulation. The application of the DNA origami platform for detecting SNPs needs to be simplified and cost-reduced to be implemented as a diagnostic system.

An interesting application of DNA nanotechnology involves extension of the study of kinetics and conformational changes to different types of molecules. The kinetics of the formation

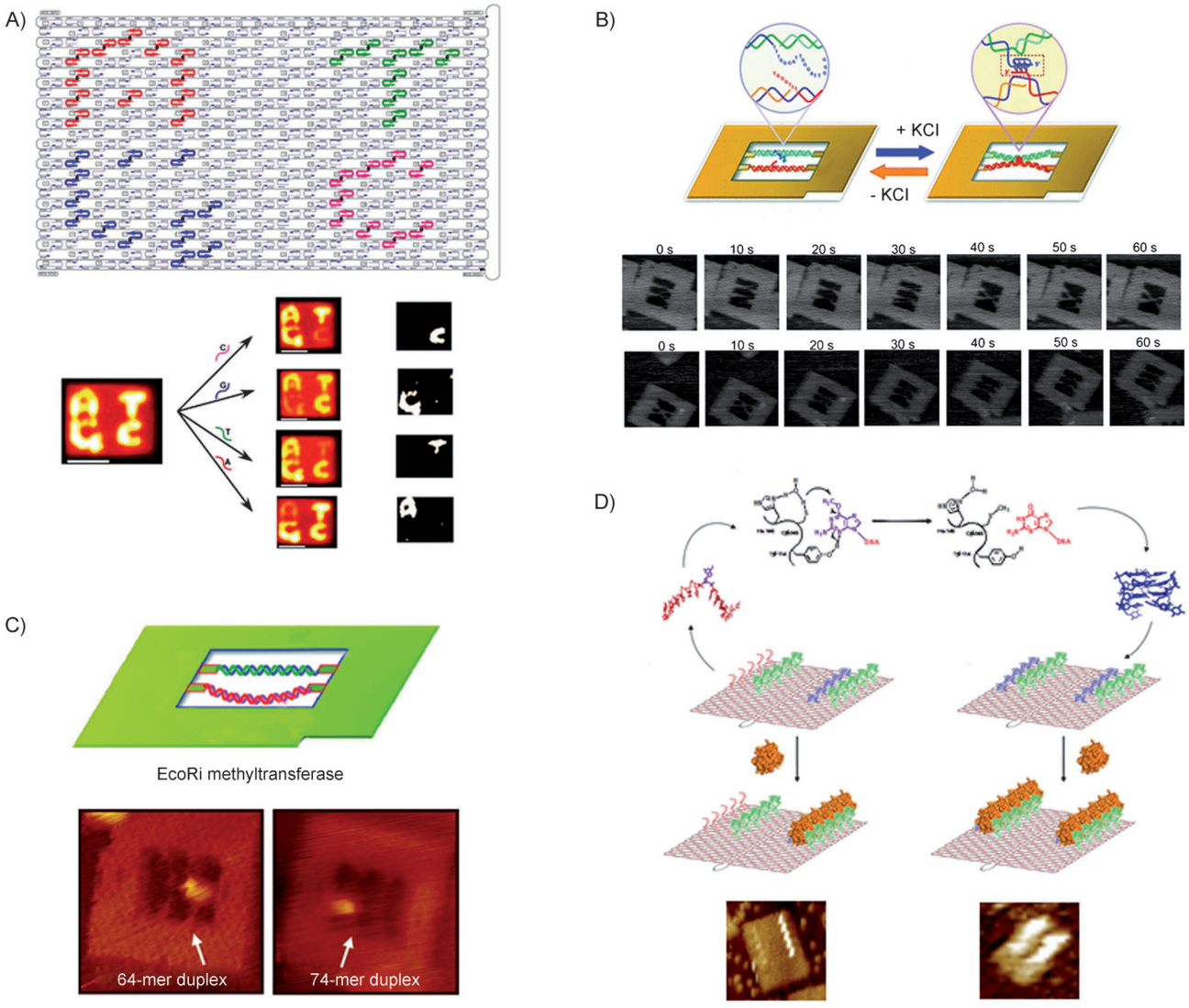

Figure 6. Study of different single-molecule reactions by the DNA origami approach. A) Detection of single nucleotide polymorphisms "SNPs"; by AFM over an origami surface. Adapted with permission from ref. [113b]. Copyright 2011, American Chemistry Society. B) Detection of the formation of G-quadruplexes in G-rich DNA sequences on a frame-like DNA origami. Adapted with permission from ref. [126]. Copyright 2010 American Chemistry Society. C) Methyl transfer reaction of EcoRI methyltransferase and analysis of the structural effect of this methylation by using a frame-like DNA origami. Adapted with permission from ref. [130]. Copyright 2010, American Chemistry Society. D) Nanosensor to analyze DNA repair activity of hAGT by α-thrombin interaction with methylated DNA aptamers, substrates of the protein. Reprinted with permission from ref. [133]. Copyright 2013, Wiley.

of a duplex DNA structure can be monitored on an origami tile—studying in real time the binding and unbinding events and estimating association/dissociation rates. As well as static analysis, dynamic processes in the sub-second range can be investigated on an origami platform in real time, and the results are comparable with those obtained by traditional methods to detect ensemble events.[125] In addition, conformational changes of biomolecules can also be analyzed with this platform. A novel method to detect the formation of G-quadruplexes in G-rich DNA sequences was developed by Sugiyama's group.[126] G-quadruplexes are four-stranded structures formed by the square arrangement of a tetrad of guanines, stabilized by the formation of Hoogsteen bonds.[127] They are promising anticancer agents, as they inhibit telomerase.[128] A DNA origami frame structure was designed: two sets of connection sites were introduced for the hybridization of duplex DNA. Each duplex contained a single strand rich in guanines in the upper and lower region in the presence of K^+ it changed its conformation to a G-quadruplex. This event was visualized by AFM in real time (Figure 6B).

The secondary DNA binding site of human topoisomerase I was identified by using an origami construct designed by Knudsen and co-workers.[129] A bait DNA protrusion was attached to the rectangular DNA nanoarray, by a 21-nucleotide extension of one of the staple strands. The secondary interaction of topoisomerase was discovered by adding either TopoIB–DNA complex (T_1 mode) or by stepwise addition of the TopoIB and cleavage complex (T_2 mode), and by monitoring the process by AFM. These results led to the conclusion that topoisomerase can bind positively and negatively supercoiled DNA. However, this should be confirmed by other methods, as this was the first time that a second binding site for topoisomerase was identified.

The study of the mechanism of enzymatic reactions in real time is crucial for understanding their biological functions, and great advances in DNA nanotechnology could help. Numerous publications have described the detection of enzymatic activity by DNA origami, and most of the studied enzymes have biomedical implications. Regulation of DNA methylation by using different tensions of double strands was studied and monitored by AFM by Sugiyama and co-workers.[130] They introduced two different double-helical tensions (tense and relaxed) into an origami frame, to control the methyl transfer reaction of EcoRI methyltransferase and examine the structural effect of this methylation (Figure 6C).[130] A further development was a versatile nanochip for direct analysis of DNA base-excision repair by 8-oxoguanine glycosylase and T4 pyrimidine dimer glycosylase.[131] The exact positioning and displacement of the enzymes in the reaction were monitored and analyzed. By using the same origami model, Suzuki et al.[132] developed a method for the visualization of Cre-mediated site-specific recombination events. Controlling the orientation and topology of the loxP substrate in a DNA frame nanoscaffold the process was regulated, thus influencing the synapsis and the outcome of the reaction. These systems could be extended to the direct observation of various enzymatic phenomena in designed nanoscale spaces, even though currently the methodology is only useful for DNA-related mechanisms.

Another study of DNA methylation was conducted in our lab:[133] the use of the DNA origami as a nanosensor to analyze the DNA repair activity of human O^6-methylguanine alkyltransferase (hAGT) by α-thrombin interaction with methylated DNA aptamers, substrates of the hAGT. This DNA repair enzyme is a cancer prognosis indicator. Inhibition of hAGT can enhance the efficiency of chemotherapeutic treatment. Previously, we demonstrated that introduction of a methyl group into any of the guanine tetrads of TBA destabilizes the G-quadruplex formed by this G-rich sequence, thus preventing thrombin from recognizing/binding to it.[134] The introduction of several methylated TBAs at specific positions of the origami allowed us to observe the loss of thrombin binding. When the O^6-methylguanine of the modified TBA was repaired by hAGT, α-thrombin was able to bind to the aptamers, as they could form the quadruplex structure required for the interaction (Figure 6D). This detection of the DNA repair activity of hAGT in an origami could be further developed to design hAGT activity assays for the identification of potential inhibitors as chemotherapy enhancers.

Accurate quantitative determination of microRNA was performed on a DNA origami motif. Zhu et al. developed a method for detecting single-strand displacement based on the interaction of streptavidin and quantum dots, measured by AFM in a linear and direct way.[135] This methodology has advantages over fluorescence signal detection: it is simple, time- and material-saving, potentially multitarget in one unique motif, and accurate enough for certain impure samples, as the signals are directly counted by AFM.

All these studies assumed that immobilization of biomolecules on a 2D platform does not affect their activity. By using fluorescence-based assays, Tinnefeld demonstrated that DNA origami does not influence the function of biomolecules (by comparison with data obtained in solution), and confirmed that DNA origami is a biocompatible surface.[136]

2.2.3. Carriers for delivery: In previous sections, we mostly reviewed applications of 2D DNA origami, as one of the most relevant features is precise positioning control on the planar surface. In contrast, many origami platforms developed as carriers for drug delivery have employed 3D nanostructures.

Many reports have described preliminary results pointing to the use of DNA origami as nanocarriers for cellular delivery. An important consideration is stability of these nanostructures under physiological conditions (maintenance of folding): DNA double helical domains and the connecting cross-overs should remain intact for the correct performance. Dietz's group reported that DNA origami objects built with a average staple length and cross-over density can be safely incubated at 37 °C (typical for cell-culture application).[73] They also proved that these nanoconstructs are stable in cell-culture medium (DMEM), and in Tris buffer with BSA or salted dextran (crowding agents), and at low pH. Furthermore, they tested stability in the presence of different nucleases, and found that their scaffolds were stable against T7 exonuclease, *E. coli* exonuclease, Lambda nuclease, and *Micrococcus* MseI restriction exo-

nuclease. However, they were degraded by DNAseI and T7 endonuclease, although they were more stable to DNAseI than double stranded DNA (degraded after 1 hour instead of 5 min at 37 °C). In addition, Mei et al. demonstrated that DNA origami are stable in cell lysate; this allows them to be easily separated from lysate mixtures, unlike natural single- and double-stranded DNA.[137] These findings illustrate the potential of DNA origami in cellular applications, and overcome some of the main problems that other delivery systems suffer.

Visualization of the intracellular location and stability of DNA origami with a label-free fluorescent probe was performed successfully by Shen et al.[138] They reported a strategy to study the distribution and stability of DNA origami nanostructures in living cellular systems, by using carbazole-based biscyanine as a probe. After 12 h incubation, most DNA origami nanostructures were localized in lysosome. After 60 h, most were disassembled or unfolded. Their results provide important information for the development of DNA origami as a biocompatible drug delivery vehicle, with the potential to accomplish controlled release.

Kjem, Gothelf and co-workers designed an origami box with a controllable lid; opening and closing was demonstrated by FRET experiments (Figure 7A).[56] Programmable access to the interior of the box could yield several interesting applications, for example the controlled release of nanocargos. A further development of this is the logic-gated DNA nanopill that was designed by Douglas et al. for the selective delivery of molecular payloads to the cell.[139] These nanopills are capable of inducing a great variety of responses in cell behavior. The biologically active payloads can be bound indirectly by antibody fragments, thus enabling applications in which the nanorobot is able to stimulate signals for activation and inhibition tasks before target delivery (Figure 7B).

Another cutting-edge cellular application of DNA origami was the design of DNA-based channel that can introduce pores into the cell's lipid membrane (Figure 7C). Single-mole-

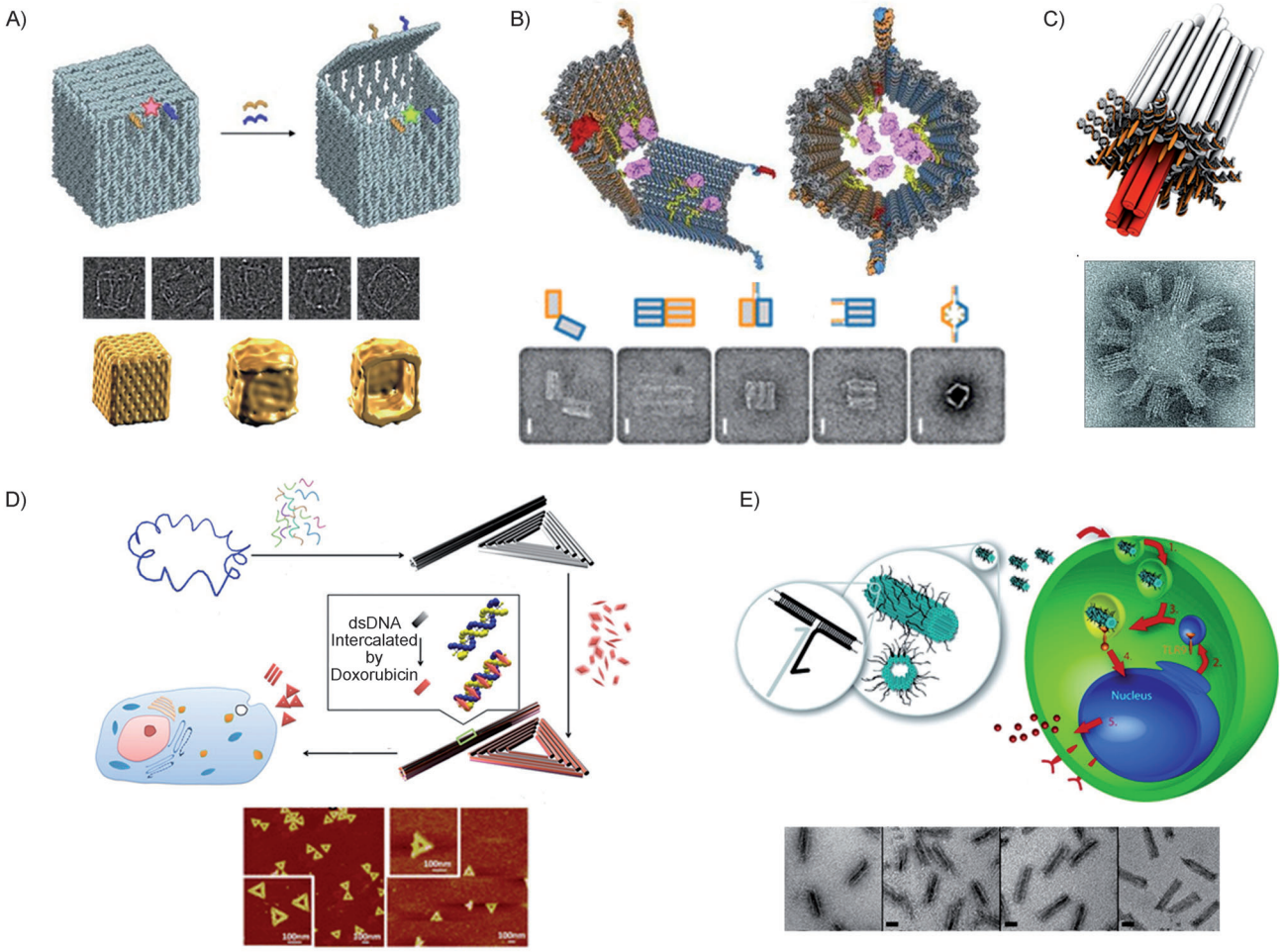

Figure 7. 3D origami structures (and AFM or TEM images) for cellular delivery. A) DNA box with a controllable lid (potential drug carrier). Reprinted with permission from ref. [56]. Copyright 2009 Nature Publishing Group. B) Logic-gated DNA nanopill for selective delivery of molecular payloads. Reprinted with permission from ref. [139]. Copyright 2012, American Association for the Advancement of Science. C) DNA-origami based channel to punch pores into the cell membrane, with ability to discriminate single DNA molecules. Reprinted with permission from ref. [141]. Copyright 2012, American Association for the Advancement of Science. D) DNA origami as a carrier for circumvention of doxorubicin resistance. Adapted with permission from ref. [142]. Copyright 2012 American Chemistry Society. E) Incorporation of CpG oligonucleotides into a DNA origami for the induction of strong immune responses. Adapted with permission from ref. [143]. Copyright 2011, American Chemistry Society.

cule translocation experiments showed that the synthetic DNA channels can be used to discriminate single DNA molecules.[140]

DNA origami has also been used as a carrier to circumvent drug resistance.[141] Doxorubicin (a well-known anticancer drug) was attached to a DNA origami by intercalation, thereby achieving high efficiency of drug loading when the nanostructures were administered. As a result, the cellular internalization of doxorubicin was increased, thus contributing significantly to enhance the cell-killing effect in doxorubicin-resistant MCF-7 cells (Figure 7D). In addition, Högberg developed two DNA origami structures with precise degrees of global twist to deliver doxorubicin in three different breast cancer cell lines.[142] They were able to regulate encapsulation efficiency and the drug release kinetics by tuning the nanostructure. With the aid of these DNA tiles, the cytotoxicity of doxorubicin was increased as the intracellular elimination rate was decreased, as compared to free drug. These results suggest that DNA origami has immense potential as an efficient and biocompatible drug delivery vehicle, although how exactly the origami nanostructures deliver the anticancer drugs remains unclear.

As mentioned above, many functional nucleic acids (including aptamers, antisense oligonucleotides, short interference RNA, and microRNA) have high diagnostic and therapeutic potential. As the carrier and the cargo are essentially the same type of molecule, the loading process can be simplified: nucleic acid hybridization or integration of the required sequence into the carrier. However, it is necessary to take architectural issues into account when designing the nanostructure, to avoid undesired interactions (between the cargo and the carrier) that could reduce the efficacy of the delivery process. The incorporation of cytosine-phosphate-guanosine (CpG) oligonucleotides to a DNA origami tube represents a good examination of this. Schüller et al.[143] tested the immune responses induced by hollow 30-helix DNA origami tubes covered with up to 62 CpG sequences in freshly isolated spleen cells (Figure 7E). The DNA constructs showed no detectable toxicity (in contrast to lipofectamine) and did not affect the viability of the splenocytes, but triggered a strong immune response, characterized by cytokine production and immune cell activation. Given that DNA oligonucleotides can be easily modified to incorporate a wide variety of biomolecules, this approach could be extended to combinations with viral moieties to generate vaccines and enhancers designed with nanometer precision and high biocompatibility.

2.2.4. DNA nanomachines and nanodevices: In addition to the static DNA origami structures, continuous advances in DNA nanotechnology have made possible the construction dynamic nanosystems that combine walkers, cargo, tracks and drive mechanisms to achieve complex motion on 2D or 3D surfaces. These DNA nanomachines and nanodevices are promising for biological applications.

Several nanomachines have been reported, such as a system that integrates a spider-like molecular walker with ability to move along a 2D substrate track assembled on a DNA origami array.[104b] DNA transporters that moved along a designed track were constructed on a DNA origami device, and the multistep motion of the motor strand was traced by AFM and TEM.[104a,144] Reck-Peterson and co-workers built a programmable synthetic cargo by using 3D DNA origami to which different DNA oligonucleotide-linked motors were attached, thereby allowing control of motor type, number, spacing, and orientation.[145] This cargo system was useful to determine and characterize the motile behavior of microtubule-based motor ensembles, depending on polarity of orientation. The behavior was found to be similar to that observed in vivo. Further development of these nanoconstructs might result in bidirectional powerful transport nanodevices to investigate the motile properties of motors and the mechanisms of motor regulation.

A DNA origami nanomachine with the potential for in vivo biosensing and intelligent delivery of biological activators was produced by Firrao's group.[146] This 3D DNA nanodevice performed its function in response to an external signal: in the presence of a small amount (picomols) of its target DNA, the robot moved a flap, thereby exposing its cargo DNA and self-assembly of the latter into a stable DNAzyme.

A versatile sensing system for the detection of a variety of chemical and biological targets at molecular resolution was designed by Kuyuza et al.[147] Their sensing methodology was based on a nanomechanical device formed by two DNA origami levers connected by a fulcrum, and was used to visually detect (by AFM) the biomolecule and its shape. All of the described mechanical detection mechanisms are suitable for targets of interest and can be used orthogonally with differently shaped origami devices in the same mixture on a single platform.

A development of previous work concerning material organization and single-molecule reactions[94,95,117] was conducted by Fan and co-workers.[148] They designed DNA nanostructures with unprecedented properties as nanoscale bioreactors, to study enzyme activities and cascades in highly organized and crowded cell-mimicking environments. These artificial systems were developed in a reliable and single-step strategy with high speed and cooperativity.

A different type of biological application was addressed by Lin et al.[149] They designed sub-micrometre nanorods that act as fluorescent barcodes and produce up to 216 barcodes that can be decoded unambiguously by using epifluorescence or total internal reflection fluorescence microscopy. The potential applications of this novel approach are of great variety: they could be used to improve tagging techniques, to develop a set of versatile imaging tools for single-molecule biological reactions and for biomedical diagnostics. They could also be modified with diverse biomolecules, such as monoclonal antibodies for immunophenotyping applications, or they could be used for in situ labeling of multiple cell types. By following the same approach, Yin and co-workers developed a multiplexed 3D cellular super-resolution technique for imaging, by using DNA origami to obtain multiplexed images for studying complex biomolecular systems in cell cultures.[150]

Upon refinement of their features and performance, these dynamic nanodevices could be further developed for many different biological and biomedical applications because of their predictable biophysical and biomechanical behavior and interaction with the cellular environment.

Outlook and Prospects

The biological applications reviewed here are just a starting point to show the potential of DNA nanotechnology for biomedical applications. Since the establishment of structural DNA nanotechnology as a field of research, scientists from different disciplines have been working together to develop numerous innovations over more than three decades. It has advanced from static scaffolds to dynamic functional devices that include other synthetic and natural materials. It has been applied for a variety of purposes from nanoelectronics, nanophotonics, and nanorobotics to more biological implementations, which could evolve into diagnostic and therapeutic tools.

However, some current difficulties must be addressed for the application of nanotechnology for biomedical purposes. Yield and scale-up of complex constructs remain a challenge; apparently, both are inversely related to the complexity and density of the desired structures. Deeper investigation into the kinetics and thermodynamics of annealing and assembly might come up with solutions to increase the stability and yield of the nanodevices and thus enable better prospects for in vivo application. Methods to expand the dimensions of the constructs should be addressed, as well as to increase the rate of encapsulation of biomolecules and inorganic material for delivery, and to broaden the diagnostic and therapeutic possibilities. The performance of single-molecule analytical techniques requires improvement of spatial resolution and timescale, and additional methodologies will be required for a better understanding of unimolecular processes, and the application to diagnostics.

A number of previously unfulfilled goals have been achieved, thus leading to successful progress of DNA nanotechnology. On this basis, we believe that further development of these techniques holds great potential for biological applications, hopefully with highly programmable and controllable capabilities in the very near future.

Acknowledgements

The Communities FUNMOL, "Fondo de Investigaciones Sanitarias" (grant PI06/1250) and by "Ministerio Ciencia e Innovación" (grant CTQ-2010-20541-C03-03) are acknowledged for financial support. C.F is grateful to Generalitat de Catalunya and Instituto de Salud Carlos III for a SNS Miguel Servet contract. M.T. was supported by a pre-doctoral fellowships from MINECO.

Keywords: biosensors · DNA nanotechnology · DNA origami · DNA structures · DNA tiles · nanostructures

[1] J. D. Watson, F. H. Crick, *Nature* **1953**, *171*, 737 – 738.
[2] a) F. Sanger, G. M. Air, B. G. Barrell, N. L. Brown, A. R. Coulson, C. A. Fiddes, C. A. Hutchison, P. M. Slocombe, M. Smith, *Nature* **1977**, *265*, 687 – 695; b) K. B. Mullis, F. A. Faloona, *Methods Enzymol.* **1987**, *155*, 335 – 350; c) F. W. Studier, *Proc. Natl. Acad. Sci. USA* **1989**, *86*, 6917 – 6921; d) A. Martin-Gallardo, W. R. McCombie, J. D. Gocayne, M. G. FitzGerald, S. Wallace, B. M. B. Lee, J. Lamerdin, S. Trapp, J. M. Kelley, L.-I. Liu, M. Dubnick, L. A. Johnston-Dow, A. R. Kerlavage, P. de Jong, A. Carrano, C. Fields, J. C. Venter, *Nat. Genet.* **1992**, *1*, 34 – 39; e) X. C. Huang, M. A. Quesada, R. A. Mathies, *Anal. Chem.* **1992**, *64*, 2149 – 2154.
[3] L. M. Demers, C. A. Mirkin, R. C. Mucic, R. A. Reynolds III, R. L. Letsinger, R. Elghanian, G. Viswanadham, *Anal. Chem.* **2000**, *72*, 5535 – 5541.
[4] J. Fu, M. Liu, Y. Liu, H. Yan, *Acc. Chem. Res.* **2012**, *45*, 1215 – 1226.
[5] N. C. Seeman, *J. Theor. Biol.* **1982**, *99*, 237 – 247.
[6] E. Winfree, F. Liu, L. A. Wenzler, N. C. Seeman, *Nature* **1998**, *394*, 539 – 544.
[7] J. H. Chen, N. C. Seeman, *Nature* **1991**, *350*, 631 – 633.
[8] Y. Zhang, N. C. Seeman, *J. Am. Chem. Soc.* **1994**, *116*, 1661 – 1669.
[9] P. W. K. Rothemund, *Nature* **2006**, *440*, 297 – 302.
[10] N. C. Seeman, *J. Biomol. Struct. Dyn.* **1990**, *8*, 573 – 581.
[11] a) U. Feldkamp, R. Wacker, H. Schroeder, W. Banzhaf, C. M. Niemeyer, *ChemPhysChem* **2004**, *5*, 367 – 372; b) U. Feldkamp, H. Rauhe, W. Banzhaf, *Genet. Program. Evolvable Machines* **2003**, *4*, 153 – 171.
[12] A. Brenneman, A. Condon, *Theor. Comput. Sci.* **2002**, *287*, 39 – 58.
[13] N. C. Seeman, H. Wang, X. Yang, F. Liu, C. Mao, W. Sun, L. Wenzler, Z. Shen, R. Sha, H. Yan, M. H. Wong, P. Sa-Ardyen, B. Liu, H. Qiu, X. Li, J. Qi, S. M. Du, Y. Zhang, J. E. Mueller, T.-J. Fu, Y. Wang, J. Chen, *Nanotechnology* **1998**, *9*, 257.
[14] N. C. Seeman, *Annu. Rev. Biophys. Biomol. Struct.* **1998**, *27*, 225 – 248.
[15] W. M. Shih, J. D. Quispe, G. F. Joyce, *Nature* **2004**, *427*, 618 – 621.
[16] Y. Wang, J. E. Mueller, B. Kemper, N. C. Seeman, *Biochemistry* **1991**, *30*, 5667 – 5674.
[17] a) Y. Li, Y. D. Tseng, S. Y. Kwon, L. d'Espaux, J. S. Bunch, P. L. McEuen, D. Luo, *Nat. Mater.* **2004**, *3*, 38 – 42; b) Y. Li, Y. T. H. Cu, D. Luo, *Nat. Biotechnol.* **2005**, *23*, 885 – 889.
[18] N. C. Seeman, Y. Zhang, J. Chen, *J. Vac. Sci. Technol. A* **1994**, *12*, 1895.
[19] a) J. Malo, J. C. Mitchell, C. Vénien-Bryan, J. R. Harris, H. Wille, D. J. Sherratt, A. J. Turberfield, *Angew. Chem. Int. Ed.* **2005**, *44*, 3057 – 3061; *Angew. Chem.* **2005**, *117*, 3117 – 3121; b) C. Mao, W. Sun, N. C. Seeman, *J. Am. Chem. Soc.* **1999**, *121*, 5437 – 5443.
[20] Y. He, Y. Tian, Y. Chen, Z. Deng, A. E. Ribbe, C. Mao, *Angew. Chem. Int. Ed.* **2005**, *44*, 6694 – 6696; *Angew. Chem.* **2005**, *117*, 6852 – 6854.
[21] a) H. Yan, S. H. Park, G. Finkelstein, J. H. Reif, T. H. LaBean, *Science* **2003**, *301*, 1882 – 1884; b) S. H. Park, P. Yin, Y. Liu, J. H. Reif, T. H. LaBean, H. Yan, *Nano Lett.* **2005**, *5*, 729 – 733.
[22] S. H. Park, C. Pistol, S. J. Ahn, J. H. Reif, A. R. Lebeck, C. Dwyer, T. H. LaBean, *Angew. Chem.* **2006**, *118*, 749 – 753; *Angew. Chem. Int. Ed.* **2006**, *45*, 735 – 739.
[23] D. Liu, M. Wang, Z. Deng, R. Walulu, C. Mao, *J. Am. Chem. Soc.* **2004**, *126*, 2324 – 2325.
[24] T. J. Fu, N. C. Seeman, *Biochemistry* **1993**, *32*, 3211 – 3220.
[25] S. Rinker, Y. Liu, H. Yan, *Chem. Commun.* **2006**, 2675 – 2677.
[26] T. H. LaBean, H. Yan, J. Kopatsch, F. Liu, E. Winfree, J. H. Reif, N. C. Seeman, *J. Am. Chem. Soc.* **2000**, *122*, 1848 – 1860.
[27] D. Liu, S. H. Park, J. H. Reif, T. H. LaBean, *Proc. Natl. Acad. Sci. USA* **2004**, *101*, 717 – 722.
[28] a) B. Ding, R. Sha, N. C. Seeman, *J. Am. Chem. Soc.* **2004**, *126*, 10230 – 10231; b) N. Chelyapov, Y. Brun, M. Gopalkrishnan, D. Reishus, B. Shaw, L. Adleman, *J. Am. Chem. Soc.* **2004**, *126*, 13924 – 13925.
[29] Y. He, Y. Chen, H. Liu, A. E. Ribbe, C. Mao, *J. Am. Chem. Soc.* **2005**, *127*, 12202 – 12203.
[30] Y. He, Y. Tian, A. E. Ribbe, C. Mao, *J. Am. Chem. Soc.* **2006**, *128*, 15978 – 15979.
[31] Z. Shen, H. Yan, T. Wang, N. C. Seeman, *J. Am. Chem. Soc.* **2004**, *126*, 1666 – 1674.
[32] H. Yan, X. Zhang, Z. Shen, N. C. Seeman, *Nature* **2002**, *415*, 62 – 65.
[33] a) K. V. Gothelf, T. H. LaBean, *Org. Biomol. Chem.* **2005**, *3*, 4023 – 4037; b) N. C. Seeman, *Methods Mol. Biol.* **2005**, *303*, 143 – 166; c) N. C. Seeman, *Trends Biochem. Sci.* **2005**, *30*, 119 – 125; d) U. Feldkamp, C. M. Niemeyer, *Angew. Chem. Int. Ed.* **2006**, *45*, 1856 – 1876; *Angew. Chem.* **2006**, *118*, 1888 – 1910; e) C. Lin, Y. Liu, S. Rinker, H. Yan, *ChemPhysChem* **2006**, *7*, 1641 – 1647.
[34] N. C. Seeman, *Curr. Opin. Struct. Biol.* **1996**, *6*, 519 – 526.
[35] Y. Zhang, N. C. Seeman, *J. Am. Chem. Soc.* **1994**, *116*, 1661 – 1669.
[36] P. J. Paukstelis, J. Nowakowski, J. J. Birktoft, N. C. Seeman, *Chem. Biol.* **2004**, *11*, 1119 – 1126.
[37] N. C. Seeman, *DNA Cell Biol.* **1991**, *10*, 475 – 486.
[38] X. Zhang, H. Yan, Z. Shen, N. C. Seeman, *J. Am. Chem. Soc.* **2002**, *124*, 12940 – 12941.

[39] R. P. Goodman, R. M. Berry, A. J. Turberfield, *Chem. Commun.* **2004**, 1372 – 1373.
[40] R. P. Goodman, I. A. T. Schaap, C. F. Tardin, C. M. Erben, R. M. Berry, C. F. Schmidt, A. J. Turberfield, *Science* **2005**, *310*, 1661 – 1665.
[41] R. P. Goodman, M. Heilemann, S. Doose, C. M. Erben, A. N. Kapanidis, A. J. Turberfield, *Nat. Nanotechnol.* **2008**, *3*, 93 – 96.
[42] F. F. Andersen, B. Knudsen, C. L. P. Oliveira, R. F. Frøhlich, D. Krüger, J. Bungert, M. Agbandje-McKenna, R. McKenna, S. Juul, C. Veigaard, J. Koch, J. L. Rubinstein, B. Guldbrandtsen, M. S. Hede, G. Karlsson, A. H. Andersen, J. S. Pedersen, B. R. Knudsen, *Nucleic Acids Res.* **2008**, *36*, 1113 – 1119.
[43] a) C. M. Erben, R. P. Goodman, A. J. Turberfield, *J. Am. Chem. Soc.* **2007**, *129*, 6992 – 6993; b) C. Zhang, M. Su, Y. He, Y. Leng, A. E. Ribbe, G. Wang, W. Jiang, C. Mao, *Chem. Commun.* **2010**, *46*, 6792 – 6794.
[44] F. A. Aldaye, H. F. Sleiman, *J. Am. Chem. Soc.* **2007**, *129*, 13376 – 13377.
[45] Y. He, T. Ye, M. Su, C. Zhang, A. E. Ribbe, W. Jiang, C. Mao, *Nature* **2008**, *452*, 198 – 201.
[46] C. Zhang, M. Su, Y. He, X. Zhao, P.-a. Fang, A. E. Ribbe, W. Jiang, C. Mao, *Proc. Natl. Acad. Sci. USA* **2008**, *105*, 10665 – 10669.
[47] C. Zhang, S. H. Ko, M. Su, Y. Leng, A. E. Ribbe, W. Jiang, C. Mao, *J. Am. Chem. Soc.* **2009**, *131*, 1413 – 1415.
[48] J. Zimmermann, M. P. J. Cebulla, S. Mönninghoff, G. von Kiedrowski, *Angew. Chem. Int. Ed.* **2008**, *47*, 3626 – 3630; *Angew. Chem.* **2008**, *120*, 3682 – 3686.
[49] J. W. Lough, W. I. Wainer, *Chirality in Natural and Applied Science*, CRC, Oxford, **2002**.
[50] *Chiral Drugs* (Ed.: C. A. Challener), Willey, Hampshire, **2001**.
[51] J. Rebek, Jr., *Angew. Chem. Int. Ed.* **2005**, *44*, 2068 – 2078; *Angew. Chem.* **2005**, *117*, 2104 – 2115.
[52] *Methods in Molecular Biology: Vol. 243: Chiral Separations: Methods and Protocols* (Eds.: G. Gübitz, M. G. Schmid), Human, Totowa, **2004**.
[53] J. C. Mitchell, J. R. Harris, J. Malo, J. Bath, A. J. Turberfield, *J. Am. Chem. Soc.* **2004**, *126*, 16342 – 16343.
[54] Y. He, M. Su, P.-a. Fang, C. Zhang, A. E. Ribbe, W. Jiang, C. Mao, *Angew. Chem. Int. Ed.* **2010**, *49*, 748 – 751; *Angew. Chem.* **2010**, *122*, 760 – 763.
[55] T. Liedl, B. Högberg, J. Tytell, D. E. Ingber, W. M. Shih, *Nat. Nanotechnol.* **2010**, *5*, 520 – 524.
[56] E. S. Andersen, M. Dong, M. M. Nielsen, K. Jahn, R. Subramani, W. Mamdouh, M. M. Golas, B. Sander, H. Stark, C. L. P. Oliveira, J. S. Pedersen, V. Birkedal, F. Besenbacher, K. V. Gothelf, J. Kjems, *Nature* **2009**, *459*, 73 – 76.
[57] A. Kuzuya, M. Komiyama, *Chem. Commun.* **2009**, 4182 – 4184.
[58] Y. Ke, J. Sharma, M. Liu, K. Jahn, Y. Liu, H. Yan, *Nano Lett.* **2009**, *9*, 2445 – 2447.
[59] a) S. M. Douglas, H. Dietz, T. Liedl, B. Hogberg, F. Graf, W. M. Shih, *Nature* **2009**, *459*, 414 – 418; b) Y. Ke, S. M. Douglas, M. Liu, J. Sharma, A. Cheng, A. Leung, Y. Liu, W. M. Shih, H. Yan, *J. Am. Chem. Soc.* **2009**, *131*, 15903 – 15908; c) Y. Ke, N. V. Voigt, K. V. Gothelf, W. M. Shih, *J. Am. Chem. Soc.* **2012**, *134*, 1770 – 1774.
[60] H. Dietz, S. M. Douglas, W. M. Shih, *Science* **2009**, *325*, 725 – 730.
[61] D. Han, S. Pal, J. Nangreave, Z. Deng, Y. Liu, H. Yan, *Science* **2011**, *332*, 342 – 346.
[62] D. Han, S. Pal, Y. Liu, H. Yan, *Nat. Nanotechnol.* **2010**, *5*, 712 – 717.
[63] a) K. Fujibayashi, R. Hariadi, S. H. Park, E. Winfree, S. Murata, *Nano Lett.* **2008**, *8*, 1791 – 1797; b) R. D. Barish, R. Schulman, P. W. K. Rothemund, E. Winfree, *Proc. Natl. Acad. Sci. USA* **2009**, *106*, 6054 – 6059.
[64] a) Z. Li, M. Liu, L. Wang, J. Nangreave, H. Yan, Y. Liu, *J. Am. Chem. Soc.* **2010**, *132*, 13545 – 13552; b) A. Rajendran, M. Endo, Y. Katsuda, K. Hidaka, H. Sugiyama, *ACS Nano* **2011**, *5*, 665 – 671.
[65] W. Liu, H. Zhong, R. Wang, N. C. Seeman, *Angew. Chem. Int. Ed.* **2011**, *50*, 264 – 267; *Angew. Chem.* **2011**, *123*, 278 – 281.
[66] Z. Zhao, H. Yan, Y. Liu, *Angew. Chem. Int. Ed.* **2010**, *49*, 1414 – 1417; *Angew. Chem.* **2010**, *122*, 1456 – 1459.
[67] E. Pound, J. R. Ashton, H. A. Becerril, A. T. Woolley, *Nano Lett.* **2009**, *9*, 4302 – 4305.
[68] B. Högberg, T. Liedl, W. M. Shih, *J. Am. Chem. Soc.* **2009**, *131*, 9154 – 9155.
[69] T. Tørring, N. V. Voigt, J. Nangreave, H. Yan, K. V. Gothelf, *Chem. Soc. Rev.* **2011**, *40*, 5636 – 5646.
[70] M. Endo, S. Yamamoto, K. Tatsumi, T. Emura, K. Hidaka, H. Sugiyama, *Chem. Commun.* **2013**, *49*, 2879 – 2881.
[71] a) E. S. Andersen, A. Lind-Thomsen, B. Knudsen, S. E. Kristensen, J. H. Havgaard, E. Torarinsson, N. Larsen, C. Zwieb, P. Sestoft, J. Kjems, J. Gorodkin, *RNA* **2007**, *13*, 1850 – 1859; b) E. S. Andersen, M. Dong, M. M. Nielsen, K. Jahn, A. Lind-Thomsen, W. Mamdouh, K. V. Gothelf, F. Besenbacher, J. Kjems, *ACS Nano* **2008**, *2*, 1213 – 1218.
[72] S. M. Douglas, A. H. Marblestone, S. Teerapittayanon, A. Vazquez, G. M. Church, W. M. Shih, *Nucleic Acids Res.* **2009**, *37*, 5001 – 5006.
[73] C. E. Castro, F. Kilchherr, D.-N. Kim, E. L. Shiao, T. Wauer, P. Wortmann, M. Bathe, H. Dietz, *Nat. Methods* **2011**, *8*, 221 – 229.
[74] a) C. Mao, T. H. LaBean, J. H. Relf, N. C. Seeman, *Nature* **2000**, *407*, 493 – 496; b) G. Seelig, D. Soloveichik, D. Y. Zhang, E. Winfree, *Science* **2006**, *314*, 1585 – 1588; c) L. Qian, E. Winfree, *Science* **2011**, *332*, 1196 – 1201.
[75] C. A. Mirkin, R. L. Letsinger, R. C. Mucic, J. J. Storhoff, *Nature* **1996**, *382*, 607 – 609.
[76] A. P. Alivisatos, K. P. Johnsson, X. Peng, T. E. Wilson, C. J. Loweth, M. P. Bruchez, Jr., P. G. Schultz, *Nature* **1996**, *382*, 609 – 611.
[77] a) S. Xiao, F. Liu, A. E. Rosen, J. F. Hainfeld, N. C. Seeman, K. Musier-Forsyth, R. A. Kiehl, *J. Nanopart. Res.* **2002**, *4*, 313 – 317; b) J. D. Le, Y. Pinto, N. C. Seeman, K. Musier-Forsyth, T. A. Taton, R. A. Kiehl, *Nano Lett.* **2004**, *4*, 2343 – 2347; c) Z. Deng, Y. Tian, S.-H. Lee, A. E. Ribbe, C. Mao, *Angew. Chem. Int. Ed.* **2005**, *44*, 3582 – 3585; *Angew. Chem.* **2005**, *117*, 3648 – 3651; d) J. Sharma, R. Chhabra, Y. Liu, Y. Ke, H. Yan, *Angew. Chem. Int. Ed.* **2006**, *45*, 730 – 735; *Angew. Chem.* **2006**, *118*, 744 – 749; e) F. A. Aldaye, H. F. Sleiman, *J. Am. Chem. Soc.* **2007**, *129*, 4130 – 4131; f) A. J. Mastroianni, S. A. Claridge, A. P. Alivisatos, *J. Am. Chem. Soc.* **2009**, *131*, 8455 – 8459.
[78] a) Y. Y. Pinto, J. D. Le, N. C. Seeman, K. Musier-Forsyth, T. A. Taton, R. A. Kiehl, *Nano Lett.* **2005**, *5*, 2399 – 2402; b) J. Zheng, P. E. Constantinou, C. Micheel, A. P. Alivisatos, R. A. Kiehl, N. C. Seeman, *Nano Lett.* **2006**, *6*, 1502 – 1504.
[79] H. Li, S. H. Park, J. H. Reif, T. H. LaBean, H. Yan, *J. Am. Chem. Soc.* **2004**, *126*, 418 – 419.
[80] S. Y. Park, A. K. R. Lytton-Jean, B. Lee, S. Weigand, G. C. Schatz, C. A. Mirkin, *Nature* **2008**, *451*, 553 – 556.
[81] D. Nykypanchuk, M. M. Maye, D. van der Lelie, O. Gang, *Nature* **2008**, *451*, 549 – 552.
[82] C. M. Niemeyer, *Trends Biotechnol.* **2002**, *20*, 395 – 401.
[83] C. M. Niemeyer, M. Adler, S. Gao, L. Chi, *Bioconjugate Chem.* **2001**, *12*, 364 – 371.
[84] a) Y. Liu, C. Lin, H. Li, H. Yan, *Angew. Chem. Int. Ed.* **2005**, *44*, 4333 – 4338; *Angew. Chem.* **2005**, *117*, 4407 – 4412; b) A. S. Walsh, H. Yin, C. M. Erben, M. J. A. Wood, A. J. Turberfield, *ACS Nano* **2011**, *5*, 5427 – 5432.
[85] a) C. Lin, E. Katilius, Y. Liu, J. Zhang, H. Yan, *Angew. Chem. Int. Ed.* **2006**, *45*, 5296 – 5301; *Angew. Chem.* **2006**, *118*, 5422 – 5427; b) B. A. R. Williams, K. Lund, Y. Liu, H. Yan, J. C. Chaput, *Angew. Chem. Int. Ed.* **2007**, *46*, 3051 – 3054; *Angew. Chem.* **2007**, *119*, 3111 – 3114; c) C. Zhou, Z. Yang, D. Liu, *J. Am. Chem. Soc.* **2012**, *134*, 1416 – 1418.
[86] S. Modi, M. G. Swetha, D. Goswami, G. D. Gupta, S. Mayor, Y. Krishnan, *Nat. Nanotechnol.* **2009**, *4*, 325 – 330.
[87] M. S. Shchepinov, I. A. Udalova, A. J. Bridgman, E. M. Southern, *Nucleic Acids Res.* **1997**, *25*, 4447 – 4454.
[88] a) M. Scheffler, A. Dorenbeck, S. Jordan, M. Wüstefeld, G. von Kiedrowski, *Angew. Chem. Int. Ed.* **1999**, *38*, 3311 – 3315; *Angew. Chem.* **1999**, *111*, 3513 – 3518; b) J. S. Choi, C. W. Kang, K. Jung, J. W. Yang, Y.-G. Kim, H. Han, *J. Am. Chem. Soc.* **2004**, *126*, 8606 – 8607.
[89] a) K. M. Stewart, L. W. McLaughlin, *J. Am. Chem. Soc.* **2004**, *126*, 2050 – 2057; b) K. M. Stewart, J. Rojo, L. W. McLaughlin, *Angew. Chem. Int. Ed.* **2004**, *43*, 5808 – 5811; *Angew. Chem.* **2004**, *116*, 5932 – 5935.
[90] a) S. M. Waybright, C. P. Singleton, K. Wachter, C. J. Murphy, U. H. F. Bunz, *J. Am. Chem. Soc.* **2001**, *123*, 1828 – 1833; b) K. M. Stewart, L. W. McLaughlin, *Chem. Commun.* **2003**, 2934 – 2935; c) J. Sharma, Y. Ke, C. Lin, R. Chhabra, Q. Wang, J. Nangreave, Y. Liu, H. Yan, *Angew. Chem. Int. Ed.* **2008**, *47*, 5157 – 5159; *Angew. Chem.* **2008**, *120*, 5235 – 5237.
[91] a) T. Maier, S. Jenni, N. Ban, *Science* **2006**, *311*, 1258 – 1262; b) D. N. Dhanasekaran, K. Kashef, C. M. Lee, H. Xu, E. P. Reddy, *Oncogene* **2007**, *26*, 3185 – 3202; c) S. Raboni, S. Bettati, A. Mozzarelli, *Cell. Mol. Life Sci.* **2009**, *66*, 2391 – 2403.
[92] F. C. Simmel, *Curr. Opin. Biotechnol.* **2012**, *23*, 516 – 521.
[93] C. M. Niemeyer, J. Koehler, C. Wuerdemann, *ChemBioChem* **2002**, *3*, 242 – 245.

[94] J. Müller, C. M. Niemeyer, *Biochem. Biophys. Res. Commun.* **2008**, *377*, 62 – 67.
[95] O. I. Wilner, Y. Weizmann, R. Gill, O. Lioubashevski, R. Freeman, I. Willner, *Nat. Nanotechnol.* **2009**, *4*, 249 – 254.
[96] L. Xin, C. Zhou, Z. Yang, D. Liu, *Small* **2013**, *9*, 3088 – 3091.
[97] C. J. Delebecque, A. B. Lindner, P. A. Silver, F. A. Aldaye, *Science* **2011**, *333*, 470 – 474.
[98] a) S. Ko, H. Liu, Y. Chen, C. Mao, *Biomacromolecules* **2008**, *9*, 3039 – 3043; b) J. Li, H. Pei, B. Zhu, L. Liang, M. Wei, Y. He, N. Chen, D. Li, Q. Huang, C. Fan, *ACS Nano* **2011**, *5*, 8783 – 8789; c) G. D. Hamblin, K. M. M Carneiro, J. F. Fakhoury, K. E. Bujold, H. F. Sleiman, *J. Am. Chem. Soc.* **2012**, *134*, 2888 – 2891.
[99] a) J.-W. Keum, J.-H. Ahn, H. Bermudez, *Small* **2011**, *7*, 3529 – 3535; b) M. Chang, C.-S. Yang, D.-M. Huang, *ACS Nano* **2011**, *5*, 6156 – 6163; c) H. Lee, A. K. R. Lytton-Jean, Y. Chen, K. T. Love, A. I. Park, E. D. Karagiannis, A. Sehgal, W. Querbes, C. S. Zurenko, M. Jayaraman, C. G. Peng, K. Charisse, A. Borodovsky, M. Manoharan, J. S. Donahoe, J. Truelove, M. Nahrendorf, R. Langer, D. G. Anderson, *Nat. Nanotechnol.* **2012**, *7*, 389 – 393.
[100] a) C. M. Erben, R. P. Goodman, A. J. Turberfield, *Angew. Chem. Int. Ed.* **2006**, *45*, 7414 – 7417; *Angew. Chem.* **2006**, *118*, 7574 – 7577; b) D. Bhatia, S. Mehtab, R. Krishnan, S. S. Indi, A. Basu, Y. Krishnan, *Angew. Chem. Int. Ed.* **2009**, *48*, 4134 – 4137; *Angew. Chem.* **2009**, *121*, 4198 – 4201.
[101] A. J. M. Wollman, C. Sanchez-Cano, H. M. J. Carstairs, R. A. Cross, A. J. Turberfield, *Nat. Nanotechnol.* **2014**, *9*, 44 – 47.
[102] J.-W. Keum, H. Bermudez, *Chem. Commun.* **2009**, 7036 – 7038.
[103] a) S. Helmig, A. Rotaru, D. Arian, L. Kovbasyuk, J. Arnbjerg, P. R. Ogilby, J. Kjems, A. Mokhir, F. Besenbacher, K. V. Gothelf, *ACS Nano* **2010**, *4*, 7475 – 7480; b) B. Ding, Z. Deng, H. Yan, S. Cabrini, R. N. Zuckermann, J. Bokor, *J. Am. Chem. Soc.* **2010**, *132*, 3248 – 3249; c) S. Pal, Z. Deng, B. Ding, H. Yan, Y. Liu, *Angew. Chem. Int. Ed.* **2010**, *49*, 2700 – 2704; *Angew. Chem.* **2010**, *122*, 2760 – 2764; d) P. K. Dutta, R. Varghese, J. Nangreave, S. Lin, H. Yan, Y. Liu, *J. Am. Chem. Soc.* **2011**, *133*, 11985 – 11993; e) R. Schreiber, J. Do, E.-M. Roller, T. Zhang, V. J. Schüller, P. C. Nickels, J. Feldmann, T. Liedl, *Nat. Nanotechnol.* **2014**, *9*, 74 – 78.
[104] a) H. Gu, J. Chao, S. J. Xiao, N. C. Seeman, *Nature* **2010**, *465*, 202 – 205; b) K. Lund, A. J. Manzo, N. Dabby, N. Michelotti, A. Johnson-Buck, J. Nangreave, S. Taylor, R. Pei, M. N. Stojanovic, N. G. Walter, E. Winfree, H. Yan, *Nature* **2010**, *465*, 206 – 210.
[105] a) J. Liu, Y. Geng, E. Pound, S. Gyawali, J. R. Ashton, J. Hickey, A. T. Woolley, J. N. Harb, *ACS Nano* **2011**, *5*, 2240 – 2247; b) R. J. Kershner, L. D. Bozano, C. M. Micheel, A. M. Hung, A. R. Fornof, J. N. Cha, C. T. Rettner, M. Bersani, J. Frommer, P. W. K. Rothemund, G. M. Wallraff, *Nat. Nanotechnol.* **2009**, *4*, 557 – 561.
[106] J. Sharma, R. Chhabra, C. S. Andersen, K. V. Gothelf, H. Yan, Y. Liu, *J. Am. Chem. Soc.* **2008**, *130*, 7820 – 7821.
[107] B. Ding, H. Wu, W. Xu, Z. Zhao, Y. Liu, H. Yu, H. Yan, *Nano Lett.* **2010**, *10*, 5065 – 5069.
[108] S. Pal, R. Varghese, Z. Deng, Z. Zhao, A. Kumar, H. Yan, Y. Liu, *Angew. Chem. Int. Ed.* **2011**, *50*, 4176 – 4179; *Angew. Chem.* **2011**, *123*, 4262 – 4265.
[109] H. T. Maune, S.-p. Han, R. D. Barish, M. Bockrath, W. A. Goddard III, P. W. K. Rothemund, E. Winfree, *Nat. Nanotechnol.* **2010**, *5*, 61 – 66.
[110] I. H. Stein, C. Steinhauer, P. Tinnefeld, *J. Am. Chem. Soc.* **2011**, *133*, 4193 – 4195.
[111] a) J. Nangreave, D. Han, Y. Liu, H. Yan, *Curr. Opin. Chem. Biol.* **2010**, *14*, 608 – 615; b) A. Rajendran, M. Endo, H. Sugiyama, *Angew. Chem. Int. Ed.* **2012**, *51*, 874 – 890; *Angew. Chem.* **2012**, *124*, 898 – 915; c) N. Michelotti, A. Johnson -Buck, A. J. Manzo, N. G. Walter, *Wiley Interdiscip. Rev. Nanomed. Nanobiotechnol.* **2012**, 4, 139 – 152; d) G. Zhang, S. P. Surwade, F. Zhou, H. Liu, *Chem. Soc. Rev.* **2013**, *42*, 2488 – 2496.
[112] A. Kuzuya, M. Komiyama, *Nanoscale* **2010**, *2*, 310 – 322.
[113] a) Y. Ke, S. Lindsay, Y. Chang, Y. Liu, H. Yan, *Science* **2008**, *319*, 180 – 183; b) H. K. K. Subramanian, B. Chakraborty, R. Sha, N. C. Seeman, *Nano Lett.* **2011**, *11*, 910 – 913.
[114] Z. Zhang, Y. Wang, C. Fan, C. Li, Y. Li, L. Qian, Y. Fu, Y. Shi, J. Hu, L. He, *Adv. Mater.* **2010**, *22*, 2672 – 2675.
[115] B. Saccà, R. Meyer, M. Erkelenz, K. Kiko, A. Arndt, H. Schroeder, K. S. Rabe, C. M. Niemeyer, *Angew. Chem. Int. Ed.* **2010**, *49*, 9378 – 9383; *Angew. Chem.* **2010**, *122*, 9568 – 9573.
[116] S. Rinker, Y. Ke, Y. Liu, R. Chhabra, H. Yan, *Nat. Nanotechnol.* **2008**, *3*, 418 – 422.
[117] J. Fu, M. Liu, Y. Liu, N. W. Woodbury, H. Yan, *J. Am. Chem. Soc.* **2012**, *134*, 5516 – 5519.
[118] a) W. Shen, H. Zhong, D. Neff, M. L. Norton, *J. Am. Chem. Soc.* **2009**, *131*, 6660 – 6661; b) R. P. Goodman, C. M. Erben, J. Malo, W. M. Ho, M. L. McKee, A. N. Kapanidis, A. J. Turberfield, *ChemBioChem* **2009**, *10*, 1551 – 1557.
[119] A. Kuzuya, M. Kimura, K. Numajiri, N. Koshi, T. Ohnishi, F. Okada, M. Komiyama, *ChemBioChem* **2009**, *10*, 1811 – 1815.
[120] A. Kuzuya, N. Koshi, M. Kimura, K. Numajiri, T. Yamazaki, T. Ohnishi, F. Okada, M. Komiyama, *Small* **2010**, *6*, 2664 – 2667.
[121] a) E. Nakata, F. F. Liew, C. Uwatoko, S. Kiyonaka, Y. Mori, Y. Katsuda, M. Endo, H. Sugiyama, T. Morii, *Angew. Chem. Int. Ed.* **2012**, *51*, 2421 – 2424; *Angew. Chem.* **2012**, *124*, 2471 – 2474; b) T. A. Ngo, E. Nakata, M. Saimura, T. Kodaki, T. Morii, *Methods* **2014**, *67*, 142 – 150.
[122] N. V. Voigt, T. Tørring, A. Rotaru, M. F. Jacobsen, J. B. Ravnsbæk, R. Subramani, W. Mamdouh, J. Kjems, A. Mokhir, F. Besenbacher, K. V. Gothelf, *Nat. Nanotechnol.* **2010**, *5*, 200 – 203.
[123] I. C. Gray, D. A. Campbell, N. K. Spurr, *Hum. Mol. Genet.* **2000**, *9*, 2403 – 2408.
[124] I. G. Panyutin, P. Hsieh, *Proc. Natl. Acad. Sci. USA* **1994**, *91*, 2021 – 2025.
[125] R. Jungmann, C. Steinhauer, M. Scheible, A. Kuzyk, P. Tinnefeld, F. C. Simmel, *Nano Lett.* **2010**, *10*, 4756 – 4761.
[126] Y. Sannohe, M. Endo, Y. Katsuda, K. Hidaka, H. Sugiyama, *J. Am. Chem. Soc.* **2010**, *132*, 16311 – 16313.
[127] a) I. Smirnov, R. H. Shafer, *Biochemistry* **2000**, *39*, 1462 – 1468; b) B. I. Kankia, L. A. Marky, *J. Am. Chem. Soc.* **2001**, *123*, 10799 – 10804; c) A. Avino, C. Fabrega, M. Tintore, R. Eritja, *Curr. Pharm. Des.* **2012**, *18*, 2036 – 2047.
[128] a) J.-L. Mergny, C. Hélène, *Nat. Med.* **1998**, *4*, 1366 – 1367; b) S. Neidle, G. Parkinson, *Nat. Rev. Drug Discovery* **2002**, *1*, 383 – 393; c) L. H. Hurley, *Nat. Rev. Cancer* **2002**, *2*, 188 – 200.
[129] R. Subramani, S. Juul, A. Rotaru, F. F. Andersen, K. V. Gothelf, W. Mamdouh, F. Besenbacher, M. Dong, B. R. Knudsen, *ACS Nano* **2010**, *4*, 5969 – 5977.
[130] M. Endo, Y. Katsuda, K. Hidaka, H. Sugiyama, *J. Am. Chem. Soc.* **2010**, *132*, 1592 – 1597.
[131] M. Endo, Y. Katsuda, K. Hidaka, H. Sugiyama, *Angew. Chem. Int. Ed.* **2010**, *49*, 9412 – 9416; *Angew. Chem.* **2010**, *122*, 9602 – 9606.
[132] Y. Suzuki, M. Endo, Y. Katsuda, K. Ou, K. Hidaka, H. Sugiyama, *J. Am. Chem. Soc.* **2014**, *136*, 211 – 218.
[133] M. Tintoré, I. Gállego, B. Manning, R. Eritja, C. Fàbrega, *Angew. Chem.* **2013**, *125*, 7901 – 7904; *Angew. Chem. Int. Ed.* **2013**, *52*, 7747 – 7750.
[134] M. Tintore, A. Aviñó, F. M. Ruiz, R. Eritja, C. Fàbrega, *J. Nucleic Acids* **2010**, *2010*, 632041.
[135] J. Zhu, X. Feng, J. Lou, W. Li, S. Li, H. Zhu, L. Yang, A. Zhang, L. He, C. Li, *PloS One* **2013**, *8*, e69856.
[136] A. Gietl, P. Holzmeister, D. Grohmann, P. Tinnefeld, *Nucleic Acids Res.* **2012**, *40*, e110.
[137] Q. Mei, X. Wei, F. Su, Y. Liu, C. Youngbull, R. Johnson, S. Lindsay, H. Yan, D. Meldrum, *Nano Lett.* **2011**, *11*, 1477 – 1482.
[138] X. Shen, Q. Jiang, J. Wang, L. Dai, G. Zou, Z.-G. Wang, W.-Q. Chen, W. Jiang, B. Ding, *Chem. Commun.* **2012**, *48*, 11301 – 11303.
[139] S. M. Douglas, I. Bachelet, G. M. Church, *Science* **2012**, *335*, 831 – 834.
[140] M. Langecker, V. Arnaut, T. G. Martin, J. List, S. Renner, M. Mayer, H. Dietz, F. C. Simmel, *Science* **2012**, *338*, 932 – 936.
[141] Q. Jiang, C. Song, J. Nangreave, X. Liu, L. Lin, D. Qiu, Z.-G. Wang, G. Zou, X. Liang, H. Yan, B. Ding, *J. Am. Chem. Soc.* **2012**, *134*, 13396 – 13403.
[142] Y.-X. Zhao, A. Shaw, X. Zeng, E. Benson, A. M. Nyström, B. Högberg, *ACS Nano* **2012**, *6*, 8684 – 8691.
[143] V. J. Schüller, S. Heidegger, N. Sandholzer, P. C. Nickels, N. A. Suhartha, S. Endres, C. Bourquin, T. Liedl, *ACS Nano* **2011**, *5*, 9696 – 9702.
[144] S. F. J. Wickham, M. Endo, Y. Katsuda, K. Hidaka, J. Bath, H. Sugiyama, A. J. Turberfield, *Nat. Nanotechnol.* **2011**, *6*, 166 – 169.
[145] N. D. Derr, B. S. Goodman, R. Jungmann, A. E. Leschziner, W. M. Shih, S. L. Reck-Peterson, *Science* **2012**, *338*, 662 – 665.
[146] E. Torelli, M. Marini, S. Palmano, L. Piantanida, C. Polano, A. Scarpellini, M. Lazzarino, G. Firrao, *Small* **2014**; DOI: 10.1002/smll.201400245.

[147] A. Kuzuya, Y. Sakai, T. Yamazaki, Y. Xu, M. Komiyama, *Nat. Commun.* **2011**, *2*, 449.
[148] Y. Fu, D. Zeng, J. Chao, Y. Jin, Z. Zhang, H. Liu, D. Li, H. Ma, Q. Huang, K. V. Gothelf, C. Fan, *J. Am. Chem. Soc.* **2013**, *135*, 696 – 702.
[149] C. Lin, R. Jungmann, A. M. Leifer, C. Li, D. Levner, G. M. Church, W. M. Shih, P. Yin, *Nat. Chem.* **2012**, *4*, 832 – 839.
[150] R. Jungmann, M. S. Avendano, J. B. Woehrstein, M. Dai, W. M. Shih, P. Yin, *Nat. Methods* **2014**, *11*, 313 – 318.

Received: February 6, 2014
Published online on June 20, 2014

Chapter 4

A fluorescence biosensor for hAGT activity.

A fluorescence biosensor for hAGT activity.

Maria Tintoré,[1] Santiago Grijalvo,[1] Ramon Eritja[1] and Carme Fàbrega[1]

In preparation.

[1] IQAC-CSIC, CIBER-BBN Networking Centre on Bioengineering Biomaterials and Nanomedicine. c/ Jordi Girona 18-26. 08034 Barcelona (Spain).

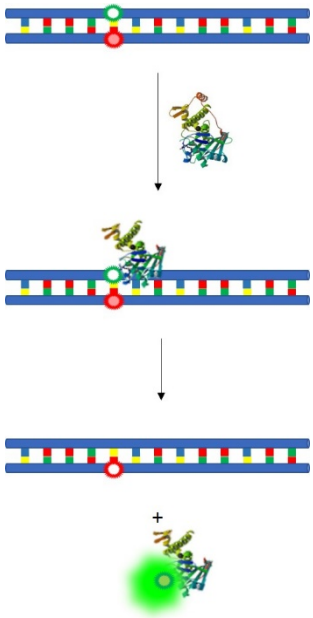

O^6-alkylguanine-DNA alkyltransferase (hAGT) activity provides resistance to cancer chemotherapeutic agents and its inhibition enhances chemotherapy. In chapter 4, we present the development of a novel fluorescence assay based on the fluorescence transfer from a duplex oligonucleotide containing a fluorophore-quencher pair to the active site of hAGT, for the detection of its DNA repair activity. For this purpose, we designed a double-stranded DNA sequence containing a fluorophore-quencher pair, where the fluorophore was attached to a synthetic 0^6-benzylguanine. This precursor was synthetized through a novel route which comprises the use of the Mitsunobu reaction for the introduction of the benzyl group into the O^6 position of the guanine. We performed HPLC studies of the repair of this benzylguanine by hAGT, to ensure that this bulky substituent can enter the active site of the protein. The repair activity of hAGT was detected by fluorescence transfer, producing an increase in intensity upon repair of the alkylguanine. This assay can be used for the evaluation of potential inhibitors of hAGT in a straightforward manner and avoiding radioactivity.

The compounds described in chapter 1 as possible candidates to inhibid hAGT activity were tested by this methodology and the preliminary results obtained are included as Appendix 4.

A fluorescence biosensor for hAGT activity.

M. Tintoré,[a,b] S.Grijalvo,[a,b] R.Eritja [*a,b] and C.Fàbrega [*a,b]

[a] Institute for Advanced Chemistry of Catalonia (IQAC), Spanish National Research Council (CSIC), C/ Jordi Girona 18-26, 08034 Barcelona, Spain; Tfn: +34 93 4006100. Fax: +34 93 2045904

e-mail: cgcnqb@cid.csic.es; recgma@cid.csic.es.

[b] Networking Center on Bioengineering, Biomaterials and Nanomedicine (CIBER-BBN).

Keywords: Biosensor, fluorescence, DNA repair, O^6-alkylguanine-DNA alkyltransferase, inhibition-activity

Abstract:

O^6-alkylguanine-DNA alkyltransferase (hAGT) activity provides resistance to cancer chemotherapeutic agents and its inhibition enhances chemotherapy. We herein present the development of a novel fluorescence assay based on a duplex oligonucleotide containing a fluorophore-quencher pair for the detection of the DNA repair activity of hAGT. This assay can be used for the evaluation of potential inhibitors of hAGT in a straightforward manner and avoiding radioactivity.

1. Introduction

Alkylating agents are chemotherapeutic anticancer drugs that produce their cytotoxic effect by generating adducts at multiple sites in DNA.[1] The most relevant adduct in terms of mutagenesis and carcinogenesis is the alkylation of the O^6 position of guanines.[2] In particular, the alkylating agent 1,3-bis-(2-chloroethyl)-1-nitrosourea (BCNU) initially attacks at the O^6 guanine position, causing its cross-link with the opposite cytosine, blocking DNA replication and producing G_2/M arrest.[3] In addition to the well-known side effects and limitations of chemotherapeutic agents, these substances also show acquired tumour resistance problems. The DNA-repair protein human O^6-alkylguanine DNA alkyltransferase(hAGT or MGMT) is responsible for removing alkyl adducts from the O^6 position of guanines, thereby blocking the cytotoxic effects of the alkylating agents and making a crucial contribution to the resistance mechanism.[4] It is well established that tumoral cells show greater expression of this protein, which explains their low sensitivity to chemotherapeutic drugs in a large number of cancers.[5] On the contrary, the promoter methylation of hAGT has been associated with patients' longer survival.[6] Therefore, pharmacological inhibition of hAGT has the potential to enhance the cytotoxicity of a diverse range of anticancer agents.[7]

hAGT is a DNA-binding protein that contains a highly conserved internal cysteine, which acts as the acceptor site for alkyl groups. It behaves like a suicidal non-enzyme, inactivating itself since the S-alkylcysteine formed is not regenerated.[8] For this reason, intense research effort has been devoted to the identification of small molecules capable of inhibiting hAGT activity and significantly enhancing the cytotoxic effect of BCNU in prostate, breast, colon and lung tumour cells.[7]

Given the potential relevance of hAGT as a prognostic marker of cancer and as a therapeutic target, several methods are available to characterize its activity. Moreover, they are also able to evaluate the capacity of small molecules for inhibiting hAGT. Most of these methods involve radioactivity assays, while others are based on multiple-step enzymatic reactions.[9] However, the first methods require the use of rigorous safety procedures and the others are discontinuous and time-consuming due to the necessity of multiple steps. Recently, two methods based on the conformational change of an intramolecular G-quadruplex were developed by our group.[10]

In this paper we describe the development of a one-step FRET assay which improves the efficiency of our previous methods because it increases the repair rate of hAGT by using double-stranded DNA, the natural substrate of the protein. In

addition, the detection of a fluorescence increase that is proportional to the repair rate of hAGT represents a low-cost, straightforward and rapid method.

For this purpose, we designed a double-stranded DNA sequence containing a fluorophore-quencher pair (Scheme 1). The fluorophore was post-synthetically and covalently attached to a modified O^6-benzylguanine (^{F}dG) and the quencher was introduced in a very close position of the complementary strand of the duplex (^{Q}dT-complementary or ^{Q}dT-missmatch), blocking the fluorescence. The fluorophore was transferred together with the benzyl group to hAGT's active site when the protein repaired the DNA, restoring the guanine. The removal of the fluorophore brought it apart from the quencher, producing a significant increase in fluorescence which allowed to measure the repair reaction of hAGT.

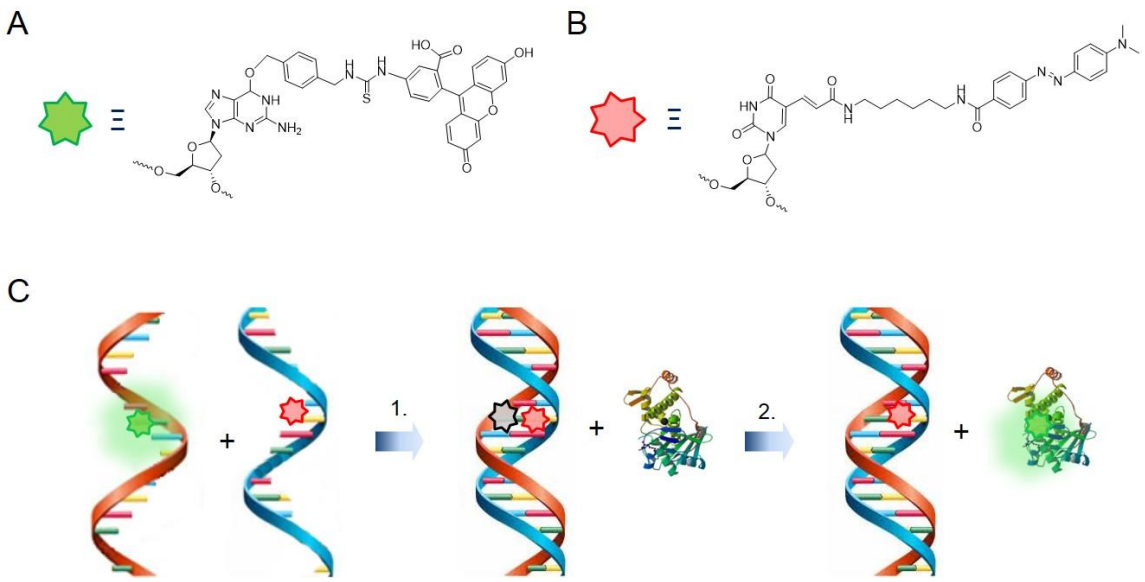

Scheme 1. A. Chemical structure of the O^6-benzylguanine with the fluorophore covalently attached to the alkyl group. **B.** Chemical structure of the quencher group (Dabcyl), covalently attached to a thymidine. **C.** Schematic representation of the fluorescence assay. 1). Annealing of the two strands containing a fluorophore and a quencher group, with the correspondent extinction of fluorescence. 2). hAGT repair activity over the benzylguanine, dragging the fluorescein group and significantly increasing fluorescence.

2. Results and Discussion

The ^{A}dG oligonucleotide was prepared using the appropriate modified guanosine phosphoramidite (**7**) in the automated DNA synthesizer using standard protocols[11]. Derivative **7** was prepared from 2'-deoxyguanosine and the protected 4- trifluoroacetyl-aminomethylbenzyl alcohol (**1**) (Scheme 2A). Its incorporation at the O^6 position of the

guanine was performed through a Mitsunobu reaction. The guanine amino function was protected with dimethylaminomethyliden protecting group. Finally, the protection and functionalization of the two hydroxyl groups were carried out under standard conditions.

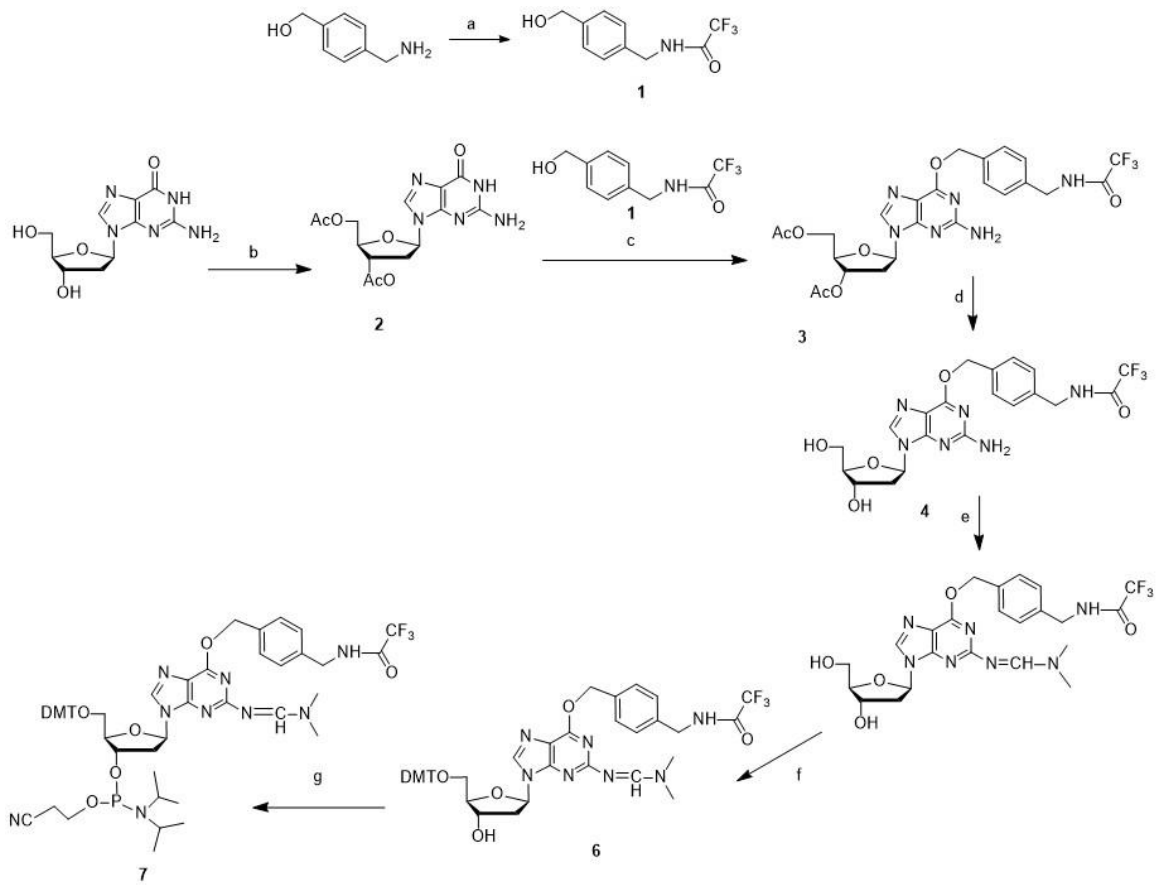

Scheme 2. A) Chemical synthesis of the O^6-benzyl-2'-deoxyguanosine phosphoramidite. a) TEA, EtTFA in DCM, 0ºC to r.t. o/n b) Ac_2O, DMAP, TEA in DMF, r.t. 4h; c) Compound 1, PPh_3, DEAD in Dioxane, r.t. o/n: d) MeOH:NH_3 (1:1), 55ºC 4h; e) $(CH_3O)_2CH\text{-}N(CH_3)_2$ in DMF; f) DMT-Cl, DIEA in Pyr, r.t. o/n; g) DIEA, $CNEOP(Cl)N(iPr)_2$ in DCM, r.t.

The benzylguanine-containing oligonucleotide and its complementary strands with a quencher group (dabcyl, Q) either at the complementary position or at one nucleotide shift were synthesized, purified by HPLC and characterised by MALDI-TOF (see Supplementary Data). Subsequently, the fluorescein label (F) was attached to the O^6- benzylguanosine amino group through a fluorescein isothiocyanate (FITC) reaction.[12] The DNA duplexes, one complementary and the other containing a mismatch due to the positioning of the T-quencher fosforamidite pairing with the modified ^{F}G, were prepared from the fluorophore-quencher pair of oligonucleotides under proper annealing conditions (Table 1). We explored to different positions of the quencher group in the complementary sequences to ensure the maximal quenching of fluorescence and to minimize steric effects and complementary discrepancies. In the first

duplex, the placement of the quencher in the complementary base of the modified guanosine provokes a mismatch in the sequence (G:T) instead of a (G:C) pair due to the fact that there is no commercially available cytidine covalently modified with the dabcyl group and the use of a thymidine was required. The second duplex contains the quencher group at one nucleotide shift with respect to the benzylguanine in the complementary sequence avoiding the introduction of a mismatch and expecting that the fluorescence extinction would remain efficient.

Name	Sequence
Oligo-^{F}dG: Complementary-^{Q}T	5'-ATC TTC TC ^{F}**G**ATT CA-3'
	3'-TAG AAG AGC^{Q}**T**AA GT-5'
Oligo-^{F}dG:Mismatch-^{Q}T	5'-ATC TTC TC ^{F}**G**ATT CA-3'
	3'-TAG AAC AG^{Q}**T**TAA GT-5'

Table 1. Sequences of the two different duplexes used in this work.

First, to see the possible effect of this two bulky groups in the duplex formation, their thermal stability was studied at 260 and 485 nm and compared to each other (see Table S2 at Supplementary Data, SD). In general, we observed destabilization of the duplex at 260 nm in the presence of the bulky substituent in the O^6 position of the central guanine, compared to the controls. However, both duplexes are stable at 30ºC. CD spectra of the two duplexes were recorded, showing that both structures formed a duplex at 25ºC (See Figure S1, SD). In order to be able to use these two duplexes in a fluorescence-quenching assay, we studied how the stability of the duplexes affects the emission of fluorescence by monitoring the emitted fluorescence at excitation wavelength of 485 nm (See Figure S2, SD). Significant differences in the melting temperature were observed due to the release effect of the quencher and a great increase in the fluorescent signal was detected. In the case of the mismatched sequence, this increase in fluorescence is produced at 26 ºC while in the fully complementary duplex, the quencher effect persisted until 53 ºC, allowing us to use it at the enzymatic temperature range for hAGT activity.

Efficient reaction with hAGT requires the ^{F}G modification to correctly accommodate in the active site. This brings the CH_2 which is attached at the O^6 position in closer proximity to the thyolated ion Cys145, making the reaction possible. For this reason, we performed a study on the hAGT dealkylation activity over the F-benzyl modified double-stranded substrates. The reaction was followed by HPLC. This study

was performed in the absence and presence of the quencher in the complementary strand.

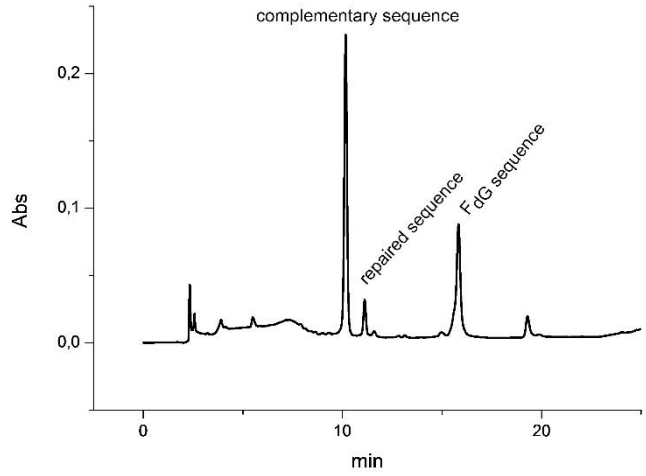

Figure 1. HPLC profile of the repair reaction of the ^{F}dG double stranded sequence in the absence of the quencher group in the complementary strand**.** The HPLC analysis was performed 37 ºC.

For this purpose, the full-length hAGT was over-expressed and purified as previously described.[10a, 13] Increasing concentrations of the protein were incubated with the double-stranded ^{F}dG sequence for 90 min at 30ºC and analyzed using HPLC. Figure 1 shows one of the HPLC profiles of the reaction's final products of hAGT at 37ºC. The appearance of a peak with a shorter retention time corresponds to the repaired sequence, formed by the removal of the F-benzyl group. Our results confirmed that hAGT has the capacity to accommodate bulky groups, including a fluorophore, in the active site without upsetting its repair activity.

We then tested the effectiveness of our proposed fluorescence method to evaluate the repair activity of hAGT. We performed the hAGT reaction using a 10 nM concentration of the fluorescently-dabcyl labelled duplex for 20 min, using different hAGT concentrations. We determined 10 nM to be the minimum amount of double-stranded DNA required to achieve a detectable and reliable difference in intensity compared to the background. As expected, the fluorophore-quencher pair gave low background fluorescence, because of the quenching effect produced by the proximity of these two groups in the base paired sequence. The presence of hAGT produced a remarkable increase in fluorescence intensity caused by the transfer of the F-benzyl group to its active site, throwing it apart from the quencher. The increase rate in fluorescence intensity correlated directly with the amount of hAGT in the reaction mixture (Figure 2). Moreover, the inactive mutant hAGT-C145S did not exhibit any decrease in fluorescence due to its inability to repair the alkylated DNA (see SD).

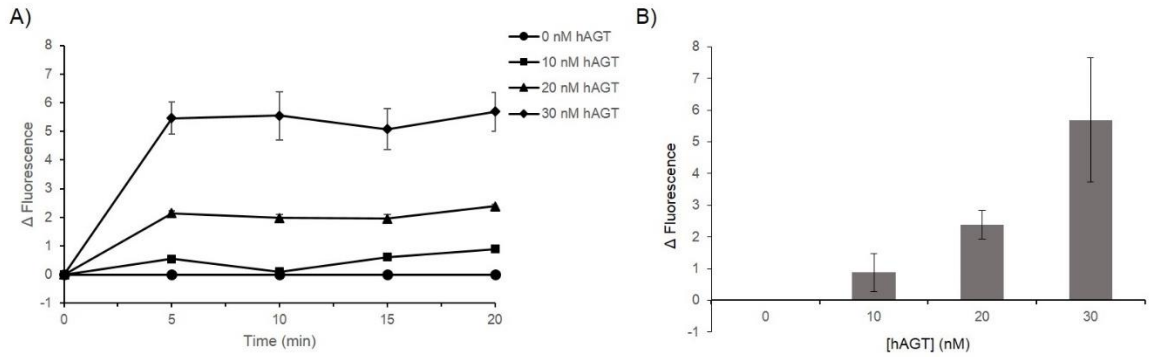

Figure 2. hAGT activity assay. A) Increase of fluorescence with respect to the background fluorescence of the oligonucleotide during 20 minutes. B) Total increase of fluorescence after 20 minutes of reaction with different concentrations of hAGT.

In view of all these observations, we corroborated that our initial hypothesis and design of the new FRET methodology is consistent.

3. Conclusions

In summary, we have described a novel route for the synthesis of a O^6-benzyl-2'-deoxyguanosine precursor which incorporated to an oligonucleotide sequence, can become a fluorescently labelled substrate for measuring hAGT repair activity. Annealing with a complementary quencher strand produces a duplex with low basal fluorescence.

Using this labelled oligonucleotide, we have developed a new assay for quantifying the DNA repair protein hAGT activity and identifying potential inhibitors as chemotherapy enhancers. The novelty of this method compared to existing ones is the single-step and real-time measurement of the reaction, representing a rapid and straightforward method that reduces cost, time and effort. In contrast with our previous developed methods to quantify hAGT activity,[10] this system uses a double-stranded oligonucleotide, which is the natural substrate for the hAGT activity, improving efficiency and reliability due to its easy quantification of the fluorescence increase upon activity. We believe that this new method will facilitate the search for new and more potent inhibitors which enhance the effect of chemotherapeutic drugs.

This methodology could be implemented for the study of hAGT dealkylation in cell culture and in animal models, through the transfection of fluorescent oligonucleotides and visualization of the increase in fluorescence using confocal microscopy. However, the thermal stability of the oligonucleotides should be improved to ensure their stability at physiological temperature. Work in this direction is currently underway.

Acknowledgements

The Communities MULTIFUN (contract NMP4-LA-2011-262943), “Fondo de InvestigacionesSanitarias” (grant PI06/1250) and by “MinisterioCiencia e Innovación” (grants CTQ-2010-20541-C03-03 and CTQ2014-52588-R) are acknowledged for financial support. M.T. was supported by a pre-doctoral fellowship (FPI) from MINECO. C.F is grateful to TV3 Marato 2012 for a research contract.

Experimental data:

Derivative **7** was prepared from 5´,3´-diaceyl-2’-deoxyguanosine and 4-aminomethylbenzyl alcohol (1.2 eq)**,** previously protected with a trifluoroacetyl group *via* a Mitsunobu reaction in the presence of diethyl azodicarboxylate (3 eq.) and triphenylphosphine (3 eq.). Then, the guanine amino function was protected with the dimethylaminomethyliden protecting group. Finally, the protection and functionalization of the two hydroxyl groups for the DNA synthesis were carried out under standard conditions. See SD for further information.

The oligonucleotide sequences were synthesized using standard protocols and purified by reversed-phase HPLC. The incorporation of the O^6-(N-4-((hydroxymethyl)benzyl)-trifluoroacetylmide)-2’-deoxyguanosinephosphoramidite (^{A}dG) in the sequence was carried out manually with a coupling time of 15 min, obtaining a yield of 75%. The length and homogeneity of the oligonucleotide were verified by MALDI-TOF (Table 1, SD). The 5’-ATCTTCTC^{A}GATTCA-3’ oligonucleotide was left to react post-synthetically with fluorescein isothiocyanate (FITC) through its free amino group. The coupling efficiency was determined by HPLC analysis. See SD for further details.

Melting curves of all the possible pairs of complementary oligonucleotides were measured by monitoring the absorbance hyperchromicity at 260 nm, heating the sample over the range 10-80 ºC. 4 µM of the duplexs in 10 mM sodium phosphate pH 7.0 and 100 mM NaCl. The CD spectra of all the possible pairs of complementary oligonucleotides were registered at 25ºC over a range of 220–320 nm using the same concentrations and buffer as for the melting temperature experiments. See SD for more detailed information.

HPLC proof of concept of the dealkylation of^{A}dG was performed by incubating the duplexes with FL hAGT 90 minutes at 30ºC and analyzing by HPLCon a Nucleosil analytical column at 37ºCwith a gradient of 10–40% acetonitrile in 20 min. See SD for more detailed information.

The fluorescence assay was performed incubating increasing concentrations of hAGT (50, 100 and 200 nM) with the fluorophore-quencher duplex substrate (10 nM). Fluorescence was measured during 20 min at excitation and emission wavelengths of 485 and 535 nm, respectively. Averages over three readings were taken for each condition tested. Each experiment was performed in triplicates.

All the experimental procedures are further detailedin the Supplementary Data.

References:

[1] M. R. Middleton, G. P. Margison, *Lancet Oncol* **2003**, *4*, 37-44.

[2] a) A. Sabharwal, M. R. Middleton, *Curr Opin Pharmacol* **2006**, *6*, 355-363; b) A. E. Pegg, B. Singer, *Cancer Invest* **1984**, *2*, 18; c) R. Saffhill, G. P. Margison, P. J. O'Connor, *Biochim Biophys Acta* **1985**, *823*, 111-145; d) B. Singer, *Cancer Res* **1986**, *46*, 4879-4885; e) K. A. Jaeckle, H. J. Eyre, J. J. Townsend, S. Schulman, H. M. Knudson, M. Belanich, D. B. Yarosh, S. I. Bearman, D. J. Giroux, S. C. Schold, *J Clin Oncol* **1998**, *16*, 3310-3315; f) M. Belanich, M. Pastor, T. Randall, D. Guerra, J. Kibitel, L. Alas, B. Li, M. Citron, P. Wasserman, A. White, H. Eyre, K. Jaeckle, S. Schulman, D. Rector, M. Prados, S. Coons, W. Shapiro, D. Yarosh, *Cancer Res* **1996**, *56*, 783-788; g) R. S. Foote, S. Mitra, B. C. Pal, *Biochem Biophys Res Commun* **1980**, *97*, 654-659; h) A. E. Pegg, *Cancer Res* **1990**, *50*, 6119-6129.

[3] a) W. P. Tong, M. C. Kirk, D. B. Ludlum, *Cancer Res* **1982**, *42*, 3102-3105; b) L. Yan, J. R. Donze, L. Liu, *Oncogene* **2005**, *24*, 2175-2183.

[4] a) T. P. Brent, P. J. Houghton, J. A. Houghton, *Proc. Natl. Acad. Sci.* **1985**, *82*, 2985-2989; b) G. Tagliabue, L. Citti, G. Massazza, G. Damia, R. Giavazzi, M. D'Incalci, *Anticancer Res.* **1992**, *12*, 2123-2125; c) R. Pepponi, G. Marra, M. P. Fuggetta, S. Falcinelli, E. Pagani, E. Bonmassar, J. Jiricny, S. D'Atri, *J. Pharmacol. Exp. Ther.* **2003**, *304*, 661-668.

[5] a) A. E. Pegg, *Mutat Res* **2000**, *462*, 83-100; b) S. L. Gerson, *J Clin Oncol* **2002**, *20*, 2388-2399; c) G. P. Margison, A. C. Povey, B. Kaina, M. F. Santibanez Koref, *Carcinogenesis* **2003**, *24*, 625-635.

[6] a) M. Esteller, J. Garcia-Foncillas, E. Andion, S. N. Goodman, O. F. Hidalgo, V. Vanaclocha, S. B. Baylin, J. G. Herman, *N Engl J Med* **2000**, *343*, 1350-1354; b) M. E. Hegi, A. C. Diserens, T. Gorlia, M. F. Hamou, N. de Tribolet, M. Weller, J. M. Kros, J. A. Hainfellner, W. Mason, L. Mariani, J. E. Bromberg, P. Hau, R. O. Mirimanoff, J. G. Cairncross, R. C. Janzer, R. Stupp, *N Engl J Med* **2005**, *352*, 997-1003; c) R. Tuominen, R. Jewell, J. J. van den Oord, P. Wolter, U. Stierner, C. Lindholm, C. Hertzman Johansson, D. Linden, H. Johansson, M. Frostvik Stolt, C. Walker, H. Snowden, J. Newton-Bishop, J. Hansson, S. Egyhazi Brage, *Int J Cancer* **2014**; d) X. Li, F. Hu, Y. Wang, X. Yao, Z. Zhang, F. Wang, G. Sun, B. B. Cui, X. Dong, Y. Zhao, *Biomed Res Int* **2014**, *2014*, 236361; e) J. M. Brandwein, J. Kassis, B. Leber, D. Hogge, K. Howson-Jan, M. D. Minden, A. Galarneau, J. F. Pouliot, *Br J Haematol* **2014**, *167*, 664-670.

[7] A. E. Pegg, K. Swenn, M. Y. Chae, M. E. Dolan, R. C. Moschel, *Biochem. Pharmacol.* **1995**, *50*, 1141-1148.

[8] a) K. S. Srivenugopal, X. H. Yuan, H. S. Friedman, F. Ali-Osman, *Biochemistry* **1996**, *35*, 1328-1334; b) M. Xu-Welliver, A. E. Pegg, *Carcinogenesis* **2002**, *23*, 823-830.

[9] a) B. D. Wilson, M. Strauss, B. J. Stickells, E. G. Hoal-van Helden, P. van Helden, *Carcinogenesis* **1994**, *15*, 2143-2148; b) M. E. Dolan, D. Scicchitano, A. E. Pegg, *Cancer Res* **1988**, *48*, 1184-1188; c) A. M. Moser, M. Patel, H. Yoo, F. M. Balis, M. E. Hawkins, *Anal Biochem* **2000**, *281*, 216-222; d) R. S. Wu, S. Hurst-Calderone, K. W. Kohn, *Cancer Res* **1987**, *47*, 6229-6235.

[10] a) M. Tintore, A. Avino, F. M. Ruiz, R. Eritja, C. Fabrega, *J Nucleic Acids* **2010**, *2010*; b) M. Tintore, I. Gallego, B. Manning, R. Eritja, C. Fabrega, *Angew Chem Int Ed Engl* **2013**, *52*, 7747-7750.

[11] C. B. Reese, *Org Biomol Chem* **2005**, *3*, 3851-3868.

[12] S. Perez-Rentero, N. Kielland, M. Terrazas, R. Lavilla, R. Eritja, *Bioconjug Chem* **2010**, *21*, 1622-1628.

[13] F. M. Ruiz, R. Gil-Redondo, A. Morreale, A. R. Ortiz, C. Fabrega, J. Bravo, *J Chem Inf Model* **2008**, *48*, 844-854.

Supplementary Data

A fluorescence biosensor for hAGT activity

M Tintoré,[a,b] S Grijalvo, [a,b] R Eritja[*a,b] and C Fàbrega[*a,b]

Table of contents:

1. Material and methods

1.1 Abbreviations:

Ac: acetyl, Ac_2O: acetic anhydride, ACN: acetonitrile, AcOEt: ethyl acetate, anh: anhydrous, Ar: aromatic, BCNU: bis-chloroethylnitrosourea, Bz: benzyl, Bzl: benzoyl, CPG: controlled pore glass, Dabcyl: dimethylamino-azobenzoic acid, DCM: dichloromethane, DEAD: diethyl azodicarboxylate, DIEA: *N,N*-diisopropylethylamine, DMAP: *N,N*-dimethylaminopyridine, DMF: *N,N*-dimethylformamide, dmf: dimethylaminomethylidene, DMT: 4,4'-dimethoxytrityl, DMT-Cl: 4,4'-dimethoxytrityl chloride, DMSO: dimethylsulfoxide, DTT: dithiothreitol, EtTFA: ethyl trifluoroacetate, F: fluorescein, ^{F}G: fluorescein-benzylguanosine, FITC: Fluorescein isothiocyanate, FRET: fluorescence resonance energy transfer, hAGT: human O^6-alkylguanine-DNA alkyltransferase, LCAA: long chain amino alkyl, MALDI: matrix-assisted laser disorption/ionization, MeOH: methanol, PPh_3: triphenylphosphine, Pyr: pyridine, ^{Q}T: (N-4'-carboxy-4-(dimethylamino)-azobenzene)-aminohexyl-3-acrylamido]-2'-deoxyuridine, RP-HPLC: reverse phase high pressure liquid chromatography, TCA: trichloroacetic acid, TEA: triethylamine, TEAA: triethylammonium acetate, THAP: trihydroxyacetophenone monohydrate, THF: tetrahydrofurane, TLC: thin-layer chromatography, TOF: time of flight, UV: ultraviolet.

1.2 Chemicals

Reagents for oligonucleotide synthesis including phosphoramidite monomers of dA^{Bzl}, dC^{Bzl}, dG^{dmf} and T, the 5'-deblocking solution (3% TCA in DCM), activator solution (0.4 M 1H-tetrazole in ACN), CAP A solution (Ac_2O /Pyr/THF), oxidizing solution (0.02 M iodine in THF/Pyr/water (7:2:1), supports and LCAA-CPG were purchased from Applied Biosystems (PEBiosystems Hispania S.A., Spain) and Link Technologies Ltd.(Scotland) and used as received. Sephadex G-25 (NAP-10) columns were purchased from GE Healtcare, USA. The 96-well Optical reaction plates were purchased to Nunc, USA. HiTrapTM FF column were purchased at GE Healthcare. FITC (isomer I) and the rest of chemicals were purchased from Aldrich, Sigma, or Fluka (Sigma-Aldrich Quimica S.A., Spain), and used without further purification. Anhydrous solvents and deuterated solvents ($CDCl_3$, CD_3OD and DMSO-d_6) were obtained from reputable sources and used as received. Thin-layer chromatography (TLC) was carried out on aluminium-backed Silica-Gel 60 F_{254} plates. Column chromatography was performed using Silica Gel (60 Å, 230 x 400 mesh).

1.3 Instrumentation

Oligonucleotide sequences were synthesized on an Applied Biosystems 3400 DNA Synthesizer (Applied Biosystems, USA). RP-HPLC purifications were performed on a Waters chromatography system using Nucleosil semi-preparative 120 C_{18} (250x4 mm) columns. Analytical RP-HPLC was performed using a XBridge OST C18 2.5 µm column and a Nucleosil Analytical column 120 C18 (250x4mm). Oligonucleotides were quantified by UV absorption at 260 nm with a Jasco V650 spectrophotometer. Mass spectra were recorded on a MALDI *Perseptive* Voyager DETM RP time-of-flight (TOF)

spectrometer (Applied Biosystems, USA) equipped with nitrogen laser at 337 nm using a 3ns pulse. The matrix used contained 2,4,6-trihydroxyacetophenone (THAP, 10 mg/mL in ACN/ water 1:1) and ammonium citrate (50 mg/mL in water). NMR spectra were measured on Varian Mercury-400. Chemical shifts are given in parts per million (ppm); *J* values are given in hertzs (Hz). All spectra were internally referenced to the appropriate residual undeuterated solvent.

UV analyses were performed using a Jasco V-650 instrument equipped with a thermoregulated cell holder. Set temperature was controlled with an 89090A Agilent Peltier device and Hellma quartz cuvettes were used (1000 µL volume). CD spectra were recorded on a CD on a JASCO spectropolarimeter J-810. Fluorometric measurements were performed on a spectrofluorometer Jasco FP6200 at 25ºC and with a Multi-Detection Microplate Reader SpectraMax M5 (Molecular devices BioNova cientifica, Sunnyvale, USA).

2. Chemical synthesis of the 6-benzyl-2'-deoxiguanosine phosphoramidite precursor

2.1. Preparation of N-(4-(hydroxymethyl)benzyl)-trifluoroacetamide (1)

4-aminomethylbenzylalcohol (500 mg, 2.89 mmol) was dissolved in 3 ml DCM. TEA (3.0 eq, 1.169 µl, 8.4 mmol) was added dropwise and kept under argon atmosphere. Afterwards, 400 µl (1.2 eq, 3.36 mmol) of EtTFA were added dropwise and the mixture was stirred in argon atmosphere at room temperature for 4 hr. The reaction was followed up by TLC (DCM:MeOH 5%). The reaction mixture dissolved in DCM and was washed with brine and the organic phase dried with $MgSO_4$. The organic phase was filtered and evaporated. The crude of the reaction was purified by chromatography (silica gel), eluted with a gradient of 0-5% MeOH in DCM. Yield (1, 500 mg, 76%). TLC R_f=0.36 (DCM:MeOH 95:5), MS (EI 70 eV) m/z calcd for $C_{10}H_{14}F_3N_2O_2$ ($M^+ + NH_4^+$) 251.1002 found 251.1002.

^{1}H-NMR (400 MHz, $CDCl_3$) δ [ppm] 4.52 (d, 2H J=5.8 Hz, Bz-C$\underline{H}_2$NH), 4.70 (s, 2H, Bz-CH_2O), 6.5 (s, 1H, OH), 7.25 (d, 2H *J* = 8 Hz, Bz-H_{arom}), 7.37 (d, 2H *J* = 8 Hz, Bz-H_{arom}).

^{13}C NMR (100 MHz, $CDCl_3$) δ [ppm] 43.64 (Bz-$\underline{C}H_2$NH), 64.79 (Bz-$\underline{C}H_2$O), 115.70 (q, *J* = 287.9 Hz, $\underline{C}F_3$), 127.55 ($2C_{arom}$), 128.18 ($2C_{arom}$), 135.16 ($C_{q\text{-}arom}$), 141.0 ($C_{q\text{-}arom}$), 157.09 (q, *J* = 157.19 Hz, $\underline{C}OCF_3$).

^{19}F NMR (376 MHz, $CDCl_3$) δ [ppm] -75.84 (COC$\underline{F}_3$).

2.2. Preparation of 3',5'-O-diacetyl-2'-deoxyguanosine (2)

2'-Deoxyguanosine (1 g, 3.78 mmols, 1 eq.) was dried by coevaporation with anhydrous DMF and dissolved in 20 ml of anhydrous DMF. Then, 90 mg of DMAP (0.74 mmols, 0.2 eq.) were dissolved in 2 ml of anhydrous DMF and added dropwise. Next, 2.6 mL of TEA (18.5 mmols, 5.0 eq.) and 1.05 ml of Ac_2O (11.1 mmols, 3.0 eq.)

were added and the mixture dissolved completely. The solution was left to react for 4 hours at r.t. Afterwards cold DCM was added to precipitate the desired compound. The mixture was vacuum-filtered and the desired compound dried. Yield (**2**, 1.1 g, 91.6%). MS (EI 70 eV) m/z calcd for $C_{14}H_{18}N_5O_6$ ($M^+ + H^+$) 352.12 found 352.12

^{1}H-NMR (400 MHz, MeOD) δ [ppm] 1.93 (s, 3H, C$\underline{H}_3$O), 2.01 (s, 3H, C$\underline{H}_3$O), 2.47 (m, 1 H, 2'), 2.91 (m, 1H, 2''), 4.2 (m, 1 H, 4'), 4.26 (m, 2H, 5', 5''), 5.34 (m, 1H, 3'), 6.15 (m, 1H, 1'), 7.76 (s, 1H, 8).

2.3. Preparation of O^6-(N-4-((hydroxymethyl)benzyl)-trifluoroacetylmide)-3',5'-O-diacetyl-2'-deoxyguanosine (3)

3',5'-O-diacetyl-deoxyguanosine (**2**, 620 mg, 1.79 mmol) was dried 3 times by evaporation of DMF. PPh_3 (1.42 g; 5.4 mmol, 3 eq) and the protected phenol (**1**, 500 mg, 2.15 mmol, 1,2 eq) was added and left under vacuum for 2 h. Then, the mixture was dissolved in anhydrous dioxane (10.0 ml) and maintained under an argon atmosphere. Finally, DEAD (860 µl; 5.4 mmol 3 eq) was added dropwise. The reaction mixture was stirred for 4 hours at room temperature and the progress of the reaction was monitored by TLC (DCM:MeOH 9:1). The orange reaction was concentrated in vacuum to obtain a viscous oil. The oil was purified by flash chromatography using a gradient of MeOH in DCM to yield a white product (750 mg, 75%). TLC R_f=0.42 (DCM:MeOH 9:1), MS (EI 70 eV) m/z calcd for $C_{24}H_{26}F_3N_6O_7$ ($M^+ + H^+$) 567.18 found 567.181 [M^+].

^{1}H-NMR (400 MHz, $CDCl_3$) δ [ppm] 2.08 (s, 3H, C$\underline{H}_3$CO), 2.12 (s, 3H, C$\underline{H}_3$CO), 2.52 (m, 1H, 2'), 2.98 (m, 1H, 2''), 4.33 (m, 2H, 5',5''), 4.52 (m, 1H, 4'), 4.90 (s, 2H, Bz-C$\underline{H}_2$NH), 5.43 (m, 1H, 3'), 5.55 (s, 2H, Bz-C$\underline{H}_2$O), 6.28 (dd, 1H, *J* = 8 Hz, 1'), 7.27 (d, 2H, *J* = 8 Hz, Bz-H_{arom}), 7.49 (d, 2H, *J* = 8 Hz, Bz-H_{arom}), 7.74 (s, 1H, 8).

^{13}C NMR (100 MHz, $CDCl_3$) δ [ppm] 20.76 (C$\underline{H}_3$CO), 20.93(C$\underline{H}_3$CO), 36.69 (C-2'), 43.60 (Bz-C$\underline{H}_2$NH), 63.79 (C-5'), 67.51 (Bz-C$\underline{H}_2$O), 74.61 (C-3'), 82.30 (C-1'), 84.44 (C-4'), 115.85 (q, *J* = 287 Hz, CF_3), 116.11 (C-5), 128.06 ($2C_{arom}$), 128.77 ($2C_{arom}$), 135.74 (C-8), 136.49 ($C_{q\text{-}arom}$), 137.56 ($C_{q\text{-}arom}$), 153.53 (C-4), 156.63-157.74 (q, *J* = 37 Hz $\underline{C}OCF_3$), 159.15 (C-2), 160.87 (C-6), 170.27 (CO), 170.61 (CO).

^{19}F NMR (376 MHz, $CDCl_3$) δ [ppm] -75.76 (COC$\underline{F}_3$).

2.4. Preparation of the deprotected O^6-(N-4-((hydroxymethyl)benzyl)-trifluoro-acetylmide)-2'-deoxyguanosine (4)

Compound (**3**) was dissolved in 3 ml of MeOH and transferred to a polypropylene conical tube (50 ml) with a stirring bar. Ammonium hydroxide (20%) 3 mL was added and the mixture was stirred during 2 hours. The reaction was followed up by TLC. The solvent was evaporated and the crude was purified by flash chromatography (DCM:MeOH 95:5 to 90:10), yielding the expected compound **5** (112 mg, 46 %). TLC

R_f=0.18 (DCM:MeOH 95:5), MS (EI 70 eV) m/z calcd for $C_{20}H_{22}F_3N_6O_5$ (M^+ + H^+) 483.1598 found 483.1599 [M^+].

^{1}H-NMR (400 MHz, MeOD) δ [ppm] 2.31 (m, 1H, 2'), 2.75 (m, 1H, 2''), 3.73 (dd *J* = 12 Hz, *J* = 3, 1H, 5'), 3.83 (dd *J* = 12 Hz, *J* = 3, 1H 5''), 4.03 (m, 1H, 4'), 4. 43 (s, 2H, Bz-C$\underline{H}_2$NH$_2$), 4.54 (m, 1H, 3'), 5.48 (s, 2H, Bz-C$\underline{H}_2$O), 6.28 (dd, 1H *J* = 8 Hz, *J* = 6 Hz, 1'), 7.27 (d, 2H *J* = 8 Hz, Bz-H$_{arom}$), 7.45 (d, 2H *J* = 8 Hz, Bz-H$_{arom}$), 8.01 (s, 1H, 8).

^{13}C NMR (100 MHz, MeOD) δ [ppm] 39.73 (C-2'), 42.58 (Bz-$\underline{C}$H$_2$NH), 62.32 (C-5'), 67.25 (Bz-$\underline{C}$H$_2$O), 71.73 (C-3'), 85.39 (C-1'), 88.24 (C-4'), 114.55 (C-5), 116.049 (q *J* = 286.7 Hz, CF3), 127.4 (2C$_{arom}$), 128.31 (2C$_{arom}$), 135.91 (C-8), 137.01 (C$_{q\text{-}arom}$), 138.65 (C$_{q\text{-}arom}$), 152.87 (C-4), 157.54 (q, *J* = 37 Hz $\underline{C}$OCF$_3$), 159.9 (C-2), 160.66 (C-6).

^{19}F-NMR (376 MHz, MeOD): δ [ppm] -77.20 (C$\underline{F}_3$)

2.5. Preparation of the N^2-(N',N'-dimethylamino)methylen)-O^6-(N-4-((hydroxymethyl)-benzyl)-trifluoroacetylamide)-2'-deoxyguanosine (5)

The product (**4,** 0.23 mmol**)** was dried by evaporation with anhydrous DMF and dissolved in 2 ml of DMF under argon. Dmf protecting group 125 µL (4 eq, 0.93 mmol) was added and the mixture was stirred during 4 hours. The reaction was followed by TLC. The solvent was evaporated and crude was purified by flash chromatography over silica gel yielding the expected compound **5** (112 mg, 46 %). TLC R_f=0.28 (DCM:MeOH 90:10), MS (EI 70 eV) m/z for $C_{23}H_{27}F_3N_7O_5$ (M^+ + H^+) 538.202 found 538.2017 [M^+].

^{1}H-NMR (400 MHz, MeOD) δ [ppm] 2.39 (m, 1H, 2'), 2.76 (m, 1H, 2''), 3.08 (s, 3H, N(C$\underline{H}_3$)$_2$), 3.14 (s, 3H, N(C$\underline{H}_3$)$_2$), 3.73 (dd *J* = 12 Hz, *J* = 3, 1H, 5'), 3,79 (dd *J* = 12 Hz, *J* = 3, 1H 5''), 4.01 (m, 1H, 4'), 4.43 (s, 2H, Bz-C$\underline{H}_2$NH), 4.56 (m, 1H, 3'), 5.57 (s, 2H, Bz-C$\underline{H}_2$O), 6.41 (dd, 1H *J* = 8 Hz, *J* = 6 Hz, 1'), 7.29 (d, 2H *J* = 8 Hz, Bz-H$_{arom}$), 7.48 (d, 2H *J* = 8 Hz, Bz-H$_{arom}$), 8.24 (s, 1H, 8), 8.65 (s, 1H, C$\underline{H}$=N).

^{13}C NMR (100 MHz, MeOD) δ [ppm] 34.58 (C-2'), 40.62, 40.73 (2C, N($\underline{C}$H$_3$)$_2$), 43.14 (Bz-$\underline{C}$H$_2$NH$_2$), 62.54 (C-5'), 68.02 (Bz-$\underline{C}$H$_2$O), 71.88 (C-3'), 85.38 (C-1'), 88.63 (C-4'), 116.77 (q *J* = 286.7 Hz, CF3), 117.60 (C-5), 128.01 (2C$_{arom}$), 128.56 (2C$_{arom}$), 136.77 (C-8), 137.57 (C$_{q\text{-}arom}$), 140.62 (C$_{q\text{-}arom}$), 153.42 (C-4), 158.94 (q, *J* = 37 Hz $\underline{C}$OCF$_3$), 159.6 (C-2), 160.41 (C-6), 162.60 ($\underline{C}$H=N).

^{19}F-NMR (376 MHz, MeOD): δ [ppm] -77.16 (CF$_3$).

2.6. Preparation of 5'-O-(4,4'-dimetoxytrityl)-[N^2-(N,N'-dimethylamino)-O^6-(N-4-((hydroxymethyl)benzyl)-trifluoroacetylmide)-2'-deoxyguanosine (6)

A solution of (90 mg, 167 µmols) of product **(5)** was dried three times with anhydrous pyridine (3 × 5 mL) and finally dissolved in anh. pyr (4 ml) and placed under argon. Then, 125 mg (1.4 eq, 0.32 mmols) of DMT-Cl and 14 mg (0.5 eq, 0.115 mmols) of DMAP were added. The reaction was stirred under argon over night at room

temperature and protected from the light. The product formation was followed up by TLC. Then, the reaction was quenched with 1 ml of MeOH and the solvent was evaporated. The crude product was purified by flash chromatography over silica gel (DCM 100%, DCM:MeOH 1-10% + 2% Et_3N) to give 117 mg (83%) of compound **6**. TLC R_f=0.68 (DCM:MeOH 95:5).

^{1}H-NMR (400 MHz, $CDCl_3$) δ [ppm] 2.49 (m, 1H, 2'), 2.65 (m, 1H, 2''), 2.92 (s, 6H, N($C\underline{H}_3$)$_2$), 3,41 (m, 2H, 5' 5''), 3.66 (s, 6H, DMT-O-$C\underline{H}_3$), 4.14 (m, 1H, 4'), 4.40 (s, 2H, Bz-$C\underline{H}_2$NH), 4.58 (m, 1H, 3'), 5.44 (s, 2H, Bz-$C\underline{H}_2$O), 6.33 (t, 1H *J* = 6 Hz, 1'), 6.66 (d, 2H *J* = 8 Hz, DMT-H_{arom}), 6.68 (d, 2H *J* = 8 Hz, DMT-H_{arom}), 7.06-7.34 (m, 13H DMT-$H_{arom,}$ Bz-H_{arom}), 7.87 (s, 1H, 8), 9.32 (s, 1H, N=C$\underline{H}$).

^{19}F-NMR (376 MHz, $CDCl_3$): δ [ppm] -75.56 (CF_3).

2.7. Preparation of 5'-O-(4,4'-dimetoxytrityl)-[N^2-(N,N'-dimethylamino)-O^6-(N-4-((hydroxymethyl)benzyl)-trifluoroacetylmide)-2'-deoxyguanosine-3'-O-(N,N-diisopropyl-2-cyanoethyl phosphoramidite (7)

A solution of product **(6)** (117 mg, 136 µmols) was dissolved in anhydrous CH_2Cl_2 under argon and at 0ºC. Then, DIPEA (95 µL, 540 µmol, 4 eq) and 2-cyanoethyl diisopropylphosphoramidochloridite (50 µL, 204 µmol) were added. After 15 min the reaction was allowed to reach r.t and stirred for 1 hour. The reaction was quenched with brine, extracted with CH_2Cl_2, dried ($MgSO_4$) and concentrated. The residue was used directly without further purification for oligonucleotide synthesis**.** TLC R_f=0.68 (hexane/EtOAc 20:70 + + 2% Et_3N).

^{1}H-NMR (400 MHz, CDC_3) δ [ppm] 1.25 (s, 6H, NCH($C\underline{H}_3$)$_2$), 1.26 (s, 6H, NCH($C\underline{H}_3$)$_2$), 2.50 (m, 1H, 2'), 2.65 (m, 3H, 2'', $C\underline{H}_2$CN), 2.92 (s, 6H, N($C\underline{H}_3$)$_2$), 3.24 (m, 2H, 5' 5''), 3.41 (m, 4H, $CH_2C\underline{H}_2$OP, NC$\underline{H}$(CH_3)$_2$), 3.66 (s, 6H, DMT-O-$C\underline{H}_3$), 4.14 (m, 1H, 4'), 4.42 (s, 2H, Bz-$C\underline{H}_2$NH), 4.58 (m, 1H, 3'), 5.54 (s, 2H, Bz-$C\underline{H}_2$O), 6.33 (t, 1H *J* = 6 Hz, 1'), 6.65 (dd, 4H *J* = 7 Hz, DMT-H_{arom}), 7.06-7.34 (m, 13H DMT-$H_{arom,}$ Bz-H_{arom}), 7.87 (s, 1H, 8), 9.32 (s, 1H, C$\underline{H}$=N).

^{13}C NMR (100 MHz, MeOD) δ [ppm] 20.45 ($\underline{C}H_2$CN), 24.47, 24.52, 24.54, 24.59 (4C, P-NCH($\underline{C}H_3$)$_2$), 39.28 (C-2'), 43.18 (2C, N($\underline{C}H_3$)$_2$), 43.31 (2C, $\underline{C}$(CH_3)$_2$), 43.55 (Bz-$\underline{C}H_2NH_2$), 55.16 (2C, DMT-O$\underline{C}H_3$), 57.94 ($CH_2\underline{C}H_2$OP), 63.48 (C-5'), 68.31 (Bz-$\underline{C}H_2$O), 74.38 (C-3'), 84.59 (C-1'), 85.80 (C-4'), 86.43 (DMT-C_q), 113.11 (4C, DMT-C_3), 117.46 (CF3), 117.69 (CN), 119.15 (C-5), 127.28 (2C, C_{arom}), 128.05 (2C, C_{arom}), 128.18, 128.72, 129.93, 129.95 (9C, DMT-$C_{3\text{-}arom}$), 135.05 (2C, DMT-$C_{q\text{-}arom}$), 135.56 (Bz-$C_{q\text{-}arom}$), 135.97 (C-8), 140.12 (Bz-C_{qArom}), 140.70 (DMT-C_{qArom}), 151.45 (2C, DMT-C_{qArom}), 152.50 (C-4), 158.47 (2C, $\underline{C}OCF_3$, C-2), 160.57 (C-6), 162.56 (N=CH).

^{19}F-NMR (376 MHz, $CDCl_3$): δ [ppm] -75.56 (CF_3).

^{31}P-NMR (161 MHz, $CDCl_3$): δ [ppm] 148.83.

3. Synthesis and purification of oligonucleotides

3.1. Oligonucleotide synthesis

The oligonucleotide sequences were synthesized at 1 µmol scale using the standard protocols (Table 1). The incorporation of the O^6-(N-4-((hydroxymethyl)benzyl)-trifluoroacetylmide)-2'-deoxyguanosinephosphoramidite (^{A}dG) in the sequence was carried out manually with a coupling time of 15 min, obtaining a yield of 75%. The incorporation of the ^{Q}T-nucleobases to the complementary sequences was automatically performed on the synthesizer. In all the syntheses we used dimethylformamidino-protected guanine phosphoramidite (**7**). The syntheses were completed using the DMT-OFF protocol, except for the sequence containing ^{A}dG, which was synthesized in DMT-ON mode to help purification.

3.2. Oligonucleotides deprotection and purification.

After oligonucleotide synthesis, the solid supports were transferred to screw-cap vials and incubated with a solution of concentrated aqueous ammonia overnight at room temperature, and additional 15 min incubation at 55ºC were needed for the sequence containing ^{Bz}G. The solutions were then filtered using sterile cotton and transferred into a 2 mL eppendorf tube. The solutions were evaporated using a nitrogen system to remove the ammonium. The resulting products were desalted by Sephadex G-25 using water as eluent.

The sequence containing ^{Bz}G was purified by reversed-phase HPLC using the DMT-ON protocol in a Nucleosil 120 10-C18 10 µm (250x8 mm) column with a flow rate of 3 mL/min and an increasing gradient of ACN (15% to 80%) over 0.1 M aqueous TEAA pH 6.5, during 20 minutes. The retention time for the oligonucleotide was 10.23 min. The pure fractions were combined and evaporated to dryness. The obtained residues were detritylated by adding 1 mL of 80% acetic acid solution for 30 min at room temperature. The deprotected oligonucleotides were desalted and further purified by a second round of chromatography, using the DMT-OFF protocol: 20 minutes of linear gradient from 5% to 50% ACN over 0.1 M aqueous TEAA pH 6.5. The yield and purity obtained for the products was around 85% in all cases. The length and homogeneity of the oligonucleotide were verified by MALDI-TOF (table 1).

The DNA-strand concentration was determined by absorbance measurements (260 nm) and its extinction coefficients. Oligonucleotide samples were kept at 4 ºC until further use.

3.3. Preparation of the fluorescent ^{F}G oligonucleotide.

The 5'-ATCTTCTC^{Bz}GATTCA-3' oligonucleotide was left to react with fluorescein isothiocyanate (FITC) through its free amino group as follows. 5 O.D. of the oligonucleotide were dissolved in 250 µL of an aqueous solution of 0.2 M $NaHCO_3$ (pH 9) and 10 eq of a solution of FITC solved in 250 µL DMF were added and left to react at rt for 8h. Then, 100 µL of an aqueous solution of 0.2 M $NaHCO_3$ (pH 9) and an

additional 10 equiv of FITC in 100 µL of DMF were added and the mixture was left to react overnight at rt. The mixtures were concentrated to dryness and the residue resuspended in 1 mL of water. The solution was purified by Sephadex G-25 and analyzed by RP-HPLC using an XBridge OST C18 2.5 µm column. The coupling efficiency was determined by HPLC analysis (86 %). The purified oligomers were analyzed by MS (MALDI-TOF), see table 1.

DNA duplexes were obtained by annealing equimolar concentrations of the control, ^{Bz}G and ^{F}G sequences with the complementary oligonucleotide strands at 72 ºC for 5 min and then allowing them to slowly cool down to room temperature.

4. hAGT expression and purification

In vitro assays were carried out using recombinant hAGT, overexpressed and purified as previously described.[13] Briefly, hAGT protein was expressed in the *E. coli* strain Rosetta, induced by adding 1 mM IPTG and left to express for 4 h at 30 °C. The pellet was disrupted by sonication and centrifuged. The supernatant was filtered, loaded into a HiTrapTM FF column and eluted with an Imidazole gradient (20-500 mM) in the following buffer of 350 mM NaCl, 20 mM Tris pH 8, and 1 mM BME. Finally, the protein was loaded into a Superdex 75 16/60 being the buffer 200 mM NaCl, 20 mM Tris pH 8.0, 10 mM DTT and 0.1 mM EDTA. The protein was concentrated to 2 mg/ml in this buffer and kept at -20 °C in the presence of 40 % glycerol. The same protocol was used for the purification of the inactive mutant hAGT-C145S expressed in the *E. coli* strain BL21. This mutant was used as negative control in many experiments.

5. Thermal stability studies.

Melting curves of all the possible pairs of complementary oligonucleotides were measured by monitoring the absorbance hyperchromicity at 260 nm. UV/Vis absorption spectra were recorded at 1ºC/min intervals, with a 1-min equilibration time at each temperature; the sample was heated over the range 10-80 ºC. The buffer solutions used were 10 mM sodium phosphate pH 7.0 and 100 mM NaCl. Sample concentration was around 4 µM. Each sample was allowed to equilibrate at the initial temperature without any external control of temperature for 5 min before the melting experiment began. The melting temperatures (Tm) are the average value of at least one pair of Tm experiments. The data were analyzed by the denaturation curve processing program, MeltWin v. 3.0. Melting temperatures (Tm) were determined by computer fitting of the first derivative of absorbance with respect to 1/T.

Thermal stability experiments recording the emitted fluorescence at excitation wavelength of 485 nm were also performed for the double strands containing a fluorophor or a fluorophor-quencher pair. These experiments were realized in the same conditions, concentration, range of temperature and buffer described above.

6. Circular Dichroism

The CD spectra of all the possible pairs of complementary oligonucleotides were registered at 25ºC over a range of 220–320 nm, with a scanning speed of 50 nm·min^{-1}, a response time of 4s, data pitch of 0.5 nm, and a bandwidth of 1nm. The duplexes concentration was 2 µM in a buffer solutions of 10 mM sodium phosphate pH 7.0 and 100 mM NaCl. The samples were annealed before recording of spectra.

7. HPLC analysis of hAGT dealkylation.

In order to measure the dealkylation of ^{F}G, 142 pmol and 350 pmol of the duplexes were incubated with 40 pmol of full-length-hAGT to a final volume of 400 µl in a reaction buffer (200 mM NaCl, 50 mM Tris pH 8.0, 1 mM DTT, 5 mM EDTA). The reaction was incubated for 90 min at 37 ºC and stopped by heating the samples at 72 ºC for 5 min. The reaction products were analyzed by HPLC on a Nucleosil analytical column at 37ºC. The HPLC flow rate was 1 ml/min, and a gradient of 10–40% acetonitrile in 20 min was used.

8. Fluorescence assay for hAGT activity.

The fluorescence assay was performed with full-length hAGT and the hAGT-C145S (inactive mutant) was used as a negative control. The reaction was accomplished in a total volume of 50 µl in each well, incubating increasing concentrations of hAGT (50, 100 and 200 nM) in reaction buffer (200 mM NaCl, 50 mM Tris pH 8.0, 1 mM DTT, 5 mM EDTA, 20 mM KCl). The assay was initiated by the addition of 5 µl of fluorophore-quencher duplex substrate (10 nM, 0.5 pmol) and this solution was then placed in a microplate reader system. Fluorescence was measured every minute for 20 min at excitation and emission wavelengths of 485 and 535 nm, respectively. Averages over three readings were taken for each condition tested. Each experiment was performed in triplicates.

Table S1: Sequence of oligonucleotides and its characterization by MALDI-TOF

Name	Sequence	Mass found (calculated)
Oligo-^{Bz}G	5'-ATC TTC TC**^{Bz}G** ATT CA-3'	4310.9 (expected 4306,94)
Oligo-^{F}G	5'-ATC TTC TC**^{F}G** ATT CA-3'	4702.2 (expected 4695.31)
Control	5'-ATC TTC TCG ATT CA-3'	4190.0 (expected 4187.77)
Complementary	5'-TGA ATC GAG AAG AT-3'	4333.8 (expected 4332.77)
Complementary-^{Q}T	5'-TGA A**^{Q}T**C GAG AAG AT-3'	4741.2 (expected 4740.38)
Mismatch-T	5'-TGA ATT GAG AAG AT-3'	4348.2 (expected 4347.77)
Mismatch-^{Q}T	5'-TGA AT**^{Q}T** GAG AAG AT-3'	4757.0 (expected 4755.39)

Sequences of the different oligonucleotide used in the development of the hAGT fluorescence assay. **^{Bz}G** represents O^6-benzyl-2'-deoxyguanine. **^{F}G** corresponds to the O^6- Fluorescein-benzyl-2'-deoxyguanine, where fluorescein is a fluorophore group. ^{Q}T represents a modified T with the quencher group (Dabcyl). Mass spectrometry analysis (MALDI-TOF) and expected mass.

Table S2. Melting temperatures of the duplexes.

$^{5'}$-ATCTTCTC XA TTCA-$^{3'}$
$^{3'}$-TAGAAGA ZW TAAGT-$^{3'}$

Name	XA	ZW	Tm (260 nm)	Tm (485 nm)
Control:Complementary	GA	CT	54.6	Nd
Control: Mismatch-T	GA	TT	45.0	Nd
Oligo-^{Bz}G:Complementary	^{Bz}GA	CT	33.3	Nd
Oligo-^{Bz}G:Mismatch-T	^{Bz}GA	TT	36.4	Nd
Oligo-^{Bz}G:Mismatch-^{Q}T	^{Bz}GA	^{Q}TT	40.2	Nd
Oligo-^{Bz}G: C^{Q}T	^{Bz}GA	C^{Q}T	41.3	Nd
Oligo-^{F}G:Complementary	^{F}GA	CT	33.0	Nd
Oligo-^{F}G: C ^{Q}T	^{F}GA	C^{Q}T	30.3	28.0/54.1
Oligo-^{F}G:Mismatch-T	^{F}GA	TT	27.9	Nd
Oligo-^{F}G:Mismatch-^{Q}T	^{F}GA	^{Q}TT	34.3	26.1

nd: not determined.

Figure S1: CD spectra of the different duplexes. A) CD spectra of complementary duplexes. B) CD of the mismatch duplexes. All de experiments were performed in 10 mM sodium phosphate pH 7.0 and 100 mM NaCl with a 2 uM of duplexes.

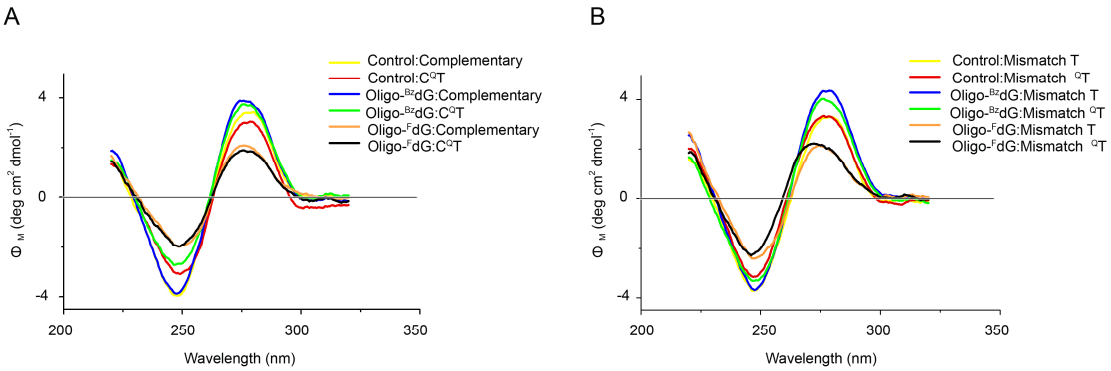

Figure S2: Curves of the melting temperatures of the two fluorescent-quencher duplexes at 485nm.

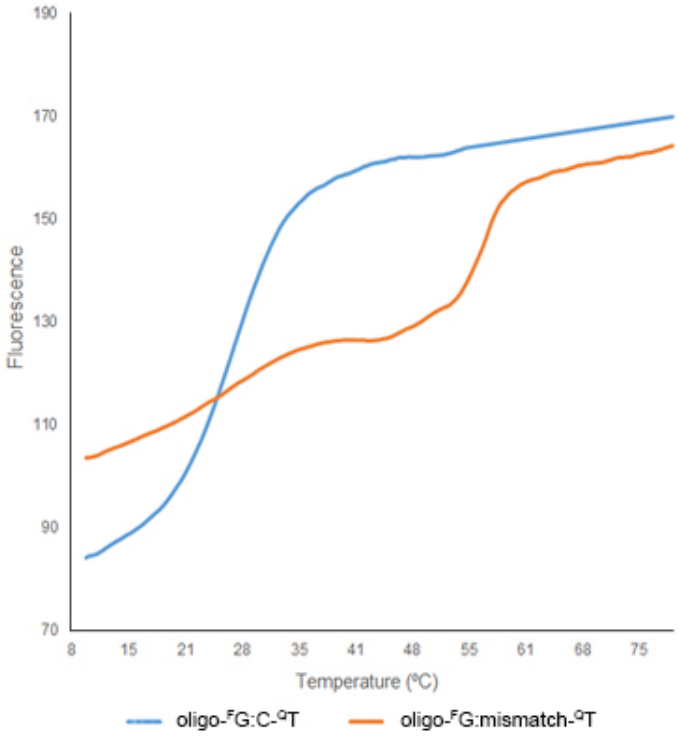

Figure S3: HPLC profiles of the control sequences. A) unmodified oligonucleotide sequence with its complementary strand. **B)** fluorescein-benzyl-modified oligonucleotide sequence with its complementary strand. The HPLC was performed at 37 ºC.

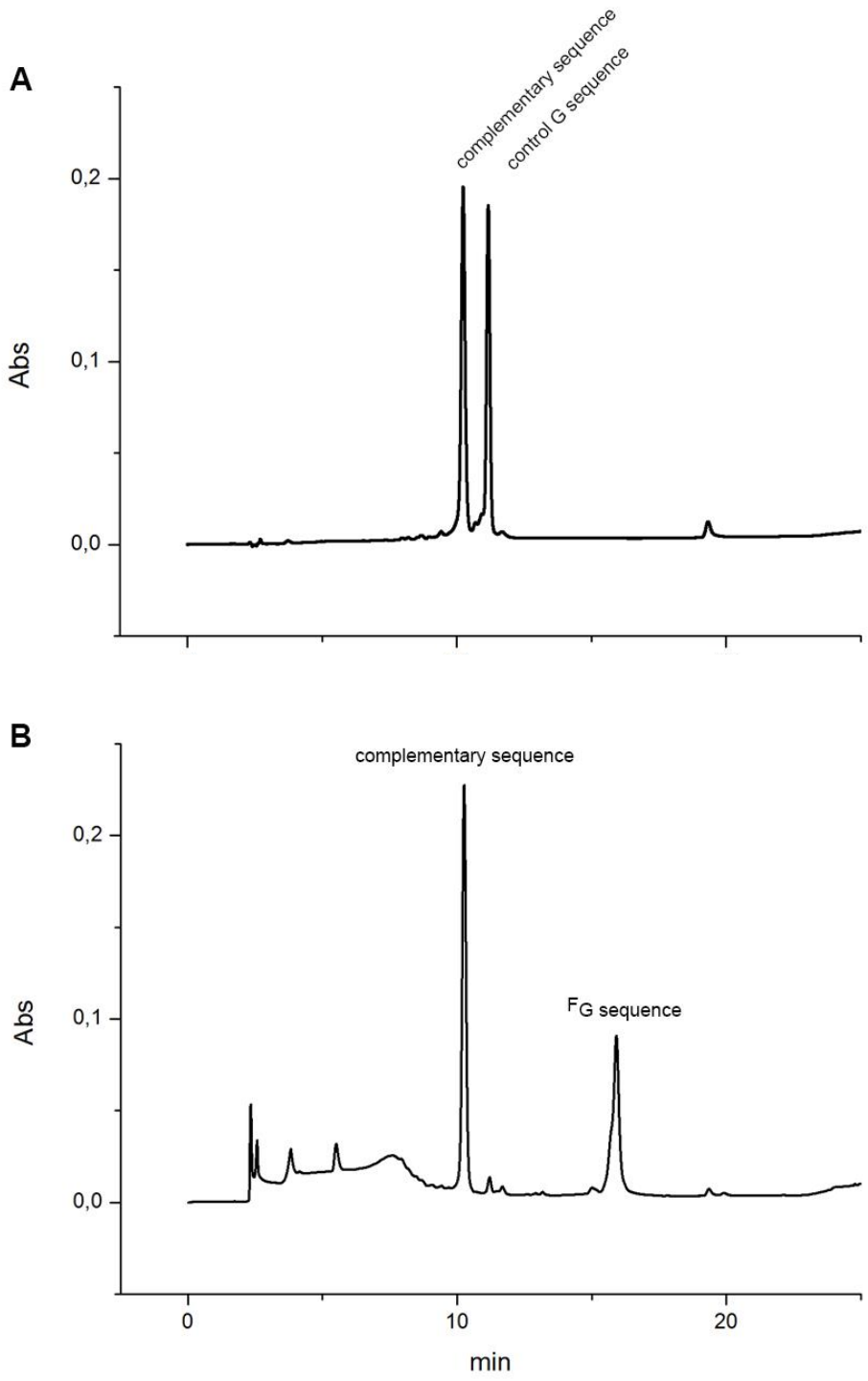

Figure S4: Control experiments of the fluorescence assay. The background fluorescence of the double stranded sequence is observed in the absence of hAGT and in the presence of an inactive mutant. An increase of fluorescence is observed in the presence of the same concentration of active hAGT (150 nM).

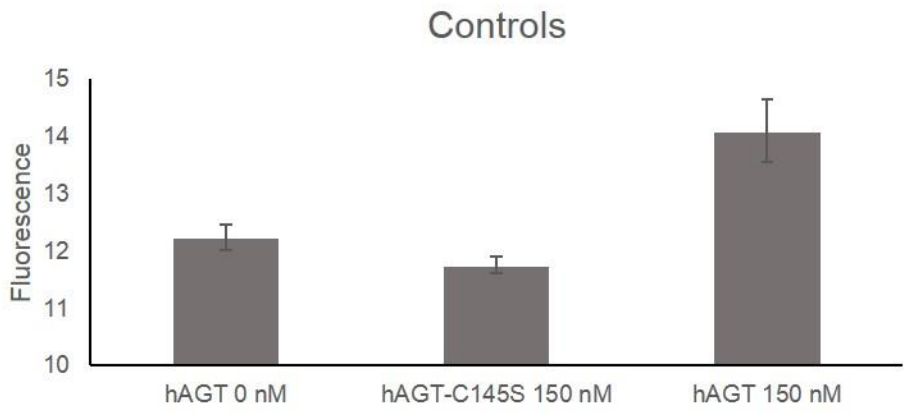

Figure S5. Kinetic data of figure 2 (main text). The emission of fluorescence corresponding to 3 concentrations of hAGT (10, 20 and 30 nM) is measured for 20 minutes.

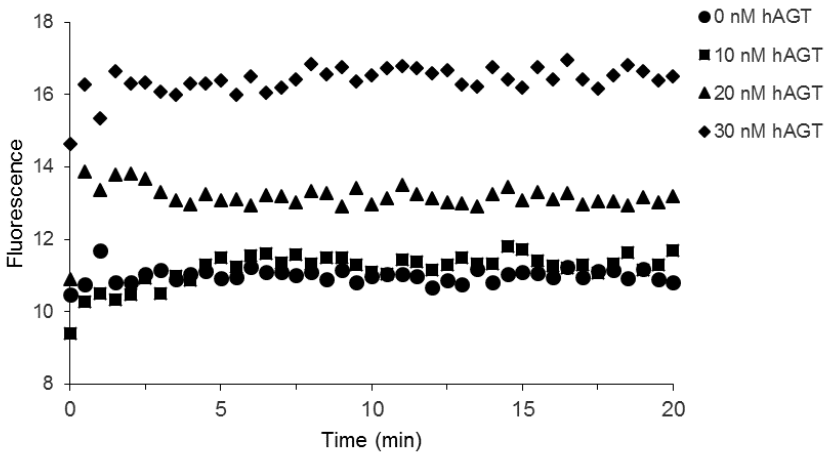

^{1}H-NMR, ^{13}C-NMR ^{19}F-NMR and ^{31}P-NMR spectra

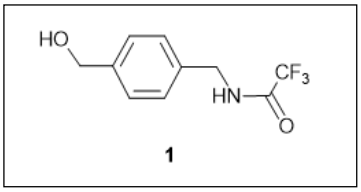

1

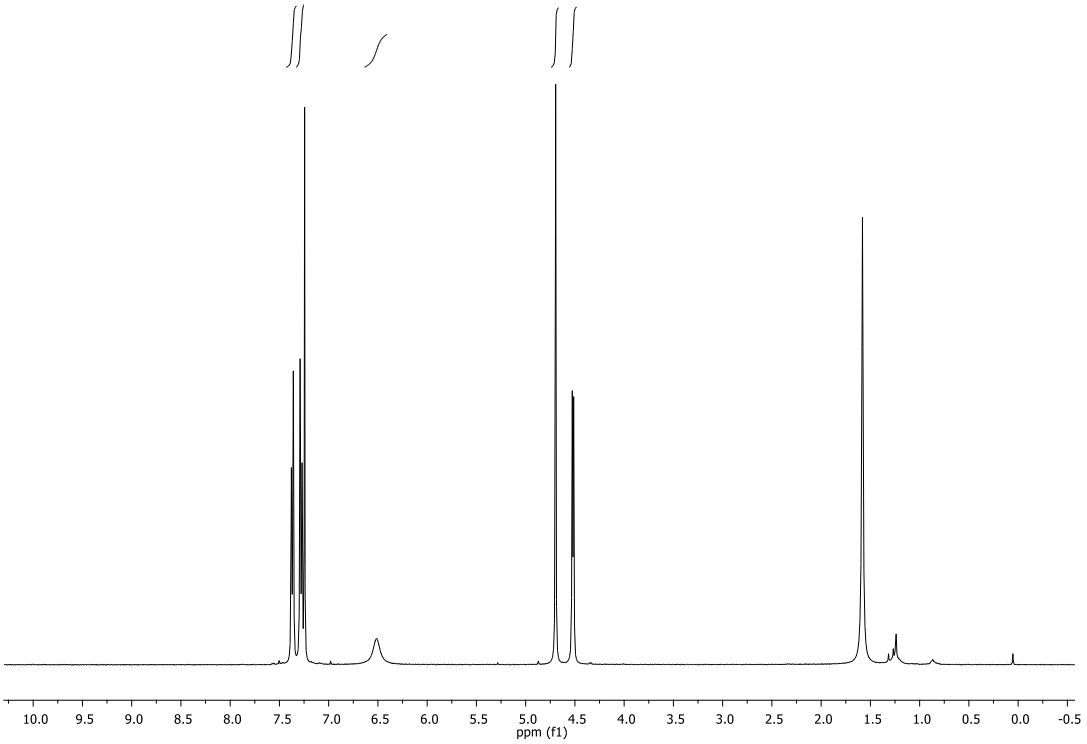

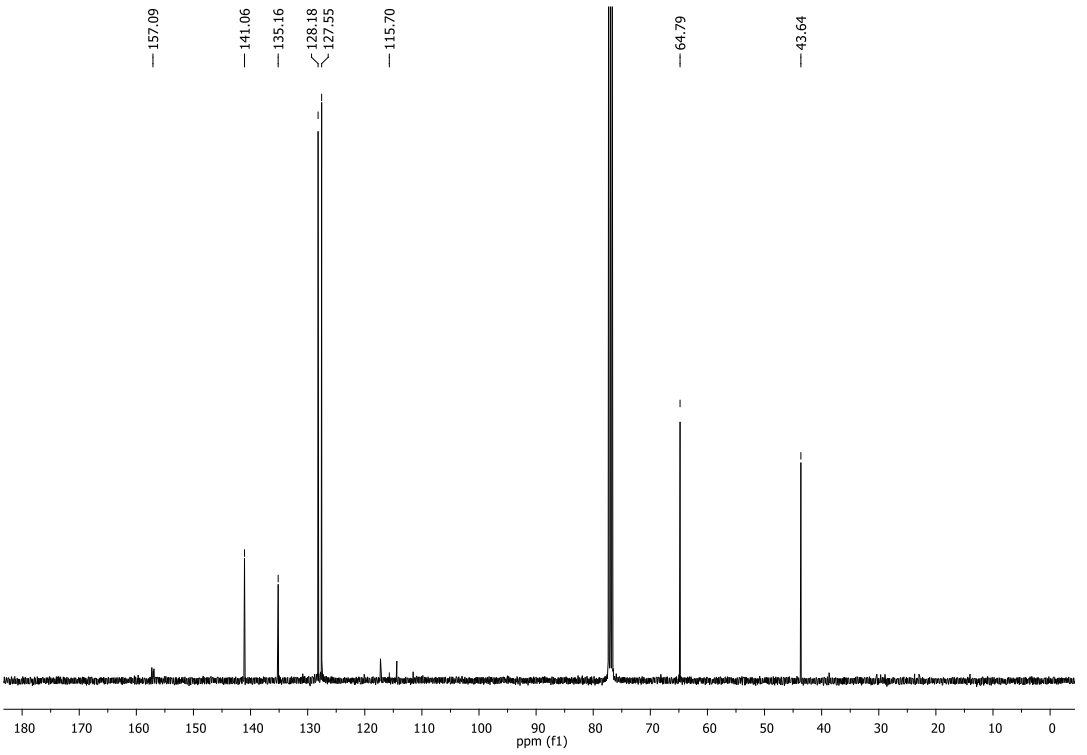

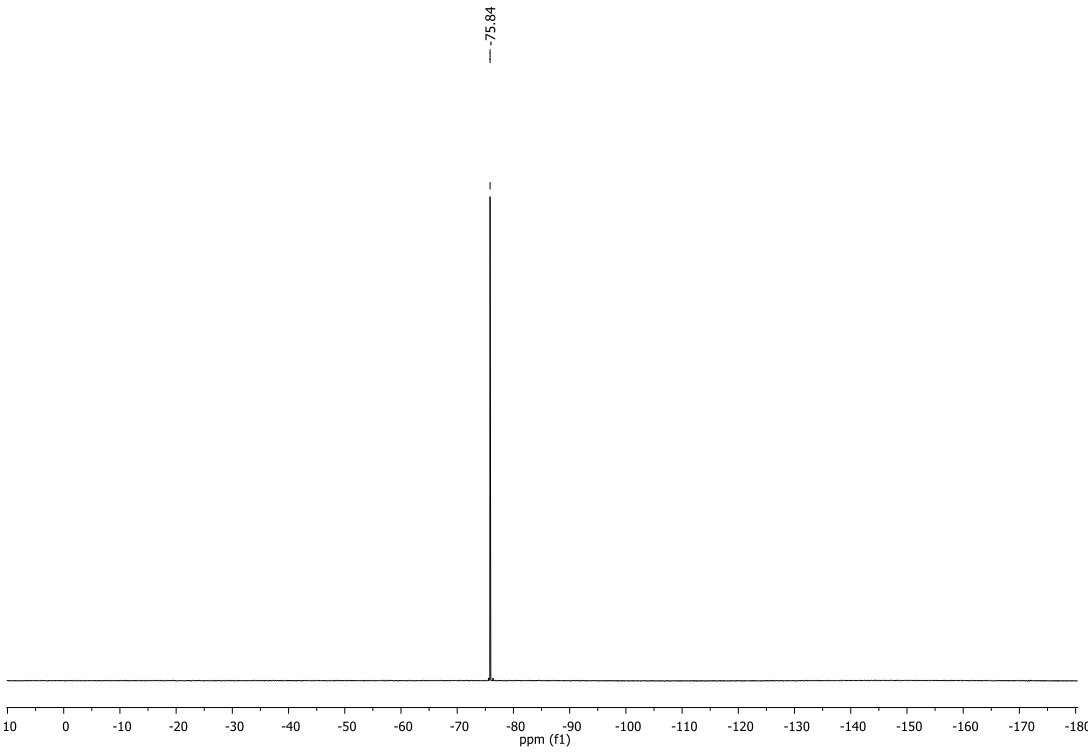
-75.84
10
0
-10
-20
-30
-40
-50
-60
-70
-80
-90
-100
-110
-120
-130
-140
-150
-160
-170
ppm (f1)

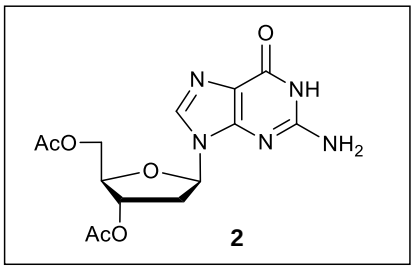
O
N
NH
AcO
N
N
NH2
O
AcO

2

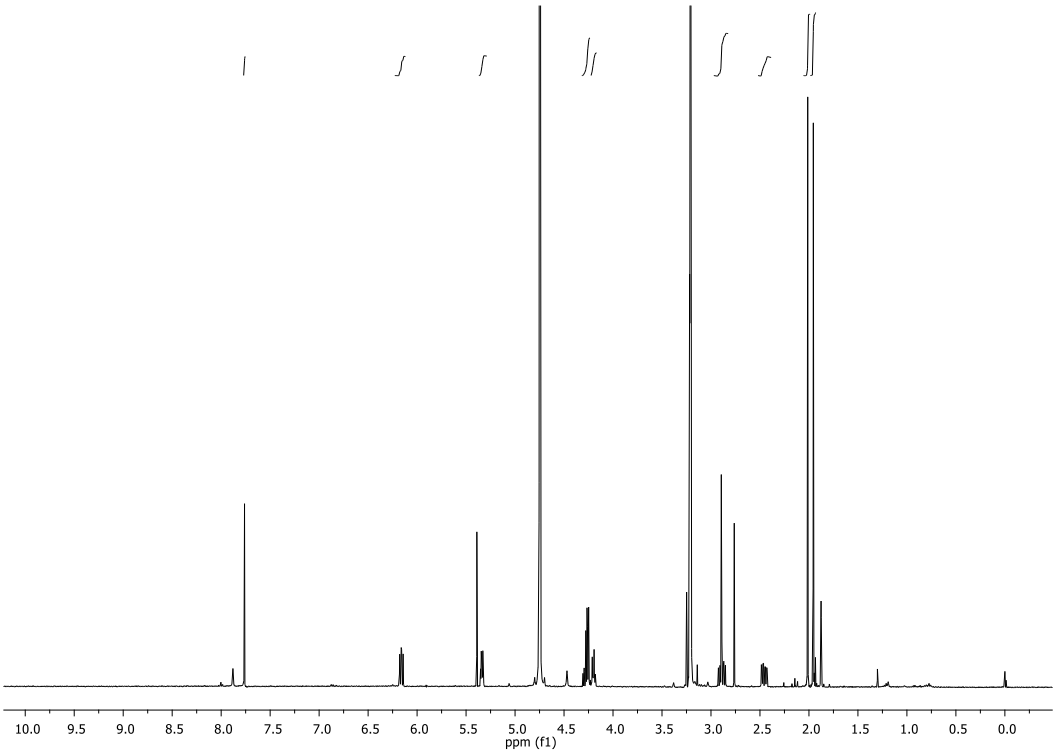
10.0 9.5 9.0 8.5 8.0 7.5 7.0 6.5 6.0 5.5 5.0 4.5 4.0 3.5 3.0 2.5 2.0 1.5 1.0 0.5 0.0
ppm (f1)

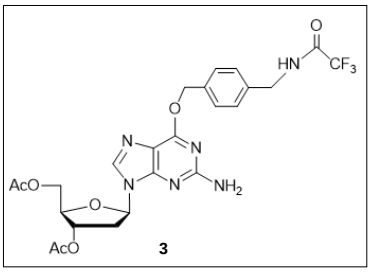
O
HN
CF3
O
N
N
N
N
NH2
AcO
O
AcO
3

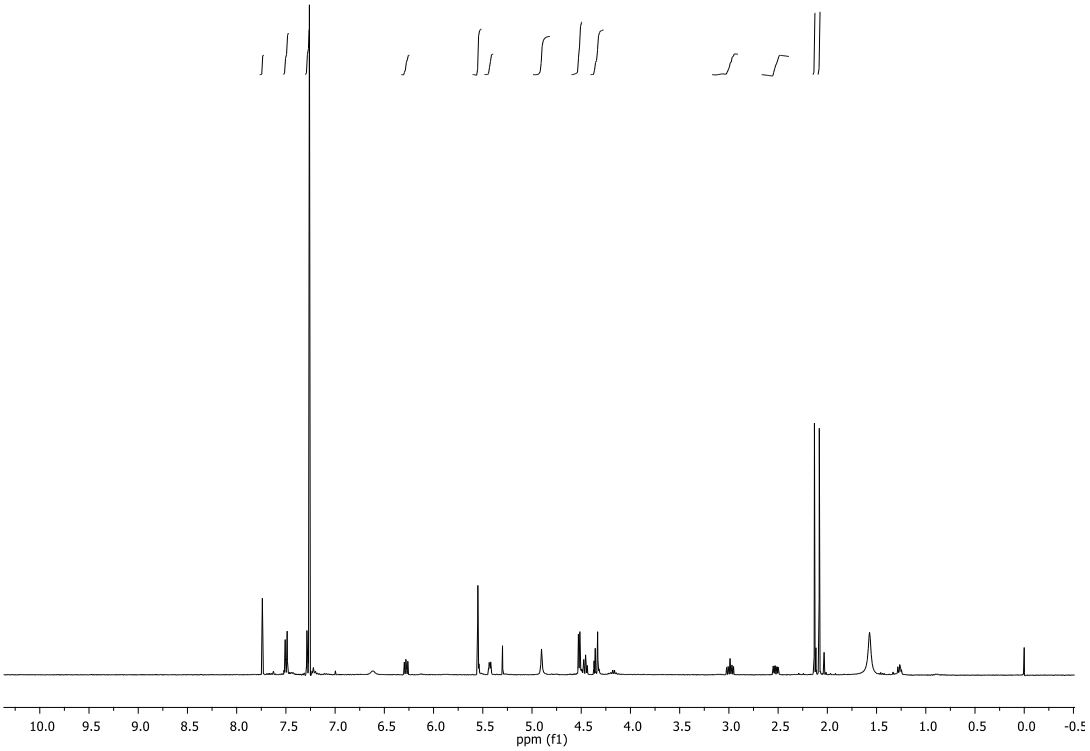
10.0 9.5 9.0 8.5 8.0 7.5 7.0 6.5 6.0 5.5 5.0 4.5 4.0 3.5 3.0 2.5 2.0 1.5 1.0 0.5 0.0
ppm (f1)

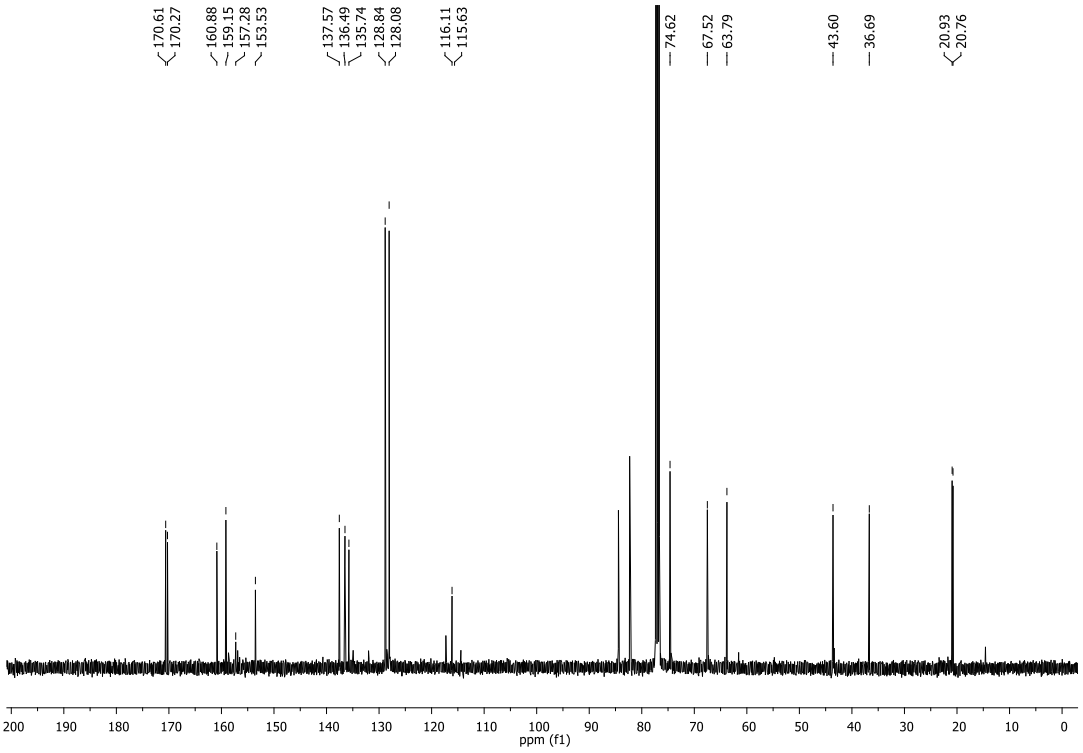
170.61
170.27
160.88
159.15
157.28
153.53
137.57
136.49
135.74
128.84
128.08
116.11
115.63
74.62
67.52
63.79
43.60
36.69
20.93
20.76
200 190 180 170 160 150 140 130 120 110 100 90 80 70 60 50 40 30 20 10 0
ppm (f1)

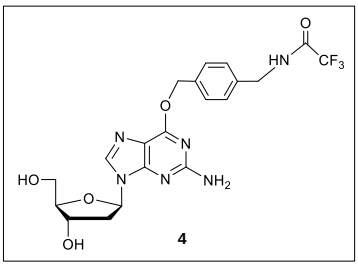
O
HN
CF3
O
N
N
N
N
NH2
HO
O
OH

4

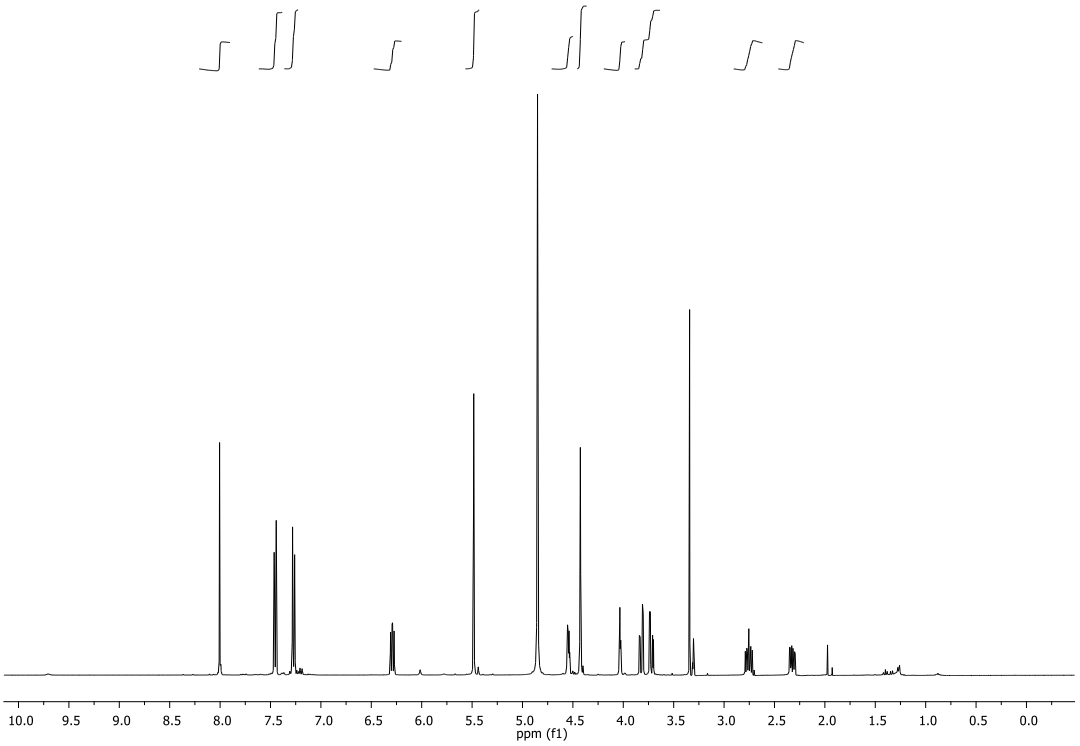
10.0 9.5 9.0 8.5 8.0 7.5 7.0 6.5 6.0 5.5 5.0 4.5 4.0 3.5 3.0 2.5 2.0 1.5 1.0 0.5 0.0
ppm (f1)

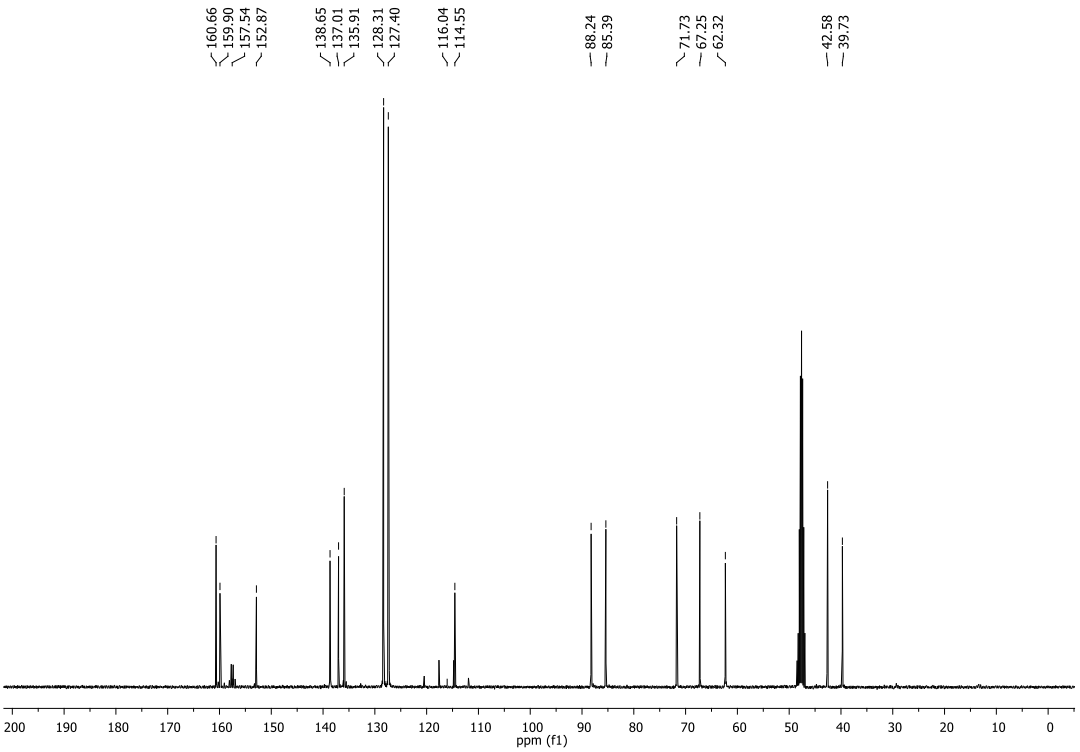
160.66
159.90
157.54
152.87
138.65
137.01
135.91
128.31
127.40
116.04
114.55
88.24
85.39
71.73
67.25
62.32
42.58
39.73
200 190 180 170 160 150 140 130 120 110 100 90 80 70 60 50 40 30 20 10 0
ppm (f1)

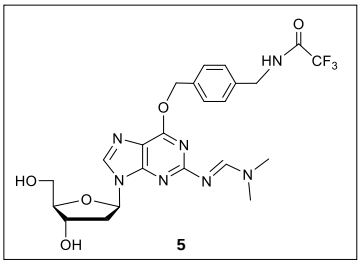
O
HN
CF3
O
N
N
N
N
N
HO
O
OH

5

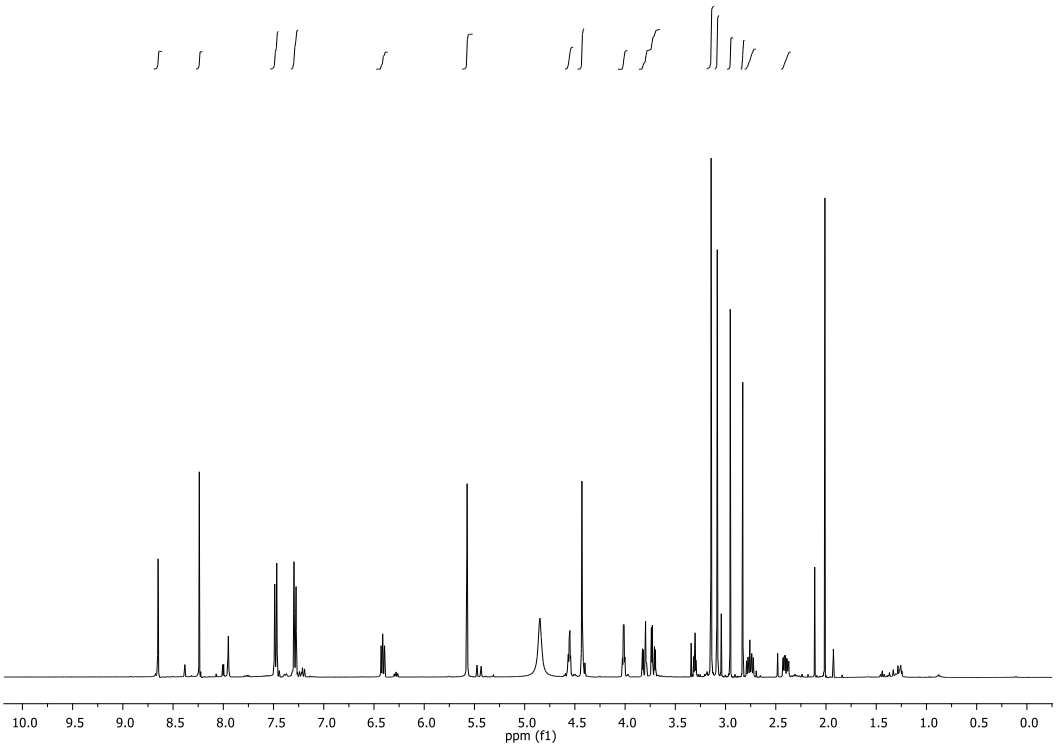
10.0 9.5 9.0 8.5 8.0 7.5 7.0 6.5 6.0 5.5 5.0 4.5 4.0 3.5 3.0 2.5 2.0 1.5 1.0 0.5 0.0
ppm (f1)

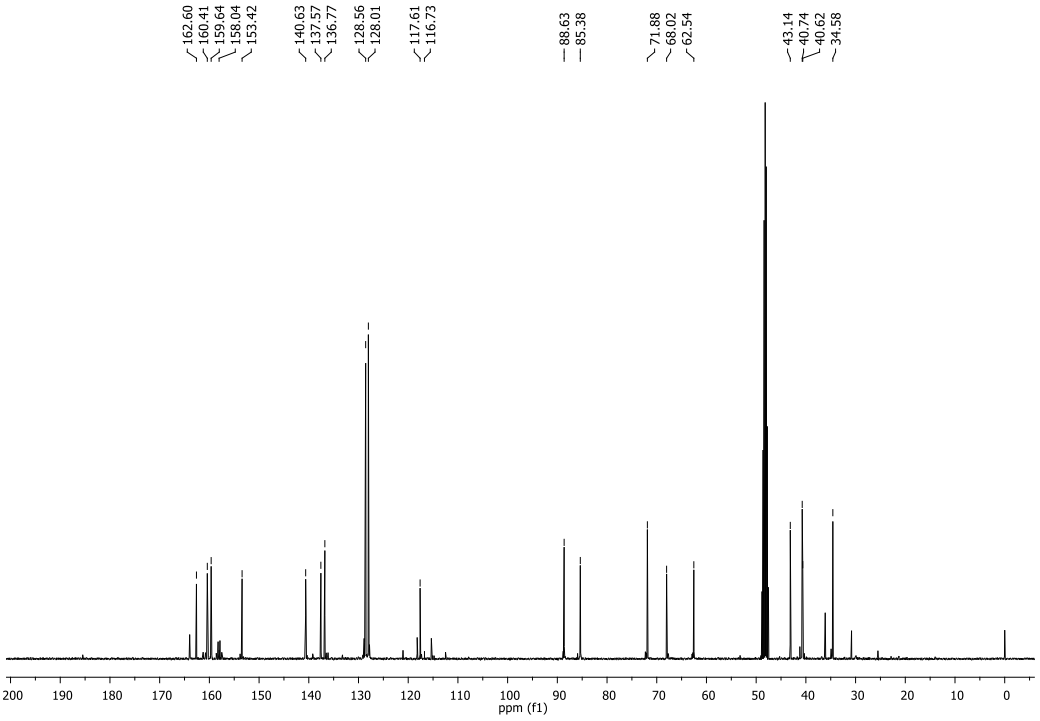
162.60
160.41
159.64
158.04
153.42
140.63
137.57
136.77
128.56
128.01
117.61
116.73
88.63
85.38
71.88
68.02
62.54
43.14
40.74
40.62
34.58
200 190 180 170 160 150 140 130 120 110 100 90 80 70 60 50 40 30 20 10 0
ppm (f1)

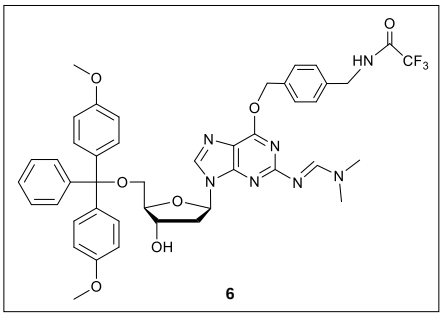
HN
O
CF3
O
N
N
N
N
N
N
O
O
O
OH
O

6

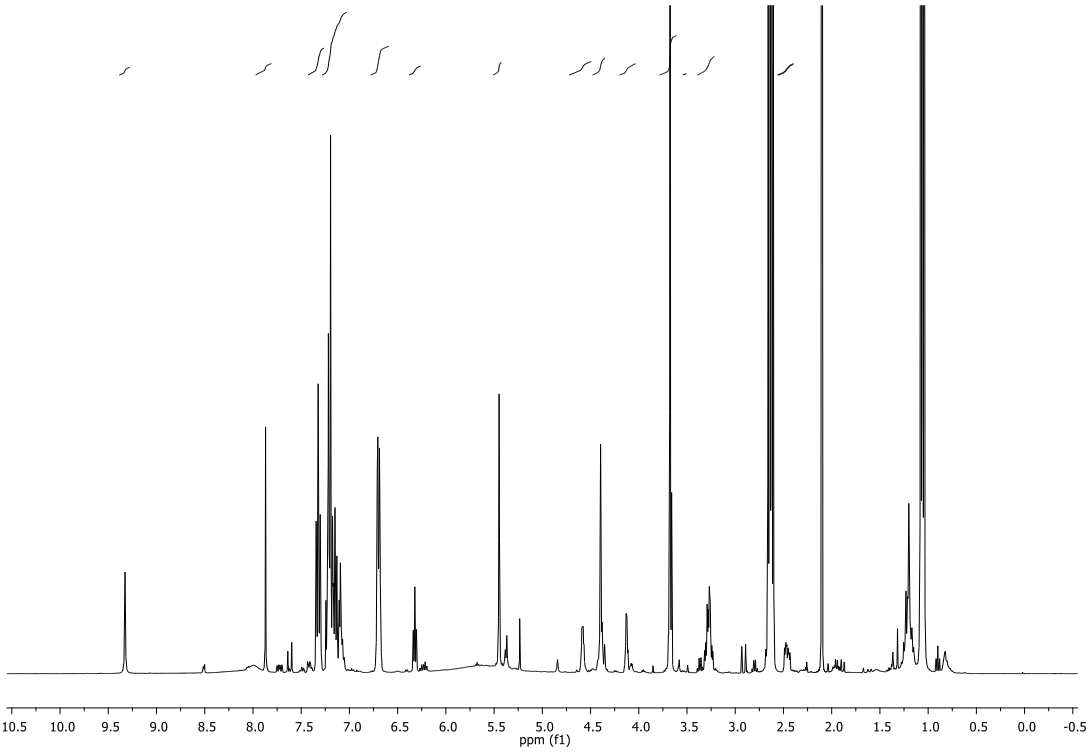
10.5
10.0
9.5
9.0
8.5
8.0
7.5
7.0
6.5
6.0
5.5
5.0
4.5
4.0
3.5
3.0
2.5
2.0
1.5
1.0
0.5
0.0
-0.5
ppm (f1)

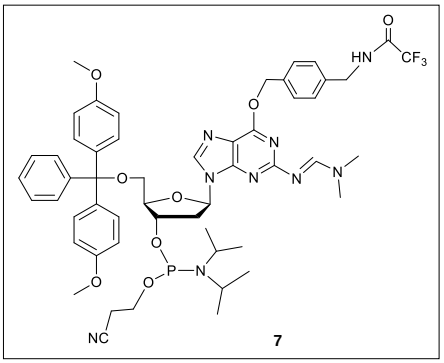
HN
O
CF3
O
N
N
N
N
N
O
O
O
O
P
N
O
O
NC

7

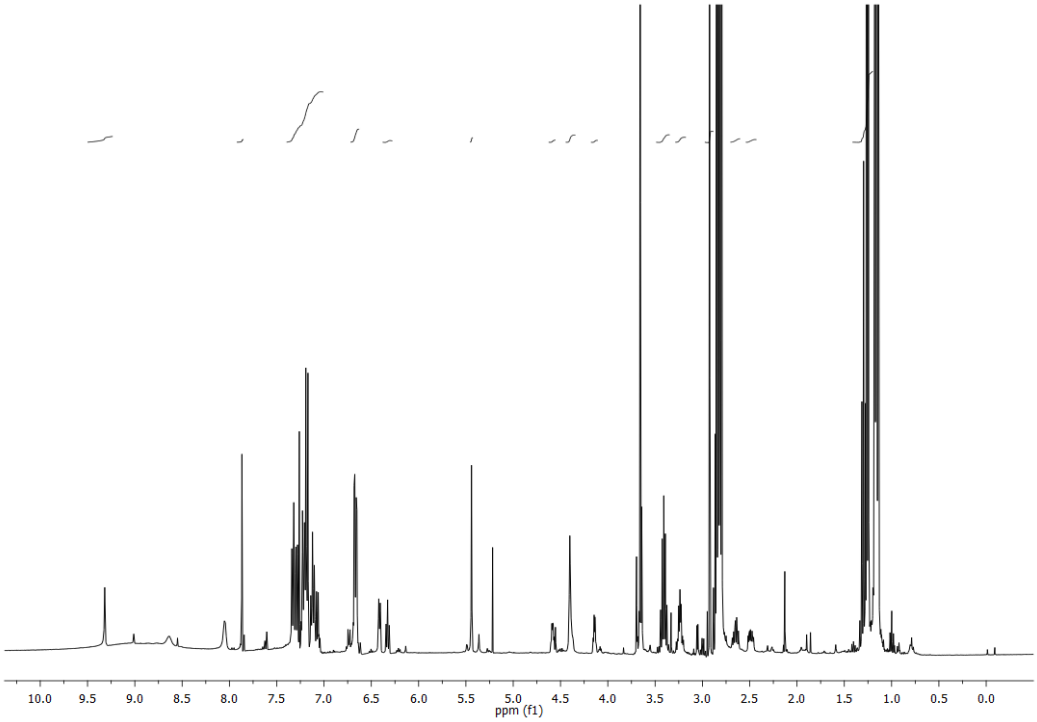
10.0
9.5
9.0
8.5
8.0
7.5
7.0
6.5
6.0
5.5
5.0
4.5
4.0
3.5
3.0
2.5
2.0
1.5
1.0
0.5
0.0
ppm (f1)

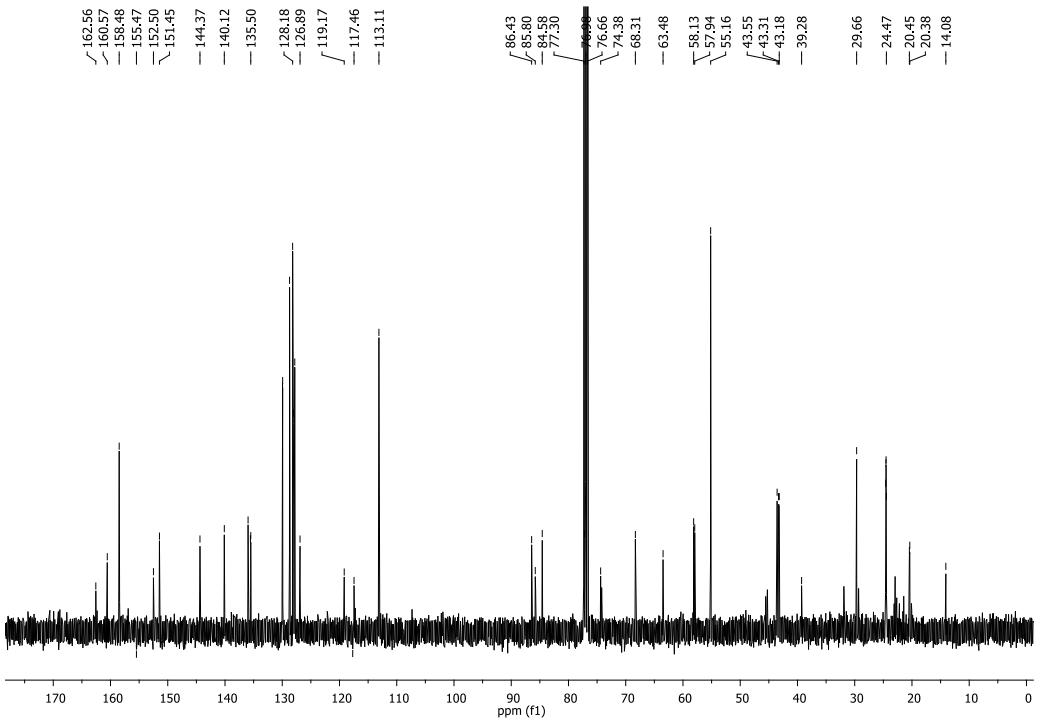
162.56
160.57
158.48
155.47
152.50
151.45
144.37
140.12
135.50
128.18
126.89
119.17
117.46
113.11
86.43
85.80
84.58
77.30
76.66
74.38
68.31
63.48
58.13
57.94
55.16
43.55
43.31
43.18
39.28
29.66
24.47
20.45
20.38
14.08
170
160
150
140
130
120
110
100
90
80
70
60
50
40
30
20
10
0
ppm (f1)

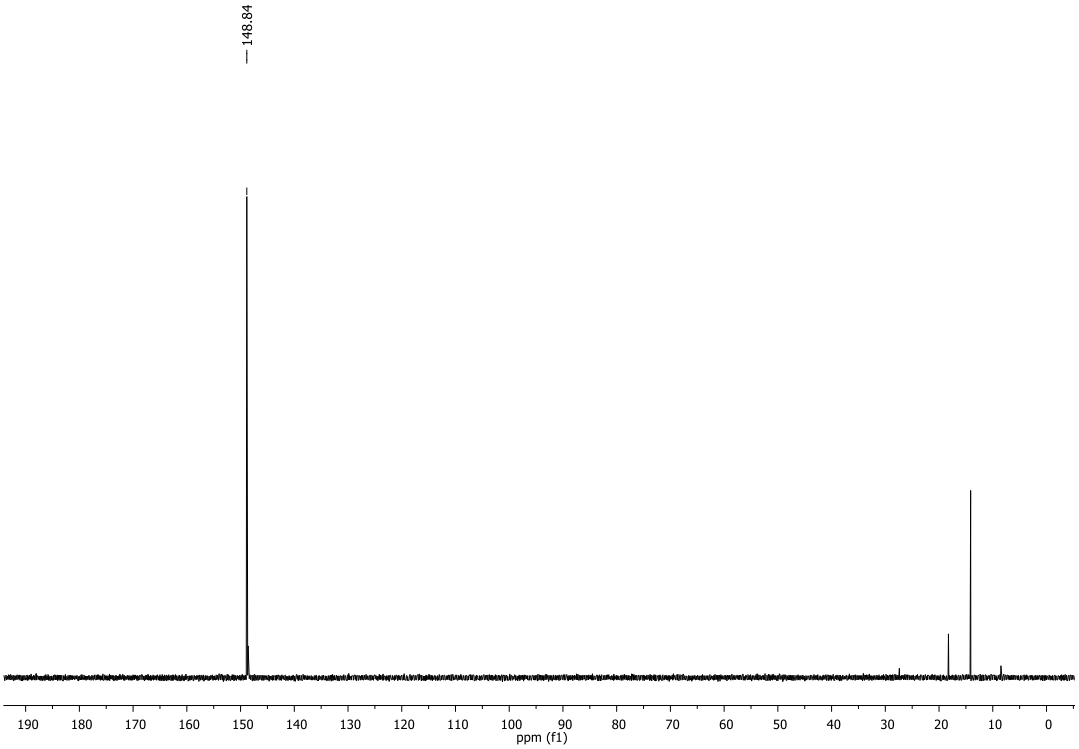
148.84
190 180 170 160 150 140 130 120 110 100 90 80 70 60 50 40 30 20 10 0
ppm (f1)

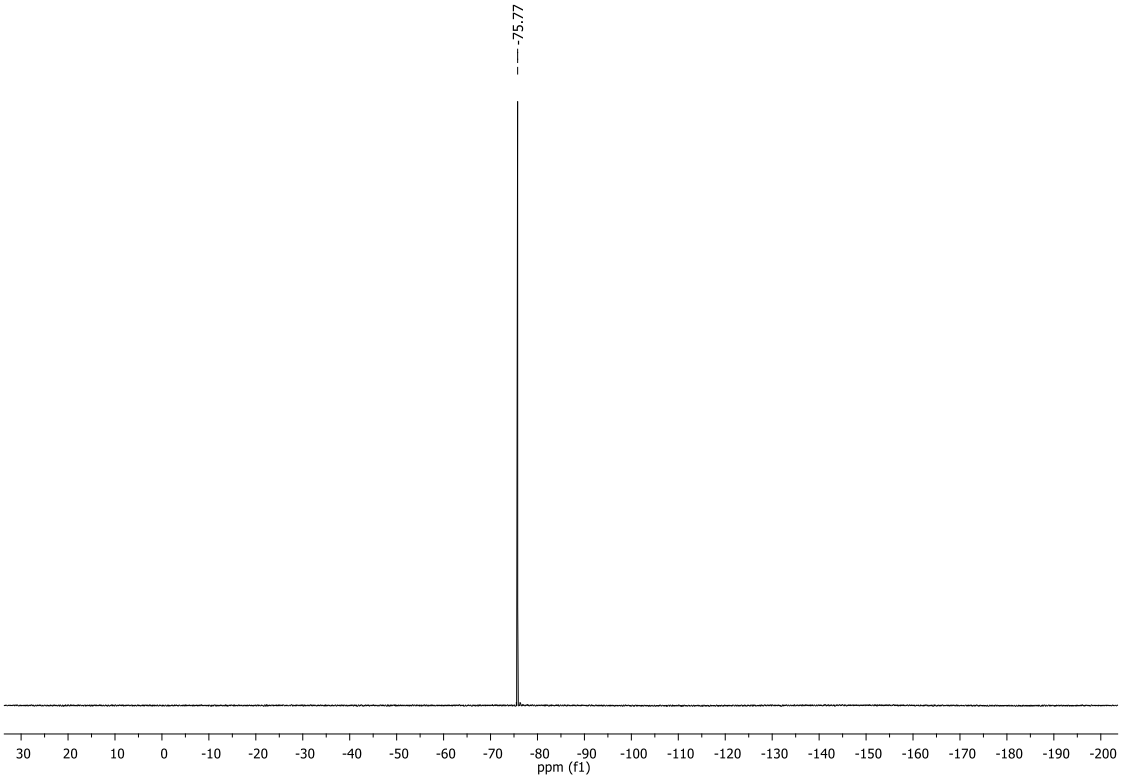
-75.77
30 20 10 0 -10 -20 -30 -40 -50 -60 -70 -80 -90 -100 -110 -120 -130 -140 -150 -160 -170 -180 -190 -200
ppm (f1)

Appendix 4

In vitro assay to evaluate potential inhibitors of hAGT by a new fluorescence method: preliminary results

In vitro assay to evaluate potential inhibitors of hAGT by a new fluorescence method

In chapter 4 we describe the development of a novel methodology to measure hAGT activity through the fluorescence transfer from a labelled alkyl-guanine to the active site of hAGT. The repair reaction produces the removal of fluorescein, which is withdrawn with the alkyl group and brought apart from the quencher group, which remains in the duplex sequence. Using this methodology, we have performed a first screening of the compounds described in chapter 1. The results obtained are preliminary, but represent a proof of concept of the usability of the assay for the evaluation of potential inhibitors of hAGT.

The assay was performed using the mismatch duplex described in chapter 4. hAGT was incubated with each compound at 30ºC during 30 minutes before adding the fluorescent duplex. Immediately, emission of fluorescence was monitored at 25ºC during 20 minutes. Figure 1 represents the kinetic data obtained for compounds 1 to 9.

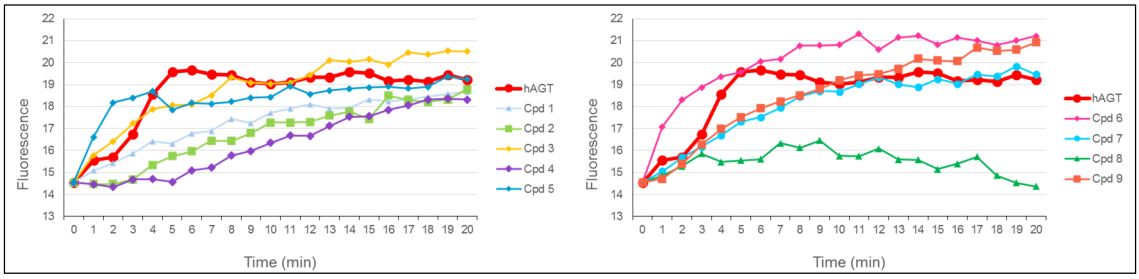

Figure 1. Kinetic data of the inhibitory activity of compounds 1 to 9.

This results suggest that compounds 1, 2, 4 and 8 may inhibit hAGT activity *in vitro*, while compounds 3, 6, 7 9 do not seem to affect hAGT activity. Compound 5 seems to slightly inhibit hAGT during the first minutes of the assay but at minute 20 seems to reach the same fluorescence as hAGT. Inhibition at 20 minutes is represented in figure 2.

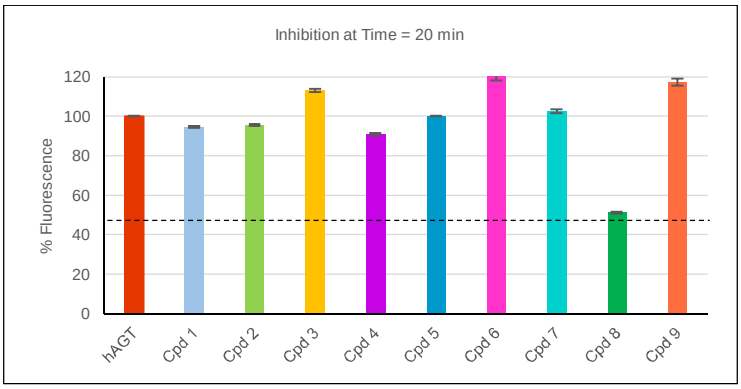

Figure 2. Inhibition of hAGT by compounds 1 to 9 at 20 min, calculated from the increase of fluorescence with respect to time 0. The basal increase of fluorescence of the duplex was subtracted from all the measurements.

Compound 8 seems to be the most promising inhibitor *in vitro*, judging by the results obtained in these experiments. This is in agreement with the results described in chapter 1, where compound 8 was found to form a complex with hAGT by ESI-MS and was observed to be non-toxic *per se* and a good enhancer of carmustine activity in cellular experiments. However, these experiments are preliminary and should be confirmed by the repetition of the assays at 37ºC.

Experimental details:

The fluorescence assay was performed using previously overexpressed and purified full-length hAGT (chapter 1). The reaction was accomplished in a total volume of 50 µl in each well, incubating 150 nM of hAGT with 750 nM of each compound (hAGT:compound 1:5) in reaction buffer (200 mM NaCl, 50 mM Tris pH 8.0, 1 mM DTT, 5 mM EDTA, 20 mM KCl). The compounds were dissolved in 1 mL of DMSO to prepare a stock concentration of 100 µM. Enough volume of each compound was added and left to incubate with hAGT during 30 minutes prior to the repair reaction with DNA. The assay was initiated by the addition of 5 µl of fluorophore-quencher duplex substrate (15 nM) and this solution was then placed in 96-well plates with black bottom (Nunc). Fluorometric measurements were performed on a spectrofluorometer Jasco FP6200 at 25ºC and with a Multi-Detection Microplate Reader SpectraMax M5 (Molecular devices BioNova cientifica, Sunnyvale, USA). Fluorescence was measured every minute for 20 min at excitation and emission wavelengths of 485 and 535 nm, respectively. Averages over three readings were taken for each condition tested. Each experiment was performed in triplicates.

Chapter 5

Molecular biosensing using gold-coated superparamagnetic nanoparticles functionalized with DNA aptamers.

Molecular biosensing using gold-coated superparamagnetic nanoparticles functionalized with DNA aptamers.

Maria Tintoré,[1] Stefania Mazzini,[2] Laura Polito,[3] Marcello Marelli,[3] Alfonso Latorre,[4] Álvaro Somoza,[4] Anna Aviñó,[1] Carme Fàbrega,[1] and Ramon Eritja[1*].

ChemBioChem, submitted

[1] IQAC-CSIC, CIBER-BBN Networking Centre on Bioengineering Biomaterials and Nanomedicine. c/ Jordi Girona 18-26. 08034 Barcelona (Spain).

[2] Department of Food, Environmental and Nutritional Sciences (DEFENS), Division of Chemistry and Molecular Biology, University of Milan,
Via Celoria 2, 20133 Milan, Italy.

[3] Institute of Molecular Science and Technologies, ISTM-CNR,
Via G. Fantoli 16/15, 20138 Milan, Italy.

[4] IMDEA Nanociencia & Nanobiotecnología (IMDEA-Nanociencia), Unidad Asociada al Centro Nacional de Biotecnología (CSIC) Madrid, Spain

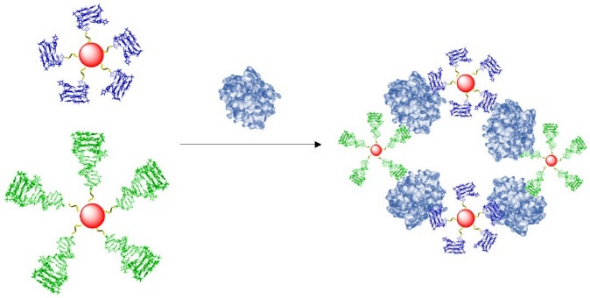

Gold and iron-based magnetic nanoparticles seem to be one of the most promising nanoparticles for biomedical applications due to their unique properties. The combination of a gold coating over a magnetic core provides the benefits from both nanoparticles, adding the magnetic properties to the robust chemistry provided by the thiol functionalization of the gold coating. In this chapter, we describe the use of gold-coated magnetic nanoparticles for molecular biosensing. Binding of α-thrombin to two aptamers conjugated to these nanoparticles causes aggregation, given that the aptamers bind cooperatively to opposite sites of the protein, forming a molecular network. This phenomenon can be observed by UV, DLS and MRI. These techniques discriminate even a single methylation in one of the aptamers, which prevents aggregation due to the inability of α-thrombin to recognize it when it is not correctly folded. A parallel study with gold and ferromagnetic nanoparticles is also detailed, concluding that the gold coating of Fe_3O_4 nanoparticle does not affect the performance of the iron-based nanoparticles and that they are suitable for the development of more complex biosensors. These results prove the high detection potency of gold coated superparamagnetic nanoparticles for biomedical applications.

This work is the result of a doctoral short stay in the University of Milan and in the CNR. The long-term objective of this detection method is to implement it as a detection method for hAGT repair activity, as it is able to detect a single methylation in guanines, the substrate for hAGT repair activity.

Molecular biosensing using gold-coated superparamagnetic nanoparticles functionalized with DNA aptamers.

Maria Tintoré,[a] Stefania Mazzini,[b] Laura Polito,[c] Marcello Marelli,[c] Alfonso Latorre,[d] Álvaro Somoza,[d] Anna Aviñó,[a] Carme Fàbrega,[a] and Ramon Eritja*[a]

Abstract: Au- and iron-based magnetic nanoparticles (NPs) are promising NPs for biomedical applications due to their unique properties. The combination of a gold coating over a magnetic core provides the benefits from adding the magnetic properties to the robust chemistry provided by the thiol functionalization of gold. Here, the use of Au-coated magnetic NPs for molecular biosensing is described for the first time. Binding of α-thrombin to two aptamers conjugated to these NPs causes aggregation, a phenomenon that can be observed by UV, DLS and MRI. These techniques discriminate a single methylation in one of the aptamers, preventing aggregation due to the inability of α-thrombin to recognize it. A parallel study with gold and ferromagnetic NPs is detailed, concluding that the Au coating of Fe3O4 NP does not affect their performance and that they are suitable for the development of complex biosensors. These results prove the high detection potency of Au-coated SPIONs for biomedical applications.

Introduction

In recent years, a great variety of chemical methods has been developed to synthesize functionalized nanoparticles for biomedical applications such as drug delivery, cancer therapy, diagnostics, tissue engineering and molecular biology, and the structure-function relationship of these functionalized nanoparticles has been extensively examined.[1]

In particular, the controlled assembly of gold nanoparticles (AuNPs) has been a subject of great interest over the past decade due to the potential applications of these particles in nanobiotechnology.[2] Their unique physical properties,[3] particularly their localized surface plasmon resonance (LSPR) and their efficient interaction with molecules with a free thiol group make AuNPs attractive building blocks for nanoscale electronic and photonic devices.[4] Since the first DNA sensor was designed by Mirkin and co-workers,[5] the development of AuNPs-based colorimetric biosensors has been increasingly applied for the detection of a large variety of targets, including nucleic acids, proteins, saccharides, small molecules, metal ions, and even cells. This technique takes advantage of the color change that arises from the interparticle plasmon coupling during AuNP aggregation (red-to-purple or blue) or redispersion of an AuNP aggregate (purple-to-red).[2a, 2b, 2g] It is quickly becoming an important alternative to conventional detection techniques, as fluorescence-based assays, and holds great potential in clinical diagnostics, drug discovery and environmental contaminant analysis, among others.

In contrast, super paramagnetic iron oxide nanoparticles (SPIONs) possess different interesting features for nanomedicine. SPIONs are well known as innovative agents in diagnostics, due to their advantages as Magnetic Resonance Imaging (MRI) contrast agents.[6] In comparison with the traditional gadolinium-based contrast agents, SPIONs produce lower toxicity, stronger enhancement of proton relaxation and have a lower detection limit.[7] Furthermore, SPIONs have several other applications in biomedicine, especially for delivery purposes, due to their reduced size, the ability to be transported in biological systems[8] and the potential use for therapy by magnetic heating.[9]

Gold and iron-based magnetic nanoparticles (AuSPIONs) have a prominent potential in biomedical applications due to their unique properties. The combination of a gold coating over the magnetic core provides the benefits from both nanoparticles, adding the magnetic properties to the robust chemistry provided by the thiol functionalization of the gold coating. For this reason, there is an increasing interest on the synthesis and applications of this type of gold-coated nanoparticles.[8c, 8d, 10]

In this work, we describe for the first time the use of gold coated magnetic nanoparticles as molecular biosensors, through their functionalization with DNA aptamers that are recognized by the protein α-thrombin. For this purpose, we conjugated the α-thrombin binding aptamers 1 and 2 (TBA1 and TBA2), and a methylated version of TBA1 (O^6-MeG-TBA1) (Table 1) to gold-coated iron-oxide nanoparticles, to iron-oxide nanoparticles and gold nanoparticles, in order to assess the advantages of each type of NPs. The TBA1 and TBA2 sequences are known to bind cooperatively to two specific and almost opposite epitopes of α-thrombin, forming a “molecular sandwich” complex.[11] TBA1 (primarily fibrinogen-recognition

[a] M. Tintoré, Dr. A. Aviñó, Dr. C. Fàbrega, and Prof. R Eritja.
Department of Chemical and Biomolecular Nanotechnology
IQAC-CSIC, CIBER-BBN Networking Centre on Bioengineering, Biomaterials and Nanomedicine
C/Jordi Girona 18-26. 08034 Barcelona, Spain.
E-mail: : ramon.eritja@iqac.csic.es
[b] Dr. S. Mazzini,
Department of Food, Environmental and Nutritional Sciences (DEFENS), Division of Chemistry and Molecular Biology,
University of Milan,
Via Celoria 2, 20133 Milan, Italy.
[c] Dr. L. Polito, Dr. M. Marelli
Department Institute of Molecular Science and Technologies ISTM-CNR,
Via G. Fantoli 16/15, 20138 Milan, Italy
[d] Dr. A Latorre, Dr. A Somoza
IMDEA Nanociencia & Nanobiotecnología (IMDEA-Nanociencia), Asociada al Centro Nacional de Biotecnología (CSIC)
C/ Faraday 9, 28049 Madrid, Spain

exosite binding)[12] is a 15mer nucleotide composed of two G-tetrads that are connected by three edge-wise loops, forming a well-characterized intramolecular chair-like, antiparallel quadruplex. In contrast, TBA2 (29mer nucleotide, heparin-binding exosite) forms a combined quadruplex/duplex structure.[11]

Table 1. Oligonucleotide sequences of the three α-thrombin binding aptamers.

Name	Sequence
TBA1	5'-HS-T_{15}GGTTGGTGTGGTTGG-3'
TBA2	5'-HS-T_5AGTCCGTGGTAGGGCAGGTTGGGGTGACT-3'
O^6-MeG-TBA1	5'-HS-T_{15}GGTTG^{Me}GTGTGGTTGG-3'

The mixture of TBA1 and TBA2 conjugated nanoparticles should form a tridimensional network in presence of α-thrombin,[8e] as represented in Scheme 1. This interaction can be detected in a straightforward manner using three types of techniques: UV, Dynamic Light Scattering (DLS) and MRI. AuSPIONs and AuNPs have a maximum of absorbance due to their surface plasmon resonance at 520 nm that shifts to higher wavelengths when aggregation occurs and this change is easily detected by UV-spectroscopy. Aggregation of the three types of nanoparticles can be detected by DLS, measuring the main hydrodynamic diameter (HD) of the nanoparticles resulting in a huge increase when α-thrombin is added to the mixture of nanoparticles carrying the TBAs. Finally, SPIONs and AuSPIONs allow the detection of the complex between α-thrombin and the nanoparticles by means of MRI, because they are contrast agents for image enhancement.

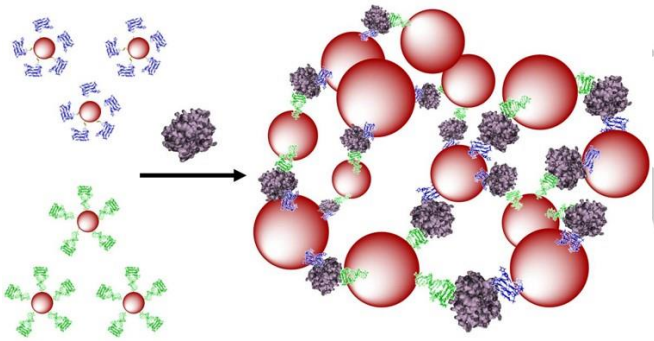

Scheme 1. Representation of the TBA-conjugated nanoparticles and the tridimensional network formation in presence of α-thrombin for the unmodified TBAs. TBA1 and TBA2 are represented folded in their chair like structure in dark blue and in green respectively α-thrombin is represented in violet.

Furthermore, we also explored the discrimination capacity of the AuSPION nanoparticles to detect a single methylation in the DNA aptamer, upon destabilizing the quadruplex structure of TBA1 by the incorporation of a methylG in one of its tetrads. In this case, the mixture does not form a tridimensional network because α-thrombin is not able to recognize this modified version of the aptamer.[13] Moreover, this inability to form the network allowed us to use this set of nanoparticles as a detection probe for a single methylation. This system can be further developed for the detection of the activity of DNA repair proteins which have alkylated guanines as substrate.

Results and Discussion

Synthesis of gold superparamagnetic iron oxide nanoparticles (AuSPION)

The preparation of the gold coated nanoparticles was performed following a process consisting of two main steps, the precipitation of the ferromagnetic seeds followed by their coating with gold acetate.[10] The precipitation of ferromagnetic seeds was obtained in good yield, and the resulting nanoparticle cores were characterized by TEM. TEM images (Figure 1A) show homogeneity in size and shape of the ferromagnetic core which is an indispensable condition to achieve the final AuSPION.

The coating of the ferromagnetic seeds with gold acetate was performed subsequently with high yield of coating. The purified gold-coated magnetic nanoparticles were analysed by TEM (Figure 1B), showing an increase of around 1.6 nm in the core diameter, which confirms that the covering was obtained successfully.

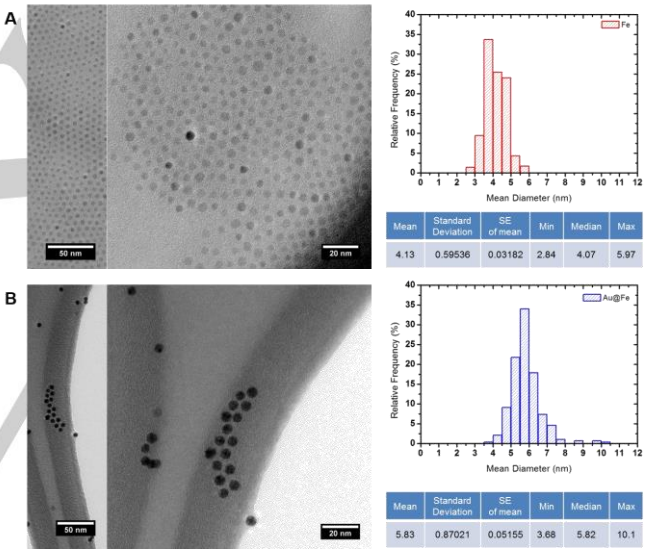

Figure 1. TEM images of the gold-coated magnetic nanoparticles, AuSPION. **A.** Images and particle size distribution of the ferromagnetic cores. **B.** Images and particle size distribution of the gold-coated SPION.

Conjugation of the AuNPs, AuSPIONs and SPIONs with TBA1, TBA2 and O^6-MeG-TBA1

TBA1 and TBA2, that bind to opposite sites of α-thrombin, and O^6-MeG-TBA1 were conjugated separately and successfully to the three types of nanoparticles selected in this work.

The conjugation of TBAs to AuNPs (commercially available) and AuSPIONs was done by incubation of NPs with thiolated-oligonucleotides followed by slow salt aging as described.[14]

The superparamagnetic nanoparticles were prepared as reported[15] and coated with dimercaptosuccinic acid (DMSA).[16] Two type of linkers (maleimide[17] and disulfide,[18] Figure 2) were used to functionalize these nanoparticles with TBAs. In order to introduce these functionalities, the carboxylate groups

of DMSA were activated using EDC/NHS and then reacted with the amino groups of the corresponding linkers bearing a maleimide or disulfide moiety. Subsequently, the resulting SPIONs were reacted with the corresponding thiolated-oligonucleotides. The degree of functionalization of SPIONs with TBAs was independent of the type of linker and they were further used indistinguishably.

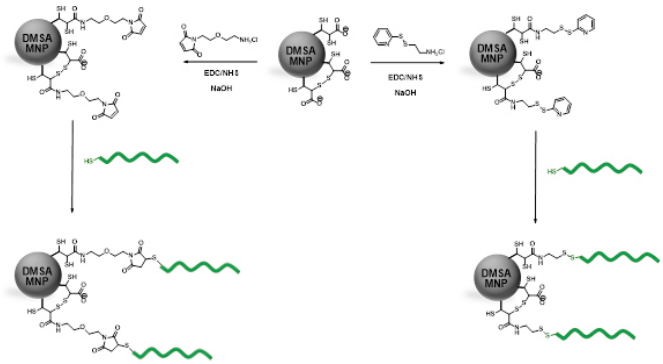

Figure 2. Schematic representation of the functionalization of SPIONs nanoparticles with TBAs (in green) using the two type of linkers maleimide (left) and disulfide (right).

The functionalization of all the nanoparticles was confirmed by the quantification of the decrease in the concentration of the oligonucleotide present in the solution, before and after conjugation (data not shown). All nanoparticles were stable after centrifugation and resuspension with aqueous buffers.

UV study of the complex formation between α-thrombin and AuNPs or AuSPIONs functionalized with TBAs

The behaviour of TBAs functionalized nanoparticles when incubated with α-thrombin was monitored by means of UV-spectroscopy observing the red-shift broadness of the surface Plasmon band. [2a, 5]

Binding interaction of the modified AuNPs-TBAs and AuSPIONs-TBAs with α-thrombin was carried out in phosphate buffer with additional K^+ at 25ºC. As expected, the UV spectrum for TBA1 and TBA2 anchored to AuNPs or AuSPIONs showed a maximum of absorption at 520 nm before incubation with α-thrombin (Figure 3). This maximum was displaced to higher wavelengths in a continuous way when α-thrombin was added, until reaching stabilization (30 nm). These results confirmed that α-thrombin was interacting with both TBA1 and TBA2, creating a NP network formed by the binding of thrombin to both TBA1 and TBA2 sequences. In addition, the formation of this network of interactions between α-thrombin and TBAs is not affected by the nature of the nanoparticles, as both AuNPs and AuSPIONs showed the same response.

In contrast, the interaction between α-thrombin and the mixture of O^6-MeG-TBA1 and TBA2 anchored to the two types of nanoparticles (AuNPs or AuSPIONs) was evidently smaller. As it can be seen in Figure 3B and 3D, at equal concentrations of α-thrombin the maximum of absorption was not changed in AuNPs (Figure 3B) or slightly displaced in Au SPIONs (Figure 3D). This small difference in the displacement rate observed in Au SPIONs (less than 10 nm), can be explained by the only interaction of AuNPs-TBA2 or AuSPIONs-TBA2 with α-thrombin. These observations proved that α-thrombin was not able to form the network with the same performance as in the case of the unmodified TBAs, and that its K_D is much higher when one guanine in the central tetrad of the TBA sequence is modified with a methyl group in the O^6 position. This simple modification prevents the formation of its quadruplex structure, and for this reason, it cannot be recognized by α-thrombin. Moreover, when we forced the concentration of α-thrombin versus TBAs (molar ratio 4:1), we could observe a small displacement of the maximum in the UV spectrum of the mixture containing the methylG-TBA1 conjugated with both types of NPs. This effect could be due to the formation of small clusters, even if in a reduced way if compared to the non-methylated mixture of TBAs (10 nm for AuSPIONs and 15 nm for AuNPs). As the protein itself is able to recognize the sequence of methylated TBA and force it to fold in its quadruplex structure suitable for the binding[13a], we presume that the methylated sequence is also recognized as a result of the excess of protein in the mixture. It is interesting to note that α-thrombin attempts to fold it and this may result in some degree of binding.

Figure 3. UV-Visible spectra of the complex formation between TBAs and α-

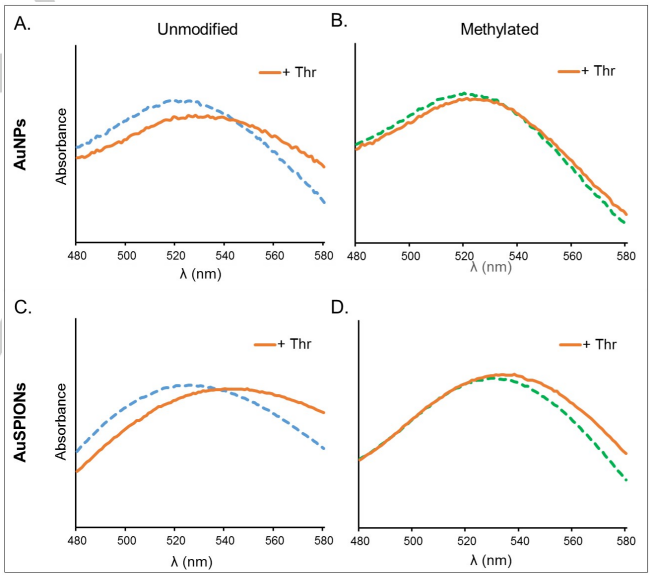

thrombin at a molar ratio of (1:1). The curves represent the mixture of NPs-TBAs in the absence (dashed lines) and in the presence (orange continuous lines) of the α-thrombin. Blue represents unmodified TBAs and green, methylated TBAs **A. and B.** display spectra recorded for AuNPs. **C.** and **D.** display spectra recorded for AuSPIONs**.**

UV seems a proper and simple way to measure the interaction between α-thrombin and the TBAs nanoparticles, as the change can be visualized within a direct step and it is not cost nor time consuming. This result confirmed that macromolecular aggregation processes can be studied indistinguishably by these two types of nanoparticles, demonstrating that the gold coating maintains the chemical and optical properties of gold itself.

DLS study of the complex formation between α-thrombin and NPs-TBAs.

The study of the complex formation between the three types of NPs-TBAs and α-thrombin by dynamic light scattering was carried out in phosphate buffer with additional K^+ at 25ºC. Figure 4 and Table 2 show the particle size distribution for the mixture of the different types of TBAs nanoparticles with and without α-thrombin. Particle size analysis was performed after the addition of α-thrombin into a mixture of TBA1 and TBA2 anchored to the three different types of nanoparticles (AuNPs, SPIONs and AuSPIONs). In all three cases the average diameter of the nanoparticles immediately increased by 25, 21.5 and 7 fold (see Table 2). Even if a small polydispersity is observed in the initial state of the mixture with AuSPION, we can clearly detect the formation of the α-thrombin-TBAs network. No precipitation was observed at these complexes concentration during the measurements. Similar results were observed for the SPIONs independently of the linker used for the functionalization.

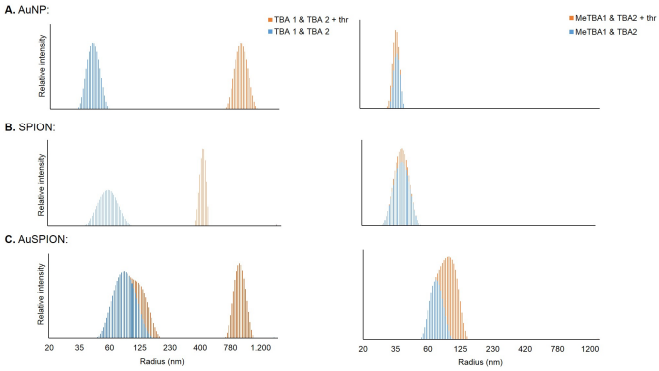

Figure 4. Particle size distribution of NPs-TBAs at 25ºC recorded by DLS. The mixtures of TBA1 and TBA2 NPs (left) and O^6-MeG-TBA1 and TBA2 NPs (right) are displayed in dashed blue, while the same NP mixtures in the presence of α-thrombin are represented in orange. In all cases, the molar ratio of α-thrombin:TBAs was 0.5:1. From top to bottom: **A.** AuNP, **B.** SPIONs and **C.** AuSPION.

In contrast, the interaction between equal concentrations of α-thrombin with the mixture of each one of the three types of O^6-MeG-TBA1 and TBA2 nanoparticles was inexistent or clearly smaller (see Table 2). These observations indicated that α-thrombin is not able to form the network with the same efficiency when the TBA1 is substituted by methylated TBA1, and thus the particle size average remains similar. In these cases, the interaction between NPs-TBA2 and α-thrombin was not identified. We presume that this may be due to the small variation in the size of the nanoparticles, which is too low to be observed by DLS.

Table 2: Size distribution (HD, nm) by DLS of TBAs nanoparticles in the absence and in the presence of α-thrombin.

Nanoparticles type		(-) α-thrombin HD (nm)	(+) α-thrombin HD (nm)
AuNPs	TBA1 & TBA2	38 ± 5	947 ± 283
	O^6-MeG-TBA1 & TBA2	38 ± 5	56 ± 7
SPIONs	TBA1 & TBA2	36 ± 5	781 ± 185
	O^6-MeG-TBA1 & TBA2	39.5 ± 11	39.5 ± 11
AuSPIONs	TBA1 & TBA2	91 ± 25	633 ± 225
	O^6-MeG-TBA1 & TBA2	91 ± 25	109 ± 34

Magnetic resonance imaging assay to compare the complex formation between α-thrombin and NPs-TBAs

The study of the complex formation between α-thrombin and the α-thrombin binding aptamers by magnetic resonance imaging was already been described by Yigit *et al*[8e]. In our work we went a step forward in the application of the MRI technique using gold-coated magnetic nanoparticles as contrast agents, studying also the effect produced in the MRI contrast when TBA1 is substituted by a methylated TBA1.

A 1:1 mixture of TBA1 or O^6-MeG-TBA1 and TBA2 anchored to SPIONs or AuSPIONs was prepared in phosphate-K^+ buffer at 25 ºC. Table 3 summarizes the formation of the molecular network due to α-thrombin binding to the nanoparticles, monitored by the changes in brightness of the T2-weighted MR images of the solution. A 2.4 ug Fe/mL concentration of the SPIONs resulted in a T2 of 50 ± 3 ms. After aggregation of the mixture by adding α-thrombin, the magnetic relaxation properties changed, reducing the T2 relaxation time to 40 ± 3 ms. Even if the concentration of the AuSPIONs nanoparticles was required to be 1000 times higher, due to the fact that the gold coating decreases the magnetic response, a similar reduction in the T2 was observed. Again, the T2 values for the mixture containing methylG-TBA1 did not decrease when α-thrombin was added, indicating that the network could not be formed. These observations are in agreement with our previous results obtained by UV and DLS studies, and prove that gold-coated magnetic nanoparticles can be used as contrast agents for MRI detection of biomolecules.

Table 3: T2 relaxation times in the absence or presence of α-thrombin. SPIONs were measured at 1/1000 (2.4 µg Fe/mL) and the AuSPIONs 1/1 (2.4 mg Fe/mL). These results represent the average of at least three independent measurements.

Nanoparticles type		Concentration of α-thrombin 0	5 nM
SPIONs	TBA1 & TBA2	50 ± 3 ms	40 ± 3 ms
	O^6-MeG-TBA1 & TBA2	51 ± 4 ms	51 ± 5 ms
AuSPIONs.	TBA1 & TBA2	70 ± 1 ms	62 ± 1 ms
	O^6-MeG-TBA1 & TBA2	63 ± 2 ms	62 ± 1 ms

Conclusions

We have obtained in high yield and purity gold-coated magnetic nanoparticles. Their functionalization with oligonucleotides is comparable with the one obtained for the gold nanoparticles. Our results prove the biosensing capacity of AuSPIONs for the first time, as they were useful for the detection of a protein by three diverse techniques. AuSPIONs were suitable for UV experiments with the same performance as AuNP, without major changes in the execution nor in the detection. AuSPIONs showed similar behaviour in DLS measurements to AuNPs and SPIONs, resulting in very similar plots of size distribution. Finally, AuSPION were useful for MRI experiments, even if they showed a shielding of the magnetic resonance due to the gold coating and required higher concentrations to reach the same signal as SPIONs.

Furthermore, this work proves that AuSPION can discriminate a normal TBA from a methylated one in the analysis of the complex formation between TBAs and α-thrombin by biophysical methods. As O^6-methylguanine is the substrate for DNA repair enzymes, critical for chemotherapy resistance, this method can also be used to monitor the activity of these DNA repair proteins. Different detection methods for the evaluation of the repair activity of one of them, alkylguanine-DNA-transferase (hAGT)[19] have been previously described.[13] These methods are also based on the conformational change of TBA upon methylation of a single guanine. Its repair restores the G-quadruplex and its recognition by α-thrombin. We envisage that AuSPIONs are useful for the development of a new methodology to detect hAGT activity in a straightforward manner. Work in this direction is currently ongoing in our laboratory. We believe that the multidisciplinary detection capacity of AuSPIONs can be evolved to design more complex biosensors for biomedical applications as well as for drug delivery and *in vivo* imaging.

Experimental Section

Abbreviations: AuNPs: gold nanoparticles, AuSPIONs: gold-coated superparamagnetic iron oxide nanoparticles, DLS: dynamic light scattering, dmf: dimethylformamidino group, DMSA: dimercaptosuccinic acid, DTT: dithiothreitol, EDC: 1-ethyl-3-(3-dimethylaminopropyl)carbodiimide, Fe_3O_4: iron oxide, hAGT: human O^6-alkylguanine-DNA alkyltransferase, HD: Hydrodynamic diameter, HPLC: high performance liquid chromatography, LSPR: localized surface plasmon resonance, MRI: magnetic resonance imaging, NHS: *N*-hydroxysuccinimide, NPs: nanoparticles, O^6-MeG: O^6-methylguanine, O^6-MeG-TBA1: O^6-methylguanine α-thrombin-binding aptamer, SPIONs: superparamagnetic iron oxide nanoparticles, T2: spin-spin relaxation time, TBA: α-thrombin-binding aptamer, TCEP·HCl: tris(2-carboxyethyl)phosphine hydrochloride, TEAAc: triethylammonium acetate, TEM: transmission electron microscopy, TMAOH: tetramethylammonium hydroxide, Tris: Tris(hydroxymethyl) aminomethane.

Chemicals:Human α-thrombin was purchased from Heamatologic Technologies Inc. All reagents and dry solvents were purchased from Sigma-Aldrich or Fluka and were used without further purification. Other chemicals from specific commercial source will be specified as they are named. Standard phosphoramidites were purchased from commercial sources. Solvents for oligonucleotide synthesis were purchased from Applied Biosystems (USA). Gold nanoparticles (10 nm) stabilized in aqueous solution of citrate were purchased from Sigma. Low binding eppendorf tubes were used in the preparation of the nanoparticles in order to avoid adsorption to the tube. Matrix for MALDI-TOF experiments were 2',4',6'-Trihydroxiacetophenone monohydrate (THAP, Aldrich) and Ammonium citrate dibasic (Fluka). Solvents for chromatographic analysis were prepared using triethylammonium acetate (TEAA, Merck) and acetonitrile (Merck) as mobile phase. Ultrapure water (Millipore, USA) was used in all experiments.

Instrumentation*:* Analytical RP-HPLC was performed using an XBridge OST C18 2.5 µm column and a Nucleosil Analytic column 120 C18 (250x4mm). Oligonucleotide sequences were detected by UV absorption at 260 nm on a JASCO V-650 instrument equipped with a thermoregulated cell holder. Mass spectra were recorded on a MALDI Voyager DE™ RP time of-flight (TOF) spectrometer (Applied Biosystems, USA). UV measurements were performed on a spectrofluorometer Jasco V-650 at 25ºC. Set temperature was controlled with an 89090A Agilent Peltier device and Hellma quartz cuvettes were used (1400 and 500 µL volume). Dynamic light scattering studies were performed on a Dynamic Light Scattering (DLS) spectrometer (LS Instruments, 3D cross correlation multiple-scattering) equipped with a He-Ne laser (632.8 nm) with variable intensity. MRI: MRI studies were carried out using a standard bore Bruker Avance AV600 spectrometer (Bruker Biospin GmbH, Rheinstetten, Germany) equipped with a 10 mm 1H micro-imaging probe and a variable-temperature control unit. Acquisition and data processing were performed with ParaVision v. 4.0 (Bruker BioSpin MRI GmbH, Ettlingen, Germany). TEM analysis was performed on a Transmission Electron Microscope (TEM) LIBRA® 200FE with an electron beam source of 200keV, a ressolution power of 0.24 nm and a magnification of 8 x - 1,000,000 x.

Oligonucleotides synthesis: The three oligonucleotide sequences (Table 1) were synthesized on an ABI 3400 DNA Synthesizer (Applied Biosystems, USA) using the 200-nmol scale synthesis and following the standard protocols. For the introduction of the thiol group at the 5'-end we used 5'-thiol modifier C6 S-S phosphoramidite from Link Technologies (Scotland, UK). For strands containing O^6-MeG, we used G^{dmf} phosphoramidite. O^6-MeG-TBA1 was deprotected in ammonia solution, overnight at room temperature. The resulting products were desalted by Sephadex G-25 (NAP-10, Amersham Biosciences, USA) and analyzed by reversed-phase HPLC. The length and homogeneity of the oligonucleotides were checked by MALDI-TOF. **$HO(CH_2)_6$-S-S-$(CH_2)_6$-T_{15}TBA1** [M]= 9617.1 (expected 9612.6), **$HO(CH_2)_6$-S-S-$(CH_2)_6$-T_{15}-O^6-MeG-TBA1** [M]=9621.4 (expected 9626.6), **$HO(CH_2)_6$-S-S-$(CH_2)_6$-T_5-TBA2** [M]=10795.5 (expected 10797.9). The DNA-strand concentration was determined by absorbance measurements at 260 nm. Oligonucleotide samples were kept dry at -20 ºC until use.

Synthesis of SPIONs: DMSA coated Fe_3O_4 nanoparticles were obtained in good yield through thermal decomposition, following the protocol reported by Salas *et. al*.[15a]

Synthesis of maleimide linker[17] *:*2-(2-aminoethoxy)ethanol (2 mL, 18 mmol) was protected with $(BOC)_2O$ in THF, followed by a standard workup. The resulting protected compound was left to react with maleimide (2.1 g, 22.5 mmol) in THF, and a freshly solution of PPh_3 (3.6 g, 13.5 mmol) and DIAD (3.6 mL, 18 mmol) following the conditions described.[17] The product was precipitated in Et_2O, filtered and purified by flash chromatography (Hexane/AcOEt 5:2 to 1:1). Then, it was deprotected with trifluoroacetic acid and purified to obtain a final yield of 89%. The resulting product had the same physical and spectroscopical properties as the one described by Weber *et. al*.[20]

Synthesis of thiopyridinyl linker (PDA*HCl).[18]: The thiopyridinyl linker was obtained following reported protocols. Briefly, to a stirred solution of aldrithiol (213 mg, 0.96 mmol) in MeOH, 2-mercaptoethylamine

hydrochloride (109 mg, 0.96 mmol) was added. After stirring 1h, the solvent was evaporated and the residue washed with cold AcOEt three times. PDA*HCl was obtained as a white solid in 51% yield. This product is the same as the one described in reference 18 and its physical and spectroscopical characterization is the same.

Functionalization of DMSA coated Fe_3O_4 nanoparticles with maleimide or PDA*HCl linker: To 1 mL of SPIONs at 2.4 mg Fe/ mL, the maleimide or PDA*HCl linker (50 mmol/g Fe), 1 equivalent of NaOH, 150 mmol of EDC/g Fe and 75 mmol of NHS/g Fe were added. This mixture was stirred at room temperature during 16 h, and was washed by iterative centrifugation and redispersion in milliQ water for at least 3 times.

Synthesis of AuSPIONs:

Synthesis of Fe_3O_4 MNP as seeds[10a]: Iron (III) acetylacetonate (0.355 g, 1 mmol) was dissolved in phenyl ether (10 mL) with oleic acid (1 mL, 3 mmol) and oleylamine (1 mL, 2 mmol) in argon atmosphere with vigorous stirring. 1,2-hexadecanediol (1.29 g, 5 mmol) was added and the solution was heated under reflux at 210 ºC for 2 hours. Then, the mixture was left to cool down to room temperature. The final solution was used in the following steps without further purification.

Reduction of Au-acetate (coating)[10b]: 2.5 mL of the Fe_3O_4 nanoparticles solution previously prepared (approximately 0.166 mmol Fe_3O_4) were diluted to a final volume of 7.5 mL in phenyl ether and mixed up with $Au(OOCCH_3)_3$ (0.55 mmol, 0.208 g), oleic acid (0.375 mmol, 0.125 mL), oleylamine (1.5 mmol, 0.75 mL) and 1,2-hexadecanediol (3 mmol, 0.775 g), under argon atmosphere with vigorous stirring. Temperature was increased following a ramp of 10ºC/min until reaching 190ºC, and the mixture was refluxed for 1.5 h. Then, AuSPIONs were precipitated with ethanol and purified by centrifugation. The precipitate was washed twice and redispersed in a 1M TMAOH solution. Then, trisodium citrate (0.04 g) was added and the pH was adjusted to 6.5. Finally, the solution was sonicated for 30 minutes, and the nanoparticles were collected using a magnet and redispersed in pure water.

Functionalization of the different type of nanoparticles:

Gold nanoparticles (AuNPs) 2-3 ODs of TBA1, -TBA2 and O^6-MeG-TBA1 were reduced with 300 uL TEAAc 0.1M and TCEP·HCl 34 uL (100 mM) at 55ºC overnight, to prevent the formation of disulfide bridges and to break the already existing ones. Next, 1 OD of the deprotected oligonucleotides were diluted in 0.5 ml of MilliQ water and were desalted with a NAP-5 column. The resulting oligonucleotide (1 mL) was mixed with 1 mL of AuNPs solution and left to conjugate overnight under agitation. Then, the solutions were brought to a final concentration of 10 mM sodium phosphate (pH 7.0). The mixtures were allowed to equilibrate before being brought to a concentration of 0.15 M NaCl stepwise over a 9 h period. The solutions were sonicated for 10 s before each addition to keep the nanoparticles dispersed during the salting procedure. The salting processes were followed by an overnight incubation at room temperature. Finally, the nanoparticles were purified by centrifugation at 13200 rpm (16100 x g) using a buffer containing 0.15M NaCl, 10 mM sodium phosphate pH 7 and NaN_3 0.01%. The centrifugation process was performed 4 times for 45 minutes at 15-20ºC. The TBAs-conjugated gold nanoparticles were analyzed by UV-visible absorption. TBAs conjugated nanoparticles were stored at 4ºC and sonicated during 5 minutes before use.

Superparamagnetic iron oxide nanoparticles (SPION): Aliquots of thiolated-aptamers (TBA1, TBA2 and O^6-Me-TBA1) for a final concentration of 245 µM were mixed with 200 µL of 2.4 mg Fe/mL Fe_3O_4 magnetic nanoparticles functionalized with maleimido and 2-thiopyridinyl groups[16] and left to react overnight at room temperature. The TBA-conjugated nanoparticles were purified by iterative centrifugation-resuspension process. The centrifugation was repeated 3 times for 30 minutes at maximum speed at room temperature and with the addition of small amounts of NaCl to enhance precipitation if required. The covalently immobilized TBA was determined by quantification of the unbound TBA in the collected supernatants. The TBAs conjugated nanoparticles were analysed by UV-visible absorption and stored at 4ºC until further use.

Gold superparamagnetic iron oxide nanoparticles (AuSPION): Equal volume of gold coated nanoparticles and thiolated DNA solution (1 OD) were mixed and left to conjugate under agitation and at room temperature for 48h. The solution followed the same salt aging process than AuNPs and the resulting suspension was centrifuged under the same conditions used for the AuNPs, resuspended in MilliQ water to remove non-conjugated oligonucleotides, and observed for any indication of aggregation. Finally, the conjugated oligonucleotides gold coated superparamagnetic nanoparticles were analyzed by UV-visible absorption. The conjugated nanoparticles were kept at 4ºC in MilliQ water until further use, due to precipitation when adding salts to the solution.

Study of the interaction between AuNPs and AuSPIONs and α-thrombin by UV: Binding between *α*-thrombin and TBA1, TBA2 and O^6-MeG-TBA1 nanoparticles was monitored by measuring changes in the UV spectrum (recorded from 650 to 400 nm) upon increasing concentrations of the protein. A mixture of NP-TBA1 and NP-TBA2 were diluted in buffer containing 10 mM phosphate pH 7 and 5 mM KCl to reach a concentration of 5 nM of nanoparticles in a volume of 500 µL. As conjugation was approximated to represent a coating of 100 oligonucleotides per nanoparticle, the concentration of DNA in the sample was considered to be around 500 nM. Each time, enough quantity (125 nM) of human α-thrombin was added. After a quick manual mix, the UV spectra were recorded. The UV spectra of the mixture and increasing concentrations of α-thrombin was recorded until reaching a final concentration of 1 uM, which represents a 2:1 molar ratio between α-thrombin and DNA. This same experiment was repeated using the modified NP-methyl TBA1 and NP-TBA2. All spectra were overlaid together to study the displacement of the maximum peak from 520 nm in case of AuNPs and 545 nm for AuSPIONs to higher wavelengths, due to the formation of a network of TBAs-α-thrombin complexes. Negative controls have been carried on by using TBA1, TBA2 and O^6-MeG-TBA1 along with increasing concentrations of hAGT and scrambled DNA along with α-thrombin. The protocol used for these studies was the same for AuNPs and for AuSPIONs.

Studies of α-thrombin interaction with TBAs nanoparticles (AuNPS, SPIONs and AuSPIONs) by DLS: Binding between α-thrombin and TBA1, TBA2 and O^6-MeG-TBA1 nanoparticles was studied by analyzing the average HD of the particles at room temperature. The molecular network originated from this binding was monitored by measuring the particles' radius enlargement upon increasing concentrations of the protein. 100 µL of a 5 nM mixture of NP-TBA1 and NP-TBA2 in buffer containing 10 mM phosphate pH 7 and 5 mM KCl were measured during 100 seconds using a 3D cross method with a scattering angle of 90º at 25ºC. Enough quantity of human α-thrombin was added to reach a 0.5:1 molar ratio between α-thrombin and DNA. After a quick manual mix, the radius length was recorded. The same experiment was repeated using the modified NP- O^6-MeG-TBA1 and NP-TBA2. The particle radius was calculated by fitting of the first cumulant parameter, and the relative intensity of the different particle complexes was calculated by fitting the contin parameter. All the experiments were performed in triplicates. The procedure of the DLS measurements was the same for AuNPs, SPIONs and AuSPIONs.

Studies of α-thrombin interaction with TBAs nanoparticles (SPIONs and AuSPIONs) by MRI: NPs-TBA1 (or NPs-O^6-MeG-TBA1) and NPs-TBA2 were mixed in 1:1 ratio and diluted in 100 mM NaCl, 25 mM KCl and 25 mM tris-HCl at pH 7.4, to reach a final concentration of nanoparticles of 2.4 µg Fe/mL in the case of the SPIONs and 2.4 mg/mL for the AuSPIONs. Then, the samples were incubated with different concentrations (0, 5, 10 and 20 nM) of α-thrombin. 100 µL of the mixed sample were loaded into a microcapillar and T2 experiments were recorded. The magnetic field strength was 14 T, corresponding to a 1 H resonance frequency of 600.1 MHz. The images were acquired at room temperature, with the following acquisition parameters: MSME (Multi Slice Multi Echo) acquisition; number of slices: 1; thickness: 1.50 mm; FOV: 0.8 mm; repetition time: 1500 ms; echo time 4.5 ms; number of echoes: 10. Two scans were performed, corresponding to a total acquisition time of 12 min. T2 values were extracted by a multi-parametric non-linear fitting y =A+B_e–t/T2 of the intensity decays. All measurements were performed three or four times in independent experiments. Acquisition and data processing were performed with ParaVision v. 4.0. The MRI measurements of the AuSPION were performed following the same protocol as the one used for the SPION.

Acknowledgements

The Communities MULTIFUN (contract NMP4-LA-2011-262943) and by "Ministerio Ciencia e Innovación" (grants CTQ-2010-20541-C03-03 and CTQ2014-52588-R) are acknowledged for financial support. M.T. was supported by a pre-doctoral fellowship (FPI) and a short stay grant (EEBB) from MINECO. C.F is grateful to Fundació La Marató de TV3 (20132032) for a research contract. We thank Dr. Susana Vilchez from the Surface Chemistry group at IQAC-CSIC for her help with the DLS experiments. LP thanks RSPPTECH – Convenzione Operativa inserita nella Raccolta Convenzioni e Contratti della Regione Lombardia (grant number 18095/RU) and the Italian Ministero dell'Università e della Ricerca (MIUR) (PRIN 2010–2011, contract number 2010JMAZML_003).

Keywords: biosensor, gold-coated superparamagnetic nanoparticles, nanotechnology, aptamers

[1] a) R. Subbiah, M. Veerapandian, K. S. Yun, *Curr. Med. Chem.* **2010**, *17*, 4559-4577; b) S. Hassan, A. V. Singh, *J. Nanosci. Nanotechnol.* **2014**, *14*, 402-414; c) A. E. Nel, L. Madler, D. Velegol, T. Xia, E. M. Hoek, P. Somasundaran, F. Klaessig, V. Castranova, M. Thompson, *Nat. Mater.* **2009**, *8*, 543-557.

[2] a) S. K. Ghosh, T. Pal, *Chem. Rev.* **2007**, *107*, 4797-4862; b) M. C. Daniel, D. Astruc, *Chem. Rev.* **2004**, *104*, 293-346; c) R. Baron, B. Willner, I. Willner, *Chem. Commun. (Camb)* **2007**, 323-332; d) E. Katz, I. Willner, *Angew. Chem. Int. Ed. Engl.* **2004**, *43*, 6042-6108; e) N. L. Rosi, C. A. Mirkin, *Chem. Rev.* **2005**, *105*, 1547-1562; f) J. J. Storhoff, C. A. Mirkin, *Chem. Rev.* **1999**, *99*, 1849-1862; g) W. Zhao, M. A. Brook, Y. Li, *ChemBioChem* **2008**, *9*, 2363-2371; h) E. C. Dreaden, A. M. Alkilany, X. Huang, C. J. Murphy, M. A. El-Sayed, *Chem Soc Rev* **2012**, *41*, 2740-2779; i) D. A. Giljohann, D. S. Seferos, W. L. Daniel, M. D. Massich, P. C. Patel, C. A. Mirkin, *Angew. Chem. Int. Ed. Engl.* **2010**, *49*, 3280-3294.

[3] S. Link, M. A. El-Sayed, *Annu. Rev. Phys. Chem.* **2003**, *54*, 331-366.

[4] a) J. H. Teichroeb, J. A. Forrest, V. Ngai, L. W. Jones, *Eur. Phys. J. E. Soft Matter.* **2006**, *21*, 19-24; b) M. Stobiecka, *Biosens. Bioelectron.* **2014**, *55*, 379-385; c) C. Ge, L. Yu, Z. Fang, L. Zeng, *Anal. Chem.* **2013**, *85*, 9343-9349; d) H. Dong, Z. Zhu, H. Ju, F. Yan, *Biosens. Bioelectron.* **2012**, *33*, 228-232; e) C. T. Ng, S. T. Dheen, W. C. Yip, C. N. Ong, B. H. Bay, L. Y. Lanry Yung, *Biomaterials* **2011**, *32*, 7609-7615; f) M. Y. Sha, H. Xu, S. G. Penn, R. Cromer, *Nanomedicine (Lond)* **2007**, *2*, 725-734; g) K. Kneipp, H. Kneipp, J. Kneipp, *Acc. Chem. Res.* **2006**, *39*, 443-450; h) S. Hwang, J. Nam, S. Jung, J. Song, H. Doh, S. Kim, *Nanomedicine (Lond)* **2014**, *9*, 2003-2022; i) W. Zhao, W. Chiuman, M. A. Brook, Y. Li, *ChemBioChem* **2007**, *8*, 727-731.

[5] R. Elghanian, J. J. Storhoff, R. C. Mucic, R. L. Letsinger, C. A. Mirkin, *Science* **1997**, *277*, 1078-1081.

[6] a) R. Weissleder, *Science* **2006**, *312*, 1168-1171; b) Z. R. Stephen, F. M. Kievit, M. Zhang, *Mater. Today* **2011**, *14*, 330-338.

[7] a) Y. X. Wang, S. M. Hussain, G. P. Krestin, *Eur. Radiol.* **2001**, *11*, 2319-2331; b) R. Weissleder, G. Elizondo, J. Wittenberg, C. A. Rabito, H. H. Bengele, L. Josephson, *Radiology* **1990**, *175*, 489-493.

[8] a) A. Z. Wang, V. Bagalkot, C. C. Vasilliou, F. Gu, F. Alexis, L. Zhang, M. Shaikh, K. Yuet, M. J. Cima, R. Langer, P. W. Kantoff, N. H. Bander, S. Jon, O. C. Farokhzad, *ChemMedChem* **2008**, *3*, 1311-1315; b) G. K. Kouassi, J. Irudayaraj, *J Nanobiotechnology* **2006**, *4*, 8; c) G. K. Kouassi, J. Irudayaraj, *Anal. Chem.* **2006**, *78*, 3234-3241; d) R. Hao, R. Xing, Z. Xu, Y. Hou, S. Gao, S. Sun, *Adv. Mater.* **2010**, *22*, 2729-2742; e) M. V. Yigit, D. Mazumdar, Y. Lu, *Bioconjug. Chem.* **2008**, *19*, 412-417.

[9] a) K. Hayashi, M. Nakamura, W. Sakamoto, T. Yogo, H. Miki, S. Ozaki, M. Abe, T. Matsumoto, K. Ishimura, *Theranostics* **2013**, *3*, 366-376; b) S. Sabale, V. Jadhav, V. Khot, X. Zhu, M. Xin, H. Chen, *J. Mater. Sci. Mater. Med.* **2015**, *26*, 5466; c) A. Hervault, N. T. Thanh, *Nanoscale* **2014**, *6*, 11553-11573; d) B. I. I.M. Obaidat, Y. Haik *Nanomaterials* **2015**, *5*, 63-89.

[10] a) I. Robinson, D. Tung le, S. Maenosono, C. Walti, N. T. Thanh, *Nanoscale* **2010**, *2*, 2624-2630; b) L. Wang, J. Luo, Q. Fan, M. Suzuki, I. S. Suzuki, M. H. Engelhard, Y. Lin, N. Kim, J. Q. Wang, C. J. Zhong, *J. Phys. Chem. B* **2005**, *109*, 21593-21601.

[11] D. M. Tasset, M. F. Kubik, W. Steiner, *J Mol Biol* **1997**, *272*, 688-698.

[12] L. C. Bock, L. C. Griffin, J. A. Latham, E. H. Vermaas, J. J. Toole, *Nature* **1992**, *355*, 564-566.

[13] a) M. Tintore, I. Gallego, B. Manning, R. Eritja, C. Fabrega, *Angew. Chem. Int. Ed. Engl.* **2013**, *52*, 7747-7750; b) M. Tintore, A. Avino, F. M. Ruiz, R. Eritja, C. Fabrega, *J Nucleic Acids* **2010**, *2010*.

[14] C. A. Mirkin, R. L. Letsinger, R. C. Mucic, J. J. Storhoff, *Nature* **1996**, *382*, 607-609.

[15] a) G. C. Salas, C.; Teran, F.J.; Miranda, R.; Serna, C.J.; Puerto Morales, M., *J. Mater. Chem.* **2012**, *22*, 21065; b) M. C. Marciello, V.; Veintemillas-Verdaguer, S.; Andrés Vergés, M.; Carrey, J.; Respaud, M.; Serna, C.J.; Puerto Morales, M., *J. Mater. Chem. B* **2013**, *1*, 5995.

[16] A. Latorre, P. Couleaud, A. Aires, A. L. Cortajarena, A. Somoza, *Eur. J. Med. Chem.* **2014**, *82*, 355-362.

[17] C. Feau, E. Klein, C. Dosche, P. Kerth, L. Lebeau, *Org. Biomol. Chem.* **2009**, *7*, 5259-5270.

[18] C. Posch, A. Latorre, M. B. Crosby, A. Celli, A. Latorre, I. Vujic, M. Sanlorenzo, G. A. Green, J. Weier, M. Zekhtser, J. Ma, G. Monico, D. H. Char, D. Jusufbegovic, K. Rappersberger, A. Somoza, S. Ortiz-Urda, *Biomed. Microdevices* **2015**, *17*, 15.

[19] A. E. Pegg, *Chem. Res. Toxicol.* **2011**, *24*, 618-639.

[20] R. W. Weber, R. H. Boutin, M. A. Nedelman, J. Lister-James, R. T. Dean, *Bioconjug. Chem.* **1990**, *1*, 431-437.

FULL PAPER

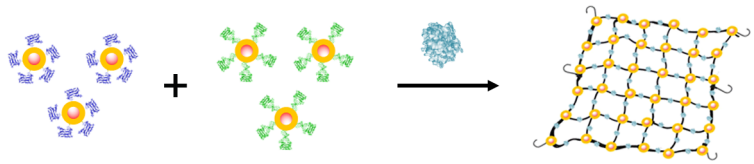

Gold coated magnetic nanoparticles combine the magnetic properties of iron and the robust chemistry provided by the thiol functionalization of gold. Their good performance in the detection of a protein-aptamer complex formation by biophysical techniques make them suitable for the development of biosensors for biomedical applications.

Maria Tintoré, Stefania Mazzini, Laura Polito, Marcello Marelli, Alfonso Latorre, Álvaro Somoza, Anna Aviñó, Carme Fàbrega, and Ramon Eritja.*

Page No. – Page No.

Molecular biosensing using gold-coated superparamagnetic nanoparticles functionalized with DNA aptamers.

General discussion

Cellular resistance to alkylating agents is a major drawback for the treatment of cancer patients.[1] One of the mechanisms responsible for this resistance is the overexpression of DNA repair enzymes, which revert the lesions produced by these chemotherapeutic drugs and lead to tumoral cell survival.[2] In particular, the human O^6-alkylguanine-DNA-alkyltransferase[3] is a DNA repair protein that removes alkyl groups from the O^6 position of guanines, restoring the DNA. For this reason, this protein represents a relevant pharmacological target in the fight against chemotherapy resistance for patients' survival.[4] In addition, the level of expression of hAGT has shown to be a prognosis biomarker of poor survival in patients who suffer from malignant gliomas.[5]

Given the relevance of hAGT as a therapeutic target, several methods are available to characterise its repair activity. Moreover, they are also able to evaluate the capacity of small molecules of inhibiting hAGT.[6] Most of these methods involve radioactivity assays,[6b, 6e] while others are based on multiple-step enzymatic reactions.[6a, 6c, 6d] However, the first methods are dangerous and require the use of rigorous safety procedures, and the others are discontinuous and time-consuming due to the necessity of multiple steps. The lack of a straightforward, rapid and costless assay to study hAGT repair activity represents a limiting step in the search of potential inhibitors as chemotherapy enhancers.

Over the last years, different small molecules with hAGT inhibitory capacity have been described, although all of them are pseudosubstrates. For example, O^6-benzylguanine (O^6-BG) inactivates hAGT *in vitro* and *in vivo*,[7] and has shown to improve the effectiveness of chloroethylating agents in clinical trials.[8] However, despite its potential for therapeutic inhibition of hAGT, there are considerable limitations in current inhibitors such as O^6-BG. First, O^6-BG has little affinity for hAGT, if compared with the affinity of O^6-alkylguanine incorporated into double stranded DNA.[9] Second, O^6-BG has low bioavailability, very low water solubility and a very high plasma clearance. In addition, clinical trials phase I and II have shown that it is very likely to produce myelosuppression.[10] A new derivative of guanine, lomeguatrib [6-(4-bromo-2-thienyl)methoxy]-purine-2-amino], was proven to be more active *in vitro* than O^6-BG.[11] The O^6-thienyl analogue was tested in phase I and II clinical trials in combination with temozolomide and, as well as O^6-BG, did not significantly increase the cytotoxic effect associated with the chemotherapeutic agent *per se*, but also caused myelosuppression.[12]

Later on, many compounds initially thought to be hAGT inhibitors have proven to be checkpoint inhibitors instead[13] and only O^6-BG is currently on the market. *In vitro* studies of O^6-(4-bromo-2-thienyl)-guanine (PaTrin-2 or PAT), a pseudosubstrate inactivator of hAGT, showed greater potency than O^6-BG. However, it causes dose-limiting

toxicities when administered with TMZ.[14] Other novel approaches to hAGT inhibition are also being studied with promising results.[13, 15]

The main objective of this thesis was the finding of new small molecules capable of inhibiting hAGT activity, to be used as chemotherapy enhancers. Due to the lack of a robust *in vitro* method to evaluate hAGT activity, we have devoted a substantial part of this thesis to the development of such method, trying to avoid radioactivity and complex multi-step reactions.

For all the *in vitro* assays and complex formation experiments described in this thesis, recombinant hAGT was used, which was overexpressed and purified following the protocols described by Ruiz *et al*.[6e] Two different constructs of hAGT were used: hAGT-FL, the human full-length protein and hAGT ΔC177-C145S, a mutant of hAGT where the cysteine of the active site was replaced by a serine, making hAGT loose its repair activity but maintaining its capacity to recognize and bind alkylguanine-DNA. The sequence of this mutant is 30 amino acids shorter than hAGT FL but preserves the folding. This modification was done to facilitate its overexpression and manipulation. This hAGT mutant was overexpressed and purified in order to use it as a negative control for the different *in vitro* assays.

Previously, a virtual screening for the selection of potential compounds candidates to interact with the active site of hAGT was realized in our group in collaboration with the Bioinformatics Unit of the CMBSO. A set of 10 compounds was selected and purchased from commercial sources. The standard procedure to evaluate the compounds would be to start by an *in vitro* evaluation of their capacity to inhibit hAGT and subsequently assess their toxicity and effectiveness *in vivo.* However, as detailed before, we do not have an adequate *in vitro* assay available currently and for this reason we started by the cell culture experiments and by the study of their ability to form a complex with hAGT by mass spectrometry.

The mass experiments realized allowed us to detect the complex formation between hAGT and 5 out of the 10 compounds studied. These results also showed that one of them (compound 8) formed a specific complex and the other four (compounds 5, 6, 7 and 9), non-specific ones. From the five compounds that showed no interaction with hAGT, one of them (compound 10) caused precipitation of hAGT immediately and did not permit the study of the complex formation. Another compound (4) showed an alteration in hAGT's mass spectrum, indicating that they interact in such a way that it destabilized in some degree its structure.

We then tested the toxicity and effectiveness of these potential inhibitors in cell culture through MTT assays in human colorectal adenocarcinoma cells. The results obtained are discussed extensively in chapter 1.

The toxicity of the 10 potential inhibitors was studied in cell culture. Two out of the ten compounds (5 and 8) were found to be non-toxic, and the other eight compounds were toxic at different concentrations. From them, three (2, 4 and 7) were toxic at LD_{50} values lower than 100 μM. Regarding their enhancement of carmustine (BCNU) toxicity, compounds 5 and 8, which were non-toxic *per se*, were found to enhance significantly the effect of carmustine, as well as compounds 4, 6 and 7 but these three were toxic. Compounds 1, 2 and 3 exhibited a relative capacity to stimulate cell death caused by carmustine and in contrast, compounds 9 and 10 were unable to increase the effect of carmustine significantly. We performed colony formation assays staining with crystal violet with compounds 5 and 8 (non-toxic and enhance BCNU in the MTT assay) and 6 and 7 (toxic at 1 μM but good enhancement of carmustine). These experiments imply the study of the recovery of the cells after treatment with the compounds in presence or absence of carmustine, and their capacity to survive and grow during the following 10 days after treatment. The results obtained are more difficult to interpret and seem to contradict in some ways the experiments of MTT: all the tested compounds except compound 5 were found to be non-toxic, allowing the growing of colonies to normal values after 7 days. In contrast, compound 5 presented a progressive reduction of colonies over concentration of potential inhibitor. These results indicate that cells are able to recover from the treatment after some days and redeem their rate of growing, except in the case of compound 5. However, their enhancement of Carmustine followed a different pattern: compounds 5, 7 and 8 improved the rate of cell death and poor survival, while compound 6 did not show a stimulating effect on carmustine. Even though, the colony formation assays are preliminary and should be reproduced before considering these results conclusive, as for example carmustine effect in the compound 6 assay did not seem to be in the same range as shown in the other assays.

From these results, we can pre-establish that compounds 8 seems to be the best candidate to enhance the effect of BCNU in cell culture, as it was found to be non-toxic at 100 μM and improved the rate of cell death when incubated with Carmustine, both in the MTT and in the colony formation assay. In addition, compound 5 showed no toxicity and good enhancement of carmustine, but it was found to be toxic in colony formation assays.

Combining the results obtained by ESI-MS and in cell culture, we can conclude that 2 compounds out of our first ten are able to form a specific (8) or non-specific (5) complex

with hAGT and are non-toxic. In addition, they seem to enhance the apoptotic effect of Carmustine in MTT and colony formation experiments, even if compound 5 was found to be toxic. These compounds represent good candidates for the study of their hAGT inhibition effect as potential chemotherapy enhancers. Following the line of this thesis, these potential inhibitors should be tested by the methods described subsequently to reveal their active concentrations and their suitability to undergo a new optimization cycle to obtain a good candidate to start preclinical studies in animal models.

At the end of this chapter, we include as an annex a work we have realized related to the search for inhibitors of another DNA repair protein, Ape1,[16] involved in the base excision repair pathway.[17] This paper reports the identification of new compounds as potential Ape1 inhibitors through a docking-based virtual screening, following by a characterization of them by similar *in vitro* techniques and cytotoxic evaluating assays as the ones described in chapter 1 for hAGT. Interaction of these compounds with the Ape1 protein was observed by mass spectrometry, and some of the compounds showed *in vitro* activities in the low-to-medium micromolar range. The ability of the candidates to inhibit the recombinant Ape1 activity *in vitro* was determined by a fluorescence-based assay described by different groups.[18] These molecules also potentiated the cytotoxicity of the chemotherapeutic agent methylmethanesulfonate in fibrosarcoma cells.

We then intended to evaluate the inhibitory capacity of the candidate molecules *in vitro*. The first intention was to employ the radioactivity assay used by Ruiz *et. al.*[6e] and firstly described by Bresnick and coworkers[19] for the *in vitro* evaluation of compounds. However, the radioactive compound used, ^{3}H-MNU (tritiated methylnitrosourea), was no longer commercially available. Other radioactivity-based assays are described, but in addition to being multi-enzymatic reactions, they require the use of rigorous safety procedures.[6b] Other assays, as ESI-MS-based experiments,[20] electrophoretic mobility shift assays[21] or HPLC assays[22] have also been conducted with the aim of studying hAGT repair. Mass spectrometry and electrophoretic detection of repaired oligonucleotides were most efficient in the case of interstrand cross-linked DNA, due to the fact that the repaired oligonucleotide without a cross-link to the complementary strand has a lower mass than the two strands covalently cross-linked, after forcing the denaturation of the duplex.[20b, 21b] Other assays reported the inhibition of restriction endonuclease followed by magnetic bead separation of products.[6a, 6d] Furthermore, a fluorescence assay was reported by Moser et al, proving useful and sensible detection of hAGT activity but it implied the use of a digestion step for the release of the fluorescent moiety.[6c] All these methods are based on multi-step complex reactions and are discontinuous and time-

consuming and the necessity to find a straightforward and sensible method for the detection of hAGT repair activity remains relevant.

For this reason, we have devoted a great effort and the main part of this thesis to the development of new *in vitro* assays for the detection of hAGT activity which allow to evaluate its inhibition by the candidate compounds. We have exploited all the resources and techniques of expertise available in our research group, whose field of interest is the chemistry and structure of nucleic acids and the application of DNA nanotechnology to biomedicine.

Chapter 2 describes a method to evaluate hAGT activity that takes advantage of the conformational change of a single stranded DNA quadruplex,[23] the thrombin binding aptamer (TBA),[24] an aptamer that is recognized by α-thrombin when it is folded into its quadruplex structure. First, we demonstrated by UV monitoring of the thermal stability of the quadruplex and by circular dichroism that the replacement of a single guanine by an O^6-methylguanine disrupts the G-quadruplex native structure of TBA, because it diminishes the amount of chemical groups available for the Hoogsteen hydrogen bonding that forms the G-quartets.

The conformational change of this G-quadruplex was used to develop a fluorescence-quencher system that reduces the emission of fluorescence when hAGT repairs the methylation introduced previously. The fluorophor and the quencher molecule were placed in opposite ends of the sequence, and the distance between them depends on its conformation: the native TBA is folded into its quadruplex structure, forcing the proximity of the fluorophor and the quencher whilst the methylated TBA, being unable to fold the quadruplex, maintains its ends in opposite senses and the fluorophor and the quencher are kept apart from each other. The reaction of hAGT represents the key to the folding and unfolding of TBA and thus to the emission or suppression of fluorescence.

Even if the methodology is rapid, simple and avoids the use of radioactivity, it had an unexpected drawback: the measurement of the loss of fluorescence was slightly delicate, as it is always more difficult to detect and reproduce a particular loss of signal than an increase of it from basal conditions. These deliberations led us to consider the robustness of this new methodology in terms of being able to implement it for the search of more potent inhibitors of hAGT activity.

For this reason, taking advantage of the expertise of other members of the laboratory in DNA Nanotechnology and making use of the conclusion obtained in chapter 2 about the distortion of the G-quadruplex when a guanine is replaced by a methylguanine,

we designed a DNA origami platform[25] as a nanotechnological device to detect hAGT activity. The DNA origami had previously been applied as platform to follow single molecule reactions,[26] even for the detection of conformational changes of a G-quadruplexes,[27] for DNA repair proteins' reaction tracking[28] and for spatial organization of proteins[29] or other nanomaterials.[30] All these advances in DNA nanotechnology lead us to envisage a new platform for hAGT repair study using DNA origami. This method is described in chapter 3. We exploited the spatial addressability of DNA origami in combination with the conformational change of a DNA G-quadruplex, TBA, to detect by AFM in real-time the complex formation with its substrate α-thrombin. This structural change is caused by a single methylation in the central guanines, as reported in chapter 2, and it causes that TBA is no longer recognized by α-thrombin. This fact was demonstrated by fluorescence and EMSA assays, and both results confirmed that the introduction of a methylated guanine prevented α-thrombin interaction, and besides, that a concentration of 10 fold of α-thrombin can be sufficient to appreciate a different pattern of union of this protein to the TBAs and methyl-TBAs-containing origami. The different behaviour of α-thrombin towards the TBA and the methylated TBA can be utilised to detect the DNA repair activity of hAGT, given that methylguanine is the substrate of this protein. In this case, we used two different types of TBA, which bind at opposite exosites of α-thrombin in a cooperative way[24] and improved the attachment of the proteins over the DNA origami, preventing the sweeping away by the AFM tip. The arrangement of α-thrombin over the surface of the DNA origami follows the distance-dependent design described by Rinker *et. al*,[29b] who found that upon placing the two aptamers at a specific distance of 5.8 nm from each other, the recognition of the protein increased by 10-fold. The introduction of several methylated TBAs in specific positions of the origami allowed to observe the loss of thrombin binding. We proved that only one of the aptamers of the pair being methylated was enough to disrupt the binding, and no α-thrombin interaction was observed by AFM while the control pairs of unmodified aptamers exhibited high rate of binding. When the O^6-methylguanine of the modified TBA was repaired by hAGT, α-thrombin was able to bind again to the repaired aptamers, as they can form the quadruplex structure required for interaction. The system is extremely effective and reliable, and the results are clearly followed by AFM. Their consistency suggests that our system could be further evolved for the study of other DNA repair enzymes. Even though, the complexity and high cost of the AFM technique hinders the application of this technology for the high throughput evaluation of potential inhibitors of hAGT.

As a result of the high impact achieved by the publication of this work, our group was invited to write a review on the state of the art of DNA nanotechnology. This work is

included as an annex of this chapter. In this review we examine recent progresses towards the potential use of DNA nanostructures for molecular and cellular biology.

In parallel, we developed a second fluorescence assay which tried to address the limitations found before (chapter 4). Studying the mechanism of action of hAGT and some reports in the literature where it is described that hAGT is more active over double stranded DNA,[31] we decided to use a double stranded oligonucleotide with a labelled alkylated guanine which could be transferred to the active site of hAGT upon DNA repair and could be quantified. This would represent a direct measurement of the activity of the protein and could be used to evaluate the effect of potential inhibitors. We synthesized a double stranded oligonucleotide where one of the two strands incorporated an alkyl-guanosine chemically modified in the O^6 position with an aminobenzyl group. We used this group because O^6-benzylguanine is reported to be the most efficiently repaired bulky adduct by hAGT[31-32] and the free amino group in the *para* position allowed the post-synthetic chemical introduction of a fluorophore (fluorescein isothiocyanate, FITC). This work implied the design of a novel synthetic route for the properly protected O^6-benzylguanosine to incorporate it to the automatized DNA synthesis cycle. This O^6-benzylguanosine was prepared from 2'-deoxyguanosine and the corresponding protected 4-aminomethylbenzyl alcohol through a Mitsunobu reaction.[33] Prior to the setting up of the fluorescence assay, we conducted HPLC studies of the repair capability of hAGT of this O^6-benzylguanine with the attached fluorescein, to ensure that this bulky substituent can be accommodated in the active site of the protein. Post-synthetically, we attached a fluorophore to this aminobenzyl group to follow the repair reaction by means of fluorescence. We incorporated a nucleotide modified with a quencher group in the complementary strand to reach very low basal fluorescence when the two strands are annealed. Two options were explored to ensure the maximal quenching of fluorescence for the background conditions of the assay: in one case, the quencher was placed in the exact complementary position, and in the other, at one nucleotide shift in the complementary sequence. The placement of the quencher in the complementary base of the modified guanosine provokes a mismatch in the sequence, due to the fact that there is no commercially available cytidine covalently modified with the dabcyl group and the use of a thymidine was required. In the case of the complementary duplex, we expected that the fluorescence extinction would remain efficient even if the quencher was not placed in the complementary position. As spatial orientation of this bulky substituents remains unclear, both were studied in terms of thermal stability and capacity to enter hAGT's active site, and finally the complementary duplex was used for the fluorescence assays because it remained stable at the temperature range required for the efficient reaction of hAGT. As

expected, once hAGT repaired the O^6 alkylguanine, it transferred the fluorophore to its active site together with the alkyl group, bringing it apart from the quencher. This resulted in an immediate increase in fluorescence that could be detected and correlated to hAGT activity. In contrast with the previous methods, and as it has been mentioned before, this system uses a double stranded oligonucleotide, which is the real substrate for the activity of hAGT *in vivo* and thus increases the efficiency of the repair reaction. In addition, as the variation in fluorescence is increasing upon activity, it is easier to quantify than the loss of fluorescence measured before. This method is currently ready to be used for the study of potential hAGT inhibitors, and some preliminary results are shown in the annex 4. These results point to compound 8 as a promising candidate to inhibit hAGT *in vitro,* which is in consonance with the results obtained in chapter 1, where it was found to form a specific complex with hAGT, to be non-toxic *per se* and to produce a significant enhancement of carmustine toxicity.

A similar approach had been described for the preparation of a fluorescent derivative of O^6-benzylguanine to be used in the detection of the hAGT activity in cells.[34] In these experiments, the O^6-alkylnucleobase is allowed to enter the cells by passive diffusion and after a certain time the excess of the fluorescent nucleobase is washed away and the remaining fluorescence measured. This remaining fluorescence inside the cells corresponds to the hAGT which has reacted, becoming fluorescently labeled. In our case, we need to evaluate in real-time the activity of hAGT and for this reason, we had to introduce the fluorescently labeled nucleoside in a DNA sequence, as well as we require the quencher molecule to be in the complementary sequence to enhance the change of fluorescence when the fluorescein molecule is transferred to hAGT. Our approach represents a more complex system which allows to measure *in vitro* the activity of hAGT in real-time.

Following with the nanotechnology, and during a short stay in the Department of Food, Environmental and Nutrition Sciences of the University of Milan, we studied the use of gold-coated magnetic nanoparticles for molecular biosensing. Binding of α-thrombin to these nanoparticles conjugated with two aptamers which recognize different sites of the protein causes aggregation,[35] a phenomenon that can be detected by three different techniques: UV, DLS and MRI. These techniques discriminate even a single methylation in one of the aptamers, preventing aggregation due to the inability of α-thrombin to recognize it. This system can be further developed for the detection of the activity of DNA repair proteins which have alkylated guanines as substrate.

We conjugated the thrombin binding aptamers 1 and 2 to gold nanoparticles (AuNPs) iron-oxide nanoparticles (SPION) and gold-coated iron-oxide (AuSPION) nanoparticles, and then comparatively studied the ability of α-thrombin to recognize a mixture of methylated and unmethylated TBA-conjugated nanoparticles. The mixture containing unmodified TBAs was able to bind α-thrombin in its both recognizing sites, forming a molecular network. In contrast, the methylated TBA1 together with the unmodified TBA2 was unable to form the network, and the aggregation process did not occur.

SPION and AuSPION allow the detection of α-thrombin by means of Magnetic Resonance Imagining, because they are contrast agents for image enhancement. The unmodified mixture of TBAs is able to interact with α-thrombin and a molecular network is formed, increasing the image contrast and its T_2 value, as reported previously.[35] AuSPION and AuNP have a surface plasmon maximum at 520 nm that shifts to higher wavelengths when precipitation occurs, allowing the use of UV-spectroscopy as a detection method. Other works have previously exploited this feature to develop biosensors for lipase activity,[36] to monitor oxidative stress[37] or to detect blood cholesterol,[38] between others. And finally, precipitation of the three types of nanoparticles can be detected by Dynamic Light Scattering, measuring the main diameter of the nanoparticles before and after thrombin addition and finding a huge increase in the case of the unmodified mixture of nanoparticles. Aggregation detected by DLS has also been used before to develop sensors for cancer biomarkers,[39] or for the detection of small molecules in solution.[40] However, this is the first time that the same nanoparticles (AuSPIONs) can be used to detect a protein by the three techniques indistinguishably, due to the combination of features provided by the magnetic core and the gold coating.

Given that the repair activity of this methylation by hAGT would imply an aggregation of the nanoparticles as a result of the dealkylation process, this platforms could be evolved to design a new methodology to detect hAGT activity. We have set the bases for this multidisciplinary methodology, allowing its use for a development of a new straight-forward and single-step assay for hAGT activity and for the testing of potential inhibitors.

References:

[1] Y. Huang, L. Li, *Transl Cancer Res* **2013**, *2*, 144-154.

[2] M. R. Middleton, G. P. Margison, *Lancet Oncol* **2003**, *4*, 37-44.

[3] a) D. S. Daniels, T. T. Woo, K. X. Luu, D. M. Noll, N. D. Clarke, A. E. Pegg, J. A. Tainer, *Nat Struct Mol Biol* **2004**, *11*, 714-720; b) D. S. Daniels, J. A. Tainer, *Mutat Res* **2000**, *460*, 151-163; c) D. S. Daniels, C. D. Mol, A. S. Arvai, S. Kanugula, A. E. Pegg, J. A. Tainer, *EMBO J* **2000**, *19*, 1719-1730.

[4] T. P. Brent, P. J. Houghton, J. A. Houghton, *Proc Natl Acad Sci U S A* **1985**, *82*, 2985-2989.

[5] a) G. P. Margison, A. C. Povey, B. Kaina, M. F. Santibanez Koref, *Carcinogenesis* **2003**, *24*, 625-635; b) S. L. Gerson, *J Clin Oncol* **2002**, *20*, 2388-2399; c) S. L. Gerson, *Nat Rev Cancer* **2004**, *4*, 296-307.

[6] a) B. D. Wilson, M. Strauss, B. J. Stickells, E. G. Hoal-van Helden, P. van Helden, *Carcinogenesis* **1994**, *15*, 2143-2148; b) M. E. Dolan, A. E. Pegg, N. K. Hora, L. C. Erickson, *Cancer Res* **1988**, *48*, 3603-3606; c) A. M. Moser, M. Patel, H. Yoo, F. M. Balis, M. E. Hawkins, *Anal Biochem* **2000**, *281*, 216-222; d) R. S. Wu, S. Hurst-Calderone, K. W. Kohn, *Cancer Res* **1987**, *47*, 6229-6235; e) F. M. Ruiz, R. Gil-Redondo, A. Morreale, A. R. Ortiz, C. Fabrega, J. Bravo, *J Chem Inf Model* **2008**, *48*, 844-854.

[7] a) M. E. Dolan, R. C. Moschel, A. E. Pegg, *Proc Natl Acad Sci U S A* **1990**, *87*, 5368-5372; b) A. E. Pegg, K. Goodtzova, N. A. Loktionova, S. Kanugula, G. T. Pauly, R. C. Moschel, *J Pharmacol Exp Ther* **2001**, *296*, 958-965; c) G. Wei, N. A. Loktionova, A. E. Pegg, R. C. Moschel, *J Med Chem* **2005**, *48*, 256-261.

[8] B. Kaina, G. P. Margison, M. Christmann, *Cell Mol Life Sci* **2010**, *67*, 3663-3681.

[9] A. E. Pegg, S. Kanugula, S. Edara, G. T. Pauly, R. C. Moschel, K. Goodtzova, *J Biol Chem* **1998**, *273*, 10863-10867.

[10] a) M. E. Dolan, M. Y. Chae, A. E. Pegg, J. H. Mullen, H. S. Friedman, R. C. Moschel, *Cancer Res* **1994**, *54*, 5123-5130; b) O. Khan, M. R. Middleton, *Expert Opin Investig Drugs* **2007**, *16*, 1573-1584.

[11] a) H. C. Ugur, M. Taspinar, S. Ilgaz, F. Sert, H. Canpinar, J. A. Rey, J. S. Castresana, A. Sunguroglu, *Mol Biol Rep* **2014**, *41*, 697-703; b) O. A. Khan, M. Ranson, M. Michael,

I. Olver, N. C. Levitt, P. Mortimer, A. J. Watson, G. P. Margison, R. Midgley, M. R. Middleton, *Br J Cancer* **2008**, *98*, 1614-1618; c) H. A. Tawbi, L. Villaruz, A. Tarhini, S. Moschos, M. Sulecki, F. Viverette, J. Shipe-Spotloe, R. Radkowski, J. M. Kirkwood, *Br J Cancer* **2011**, *105*, 773-777.

[12] K. Wang, M. Murcia, P. Constans, C. Perez, A. R. Ortiz, *J Comput Aided Mol Des* **2004**, *18*, 101-118.

[13] M. R. L. Kelley, D.; Fishel, M.L., *Future Oncol.* **2014**, *10*, 1215-1237.

[14] S. E. Golding, E. Rosenberg, B. R. Adams, S. Wignarajah, J. M. Beckta, M. J. O'Connor, K. Valerie, *Cell Cycle* **2012**, *11*, 1167-1173.

[15] a) C. H. Fan, W. L. Liu, H. Cao, C. Wen, L. Chen, G. Jiang, *Cell Death Dis* **2013**, *4*, e876; b) B. Kaina, U. Muhlhausen, A. Piee-Staffa, M. Christmann, R. Garcia Boy, F. Rosch, R. Schirrmacher, *J Pharmacol Exp Ther* **2004**, *311*, 585-593.

[16] a) P. Auerbach, R. A. Bennett, E. A. Bailey, H. E. Krokan, B. Demple, *Proc Natl Acad Sci U S A* **2005**, *102*, 17711-17716; b) D. M. Wilson, 3rd, R. A. Bennett, J. C. Marquis, P. Ansari, B. Demple, *Nucleic Acids Res* **1995**, *23*, 5027-5033; c) B. Demple, *Curr Biol* **1995**, *5*, 719-721; d) L. Harrison, A. G. Ascione, D. M. Wilson, 3rd, B. Demple, *J Biol Chem* **1995**, *270*, 5556-5564; e) L. Hughesdavies, T. Galanopoulos, L. Harrison, M. Maxwell, H. Antoniades, B. Demple, *Int J Oncol* **1995**, *6*, 749-752; f) D. M. Wilson, 3rd, M. Takeshita, A. P. Grollman, B. Demple, *J Biol Chem* **1995**, *270*, 16002-16007.

[17] a) S. S. Wallace, *DNA Repair (Amst)* **2014**, *19*, 14-26; b) A. B. Robertson, A. Klungland, T. Rognes, I. Leiros, *Cell Mol Life Sci* **2009**, *66*, 981-993.

[18] a) S. Madhusudan, F. Smart, P. Shrimpton, J. L. Parsons, L. Gardiner, S. Houlbrook, D. C. Talbot, T. Hammonds, P. A. Freemont, M. J. Sternberg, G. L. Dianov, I. D. Hickson, *Nucleic Acids Res* **2005**, *33*, 4711-4724; b) L. A. Seiple, J. H. Cardellina, 2nd, R. Akee, J. T. Stivers, *Mol Pharmacol* **2008**, *73*, 669-677.

[19] J. M. Bogden, A. Eastman, E. Bresnick, *Nucleic Acids Res* **1981**, *9*, 3089-3103.

[20] a) F. P. McManus, C. J. Wilds, *Chembiochem* **2014**, *15*, 1966-1977; b) Q. Fang, A. M. Noronha, S. P. Murphy, C. J. Wilds, J. L. Tubbs, J. A. Tainer, G. Chowdhury, F. P. Guengerich, A. E. Pegg, *Biochemistry* **2008**, *47*, 10892-10903.

[21] a) L. Liu, A. E. Pegg, K. M. Williams, F. P. Guengerich, *J Biol Chem* **2002**, *277*, 37920-37928; b) F. P. McManus, Q. Fang, J. D. Booth, A. M. Noronha, A. E. Pegg, C. J. Wilds, *Org Biomol Chem* **2010**, *8*, 4414-4426.

[22] a) K. X. Luu, S. Kanugula, A. E. Pegg, G. T. Pauly, R. C. Moschel, *Biochemistry* **2002**, *41*, 8689-8697; b) Q. Fang, S. Kanugula, J. L. Tubbs, J. A. Tainer, A. E. Pegg, *J Biol Chem* **2010**, *285*, 8185-8195; c) M. E. Dolan, D. Scicchitano, A. E. Pegg, *Cancer Res* **1988**, *48*, 1184-1188.

[23] a) S. Burge, G. N. Parkinson, P. Hazel, A. K. Todd, S. Neidle, *Nucleic Acids Res* **2006**, *34*, 5402-5415; b) S. Neidle, *Curr Opin Struct Biol* **2009**, *19*, 239-250.

[24] a) L. C. Bock, L. C. Griffin, J. A. Latham, E. H. Vermaas, J. J. Toole, *Nature* **1992**, *355*, 564-566; b) D. M. Tasset, M. F. Kubik, W. Steiner, *J Mol Biol* **1997**, *272*, 688-698.

[25] P. W. Rothemund, *Nature* **2006**, *440*, 297-302.

[26] a) N. V. Voigt, T. Torring, A. Rotaru, M. F. Jacobsen, J. B. Ravnsbaek, R. Subramani, W. Mamdouh, J. Kjems, A. Mokhir, F. Besenbacher, K. V. Gothelf, *Nat Nanotechnol* **2010**, *5*, 200-203; b) R. Jungmann, C. Steinhauer, M. Scheible, A. Kuzyk, P. Tinnefeld, F. C. Simmel, *Nano Lett* **2010**, *10*, 4756-4761; c) R. Subramani, S. Juul, A. Rotaru, F. F. Andersen, K. V. Gothelf, W. Mamdouh, F. Besenbacher, M. Dong, B. R. Knudsen, *ACS Nano* **2010**, *4*, 5969-5977; d) Y. Suzuki, M. Endo, Y. Katsuda, K. Ou, K. Hidaka, H. Sugiyama, *J Am Chem Soc* **2014**, *136*, 211-218.

[27] Y. Sannohe, M. Endo, Y. Katsuda, K. Hidaka, H. Sugiyama, *J Am Chem Soc* **2010**, *132*, 16311-16313.

[28] M. Endo, Y. Katsuda, K. Hidaka, H. Sugiyama, *Angew Chem Int Ed Engl* **2010**, *49*, 9412-9416.

[29] a) B. Sacca, R. Meyer, M. Erkelenz, K. Kiko, A. Arndt, H. Schroeder, K. S. Rabe, C. M. Niemeyer, *Angew Chem Int Ed Engl* **2010**, *49*, 9378-9383; b) S. Rinker, Y. Ke, Y. Liu, R. Chhabra, H. Yan, *Nat Nanotechnol* **2008**, *3*, 418-422; c) A. Kuzuya, M. Kimura, K. Numajiri, N. Koshi, T. Ohnishi, F. Okada, M. Komiyama, *Chembiochem* **2009**, *10*, 1811-1815; d) E. Nakata, F. F. Liew, C. Uwatoko, S. Kiyonaka, Y. Mori, Y. Katsuda, M. Endo, H. Sugiyama, T. Morii, *Angew Chem Int Ed Engl* **2012**, *51*, 2421-2424; e) K. Numajiri, T. Yamazaki, M. Kimura, A. Kuzuya, M. Komiyama, *J Am Chem Soc* **2010**, *132*, 9937-9939; f) K. Numajiri, M. Kimura, A. Kuzuya, M. Komiyama, *Chem Commun (Camb)* **2010**, *46*, 5127-5129.

[30] A. Kuzuya, N. Koshi, M. Kimura, K. Numajiri, T. Yamazaki, T. Ohnishi, F. Okada, M. Komiyama, *Small* **2010**, *6*, 2664-2667.

[31] A. E. Pegg, *Chem Res Toxicol* **2011**, *24*, 618-639.

[32] H. Zang, Q. Fang, A. E. Pegg, F. P. Guengerich, *J Biol Chem* **2005**, *280*, 30873-30881.

[33] a) K. Katsumata, T. Sumi, T. Wada, K. Katou, T. Aoki, *Gan To Kagaku Ryoho* **2004**, *31*, 1357-1360; b) O. Y. Mitsunobu, M., *Bulletin of the Chemical Society of Japan* **1967**, *40*, 2380-2382.

[34] a) A. Juillerat, C. Heinis, I. Sielaff, J. Barnikow, H. Jaccard, B. Kunz, A. Terskikh, K. Johnsson, *Chembiochem* **2005**, *6*, 1263-1269; b) A. Keppler, S. Gendreizig, T. Gronemeyer, H. Pick, H. Vogel, K. Johnsson, *Nat Biotechnol* **2003**, *21*, 86-89; c) A. Juillerat, T. Gronemeyer, A. Keppler, S. Gendreizig, H. Pick, H. Vogel, K. Johnsson, *Chem Biol* **2003**, *10*, 313-317.

[35] M. V. Yigit, D. Mazumdar, Y. Lu, *Bioconjug Chem* **2008**, *19*, 412-417.

[36] Y. Tang, W. Zhang, J. Liu, L. Zhang, W. Huang, F. Huo, D. Tian, *Nanoscale* **2015**.

[37] Z. Yasmin, E. Khachatryan, Y. H. Lee, S. Maswadi, R. Glickman, K. L. Nash, *Biosens Bioelectron* **2015**, *64*, 676-682.

[38] V. Raj, T. Johnson, K. Joseph, *Biosens Bioelectron* **2014**, *60*, 191-194.

[39] X. Liu, Q. Dai, L. Austin, J. Coutts, G. Knowles, J. Zou, H. Chen, Q. Huo, *J Am Chem Soc* **2008**, *130*, 2780-2782.

[40] O. A. Alsager, S. Kumar, G. R. Willmott, K. P. McNatty, J. M. Hodgkiss, *Biosens Bioelectron* **2014**, *57*, 262-268.

Conclusions

CONCLUSIONS:

- 10 compounds selected by a virtual screening study with potential inhibitory activity against hAGT have been analysed *in vitro* and in cell culture assays :
    - The analysis by mass spectrometry (ESI-MS) confirmed the complex formation of hAGT with 5 of them: compound 8 formed a specific complex and compounds 5, 6, 7 and 9 an unspecific one.
    - MTT cytotoxicity studies showed that 2 compounds (5 and 8) were non-toxic and the other 8 compounds presented different levels of toxicity *per se*. In addition, 5 compounds showed enhancement of carmustine toxicity (4, 5, 6, 7 and 8). Compounds 5 and 8 seem to be the best candidates for hAGT inhibition, as they enhance BCNU without being toxic by themselves.
    - Compounds 5, 6, 7 and 8 were further characterized by colony formation assays, which confirmed that compound 8 was non-toxic at long-term experiments and exhibited a stimulation effect of carmustine.

- A new method to detect hAGT activity based on the conformational change of the thrombin binding aptamer and followed by FRET has been designed and set up successfully. This technology allows the quantification of hAGT activity in a single step and in a straightforward manner, avoiding radioactivity and reaching a detection limit of 0.5 pmols of hAGT. Furthermore, this method can be easily transferred to a high throughput experiment for the evaluation of small molecules as potential hAGT inhibitors.

- The DNA origami platform has been exploited to design a new methodology to follow in real-time the repair activity of hAGT by Atomic Force Microscopy. This study combines the recognition capacity of α-thrombin, able to discriminate methyl-TBA and TBA, and the single-molecule features of the DNA origami technique, applied to the detection of DNA repair. The system is extremely effective and reliable, and the results are clearly followed by AFM, allowing the detection of single-molecule reactions, the highest detection limit possible. Their consistency suggests that our system could be further evolved to design hAGT activity assays for the identification of potential inhibitors as chemotherapy enhancers and for the study of other DNA repair enzymes.

- A new assay to detect hAGT activity by the transfer of a fluorescent moiety from the substrate oligonucleotide to the active site of the protein has been described. For this purpose:

- We have described a novel route for synthesizing an O^6-benzyl-2'-deoxyguanosine precursor which incorporated to an oligonucleotide sequence, can become a fluorescently labelled substrate for measuring hAGT repair activity.
- Annealing with a complementary quencher strand produces a stable duplex confirmed by physicochemical methods which presents a low basal fluorescence.
- We have tested the efficiency of the fluorescence substrate transfer to hAGT. This system allows the detection of 0.5 pmols of hAGT, the same obtained for the fluorescence assay based on the conformational change of a G-quadruplex.
- On theses bases, we have developed a new rapid and straightforward assay to detect hAGT activity. The system uses a double-stranded oligonucleotide, the natural substrate for hAGT activity, improving efficiency and reliability due to its easy quantification of the fluorescence increase upon activity.
- We have tested 9 compounds with potential inhibitory activity of hAGT, finding that compound 8 inhibits significantly the DNA repair activity of hAGT *in vitro*. This represents a proof of concept of the usability of our method, as well as confirms the results previously obtained in chapter 1.

- Three types of nanoparticles (AuNPs, SPIONs and AuSPIONs) have been used to detect by different techniques (UV, DLS and MRI) a single methylation in G-quadruplex. We have proven the detection capacity of AuSPION as biosensors, demonstrating that their performance is comparable to AuNPs and SPIONs. The bases for setting up a new detection platform for hAGT activity over a nanoparticle system have been accomplished.

Summary

The O^6-alkylguanine DNA alkyltransferase (hAGT or MGMT) is a DNA repair protein in charge of removing alkyl adducts from the O^6 position of guanines, blocking their cytotoxic effects and playing an important role as a resistance mechanism to chemotherapy in cancer patients. For these reasons, it is considered relevant as a prognosis marker of cancer and represents a potential therapeutic target. Intense research efforts have been devoted to the identification of small molecules capable of inhibiting hAGT activity and enhancing the cytotoxic effect of the alkylating agents in tumour cells.

In this doctoral thesis, we have explored 10 compounds with potential inhibitory activity against hAGT. The analysis by mass spectrometry (ESI-MS) confirmed the complex formation of hAGT with 5 of them (compounds 5, 6, 7, 8 and 9). MTT cytotoxicity studies in cell culture showed that 2 compounds (5 and 8) were non-toxic and showed enhancement of carmustine toxicity. This compounds were further analysed by colony formation assays, which confirmed that compound 8 was non-toxic at long-term experiments and exhibited a stimulation effect of carmustine. Compound 8 seem to be the best candidates for hAGT inhibition, as it forms a complex with hAGT and it enhances BCNU without being toxic in MTT and colony formation assays.

Due to the lack of a consistent *in vitro* assay for the activity of hAGT, we have devoted part of this doctoral thesis to the search of bio and nanotechnologies to detect hAGT activity which enable the evaluation of potential inhibitors of the protein. Chapter 2 describes the development of a new fluorescence method using the conformational change of a DNA G-quadruplex, the thrombin binding aptamer (TBA), as a molecular beacon for the detection of hAGT activity and the development of new inhibitor compounds.

The conformational change of TBA is further explored to develop a detection platform on DNA origami which allows de quantification of the repair activity of hAGT on a single molecules basis, through the direct visualization by AFM of the interaction of TBA with its target protein α-thrombin when its G-quadruplex structure is restored.

In addition, this work reports the synthesis of guanine derivatives modified at position 6 and properly functionalized for their incorporation into double stranded oligonucleotides that are used for the development of another novel fluorescence methodology to evaluate hAGT activity and to assess potential inhibitors as enhancers of chemotherapy.

Finally, during a short stay in the University of Milan, we have developed a new sensor to detect a methylation in TBA using three types of nanoparticles: AuNPs, SPIONs and AuSPIONs. AuSPIONs combine the features of the gold coating and the magnetic core,

and exhibit similar performance as AuNPs and SPIONs in UV, DLS and MRI assays to detect thrombin and a single methylation in TBA. These results provide the basis for the development of a new straightforward method to study hAGT activity and to evaluate potential inhibitors.

RESUM

La proteïna de reparació de l'ADN alquilguanina-ADN-O^6-alquiltransferasa (hAGT) elimina productes d'alquilació en la posició O^6 de les guanines, bloquejant la citotoxicitat dels agents alquilants i produint resistència a la quimioterapia. Es considera rellevant com a marcador de pronòstic en càncer i representa una potencial diana terapèutica.

L'objectiu a llarg termini d'aquesta tesi doctoral és trobar inhibidors de l'activitat d'hAGT per millorar l'efecte de la quimioteràpia en pacients amb càncer.

En primer lloc, es va avaluar la capacitat de 10 compostos, potencials inhibidors d'hAGT, de formar un complexe amb hAGT utilitzant espectrometria de masses, i es va estudiar la seva toxicitat en cultius cel·lulars a través d'assajos de MTT i de formació de colònies.

A continuació, es desenvolupen diferents mètodes per a la detecció de l'activitat d'hAGT, per a avaluar inhibidors d'aquesta proteïna *in vitro*. Dos d'aquests mètodes utilitzen el canvi conformacional que es produeix en l'aptàmer d'unió a la trombina (TBA) en introduir una O^6-metilguanina, substrat d'hAGT, en una de les seves tètrades centrals.

En el primer mètode es va emprar el TBA per generar un sensor de fluorescencia incorporant un fluoròfor i un inhibidor de fluorescència a cadascun dels seus extrems. Aquest sensor permet la detecció de la disminució en la fluorescència deguda al canvi conformacional del TBA produit per l'activitat d'hAGT.

Posteriorment, el canvi conformacional del TBA va permetre dissenyar un biosensor de l'activitat d'hAGT a nivell unimolecular sobre la superfice d'un origami d'ADN. La interacció del TBA amb la seva proteina diana, l'α-trombina, es va seguir per AFM per detectar que l'estructura de G-quàdruplex metilada es restableix per la reparació d'hAGT.

El tercer mètode es basa en la transferència de fluorescència al centre actiu d'hAGT degut a la reparació d'un oligonucleòtid que conté una guanina modificada amb un grup alquil marcat amb un fluoròfor. Amb aquest objectiu, es va portar a terme la síntesi química d'aquesta guanina modificada.

En el marc d'una estada en la Universitat de Milà, es descriu l'estudi de nanopartícules funcionalitzades amb TBAs per a detectar una metilació en una guanina utilitzant espectroscopia d'UV, DLS o MRI, amb l'objectiu de desenvolupar un nou assaig de l'activitat reparadora d'ADN d'hAGT.